Interplay between Lake and Catchment Processes in Kuhai Lake Basin, NE Tibetan Plateau, China during Late Holocene

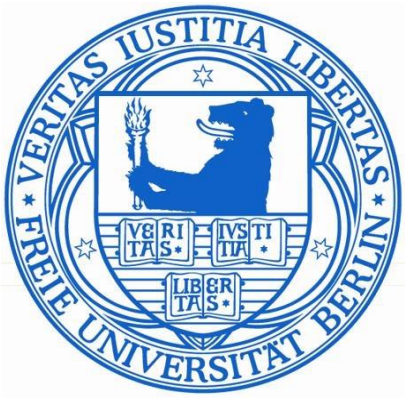

Dada YAN

Dissertation at the Department of Earth Sciences

Freie Universität Berlin

This dissertation is submitted for the degree of

Doctor in Natural Sciences

(Dr. rer.nat.)

2017

Disputation time: 19 April, 2017

Reviewers:

Prof. Dr. rer. nat. **Bernd Wünnemann** Email:wuenne@zedat.fu-berlin.de
PD. Dr. rer. nat. habil. **Peter Frenzel** Email: peter.frenzel@uni-jena.de
Prof. Dr. rer. nat. **Brigitta Schütt** Email:brigitta.schuett@fu-berlin.de

Contents

Abbreviations

>	more than	**g/l**	gram per liter
<	less than	**i.e.**	id est
°C	degree centigrade	**ka**	kilo years (=1000 years)
%	percentage	**km**	kilometer
‰	per mill	**km^2**	square kilometer
δ	delta, ratio	**kV**	kilovolt
$\delta^{18}O$	ratio of ^{18}Oxygen and ^{16}Oxygen	**m**	meter
$\delta^{13}C$	ratio of ^{13}Carbon and ^{12}Carbon	**mA**	milliampere
δD	ratio of Deuterium and Hydrogen	**max.**	maximum
a	year	**min.**	minimum
AD	anno Domini	**mg/g**	milligram per gram
AMS	Accelerator Mass Spectrometry	**mm**	millimeter
a.s.l.	Above sea level	**mS**	millisiemens
BP	Before Present (since 1950)	**N**	North
ca.	circa	**OSL**	optical stimulated luminescence
cal.	calibrated	**pers. commu.**	personal communication
CE	Current Era	**RE(s)**	reservoir error(s)
cm	centimeter	**rel.**	relative
cps	counts per second	**s**	second
E	East	**SAR**	sediment accumulation rate
EC	electrical conductivity	**SEM**	Scanning Electron Microscope
el. cond.	electrical conductivity	**sp.**	spec
e.g.	exemplī grātiā, for example	**spp.**	species
EM	endmember	**TSD**	total dissolved solids
EMMA	endmember modelling analysis	**µm**	micrometre
et al.	et alli	**vol.**	volcanic
g	gram	**VPDB**	Peedee Belemnite
GPS	Global Positioning System	**VSMOW**	Standard Mean Ocean Water

Table list

Figures list

Tables & figures list in appendix

Extended abstract

The Tibetan Plateau (TP), the largest and highest plateau in the world and important water resource region for billions of people on the Asian continent, is considered a unique area in Central Asia for deciphering the relationship between landscape evolution and climate impact. Lake basins and their catchments are therefore valuable research objects for studying the process-response behavior of individual systems as they react very sensitive to climatic and non-climatic factors that influence sediment and water flux from the sources to the sinks. Commonly, these processes are archived in sediments of lakes as long as they persist and are not subject to erosion/deflation. Hence, many researchers concentrated on lake research on the TP to elucidate the evolution of lakes in response to climate impact, for example. Especially the interplay between the Asian Monsoon system and the mid-latitude Westerlies are in the focus of such studies.

The overwhelming majority of research results based on various proxy data rely on sediment records from lakes, derived from a single sediment core, preferably retrieved from the deepest and central part of lake basins. The results imply that the proxy data, extracted from the respective sediment parameters, are spatially and temporally valid for the entire research region and beyond. In most cases, catchment dynamics and their interaction with the lake were not or less considered for the overall interpretation of climate- and/or non-climate-induced processes that influenced the lake hydrology and its evolution through time.

The Kuhai Lake Basin, located on the north-eastern TP, was selected for this study in order to combine investigations in the lake's catchment with those on the lake itself. This strategy was considered a necessary requirement for a better understanding of interrelated processes responsible for the evolution of the lake. Especially their response to climate impact by the East Asian Summer monsoon (EASM) and the Westerlies were in the focus of this study.

Geomorphological studies in the catchment of the lake were conducted with focus on the drainage systems and their sediments, combined with morphological landforms formed by aeolian processes. Thirty sediment sections were investigated by means of sediment composition (grain size) and fossil remains (ostracod), where possible. In addition, selected sediment sequences in several sections were dated by radiocarbon-AMS or OSL techniques.

Sediments from the lake were used for detailed high-resolution analysis. They comprised 57 lake surface samples covering the entire lake basin and four sediment cores with individual lengths of up to 2.75 m from different locations in the lake. The chronology of all sediment cores was achieved by radiocarbon-AMS dating on different fractions from bulk samples and/or plant remains. $^{210}Pb/^{137}Cs$ dating was used for age control of the

upper 25 cm sediment from one core. Records from the lake cover the last 4000 years of sedimentation history.

High-resolution analyses (1 or 2 cm resolution) of lake sediments from the lake comprise grain size by laser technology, geochemical components by LOI and ICP-OES, mineral identification by XRD, stable isotopes $\delta^{13}C/\delta^{18}O$ on authigenic carbonate and ostracod identification.

Morphological-sedimentological investigations in the catchment confirmed two different drainage systems on the northern and eastern side of the lake basin with slight differences in lithology of the headwater regions (Permian versus Triassic formations). Most important is the fact that the northern drainage systems are only periodically active during the rainy season in summer time, thus providing water and sediments to the lake during a limited period of the year. Conversely, the southern drainage system is active all the year round with perennial water and sediment supply, as also two other smaller systems in the south-east and south-west do. These conditions of the modern time most likely existed also during the last 4000 years.

Two distinct terrace systems bordering the main rivers are indicative of sequential incision by strong fluvial erosion of unknown age for the higher one, whereas the younger one was formed during the last few hundred years. Incision rate for the younger terrace accounts for >3mm/year which is a rather high value. It can be assumed that the incision into the own fan is the result of tectonic uplift of the catchment in combination with a lowered lake level.

Aeolian sediments in the Kuhai catchment reveal deposition of dune sand and other aeolian sand covers mainly during the early Holocene and late Holocene. Fine-grained loess deposits however, indicate the contribution of these aeolian components since the last 9 ka, mainly preserved in the upper parts of the catchment. The wide-spread dune fields in the north-eastern part of the lake basin are relatively young in age and suggest earliest accumulation at about 3 ka while the major dune bodies are not older than 2000 years.

Analyses of lake surface samples from Kuhai Lake confirm the very high spatial diversity of grain size components, minerals/geochemical elements and ostracod assemblages, all strongly affected by the contribution of the two different drainage systems, lake-internal currents and vertical water temperature gradients as well. High proportions of fine-grained lacustrine deposits (transported as suspended load) were found in the center and southern part of the lake basin. The same applied to carbonates with high proportions of Monohydrocalcite (MHC). The latter occurred in high concentrations mainly in water depths below 10 m, with water temperatures <8°C. Non-detrital High-Mg-Calcite and Dolomite were only concentrated at few locations in areas protected from inflowing rivers in water depths above 10 m.

Only two species of ostracod (*Eucypris mareotica*, *Limnocythere inopinata*), both common species with wider environment tolerance range were recorded in surface sediments, of which *L. inopinata* is considered to live in shallow water environments of lakes and ponds. They only occurred at few sites in shallow parts of the lake with water depths between 4 and <11 m, while *L. inopinata* was not found in water depths >8 m. The distribution of aquatic plants (mainly consisting of sea grass, e.g., *Potamogeton* sp.) was everywhere restricted to a water depth <6 m, while algae (not specified) were found in all water depth but with considerably low amounts in the profundal zone (~>14 m water depth).

Stable oxygen and carbon isotopes in carbonates showed a clear dependence on evaporative effects and on inflowing water. Lightest values were recorded at the river mouths and continuously increasing values (heavier) towards the lake center and the southern part of the lake, due to continued mixing with isotopically heavier lake water and evaporation. Their changes also marked the pathway of inflowing water towards the lake center. Highest values corresponded with the deposition of non-detrital High-Mg Calcite and Dolomite at protected sites with less water exchange. In general, increasing isotope values in the lake reflect the mixing process with heavier lake water and evaporation.

All parameters mentioned above were used for the estimation of water depth changes during the past 4000 years, derived from the sediment composition in cores. Sediments in the four lake records also displayed a high diversity among them and through depth and time, depending on their position to the inflowing river systems. In general, higher fluctuations of grain size components in the cores closer to the inflow regions of the two river systems corresponded with changes in energy flow. Consequently, the core from the lake center showed less variation in grain size.

Fluctuations in fine-grained lacustrine deposits which certainly included aeolian loess components as well, but likely with lower amounts, were used to identify water depth changes too, in relation to the sediment flux from the two river systems. These fluctuations corresponded with the occurrence/disappearance of MHC in favor of non-detrital High-Mg-Calcite and Dolomite and with the distribution of aquatic plants for certain time periods.

Stable oxygen isotopes in the core records support these inferences. Moreover, they displayed not only changes in water supply from the catchment but also a clear differentiation between water sources and the timing of discharges. During the summer season, local rainfall connected with the EASM effective moisture supply, enhanced discharge via all river systems toward the lake, while during the off-Monsoon season only water/snow from local water vapor recycling processes and/or from westerly-derived sources contributed to the lake's water budget, mainly via the perennial rivers. This pattern of seasonal dimension most likely influenced the isotopic composition of the lake water, from which the carbonates precipitated. The proportion of the two contributing water resources in combination with lower temperatures and reduced evaporation effects during the off-monsoon period reflected the isotopic composition of the lake carbonates.

As a result, the isotopic pattern in carbonates from Kuhai Lake was opposite to the patterns in summer monsoon-controlled speleothem records. Both data sets were used here as comparison for discussing the EASM influence in this region during the last 4000 years.

Phases of weak EASM influence accompanied by very low lake levels and related water depth occurred during the period 4-2.7 cal. ka BP (dry interlude), due to less water inflow from the episodic river systems. The core locations closer to the inflowing sites were temporally dry or experienced pond and/or wetland conditions, favorable for ostracod and plants to develop there. The low water depth in the lake center enabled the occurrence of ostracod and the growth of sea grass as well, preserved in the respective sediments.

Comparable climate conditions with weak EASM in favor to the Westerlies also occurred during the time intervals of the Dark Ages Cold Period (DACP, 1.5-1 cal. ka BP) and Little Ice Age (LIA, 0.55-0.05 cal. ka BP, ca. 1300-1900 AD) with strong negative water balances, although less pronounced in comparison to the previous longer dry interlude.

Conversely, a stable phase with stronger influence of EASM effective moisture supply and possibly slightly higher lake level as today occurred between 2.7 and 1.5 cal. ka BP. Similar conditions were recorded for the period of the Medieval Warm Period (MWP, 0.95-0.65 cal. ka BP), with fluctuation bur generally greater water depth than the preceding period.

These changes of EASM influence in favor of Westerly–derived climate during the drier and perhaps colder periods may have been due to the southwards shift of the ITCZ that reduced the atmospheric pressure gradient between the ocean and the TP, resulting in weaker influence of effective summer monsoon moisture transport to the northern latitude along the modern monsoon boundary. In addition, it seems possible that changes in solar radiation beside other possible drivers affected the water balances in the Kuhai lake region.

Erweiterte Zusammenfassung

Das Tibet Plateau (TP), größtes und höchst gelegenes Plateau der Erde und gleichzeitig wichtige Wasser-Resource für Milliarden von Menschen des asiatischen Kontinents, kann als einzigartige Region betrachtet werden, die Beziehungen zwischen Landschaftsentwicklung und Klima zu entschlüsseln. Seebecken und ihre Einzugsgebiete sind daher wertvolle Untersuchungsobjekte, um die Wirkungsgefüge zwischen Prozess und Reaktion individueller Systeme zu studieren, da diese sehr sensitiv auf klimatische und nichtklimatische Faktoren reagieren und dadurch den Sediment- und Wassertransport von der Quelle bis zum Ort der Ablagerung beeinflussen. Gewöhnlich werden diese Prozesse in Sedimenten der Seen archiviert, solange diese existieren und nicht der Abtragung durch Erosion und/oder Deflation unterliegen. Daher haben sich zahlreiche Forscher auf die Untersuchungen von Seen des Tibet Plateaus konzentriert, um die Geschichte der Seenentwicklung als Reaktionen auf den Klimaeinfluss aufzuklären. Insbesondere die Wechselbeziehungen zwischen dem Asiatischen Monsunsystem und dem Westwindsystem der mittleren Breiten liegen dabei im Fokus dieser Untersuchungen.

Die überwältigende Mehrheit der Forschungsergebnisse aus Proxidaten vertraut auf Sedimentdaten aus Seen, welche aus einem einzigen Sedimentkern entnommen wurden, vorzugsweise aus der Seemitte bzw. aus den tiefsten Teilen des Seebeckens. Es wird dabei angenommen, dass die extrahierten Proxidaten aus den Sedimenten sowohl zeitlich als auch räumlich für die gesamte Untersuchungsregion und darüber hinaus repräsentativ sind. In den meisten Fällen sind die dynamischen Wechselwirkungen zwischen dem Einzugsgebiet und dem See im Hinblick auf die Interpretation von klimarelevanten und nicht-klimatischen Prozessen, welche die hydrologische Entwicklung des Sees in der Zeit steuern, weniger betrachtet worden.

Das Kuhai-Becken im nordöstlichen Tibet Plateau wurde für diese Studie ausgewählt, um Untersuchungen im Einzugsgebiet des Beckens mit denen im See zu kombinieren. Diese Strategie wird als notwendige Voraussetzung erachtet, um das Verständnis über die Wechselwirkungen verschiedener Prozesse zu vertiefen, die für die Genese des Sees verantwortlich sind. Dabei standen die Einflüsse des Ostasiatischen Sommermonsuns (EASM) und der Westwinde auf das System im Vordergrund.

Es wurden geomorphologische Untersuchungen im Einzugsgebiet des Sees mit Fokus auf die Abflusssysteme und ihrer Sedimente in Kombination mit Landformungen durch äolische Prozesse durchgeführt. Insgesamt wurden 30 Profile untersucht und sedimentologisch mit Hilfe von Korngrößenanalysen sowie Fossilresten (Ostrakoden) ausgewertet, sofern möglich. Zusätzlich wurden ausgewählte Sedimentprofile und mit Hilfe von Radiokarbon-AMS oder Optisch Stimulierter Lumineszenz (OSL) datiert.

Sedimente aus dem Kuhai See wurden hochauflösend analysiert. Diese umfassten 57 über den See verteilte Oberflächenproben vom Seegrund sowie 4 Sedimentbohrkerne mit individuellen Kernlängen bis zu 2,75 m aus verschieden Teilen den Sees. Die

Chronologie der Sedimente aus allen Bohrkernen wurde durch Radiokarbon-AMS Datierungen an unterschiedlichen Fraktionen einer Probe sowie an fossilen Pflanzenresten ermittelt. Zusätzlich wurden an einem ausgewählten Bohrkern die obersten 25 cm Sediment mittels Blei-Cäsium Methode (^{210}Pb/^{137}Cs) datiert. Insgesamt decken die Kerne die letzten 4000 Jahre Sedimentationsgeschichte ab.

Die hochauflösende Analyse (1 cm bzw. 2 cm Auflösung) der Seesedimente umfasste Korngrößen mittels Lasertechnik, geochemische Komponenten mittels Glühverlust (LOI) und ICP-OES, Mineralbestimmung mittels Röntgendiffraktometrie (XRD), Stabile Isotope $\delta^{13}C/\delta^{18}O$ an authigenen Karbonaten sowie Ostrakodenbestimmung.

Die morphologisch-sedimentologischen Untersuchungen im Einzugsgebiet bestätigen die Existenz von zwei unterschiedlichen Drainagesystemen, östlich und nördlich des Seebeckens mit lithologisch geringfügigen Unterschieden in den Ausgangsgesteinen der oberen Einzugsgebiete (Permische versus Triassische Gesteine). Bedeutender ist allerdings die Tatsache, dass im Norden bzw. Nordosten des Sees ausschließlich periodische/episodische Systeme vorzufinden sind, die nur während der Hauptregenzeiten im Sommer aktiv sind. Im Gegensatz dazu, sind insgesamt drei dauerhaft aktive Systeme im Osten, Südosten und Südwesten aktiv, die das ganze Jahr über Wasser und Sediment dem See zuführen. Diese aktuellen Abflussbedingungen können auch für die Vergangenheit (zumindest für die letzten 4000 Jahre) angenommen werden.

Zwei markante Terrassensysteme begleiten die Flüsse und zeugen von intensiver Tiefenerosion durch fluviale Aktivität. Für die obere ältere Terrasse ist ein Alter unbekannt. Die untere jüngere ist erst in den letzten wenigen Hundert Jahren gebildet worden und weist auf eine ungewöhnlich hohe Erosionsrate von >3mm/Jahr hin. Es kann davon ausgegangen werden, dass die bisherige Einschneidung in den eigenen Schwemmfächer als Folge tektonischer Hebung des Einzugsgebietes im Verbund mit einem niedrigeren Seespiegel erfolgte.

Äolische Sedimente im Kuhai Einzugsgebiet belegen die Ablagerung von Dünensand sowie Sanddecken, welche aufgrund der Datierungen in das frühe Holozän und in das Spätholozän gestellt werden können. Feinkörnigere Lösse sind gemäß vorliegender Datierungen zumindest seit etwa 9000 Jahren abgelagert worden und sind in den höheren Lagen des Einzugsgebietes deutlich oberhalb des Sees erhalten geblieben. Das ausgedehnte Dünengebiet im Nordosten des Sees ist dagegen relativ jung und läßt auf eine Ablagerung um 3 ka schließen, wobei die Hauptteile der Dünenkörper nicht älter als 2 ka sind.

Die Analysen der Oberflächensedimente aus dem See belegen die sehr hohe räumliche Diversität der Korngrößenkomponenten, Minerale, geochemische Elemente und Ostrakoden. Diese ist durch die beiden unterschiedlichen Drainagesysteme und deren Zuläufe, durch die see-interne Wasserzirkulation und den vertikalen Temperaturgradienten im Wasser bedingt.

Hohe Anteile feinklastischer Seesedimente (transportiert als Suspensionsfracht der Flüsse) finden sich im Zentrum und im südlichen Becken des Sees. Gleiches gilt für die Ablagerung von Karbonaten, wobei Monohydrokalzit (MHC) als dominantes Mineral gefunden wurde . Letzteres tritt in höheren Konzentrationen in Wassertiefen unterhalb 10 m auf, in denen die Temperaturen entsprechend vorliegender Messungen unterhalb 8°C liegen. Nicht-detritischer Hochmagnesium-Kalzit und Dolomit trat nur an wenigen Stellen in höheren Konzentrationen oberhalb von 10 m Wassertiefe auf und dann auch nur an geschützten Stellen außerhalb des direkten Einmündungsbereiches der Flüsse an Stellen mit vermutetem geringeren Wasseraustauch.

Lediglich 2 verschiedene Ostrakodenarten konnten in den Oberflächensedimenten gefunden werden: *Eucypris mareotica* und *Limnocythere inopinata*, die beide eine größere Toleranz hinsichtlich ihrer ökologischen Lebensansprüche aufweisen, wobei *L. inopinata* als Bewohner von Seen und Kleingewässern im Flachwasser bekannt ist. Beide Arten traten nur in sehr wenigen Proben auf und dann nur in Wassertiefen zwischen 4 und <11 m. *L. inopinata* hingegen war nicht in Wassertiefen >8 m zu finden. Die Verbreitung von Wasserpflanzen (Seegras, u.a. *Potamogeton* sp.) war überall begrenzt auf Wassertiefen oberhalb 6 m, während Algen (nicht näher bestimmt) in allen Proben zu finden waren, allerdings in deutlich geringeren Anteilen im Profundal des Sees unterhalb 14 m Wassertiefe.

Stabile Sauerstoff und Kohlenstoffisotope in Karbonaten zeigten eine deutliche Abhängigkeit von Evaporation und zufließendem Wasser, wobei die leichteren Isotope im Mündungsbereich der Flüsse angetroffen wurden und seewärts durch fortschreitende Mischung mit dem Seewasser und Evaporation isotopisch schwerer wurden. Sie ezichneten aber auch den Transportweg des zufließenden Wassers nach. Schwerere Sauerstoffisotope korrespondierten mit nicht-detritischem Hochmagnesium-Kalzit und Dolomit.

Alle oben genannten Parameter wurden für eine Abschätzung der Wassertiefenverhältnisse bzw. Seespiegelveränderungen während der letzten 4000 Jahre genutzt, welche aus den Sedimentdaten der Bohrkerne angeleitet werden konnten. Sedimente der Bohrkerne zeigten ebenso wie die Oberflächenproben eine hohe Diversität untereinander und über die Tiefe/Zeit in Abhängigkeit von der jeweiligen Position der Bohrkerne zu den Drainagesystemen. Stärkere Fluktuationen im Korngrößenspektrum waren in solchen Kernen zu beobachten, die näher an den Zuflüssen lagen, womit sie das Abflussverhalten der jeweiligen Flüsse widerspiegeln. Deutlich geringere Korngrößenvariationen traten im Zentrum des Sees auf. Die Fluktuationen der Feinkomponenten, welche sicherlich auch zu einem geringeren Anteil äolische Sedimente (Löß) enthielten, wurden ebenfalls als Indikatoren für Seespiegeländerungen bzw. Wassertiefenschwankungen in Abhängigkeit vom Eintrag durch variable Flussaktivität herangezogen. Die Variationen korrespondierten mit dem Auftreten/Verschwinden von MHC zugunsten von nicht-detritischem Hochmagnesium-

Kalzit und Dolomit sowie mit der Verteilung von Wasserpflanzen (Seegras) während bestimmter Zeitabschnitte.

Variationen der stabilen Sauerstoffisotope unterstützen nicht nur diese Annahmen der Seespiegel/Wassertiefenveränderungen, sondern auch die Änderungen im Wasserdargebot über die Flüsse in Abhängigkeit saisonaler Aktivitätsphasen. Während der Sommerperiode führte der durch den EASM verursachte Niederschlag zu hohem Abfluss aller Drainagesysteme Richtung See. In den Perioden außerhalb des Monsuneinflusses (Herbst bis Frühjahr) erfolgte die (geringere) Wasserversorgung des See im Wesentlichen unter Einfluss der Westwindsysteme und -möglicherweise durch lokales Recycling von Wasserdampf begünstigt - über die perennierenden Flüsse, ähnlich den heutigen Verhältnissen.. Dieses Muster mit saisonaler Prägung hat sehr wahrscheinlich die isotopische Zusammensetzung des Wassers beeinflusst. Dabei dürfte der jeweilige Anteil der unterschiedlichen Niederschlagsquellen am gesamten Wasserdargebot neben den saisonalen Temperatur- und Verdunstungseffekten die isotopische Zusammensetzung des Seewassers beeinflusst haben, von welchem die Karbonate präzipitierten. Als Ergebnis zeigt sich deshalb ein gegenläufiges Muster zu den bekannten Isotopenmustern in den Höhlensedimenten der Monsunregion. Dieser Unterschied wurde für die Rekonstruktion des EASM Einflusses der letzten 4000 Jahre herangezogen.

Danach traten Phasen mit schwachem EASM Einfluss und resultierendem sehr niedrigen Seespiegel (geringe Wassertiefen) vor allem in der Periode zwischen 4 und 2,7 ka BP auf (Trockenperiode). Diese sind als Folge des reduzierten Abflussgeschehens vor allem über die nur episodisch aktiven Drainagesysteme zu betrachten. An den mehr ufernahen Bohrlokalitäten war der Seespiegel extrem niedrig und führte zumindest zeitweilig zur Bildung von Trockenbereichen sowie Flachwasser- bzw. Sumpfzonen, vorteilhaft für die Entwicklung der Ostrakodenpopulationen und Flora, welche in den Sedimenten der Bohrkerne gespeichert wurden.

Vergleichbare Verhältnisse eines schwachen Monsuneinflusses zugunsten der Westerlies traten auch in den kälteren und trockeneren Perioden um 1,5-1,0 ka BP („Dark Cold Ages Period“, Periode nach dem Fall des Römischen Reiches), und um 0,55-0,05 ka BP (ca. 1300-1900 AD) während der Kleinen Eiszeit auf, gekennzeichnet durch negative Wasserbilanzen des Kuhai Sees, die jedoch im Vergleich zu der vorhergehenden Periode geringer waren.

Im Gegensatz dazu konnten trotz kleinerer Schwankungen überwiegend stabile und positive Wasserbilanzen zwischen 2,7 und 1,5 ka BP sowie während der Mittelalterlichen Wärmeschwankung (MWP) zwischen ca. 0,95 und 0.65 ka BP festgestellt werden. Sie sind die auf eine Intensivierung des EASM Einflusses zurückzuführen und entsprechen weitestgehend den heutigen Bedingungen.

Fluktuationen des EASM-gesteuerten Klimaeinflusses mit stärkerer Ausprägung der Westerlies während der trockeneren und sicherlich auch kälteren Perioden gehen vermutlich auf die Südwärtsverlagerung der Innertropischen Konvergenzzone (ITC)

zurück, welche eine Abschwächung der Druckgegensätze zwischen dem Ozean (Pazifik) und dem TP begünstigte und dadurch die nordwärtige Ausdehnung des sommermonsunalen Niederschlags entlang der heutigen Monsungrenze behinderte. Darüber hinaus kann vermutet werden, dass die Schwankungen in der Solarstrahlung ebenfalls einen negativen Einfluss auf den Wasserhaushalt des Kuhai Sees ausgeübt haben können.

.

1. Introduction

The Tibetan Plateau (TP), also known as the Qinghai-Xizang Plateau, is the highest and largest plateau in the world, covering an area of more than 2.5 million square kilometer with a mean elevation exceeding 4500 m above sea level. It is therefore often called 'Roof of the world' or the 'Third Pole' (Qiu, 2008), initially formed by the collision of the Indian subcontinent with the Eurasian plate some 50 Ma ago (Molnar, 1989) and uplifted since then to its present shape. The TP does not only play a significant role in the global climate system but also serves as a prominent water resource region for more than 1.5 billion people, because several large rivers such as the Changjiang (Yangtze River), Yellow River, Indus, Yarlung Tsangpo (Brahmaputra), Yuan River (Red River) and the Ganges system originate on the plateau.

More than 3000 lakes of different size and water quality serve as important water storage systems too. These water resources directly influence economy and social life in China and surrounding countries (Immerzeel et al., 2010). Due to this extraordinary geological, environmental and climate setting it has attracted a high number of researchers from different geoscientific disciplines in order to better understand the role of the TP on the regional and global climate system. It is therefore of particular interest how and to which extent the climate system could have influenced environmental processes and responses on the land surface.

Existing palaeoclimate studies show high-frequency climate instability during the last glacial cycle. Taking the influence of the Asian Summer Monsoon as an important driver for the process-response behavior of environments with limited water variability and renewable storage capacity into account, the present and past effective moisture transport across the TP is rather important for predicting future water availability under the current climate warming scenarios (e.g., Wanner et al., 2008). Notably the two branches of the Asian Monsoon system, namely the Indian Summer Monsoon (ISM) and the East Asian Summer Monsoon (EASM), are the most prominent atmospheric systems which compete with mid-latitude westerly air masses across the TP (e.g., Domroes and Peng, 1988; Böhner, 2006), all influencing effective moisture supply in that vast region.

A comprehensive Sino-German research program during the last years (funded by the German Science Foundation, DFG) also focused on these interactions on different timescales and in different research regions. Notably, studies along sediment cascades from the sources to the sinks at the modern boundary of the EASM on the northeastern TP were subject to detailed analyses of catchment-lake interactions. I was involved in this research as a Master degree student with focus on ostracod studies.

The results already showed that a comprehensive consideration of interacting processes between the lakes (Donggi Cona, Heihai, Hala Lake) and their catchments are necessary

pre-requisites to better understand climate-induced processes as well as non-climatic factors that affected sediments in the respective regions.

Due to a new project funded by the Chinese State Government within the so-called 1000-talents program awarded to Prof. Wünnemann, Kuhai Lake close to the former research regions was selected for detailed studies.

The comprehensive study on Kuhai Lake and its catchment lead to the following scientific questions, which needed to be answered for a more comprehensive understanding of interlinked processes and their responses to climate-driven hydrological variations within the lake basin:

- How and to which extent can sediments from Kuhai Lake display spatio-temporal diversity of processes?
- Are there linkages between transport and depositional processes in the lake and its catchment?
- Is a single sediment record representative for reconstructing overall climatic influence on the lake system?
- Can the records from the Kuhai Basin monitor the climatic interplay between the East Asian Summer Monsoon and Westerlies?

This study aims at resolving the effects within a small lake-catchment which may contribute to a wider knowledge about influencing factors in a sensitive area close to the modern boundary of summer monsoon impact.

2. Scientific problems - State of knowledge

To date, it is still not well understood, how and to which extent the two climate systems – the Asian Summer Monsoons and Mid-Latitude Westerlies on the north-eastern and north-central Tibetan Plateau interact. They may have caused the out-of-phase relationship during the Holocene (Chen et al., 2008; Li et al., 2012; Jin et al., 2012). Lake stable isotopes (e.g., Henderson et al., 2010; An et al., 2012; Yan and Wuennemann, 2014; Chen et al., 2016) compared with cave and/or ice records (e.g., Yao et al., 2012; Pang et al., 2014) were applied to distinguish different moisture sources especially in northeastern Tibetan Plateau. Zhang et al. (2011) compared stable isotope records from the Indian and East Asian Summer Monsoon realms and found that the signatures do not show asynchronous climate during the Holocene which contradict other records (Herzschuh et al. 2010; Wang et al., 2010).

Li et al. (2014) published a very interesting review report about the synchrony or asynchrony of the Holocene climate and compared lake records with various climate simulations. They found some important similarities between the responses of sediment archives to the Indian Summer Monsoon (ISM) and the East Asian summer monsoon (ESAM), which at least indicate synchronous Holocene climate in the monsoon realm of south-east Asia, although climate models show certain differences to each other and cannot clearly display events such as Younger Dryas and the 8.2 ka event (Li et al., 2014; Zhang et al., 2011). With respect to the interplay between the mid-latitude Westerlies and the EASM the authors argue that speleothem records, moisture indices and climate simulations cannot fully explain the asynchronous Holocene climate records along the transitional zone of the current summer monsoon. Notably high lake levels during the climatic optimum at ca. 8 ka in northwestern China do not correlate with data from the classical monsoon area. Hence, they assume that the implication of asynchronous Holocene climate in this region inferred from lake records and climate models do not sufficiently enough consider local surface water conditions (Li et al., 2014; Yan and Wünnemann, 2014). These are effected by water vapor transport in general circulations and hydrologic processes such as impacts of surface runoff, lake evaporation, on-lake precipitation, basin-wide evaporation and to local catchment-lake effects (e.g. permafrost dynamics, mass movements, changes of river course geomorphology and local currents of water system, tectonic impact, and human activity). They altogether interact with different magnitude and amplitude.

However, despite the controversial discussion about the validity of cave records for monsoon rainfall over China, Liu et al. (2014) could show that $\delta^{18}O$ reconstructions for the last 21 ka do represent rainfall intensity of the EASM system, based on the comparison of climate simulations and observational data. Records from the Chinese loess region and modeling results indicate that precipitation increased between 8 and 3 ka BP and are synchronous with high-northern-latitude ice volume/ice cover and atmospheric CO_2, probably driven by CO_2-forced high-northern-latitude temperature

changes (Lu et al., 2013). However, modeling results by Boos and Kuang (2010) confirm the particular importance of the Himalayas as a barrier for monsoonal moisture transport into the interior of the TP and to northern latitudes by hindering the exchange of extra-tropical and tropical air masses. They conclude that the Tibetan Plateau therefore does not necessarily play a major role for monsoon development and strength over Asia.

Chen et al. (2008) postulated on the base of various lake records that the northwestern regions of China may have been much stronger influenced by westerly air masses that may have triggered early Holocene dry conditions there, thus resulting in an 'out-of-phase' mode in comparison to the monsoon domain (see also Wang et al., 2010; Li et al., 2012). Most of the used data however, relied on the qualitative interpretation of millennial-scale changes in lake status. Model simulations for testing the climate impact and effective moisture sources over the arid and semiarid regions of China indicate dry conditions during the early Holocene in that region which seem to be closely related to decreased water vapor advection (Lin et al., 2011).

Interestingly, a lake record from Ximencuo was used to infer Holocene cold events on the eastern Tibetan Plateau in comparison with other records (Mischke and Zhang, 2010). The authors conclude that the short-term cold spells in the Ximencuo record roughly match with other records on the Tibetan Plateau, but by no means with all sites. However, an overall comparison with 20 records mainly from the summer monsoon domain showed that the spatial and temporal mismatches of cold events dominated by far (Mischke and Zhang, 2010), which cannot be only explained by regional climate diversity. The same applied to records from the Tibetan Plateau for the Holocene climatic optimum. This period of ameliorated climatic conditions varied considerably in space and time (Zhang and Mischke, 2009), likely due to uncertain chronologies. Most of the available lake records, however, lack sufficient high resolution for the reconstruction of short-term spells and as such define much longer periods of dry-cold or wet-warm climate conditions (e.g., Mischke and Zhang, 2010; Mischke et al., 2010; Zhu et al., 2010).

Intra-mountain lake basins however, are considered as excellent archives that monitor environmental and climate changes, because they react very sensitive to pulses, affecting the sedimentary and hydrologic budget of the basin. Especially lakes as final recorders of interlinked sedimentary processes on a catchment scale provide important signals for high-resolution reconstruction of present and past climate-driven sediment fluxes and hydrological variations, as long as the lakes persist and the stored sediments are not subjected to erosion. Hence they can be used to infer climate variations through time.

Published records from lakes on the Tibetan Plateau and adjacent areas refer to sediment and geochemical proxies, including stable isotope data from bulk sediments (e.g., Shen et al., 2005;Henderson et al., 2010; Wu et al., 2006, 2009; Zhang and Mischke, 2009; Liu et al., 2007, 2009; Fan et al., 2012; Opitz et al., 2012, 2013; Yan and Wünnemann, 2014; Bird et al., 2014) and mineral composition (Wünnemann et al., 2010), pollen records (e.g., Zhao et al., 2011; Kramer et al., 2010; Xu et al., 2010; Wen et al., 2010;Wischnewski et al., 2011), biomarkers (e.g., Günther et al., 2011;

Aichner et al., 2012; Hou et al., 2016) and other fossil remains such as ostracods (e.g., Mischke et al., 2010; Frenzel et al., 2010; Zhai et al., 2010;Yan and Wuennemann, 2014). Most of these however, are combined records used to infer changes in lake level, salinity, ecological status and vegetation cover within a certain system as a response to changes in effective moisture availability and thus, climate. Most of them are not really able to quantitatively define water depth and lake levels throughout time.

Terrestrial sediments in combination with morphological indicators, such as palaeo-shorelines and/or lakeshore-terraces are commonly applied to estimate a lake level at a certain time, based on dated sequences. Examples for this inferences are Lagkor Tso (Lee et al., 2012), Donggi Cona (Dietze et al., 2010, 2012), Qinghai Lake (Liu et al., 2011, 2015), Paiku Lake (Wünnemann et al., 2015) and Tangra Yumco (Long et al., 2012).

Most of the reported lake level variations and highstands on the Tibetan Plateau based on paleoshoreline studies by ASTER satellite images were attributed to the Holocene period (Liu et al., 2013) of which the highest stands occurred during the early Holocene (An et al., 2012), exerting strong east-west asymmetry on the Tibetan Plateau (Hudson and Quade, 2013). All this data can explain a certain lake stand at a dated time, while potential water volume and hydrological balances can be modeled for longer time scales, if a series of shorelines exists (Krause et al., 2010; Huth et al., 2012).

Due to the different devices applied in the field for shoreline measurements, results can vary considerably. Yan et al. (2017) pointed out that the potentially wrong elevations of OSL-dated paleo-shorelines in Qinghai Lake area (Liu et al., 2011, 2015) are probably related to inaccurate GPS measurements. It would result in wrong lake level estimations without crosschecks including comprehensive catchment information, at least favoring conflicting results with other records.

Commonly, proxy data from lake records refer to a single sediment core, which was achieved from lake centers and/or the deepest part of a lake. According to several studies it is obvious that differences in sediment composition, geochemical properties, fossil remains and limnological setting occur at different lake sites and water depth (e.g., Dearing, 1997; Last, 2002; Mischke et al., 2009; Wünnemann et al., 2012), leading to incomplete interpretations of climate-driven processes if the proxy data refer to only one site. A recently published lake record from Hala Lake (Yan and Wünnemann, 2014) is currently the only record in China that provided continuous high-resolution proxy data of centennial-scale climate-driven changes in water depth that trace far back to about 24 ka BP, based on several sediment cores at different water depth combined with catchment studies. A further high-resolution lake record from Qinghai Lake (An et al., 2012) was used to infer the interplay between the EASM and Westerlies for a similar long time sequence but without taking any catchment processes into consideration. The proxy data were interpreted by changes in aeolian dust flux (so-

called Westerly index) in comparison with a Monsoon index based on other sediment proxies.

The most important aspect for defining spatio-temporal differences in climate-driven responses of lake systems is based on a reliable chronology. Commonly it is achieved by absolute age determinations, such as radiocarbon, using a linear relationship between dated sediment strata. Problems with respect to dating results arise from inherent reservoir errors that affect the sediments by the incorporation of old carbon from various sources or by modern carbon. For example, Qinghai Lake sediments indicate reservoir errors between 400 and 1600 years (Hou et al., 2012; Henderson et al., 2010). In Hala Lake reservoir errors range between 1200 and less than 240 years (Wünnemann et al., 2012; Yan and Wünnemann, 2014). Sediments from Lake Donggi Cona suggest errors between 2000 and 2300 years (Mischke et al., 2010; Opitz et al., 2012; Dietze et al., 2013). Similar errors were calculated for Zigetang Co, central Tibet Plateau (2000 years, Herzschuh et al., 2006), whereas extreme high reservoir errors were reported from Kusai Lake, (3400 years, Liu et al., 2009), Heihai Lake (> 6000 years, Lockot et al., 2015) and Bangong Lake (>6500 years, Fontes et al., 1996). For the latter two cases the incorporation of detrital carbonate from the catchment lead to these high reservoir errors known as hardwater effect (e.g., Fontes et al., 1996).

A carbon reservoir effect however, can vary in space and time and influences the true age of sediment significantly (Henderson et al., 2010; Hou et al., 2012; Mischke et al., 2013). This problem applies to many lake basins in China and thus may be also a reason that climate reconstructions derived from lake records are divers in space and time (Yan and Wünnemann, 2014). The commonly reported asynchronous climate over China as well as reverse climate trends between the atmospheric systems (Hong et al., 2003, 2005; Chen et al., 2008) may be also influenced by these errors in the respective chronologies. In Lake Heihai sediments Lockot et al. (2015) found that there exists a relationship between reservoir error and carbonate (Dolomite) variation throughout the record, enabling a correction of radiocarbon ages against individual reservoir errors through sediment depth.

Other absolute dating methods, such as Optically Stimulated Luminescence (OSL), are increasingly utilized for dating lake and shoreline sediments (Lee et al., 2012; Long et al., 2012, 2014, 2015; Lai et al., 2014) in order to overcome radiocarbon dating uncertainty. Differences between OSL dating results and radiocarbon ages can be much higher than the calculated radiocarbon reservoir error from the same sample. OSL dating results however, depend on the selection of material (Feldspar, Quartz, multi-minerals), bleaching intensity, estimation of water content and the used protocols for age calculation. New approaches by coupling OSL with ^{14}C dating results of dated lake sediments (Long et al., 2014) indicate that a more consistent chronology of lake records can be achieved.

Under- and over-interpretation of proxies would result in different environment reconstructions in lake systems, which require more comprehensive studies by integrating multi-cores, multi-proxies and catchment information (Wünnemann et al., 2010, 2012; Dietze et al., 2012; Yan et al., 2017).

For example, a comparison of lake records from the north-eastern Tibetan Plateau (Lake Kuhai, Lake Koucha) based on pollen and sediment proxies reveal some differences and even opposite trends of climate signals (Mischke et al., 2010; Wischnewski et al., 2011). This has been explained by local in-lake and catchment processes which have influenced the sediment proxies, without provision of details. Conversely, the pollen records are considered to represent true regional climate signals, although the pollen samples were taken from the same material. On the other hand, it can be shown that even pollen records from the same lake can vary considerably between different sites from the same system. For example, Ma et al. (in prep.) reported pollen data from lake-center which differ from those in shallow parts of the lake, similar to ostracods assemblages (Yan and Wünnemann, 2014). Similar differences during the Holocene were also reported from lakes Donggi Cona and Kuhai, based on sediment proxies, ostracod assemblages (Mischke and Zhang, 2010; Mischke et al., 2010) and biomarkers (Aichner et al., 2012), indicating regional and even local diversity, as also assumed for other records in adjacent regions of the Tibetan Plateau (e.g., Holmes et al., 2009; Liu et al., 2009; Zhou et al., 2010). These differences may be partly explained by the increasing impact of westerly-driven air masses. It is therefore of crucial importance that various processes and their interrelationships influence sediment transport, distribution and deposition in a lake and its catchment. They were obviously underestimated in the past.

Henderson et al. (2010) found that stable isotope records in core QING6 from Qinghai Lake cannot be interpreted in a 'classic' way used in published records (Lister et al., 1991; Liu et al., 2007), potentially due to additional influences on the isotopic composition, for example by prolonged ice-cover periods. This assumption was confirmed later by a detailed study on pond/wetland formation in the same area (Yan et al., 2017). Also, Chen et al. (2016) summarized conflicting results on published isotope records from Qinghai Lake and argued that $\delta^{18}O$ based on ostracod shells (Lister et al., 1991; An et al., 2012) may not reflect the strength of the East Asian Summer Monsoon (EASM) or the intensity of monsoon precipitation.

This again raises the question whether stable isotope data from a single lake basin can vary spatially, as indicated by data from Hala Lake. Leng and Marshall (2004) pointed out that a lot of open questions with respect to stable isotope fractionation processes in lake systems exist and may therefore limit the interpretation for climate reconstruction, if no other factors influencing the lake systems are well-considered.

Consistent high-resolution records on centennial-scale water budget changes for longer scales which are able to reasonably elucidate shifts of moisture sources throughout the Late Pleistocene and Holocene are lacking. Thus, intensified investigations related to the interplay of different processes are required to improve the understanding of long-term climate change mechanisms.

3. Study site

3.1 Geomorphological and geological setting

Lake Kuhai (35.3° N; 99.2°E, Fig.1, Fig.4) is a small closed lake basin of 49.12 km^2 in size at 4132 m a.s.l., located about 55 km north-west of the glaciated Anemaqen Mountains (阿尼玛卿山, A'Ni'Ma'Qing, up to 6283 m a.s.l.). Administratively the lake belongs to the Huashixia and Xinghai counties of Qinghai Province.

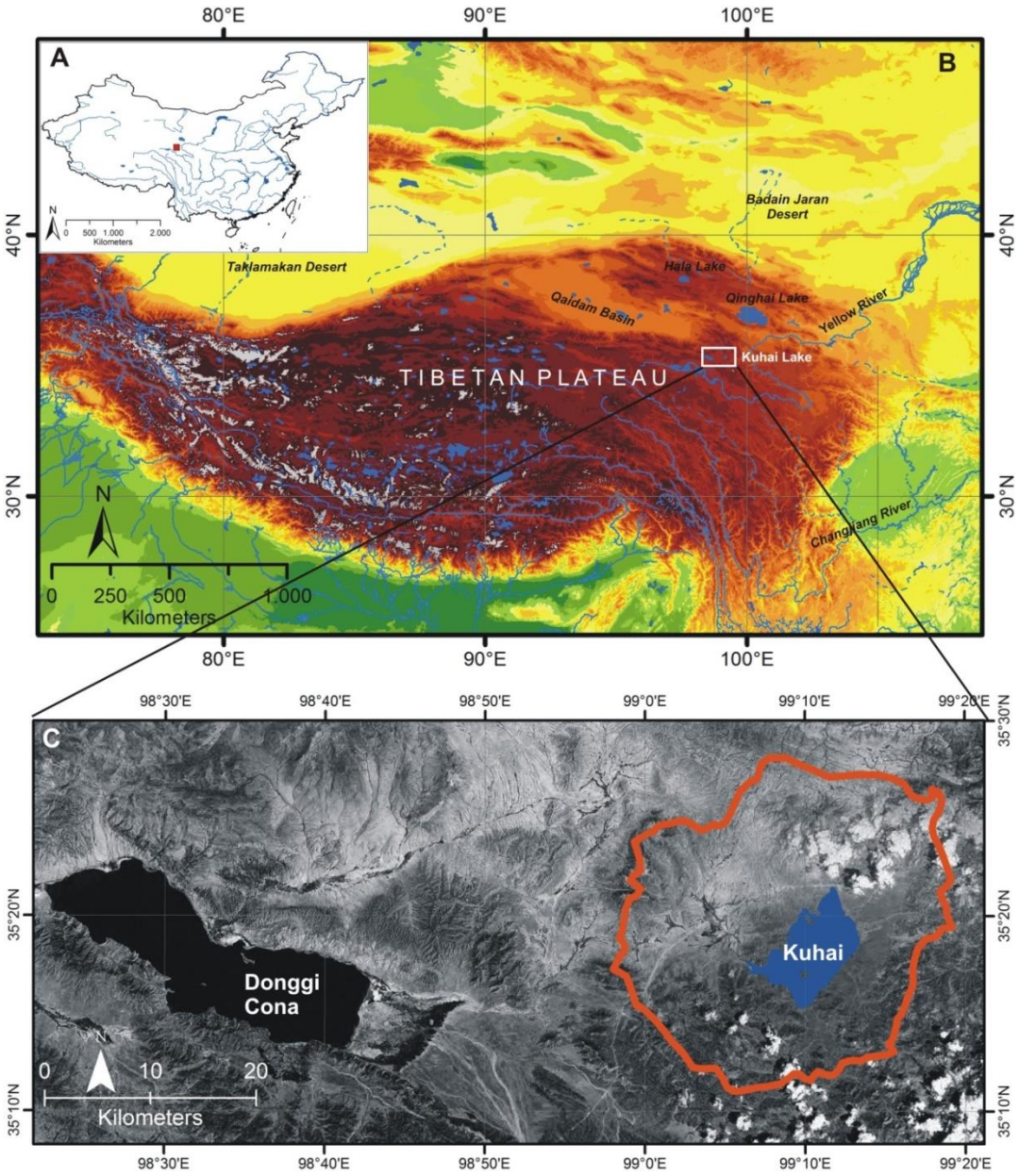

Fig. 1 Overview map of the Tibetan Plateau. **A:** Map of China with location of study site; **B:** Map of the Tibetan Plateau and adjacent regions; **C:** Detail of the study site Kuhai Lake and its catchment, adjacent to Lake Donggi Cona.

The Kuhai basin is surrounded by mountain ranges reaching elevations between 4400 and 4850 m a.s.l., lacking indications of present and former glaciated features. The highest north-south striking mountain range along the eastern border of the basin forms the watershed to the Yellow River. Wide-spread, up to 5 km wide alluvial fans are only located at the eastern, northern and north-western side of the basin (Fig.2 D) hosting several drainage systems which are episodically active during the rainy season, except for one larger system which contributes to the water budget of the lake all year round (Fig.2 A). This perennial river is one of the larger drainages originating in the eastern mountain ridge that deeply incised into the alluvial fans. As a result, a distinct terrace (T1 in Fig.2 A) of >10 m above the modern river bed developed. This terrace declines toward the lake basin reaching 3 m height there and abruptly ends before reaching the modern lake (Fig.2 B). This terrace is composed of coarse gavels overlain by alluvial sediments containing sand and scattered coarse gravels within a fine-grained matrix. A modern brown soil developed on top. V-shaped vertical cracks within the gravel layer, filled with fine-grain alluvial material point to former ice wedge formation (Fig.2 B). A second lower terrace (T2 in Fig.2 A) of 1.2 m height developed due to further incision of the river.

Similar terrace features are developed along an episodically active drainage system few kilometers farther north (Fig.2 D). Adjacent to this drainage a wide-spread area of small dunes, up to 4 m in individual height, cover the alluvial fan there (Fig.2 C), terminate at the steeper slopes of the mountains and merge into aeolian sand ramps. Most of the dunes are fixed by grass vegetation, but display bare parts on the wind-exposed sides (west to north-west) and indicate modern deflation processes and still remobilization.

The alluvial fans between the mountains and the lake form a very flat kilometer-wide are of wetland, passed by the episodically discharging river beds (Fig.2 E).

The western part of the basin in bound by relatively steep slopes of mountain groups without river discharge to the lake (Fig.2 F), except at the south western part, where a sub-basin with widespread wetlands is permanently drained towards Kuhai Lake (second perennial drainage, Fig.2 G). Exposed lake sediments above the modern water level are indications of former higher levels of Kuhai Lake.

A third perennial river with low to medium discharge originates from the south-eastern group of mid-elevation mountains. It occupies a wide-spread valley that is considered to have acted as a former outflow of the lake basin towards the Yellow river (Fig.2 I, K), once the lake level reached 4142 m a.s.l. Currently, the lake has no outflow.

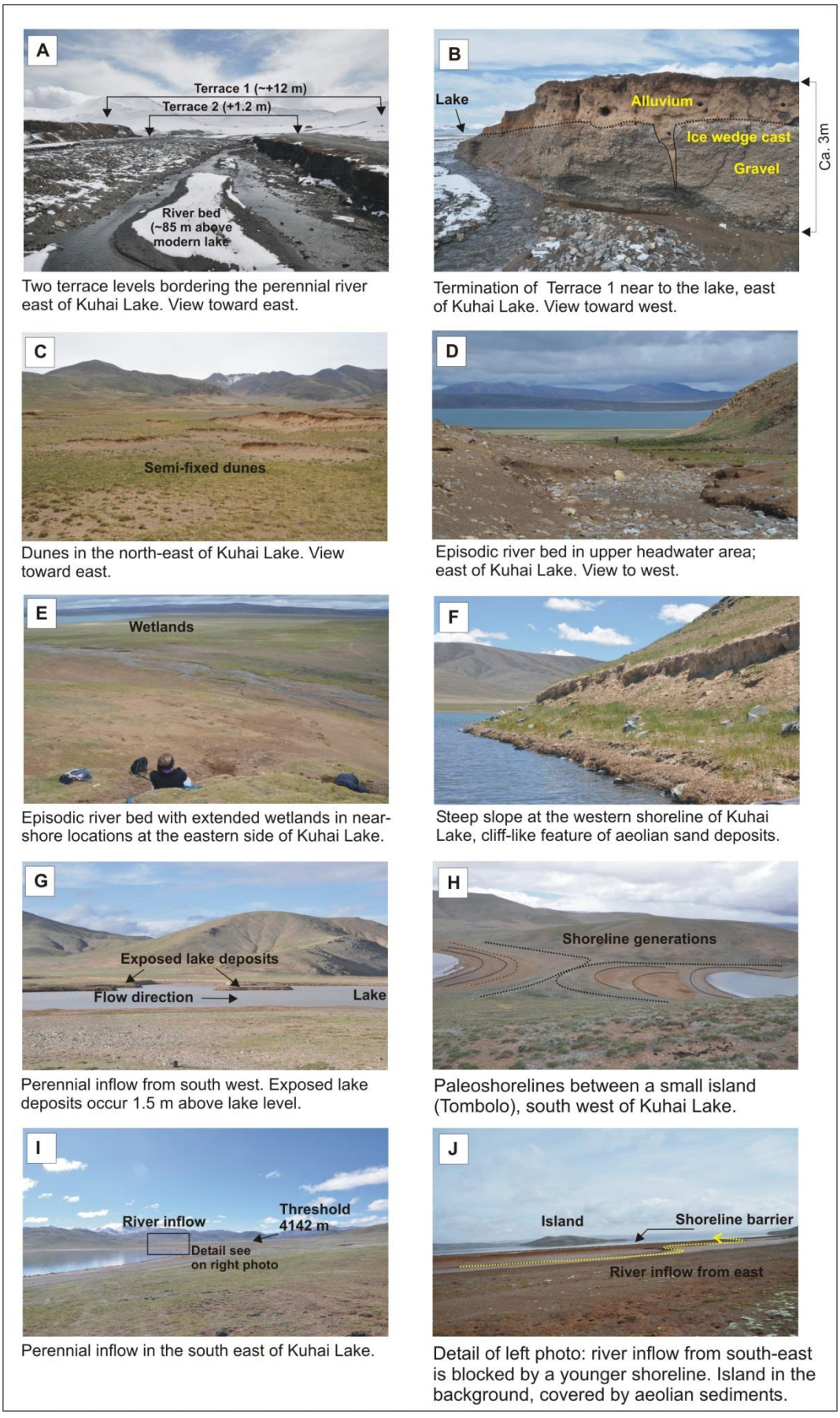

Two terrace levels bordering the perennial river east of Kuhai Lake. View toward east.

Termination of Terrace 1 near to the lake, east of Kuhai Lake. View toward west.

Dunes in the north-east of Kuhai Lake. View toward east.

Episodic river bed in upper headwater area; east of Kuhai Lake. View to west.

Episodic river bed with extended wetlands in near-shore locations at the eastern side of Kuhai Lake.

Steep slope at the western shoreline of Kuhai Lake, cliff-like feature of aeolian sand deposits.

Perennial inflow from south west. Exposed lake deposits occur 1.5 m above lake level.

Paleoshorelines between a small island (Tombolo), south west of Kuhai Lake.

Perennial inflow in the south east of Kuhai Lake.

Detail of left photo: river inflow from south-east is blocked by a younger shoreline. Island in the background, covered by aeolian sediments.

Fig. 2 Selected photos from the catchment of Kuhai Lake.

Three small islands are located on the north-western, southwestern and southern side of the lake. Two smaller ones on the western side of the lake occur as tombolo-like features, currently occurring as peninsulas. Several shoreline generations are visible there. They are comparable with shorelines around the lake. The highest one ca. 8-10 m above the present lake level was the initial shoreline that connected the former island with the surrounding land (Fig.2 H). During this stage of shoreline formation the lake may have reached the threshold of 4142 m a.s.l. in the south eastern valley (Fig.2 I) and may have resulted in an overflow to the Yellow River. However, literature confirming this overflow is lacking.

The largest island, called Cuoshiniang in the southern part of the lake is about 0.73 km^2 in size, reaching heights of up to 85 m (4217 m a.s.l.) above the present lake level. Metamorphic rocks of Paleo-Proterozoic age (Fig.3) there are covered by eolian deposits of up to 3 m in thickness.

The overall catchment comprises an area of 711.8 km^2 and is bordered in the west by the neighboring catchment of the Donggi Cona Lake.

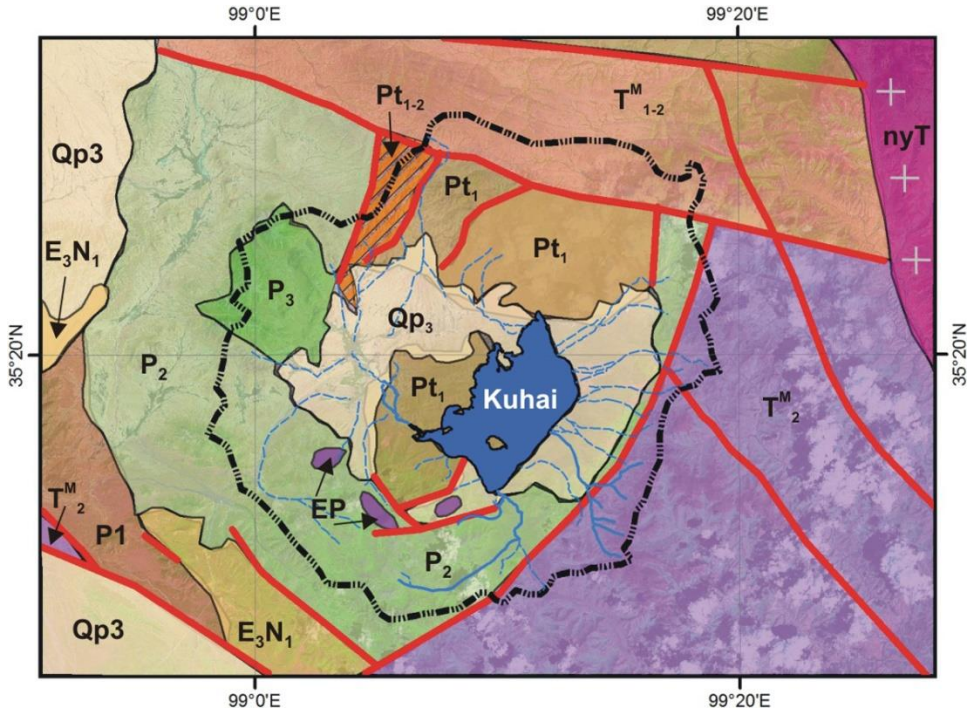

Fig. 3 Geology of Kuhai Lake catchment. **Pt_1/Pt_{1-2}**: Paleo-Proterozoic, shist, gneiss migmatite, amphibolite, marble; **P_1**: Permian, sandstone limestone, basalt; **P_2**: Permian, limestone, siltstone, volc. rocks; **P_3**: Permian, continental clastic rocks, dolostone; **$T^M_{1-2,\ 2}$**: Triassic (marine facies), sandstone, slate, limestone, siliceous rocks, intermediate-acid volc. rocks; **E_3/N_1**: Oligocene/Neogene, sandstone, conglomerate, siltstone, mudstone, **Qp3**:Late Quaternary/Pleistocene; clay, sand, gravel, loess. **EP**: Late Paleozoic ultrabasic rocks; **nyT**: Triassic granite, **Red lines**: major faults. Data source: Geol. Map of Qinghai-Xizang Tibetan Plateau and adjacent areas 1: 1.500000, Chengdu Institute of Geology and Mineral Resources, China Geological Survey, modified.

The geology of the catchment (Fig.3) is mainly composed of Paleo-Proterozoic and Paleozoic (Permian) metamorphic rocks, including shist, gneiss, migmatite, amphibolite, limestone, siltstone and volcanic rocks (Geol. Map of Qinghai-Xizang Tibetan Plateau and adjacent areas 1: 1.500000, Chengdu Institute of Geology and Mineral Resources, China Geological Survey). Late Quaternary (Pleistocene) gravels and sand surround the lake basin in the eastern and western part of the catchment. The eastern and northern mountains at the border of the catchment consist of Triassic formations (marine facies), mainly composed of sand- and limestone. Despite its location farther north the basins seems to be partly influenced by the left-lateral strike-slip Kunlun fault system (Van der Woerd et al., 2002, Fu et al.,2005), which resulted in a pull-apart basin of the Donggi Cona and a push-up structure of the Anemaqen Mts. (Van der Woerd et al., 2002). Several faults in the north, east and south of the catchment indicate this likely relationship. The lake basin itself has a bowl-shaped morphology with a maximum water depth of 22.3 m in the north-central part (Fig.4).

The lake water is saline with an electric conductivity of 19.9-22.8 mS/cm. In August 2002 and March 2003 el. cond. was higher and reached values of 28.6 mS/cm (Mischke et al., 2010b). Its pH is variable and ranged between 7.2 and 8.7, measured in 2015 and 2016. Total dissolved solids (TDS) reached values of up to 20.1 g/l, which accords to a reduced transparency of only 6-7 meters. The lake hosts high amounts of green algae and aquatic plants, such as *Potamogeton* sp., the latter only occurs down to a water depth of 6 m.

Figure 4 shows the locations of all investigated onshore sites including locations of water samples taken from flowing rivers or captured during rain/snowfall events. Investigated sites within the lake basin refer to sediment coring at different sites of which only the sediment cores KH11-14 are used in this study. Beside, surface samples, lake water samples and limnological measurements completed this research. The location of a previous studies (Mischke et al., 2010b, Wischnewski et al., 2011) based on a sediment core from the near-center part of the lake is marked too.

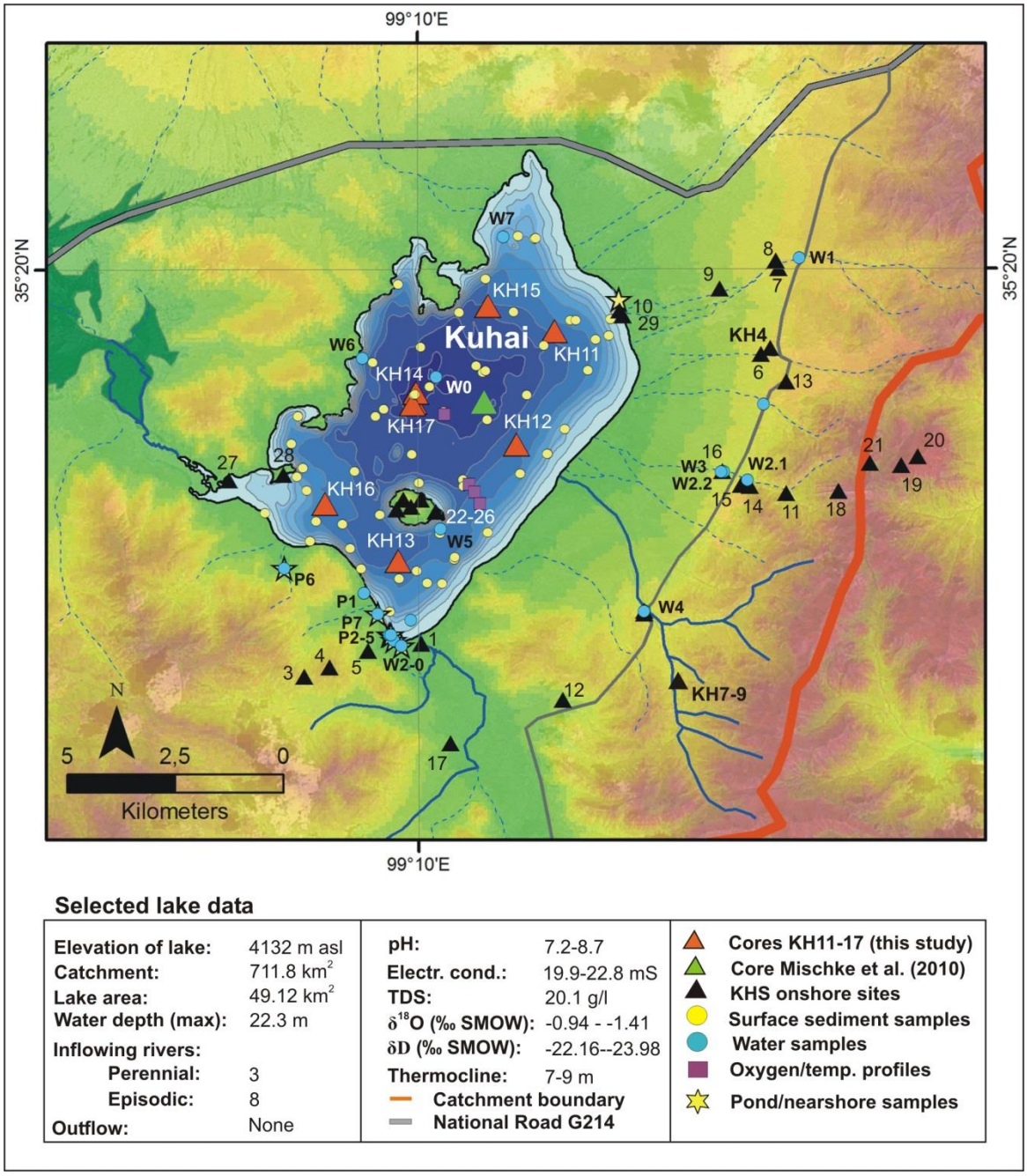

Fig. 4 Kuhai Lake with locations of drilling sites, limnological measurements, water samples, surface sampling, onshore sites and selected lake data. Numbers refer to section sites. Data source: MrSid2000, STRM-3, United States Geological Survey (USGS).

3.2 Climate and vegetation

The lake basin is located in the marginal zone of the East Asian Summer Monsoon (EASM) and Westerlies influence on the north-eastern Tibetan Plateau. Climate information is based on the observation data from the nearest weather station (Maduo county, station code: 56033) with 30 years (1981-2010) records (98.13°E, 34.55°N, 4272.3 m a.s.l., National Metrological Information Center: http://data.cma.gov.cn/data/detail/dataCode/A.0029.0004.html, Fig.5). The mean annual temperature was -3℃. Highest air temperature of 8℃ happened in July (Fig.5 D), while air temperature <0℃ occurred from autumn to early spring (October to April). The annual mean precipitation was calculated to 332.5 mm, of which 59% fell in summer (June-August, Fig.5 A). However, the mean annual evaporation is about 1000 mm (Ling, 1999).

Interestingly, highest amounts of continuous precipitation, even exceeding the long-term mean, occurred frequently in September during the last 30 years with temperatures already below 0°C and thus also apart from the main summer monsoon period (Fig.5 C.1, C2, C3). However, the longest mean continuous precipitative time of up to 19 days happened in June with a total amount of 27.1 mm only, while in July and September the total amount increased to 73.1 mm and 113.2 mm, respectively, within 16 days of continuous precipitation. The time of mean daily temperature <0 ℃ in June to August accounted for less than 10 days.

The prevailing near-surface wind at Maduo station during the last 30 years was north (N) to north-northeast wind (NNE), with mean speeds of 2.3 m/s (in December) to 3.7 m/s (in May) (Fig.5 B).

The modern vegetation in Kuhai catchment area is dominated by taxa of high-alpine meadows mainly as *Kobresia pygmaea* and *Stipa purpurea formingx*, with some alpine shrubs (e.g. *Salix orithrepha*, *Saussurea* spp. and *Dasiphora* (*Potentilla*) *fructicosa*) in the southeast catchment (Hou, 2001; Kürschner et al., 2005). Cattle (yaks, sheep and goats) are currently grazing in the lake catchment, especially along the western and southern sides of the lake.

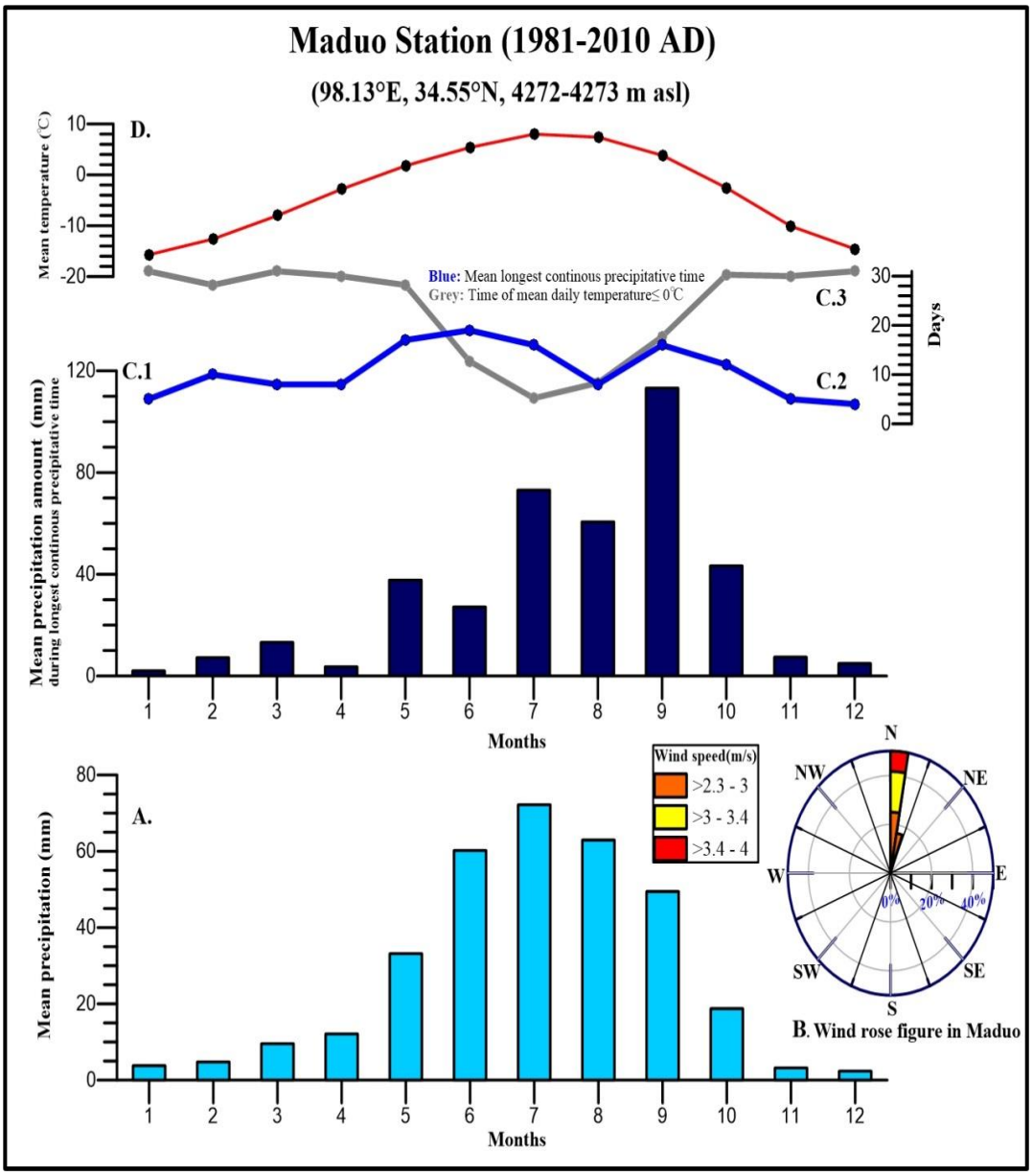

Fig. 5 Climate data from Maduo weather station, NE Tibetan Plateau for the period 1981-2010. A: mean monthly precipitation; B: wind direction and strength; C1: mean precipitation amount; C2: Mean longest continuous precipitation; C3: Time of mean daily temperature below 0°C; D: mean monthly temperature.

4. Methods

Methods of fieldwork and sediment analysis were conducted in close cooperation with the working group of Prof. Wünnemann at Freie Universität Berlin and Nanjing University, related to the topic "Interrelationships between lake and catchment processes on the Tibetan Plateau". This study focused on the Kuhai lake basin and its catchment. Tab.1 shows the contribution of all group members with respect to fieldwork and laboratory analyses. Furthermore, applied statistics were partly used in recent publications (Yan and Wünnemann, 2014; Yan et al., 2017) which can be considered as an integrative part of this study.

Tab. 1 Contributions of group members to field and lab work in Kuhai.

Items	Methods	Surface samples	Pond sampes	Water samples	Section samples	Cores						
						KH 11	KH12	KH13	KH14	KH15	KH16	KH17
Field work	4 times, 2014-2016											
Lab work												
Datings	AMS dating											
	210Pb-137Cs dating											
	OSL dating											
Geochemistry	pH/salinity etc.											
	ICP											
	Stable isotopes											
	XRD											
	XRF											
	LOI											
Sedimentology	Grainsize											
Biomarkers	Ostracods											
	Algea											
Statistics	EMMA											
	Bacon											
	Measured by group			Measured by D.Yan			Measured by M. Neyen					
	Measured by E.Runge			Measured by Y. Hu			Measured by M. Storms					
	Measured by Kiel			Dated by Beta			Measured by NIGLAS					

The flow chart in Fig.6 shows the main steps of procedures how to approach the targets in this study. Based on the Kuhai lake system along the marginal region of Asian Summer Monsoons and Westerlies influence (Fig.1), different types of proxy data from the catchment and lake were obtained and compared (**Data acquisition, Data analysis**) to achieve the objective **High-resolution records**. Lake and catchment data were strongly related to each other and needed to be compared and evaluated to figure out local effects not only by direct identification of catchment processes, but also by comparison of two data sets. They could lead to the separation of local effects from climate-forced changes in order to reconstruct the hydrological balance through time. (**Data analyses, Data interpretation: Objectives Lake-catchment integration and Hydrological balance reconstruction**).

In a further step the results from the lake-catchment needed to be compared with existing data from adjacent lake systems (e.g. Donggi Cona, Qinghai Lake) and also with speleothem records from the monsoon realm to identify climate and non-climate factors before a synoptic approach could lead to the understanding of the mechanisms related to the interplay between the Asian Summer Monsoons and Westerlies along their marginal zone on the north-eastern Tibetan Plateau (**Data interpretation, Objective of Climate inferences**).

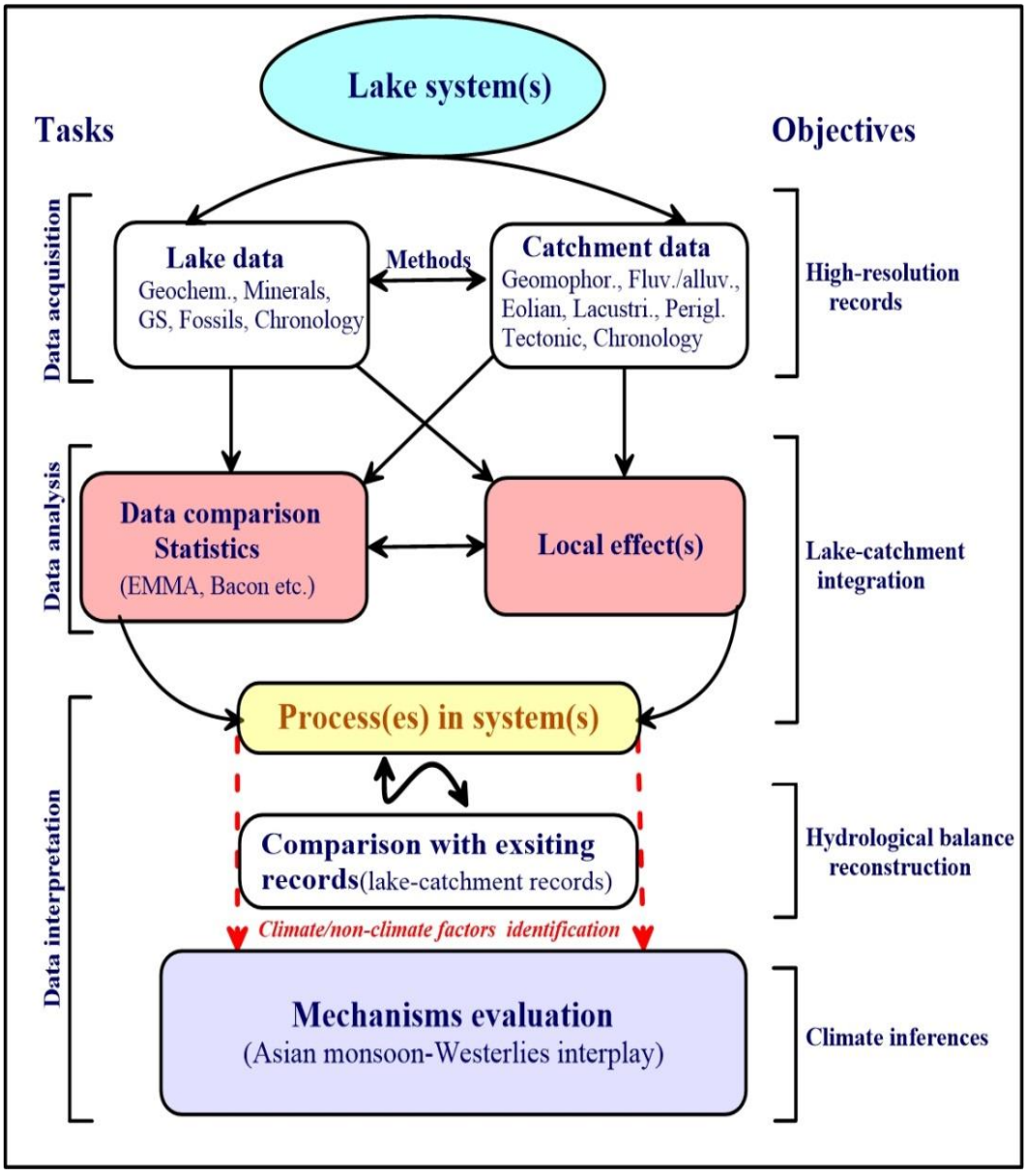

Fig. 6 Flow chart of the research strategy in this study.

4.1 Fieldwork

Fieldwork was carried out during several weeks in early summer in the years 2014 to 2016 comprising investigations on the lake and selected onshore sites within the Kuhai catchment (Fig.4, Appendix I, II). Limnological measurements refer to dissolved oxygen content and water temperature in vertical profiles using a WTW OxCal 197 instrument with a standard electrode on a 60 m long cable, measured in early June 2015 and late June 2016 at different locations (Fig.4). Electrical conductivity, pH and transparency (by Secchi disc) from surface waters around the lake was measured with standard pH/EC handheld devices. Water samples were taken at different locations from the lake water, inflowing rivers and from rain/snow. For the vertical water profile down to 20 m water depth in the center of the lake basin, we used an UWITEC water sampler which provided samples for every meter water depth. All samples were measured for pH, electrical conductivity, TDS, stable oxygen isotopes and deuterium (see appendix II).

Bathymetric measurements along several transects at Lake Kuhai were conducted by a Humminbird Echo sounder, coupled with GPS, comprising more than 6000 individual data points in total. In addition, four shallow sediment sub-bottom profiles by a 3.5 KHz single pulse profiler (GeoPulse, GeoAcoustics, UK) were applied in order to detect sediment structure along selected transects including the location of drill cores. Detailed analyses of sub-bottom profiler results are subject to a further publication elsewhere.

A UWITEC60 short core device was applied for short cores less than 3 m in length for cores KH11, 12, 13 and 14 with individual lengths of up to 275 cm (Fig.4). Cores KH15, 16 and 17 were retrieved from a UWITEC-90 double-A-platform, of which core KH17 was drilled in the center of the lake close to core KH14 as overlapping 2 m long core segments, covering a continuous sediment sequence of 7 m in PVC liners. Differently from previous UWITEC drill technology, this system uses always the same drill hole fixed by a ground plate while the piston opens at a defined depth to enable continuous coring. Possible sediment gaps at the transition from one core to the next can be compensated by overlapping drilling. Here an overlap of one meter was used to enable best possible core splicing. In total, 17 cores with individual lengths between 2.15 and 7 m were retrieved. In this study, only the cores KH11-14 were used for detailed analyses. Water depths at the respective core sites were 13.3 m (KH11), 13.7 m (KH12), 13.7 m (KH13 and 21.7 m (KH14). Cores were cut lengthwise, photographically documented, described and sampled at 1 cm intervals including subsamples for different analyses.

Surface sediments refer to 58 locations within the Kuhai Lake (Fig.4). They were obtained either by an Ekman sediment grab or by UWITEC60 short corer device. In total, 106 samples were taken, comprising the upper 0.5 to 2 cm thick sediment, followed by samples from 2-4 cm and 4-6 cm depth. In this study, only the uppermost samples were used for assigning spatial distribution patterns of selected grain size classes, geochemical elements, minerals and ostracods, deposited in the last 15 years.

Thirty sections from Kuhai catchment area were sampled either from naturally exposed river cuts at near-shore locations and river upstream sites, mainly along the eastern side of the lake or dug by hand. The latter ones comprise sites on the island in the southern part of the lake and on hillslopes and dunes (Fig.4). Sampling of the sections for further analyses (AMS dating, OSL dating, grain size analysis and loss on ignition) followed section stratigraphy and lithology (see Figs.25-37, appendix II).

4.2 Sediment analysis

4.2.1 Datings

4.2.1.1 ^{14}C AMS dating

Dateable material from Kuhai was selected in two steps: First, parallel to the sampling, organic-bearing material was selected from appropriate sequences and sent out for a first chronological overview. In a second step, additional samples were selected on the base of LOI results. Organic material from algae and potential terrestrial plants were picked from the bulk sample, identified and then sent out for dating. Dating at Beta Analytics, Miami, USA, referred to individual plant remains (aquatic plants) bulk organic matter and the alkali soluble (humic) and alkali insoluble (humin) fractions, in order to identify potential contamination by allochthonous carbon.

According to the personal communication with Beta Analytics, the procedures for dating are as follows: Commonly bulk organic matter is dated after sieving the sediment to < 180 microns in order to remove any roots or macrofossils, followed by acid washing to remove carbonates.

Dating the ‘Alkali-Soluble Fraction’, which is commonly referred to as the humic acid fraction follows a similar procedure as before, including treatment with alkali to solubilize the humic acids, which are then precipitated and dated.

Similar procedures are used for the 'Alkali-Insoluble Fraction', which is many times referred to as the humin fraction while the alkali treatment solubilizes the humic acids which are rinsed away for dating the remaining alkali insoluble fraction.

Sediments that are treated with alkali to extract humic acids (and then dated on the humic acid or humin fraction) can sometimes yield problematic results depending on the localized soil geochemistry. Alkali extractions on sediments will remove any un-bound carbon that is alkali soluble. The source of this carbon can be from more recent humic and fulvic acids or ancient labile carbon that is alkali soluble. Many times depending on the clay concentration and if the younger or older humic/fulvic acids are bound to clay particles, the alkali extractions may preferentially remove the original or older labile carbon and leave behind the younger clay bound humic and fulvic acids, or visa-versa. Typically, the acid washed and sieved bulk fraction will yield the most accurate date, or a date somewhat more recent if there are more recent mobilized humic acids present, but at least the error (if any) is always in one direction and not perhaps yielding an age that is too old one time and too recent the next.

With respect to the cores KH11-14 sixteen samples were dated on different fractions and yielded quite different results (Tab.2, Fig.9 A, B, Reimer et al., 2013). As only four from at least seven sediment cores taken from different parts of the lake (see Fig.4) were used in this study, the final chronology of each core had to be adjusted to all cores based on a so-called master chronology of the longest record (KH17). This work was done by B. Wünnemann et al. (in prep.) and will be published elsewhere as comprehensive chronological constraints of the last 14 ka BP. Hence, this study refers to this chronology covering the last 4 ka BP of lake records.

Previous dating results from Kuhai Lake (Mischke et al., 2010b) provided a reservoir-corrected age model based on dating of humic and humin fractions, which is different from the dating results presented in this study. Here, individual age models for every core were used and compared with the core lithology and inferred sediment accumulation rates. As a result, the age-depth relation is most likely a non-linear function with different reservoir errors on different dating methods and at different locations from the same lake system. Previous reports from Hala Lake (Wünnemann et al., 2012; Yan and Wünnemann, 2014) and Qinghai Lake (Henderson et al., 2010) as well as from multiple sites (Hou et al., 2012; Mischke et al., 2013) already reported various reservoir errors in lake systems, which affected the chronology accordingly. Consequently, nearly 51 samples from Kuhai and its catchment were applied for establishing the chronological framework of lake development and catchment dynamics.

4.2.1.2 ^{210}Pb/^{137}Cs dating

^{210}Pb/^{137}Cs dating is frequently used for the upper 10-20 cm sediment in cores to trace records back to the last ca. 100 - 200 years (Henderson et al., 2010； Zhang et al., 2005). The ^{137}Cs signal with highest peaks is commonly assigned to highest ^{137}Cs emissions related to atomic bomb tests in the 1960th or to the nuclear catastrophe of Chernobyl in 1986. According to the available literature, highest ^{137}Cs values commonly refer to the year 1963 AD (Henderson et al., 2010). Meanwhile, the first zero-value was considered to represent the earliest age without ^{137}Cs nuclear influence, commonly assigned to the years 1950 AD, 1952 AD or 1953 AD, depending on references and investigated regions. Once all years are assigned, different sediment accumulation rates (SAR) can be calculated within dated samples (in general 10-15 cm maximum). However, there are samples with weak or even no ^{137}Cs signal in lakes of the Tibetan Plateau (e.g. Qinghai Lake, Daotanghe Pond, Yan et al., 2017) Furthermore, increased ^{137}Cs values related to the Chernobyl fallout were not traced in this study.

^{210}Pb results can be used to calculate average SAR of dated samples after logarithmic fitting [Y=a*ln(x)+b, of which, Y is the depth, x is ^{210}Pbex values at each depth, SAR=|a|*λ, λ=0.0311] with precondition that sediment accumulation is continuous. The sediment density and variable water content as well however, are not considered in this calculation. Additionally, sediment components affect dating results too. The finer (e.g. clay, silt) the material, the better signals could be traced, which would in turn mean that coarse grain size may not preserve appropriate signals (Pers. comm. Dr. Xia Weilan, Nanjing Institute of Geography and Limnology, Chinese Academy of Sciences).

In this study, ^{210}Pb/^{137}Cs dating was performed on core KH 13 with a resolution of 1 cm for the upper 25 cm sediment sequences. The results are shown in Fig.11.

4.2.1.3 Optical stimulated luminescence (OSL) dating

A total of 25 samples from sections containing aeolian deposits in Kuhai catchment were dated with OSL method in two luminescence dating laboratories (Nanjing Institute of Geography and Limnology, Chinese Academy of Sciences and Nanjing University). Owing to low luminescence intensity of quartz in these sediments, the K-feldspar fractions were selected for dating. Sample preparation followed the methods provided by Long et al. (2014). Under the subdued red light, the daylight-exposed outer part of the samples was scraped off for dose rate measurement. The remaining materials (non light-exposed) was used for equivalent dose (D_e) measurement. For D_e determination coarse grain (CG) fraction (150-200 μm) was extracted by wet sieving, and then treated

with 30% H_2O_2 and 10% HCl, respectively to remove organic materials and carbonates, followed by heavy liquid density separation with sodium poly-tungstate to separate the K-rich feldspar (<2.58 g/cm^3). The obtained K-rich feldspar was not treated with HF since HF etching on feldspar tends to cause deep pitting rather than removing a uniform shell from the grains (Duller, 1994).

D_e measurements were performed on the automated luminescence reader Risø TL/OSL-20, equipped with a $^{90}Sr/^{90}Y$ beta source. For K-feldspar luminescence measurement, infrared (IR) LEDs (870 nm) were used, and the IR-stimulated luminescence (IRSL) signal of K-feldspar minerals was detected through a combination of Schott BG-39 and BG-3 filters in the blue light spectrum between 320 and 450 nm. Using single aliquot regenerative-dose (SAR) protocol, the IRSL signal observed at 150^o C following a prior IR stimulation at 50^o C (i.e., post-IR IRSL signal, abbreviated pIRIR150) (Madsen et al., 2011; Reimann et al., 2011; Long et al., 2015) was used for D_e measurement of K-feldspar (Tab.3, Fig.12). For each sample 8-12 discs were measured for D_e calculation. The scraped material was first dried for the calculation of in-situ water content (WC) and then homogenized to determine dose rate. The concentration of radioactive nuclides (U, Th and K) in all samples was measured by neutron activation analysis (NAA) in the China Institute of Atomic Energy (Beijing) and inductively coupled plasma mass spectrometry (ICP-MS) in Chang'an University (Xi'an). All dose rate calculations (for alpha dose rate, external dose rate, internal dose rate, and cosmic dose rate) follow a detailed description according to Long et al. (2014) and references therein. However, G-values and fading results were not provided.

4.2.2 Loss On Ignition (LOI)

Loss On Ignition was used to determine organic matter (OM) and carbonate content. Totally 1224 samples from cores KH11-KH14 including onshore sections were dried and powdered. Burning in an oven at 550°C for three hours provided the percent content of OM by weight loss on the base of individual bulk samples. The same samples were burned again at a temperature of 880-900°C for three hours to enable the release of carbonate-bound carbon dioxide (CO_2), converted to the amount of carbonate (CO_3) by stoichiometry (Dean, 1974).

LOI measurements are a suitable and relatively fast method to determine the quantity of total organic carbon (TOC) fixed in organic matter (Heiri et al., 2001). Parallel measurements of TOC on samples from lake deposits (Wünnemann et al., 2010, 2012)

reveal comparable trends in records, although the amount of TOC in OM from lake sediments of the Tibetan Plateau can vary considerably.

Quantitative analyses of carbonates by LOI also show high correlation with Ca counts measured by X-ray Fluorescence (XRF), as long as the major carbonates are related to Ca-bearing minerals (Wünnemann et al., 2010).

4.2.3 X-ray fluorescence (XRF) analysis

XRF analysis was performed with 2 mm resolution on a GeoTek multi-sensor core logger (run with 20 and 40 kV, 2 mA, 15 s count time) at Nanjing Normal University. Parts of the cores were also measured by an Avaatech XRF core scanner with line-scan camera for RGB color and multiple elements (run with 10, 30, 50 kV, 2 mA, 15 s count time) at Yunnan Normal University. The former one can provide multi-proxies including laser profile, magnetic susceptibility, Munsell color and multiple elements within a single scan, while operating power limits (20 and 40 kV) are restricted to less elements, compared with Avaatech core scanner. The latter equipment can detect more elements due to a wider power range but parallel scans as in the former instrument are not available.

Cleaned cores with a very flat scan surface were necessary for the sensor to provide reliable data. In some cores from Kuhai Lake, the upper sediment sequences were too soft for the sensor to detect reliable signals due to high water content. XRF results were excluded from this study and will be presented separately.

4.2.4 Inductively coupled plasma optical emission spectrometry (ICP-OES) analysis

In this study, 106 surface samples were treated by HCl-digestion for ICP-OES analysis. Ca. 0.2 g of the dry sample (dried at 105°C for 12 hrs) was filled into a 100 ml glass flask. 5 ml 1nHCl was added and shaked for 3 hrs. The solution was filled with bi-distilled aqua dest. up to the 100 ml calibration mark. The flask was shaken again before filtering into a 100 ml polyethylen (PE) flask. The HCl-solution was measured shortly after the solution was produced. Samples were analyzed for major elements (Ca, Fe, K, Mg, Mn, Na, P, S, and Sr) using an inductively coupled plasma optical emission spectrometer (ICP-OES Perkin Elmer Optima 2100DV). As a data quality control $CaCO_3$ in different concentrations (100 %; 34 % and 7 %) and Gypsum ($CaSO_4 \cdot 2H_2O$) were measured for Ca. The relative standard is ± 5 %. Retrieved quantitative values of the traced elements rely on grain size distribution of the original material. In general, fine grain size components (<63 µm) provide higher concentrations of elements than coarser ones (pers. comm. Philipp Holzmann, Freie Universität Berlin) due to higher adsorption capacity of

finer components and, in turn, dilution effects by coarser grains. This aspect has to be considered when interpreting results from different locations within one lake system (this study).

4.2.5 Stable isotope analysis

Stable oxygen and carbon isotopes on 599 bulk sediments, and selected ostracod shells from surface samples and cores were measured at Leibniz Laboratory for Radiometric Dating and Isotope Research, Kiel, Germany. Standard deviations for each sample were less than 0.04‰. Samples containing High-Mg-Calcite, Monohydrocalcite (MHC, $CaCO_3 \cdot H_2O$) and Dolomite were measured with different reaction times, according to the solubility of the respective carbonates.

Fifty-seven water samples (including rain, river water and lake water) were measured four times on a Flash HT-Thermo MAT 253 isotope ratio mass spectrometer after filtering with a 0.2 µm membrane filter. Twenty-five water samples (standard deviations of each samples ranged between 0.02‰-0.21‰) were measured in the Organic/Stable Isotope Geochemistry Lab. affiliated to State Key Laboratory for Mineral Deposits at Nanjing University. Thirty-four samples were measured at Nanjing Institute of Geography and Limnology, Chinese Academy of Sciences, with standard deviations of less than 0.12‰.

4.2.6 X-ray diffraction (XRD) analysis

X-ray diffraction is a commonly used technique to identify minerals in sediments based on powdered samples. In total 477 samples from cores KH11-14 and surface samples were dried at 60°C for minimum 24 hours and afterwards ground using a Fritsch Pulverisette 6 Mono Mill for 5 minutes at Nanjing University. X-ray diffraction (XRD) analysis was performed at Freie Universität Berlin using a Rigaku Miniflex 600 (copper kα radiation, 40 kV, 15 mA, °Theta 3-60). Minerals were identified by X'pert Highscore software, using Pdf2 mineral database. Once minerals were identified by individual cross-checks of several available reference cards, the same references were applied to all samples of each dataset (KH11-KH14 and surface samples) to enable comparability between the records.

In general, XRD analysis is a semi-quantitative measure with respect to the mineral composition of each sample. There are three different methods to semi-quantitatively estimate the percentage of each mineral component, provided by the software: i) the Relative Intensity Ratio (RIR) automatically provided percentages of identified minerals, if the used mineral reference provides a so-called RIR value. A disadvantage is that RIR

values only can be provided for minerals which are in the pattern list; hence reducing the reference cards considerably; ii) the Area Value (AV), which calculates the space of an identified mineral below its primary reflex, taking neighboring mineral reflexes into account. Unfortunately, not all identifiable minerals are stored in the reference database. Hence, area calculation is not possible for those minerals which are not presented by a reference. This applies to High-Mg-Calcite, for example; iii) the intensity of primary (100%) peaks in terms of counts per second (cps), while the total cps of all identified minerals account for 100%. All three methods provide different results by overestimating mineral abundances such as Amphibole, Chlorite, Kaolinite, Aragonite and Gypsum (RIR method), underestimating carbonate facies, such as Monohydrocalcite (MHC), Mg-Calcite, Aragonite and Dolomite (AV method) and in general overestimating clay minerals (CM) and MHC, while underestimating Pyrite, Halite and Feldspars (cps-method).

In this study, the cps-method was selected as the most appropriate semi-quantitative method for direct comparison between the records. This method has been successfully demonstrated by Wünnemann et al. (2010, 2012).

In this study, all minerals in samples were identified, but only clay minerals, carbonate minerals (e.g. Calcite, MHC, High-Mg-Calcite, Dolomite and Aragonite), Gypsum and Feldspars were presented for discussion.

4.2.7 Grain size analysis

Grain size analysis was performed on 851 samples from the cores KH11-14, surface samples and sections, following the procedures according to ISO Norm 14688-1 (2011).

For the core samples, mainly composed of fine-grained sediment, ca. 1 g dried material was used for pretreatment with 10% HCl to remove carbonate. Afterwards the samples were washed with aqua dest. until neutral pH. Due to relatively high content of aquatic plants in the core samples, larger plant remains were picked out before adding H_2O_2 for the removal of organic matter. Depending on the organic content, this procedures lasted for several days. HCl treatment before adding H_2O_2 enabled a shortening of the reaction time for organic matter removal because plants were not fixed with carbonate anymore. After several times washing, $Na_4P_2O_7$ was added to the sample for dispersion.

Grain size distributions between 0.02 and 2000 μm were determined, using a Malvern Mastersizer 2000 Analyzer at Nanjing University, China. All samples were measured three times and the mean value was used for further data analyses. All resulting data was based

on the Mie theory which is commonly used for fine-grained particles to ensure a better performance than by Fraunhofer approximation. The division of grain size classes was based on the international scale (modified Wentworth classes, Doeglas, 1968) which set the boundary between clay and fine silt at 2µm.

4.2.8 Ostracod analysis

Following Yan and Wünnemann (2014), ostracod analysis on surface samples and cores were performed with support of PD Dr. Peter Frenzel, Friedrich-Schiller-Universität Jena.

1550 samples from cores KH11-14, including all 106 surface samples and selected samples from the onshore sites were used for ostracod identification.

About 3 g of sediment was treated according to Mischke et al. (2003), using ca. 5% H_2O_2. Dispersed samples were wet-sieved using 125 µm and 250 µm meshes. Ostracod species identification and counting under a stereoscopic microscope was performed with reference to Meisch (2000), Griffiths and Holmes (2000) and Yan and Wünnemann (2014). Samples containing less than 200 valves were completely counted. Larger amounts were calculated from splits of the sieve residues.

Relative abundance in percentage of each species is presented in this study (see Fig.21 A, B). A transform function was not applied due to low variety of ostracod species. Log-transformed sum of ostracods [ln (x+1)] was provided in this study because relative abundances overprinted the differences between samples with huge amounts and low ones. References to ostracod habitats, especially those from the Tibetan Plateau are restricted due to the limited knowledge of some species about ecological conditions based on living specimen (Akita et al., 2016) and identifications of some species in existing publications in this region are doubtful (Li et al., 2010; Mischke et al., 2010; Yan et al., 2017) .

Twenty shells from different species were selected for scanning electron microscopy (SEM) at Freie Universität Berlin and Friedrich-Schiller-University, Jena. Respective plates and description of main documented species are presented in Fig.16 and appendix II 4.

4.3 Statistics

4.3.1 Bacon modelling

Bacon (Blaauw and Christen, 2011) is an approach to age-depth modelling based on Bayesian statistics to reconstruct Bayesian accumulation histories for deposits, combining radiocarbon and other dates with prior information within 95% confidence intervals. Final results of Bacon age-depth model are calculated according to the 'best' model based on the weighted mean age for each depth (Blaauw and Christen, 2011, appendix II), which can be different from the calibrated dated ages. However, the Bacon software is implemented in 'R', based on programming within a console. Hence, there is no graphical user interface. Bacon is based on Bayesian statistics which means, in a mathematical point of view, the age models which analysts obtain, might be correct but sometimes there are some 'errors', for example with respect to grain size variations, which make no sense from a sedimentological point of view. In such cases, the software does not consider ages, which are 'too young' or 'too old' (pers. comm. Dr. Thomas Kasper, Institute of Geography at Friedrich-Schiller-University Jena) so that such ages ('too old' or 'too young') should be excluded before running the program. This applies to clearly identified outliers within age-depth-relations, for example. Otherwise, the calculation is negatively affected. Reservoir error corrections need to be provided by users before running this software. Changes in parameter settings (e.g., hiatus and resolution) can result in age calculations, which are different from a mean sediment accumulation rate (SAR), not considered in calculation procedures by Bacon and thus may require separated runs. However, spatio-temporal changes of sediment accumulations during some sediment depths without dated ages might be overprinted, if only the software-supported mean SAR of the whole core is applied, although this kind of abrupt change in sedimentology is meaningful and thus cannot be excluded from age-depth models. As the Bacon model does not provide sequential changes, corrections on the original data considering grain size, water content and compaction effect need to be done prior to the model run. The relatively high number of different ages obtained from AMS dating results in combination with grain size variations and respective SAR made it possible to define the likely radiocarbon ages for each Bacon-based age-depth model.

4.3.2 End-member modelling (EMMA)

Dietze et al. (2012) modified the endmember modelling analysis with a basic concept of eigenspace analysis based on grain size data sets, which was applied for the interpretation of sedimentological processes (Dietze et al., 2012, Wang et al., 2015, Ijmker et al., 2012). In this study, EMMA was applied to all KH sediment cores and to selected onshore sections.

However, the precondition of applying EMMA is that each process assigned to EM interpretation identified in a certain system should be unique and independent. These conditions however, are very rare in fact. For example, grain size compositions of aeolian and suspended load sediments may possess similar distribution modes, hence sometimes hard to distinguish. As a result, multi-modes of grain-size distribution curves presented in endmember curves may include several processes, which need to be individually considered for a more convincing interpretation with respect to inherent processes (Yan et al., 2017 and this study). Currently, the used EMMA algorithm is limited in this respect.

Due to measurement limitations, obtained grain size data with classes of <2 µm and/or >500 µm are out of or close to laser detecting range and thus may require elimination of those grains size values including re-calculation of percentages of each class to avoid overestimation and/or over-interpretation of too fine and/or too coarse parts by statistics. Interpretations of end-members are not universal and thus equally applicable to all systems. Hence, endmember results are here interpreted in the context of lake-catchment relationships as a necessary pre-requisite (Dietze et al., 2012; Wang et al., 2015; Yan et al., 2017).

In this study, sediment with similarities in grain size composition induced by different processes (e.g. sheet flood, aeolian, soil wasting and other reworking processes) cannot be fully unmixed, may cast doubts on the interpretation of end-member curves as a single process, for example as aeolian processes in Kuhai area.

4.4 Data processing and presentation

Within this study, different softwares were applied to manage data processing and presentation.

For the overview figures including processing of the bathymetry map of Kuhai Lake, ArcGis10 software was applied. Spatial distribution patterns of proxy data from surface samples were achieved by Topo-to-Raster and Inverse Distance Weighted (IDW) interpolation procedures in ArcGiS10. Most of the individual graphs presented here refer to Graphers 10 software. Statistical approach for endmember analyses was performed by Matlab software. As already mentioned, mineral identification was based on X'pert software and the age models were run with Bacon in R (Blaauw and Christen, 2011).

5. Results

5.1 Limnological parameters: water temperature and dissolved oxygen

Water temperature and dissolved oxygen content were measured in vertical profiles at several locations within Kuhai Lake. According to Fig.7, the surface temperature in early June 2015 reached 9-10°C in the lake center (Fig. 4), remained constant until 6 m water depth and declined afterwards to a temperature of 0.8°C from 16 m water depth down to the bottom. The thermocline, expressed as a sudden drop in temperature of about 4°C was well developed between 6.5 and 8 m water depth. End of June 2016 the surface water temperature reached 13°C, dropped to 12°C one meter deeper and remained almost constant until 6 m water depth, declined slightly afterwards to 6°C until 13 m water depth, followed by a sharper decline towards 2.6°C at 16 m depth and remained constant until the lake bottom. The thermocline end of June 2016 was weaker than at the beginning of June 2015.

Dissolved oxygen developed similar during the two measure periods in 2015 and 2016. The upper 6 m water column displayed constantly high values close to 100% and declined afterwards, reaching 30% at the lake bottom.

Higher values above 100% were only recorded between 7 and 9 m water depth in June 2015. Electric conductivity, total dissolved solids and pH were measured at several sites on the lake and reached values in 2016 between 19.9 and 22.8 mS (el. cond.), 20.1g/l (TDS, mean) and 7.2-8.7 (pH).

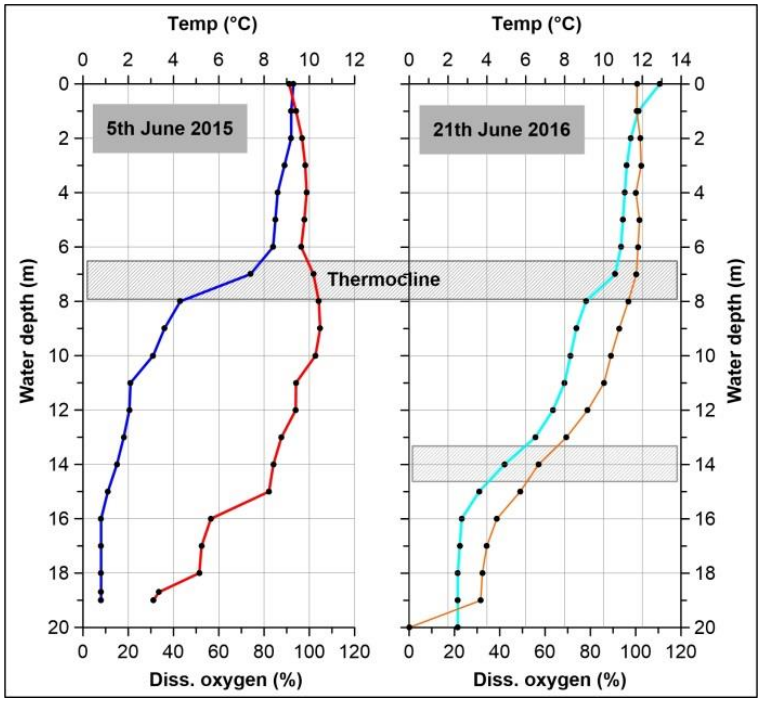

Fig. 7 Water temperature and dissolved oxygen in Kuhai Lake, measured on 5th June 2015 and 21th June 2016 in the center part of the lake.

5.2 Lithology of sediment cores and chronological framework

5.2.1 Lithology of cores KH11-KH14

The lithology of cores KH11-14 is composed of fine-grained mud with dominance of silt-sized particles (Fig.9 A, B). The upper 8-10 cm sediment in all cores displayed layered clayey silt, partly with intermittent thin silty-sandy layers. The brownish colour indicates the presence of well-ventilated (oxygenized) bottom sediments at all respective water depth. Down-core, massive algae (green algae, not specifically identified) formed a thick felt layer until about 18 cm sediment depth (in core KH14 only until 15 cm depth, see Fig.8), followed by dark-grey (light brown in colour after oxidized exposed surface) laminated clay-silt to silty sequences with differences in layer thickness and sediment composition among the cores. Pure sand or gravels were not found in all cores.

KH11 in the north-east of the lake displayed clayey mud with weak lamination from 43-85 cm depth. Silty mud with intercalated thin sandy layers followed until 140 cm depth. From 140 to 190 cm depth silt and clayey silt layers followed, partly weakly laminated. The bottom sediment from190 cm down to the bottom was composed of laminated silty-sandy mud.

KH12 farther south of KH11 in the eastern part of the lake close to the inflow region of the perennial river showed a more uniform sediment composition, mainly of laminated clayey to silty mud until 195 cm sediment depth, followed by strong variations in sediment composition down-core from carbonate-rich clayey silt to organic-rich silty-sandy mud. This sequence included plenty of plant remains in individual layers, consisting of algae and seagrass (e.g., *Potamogeton* sp.).

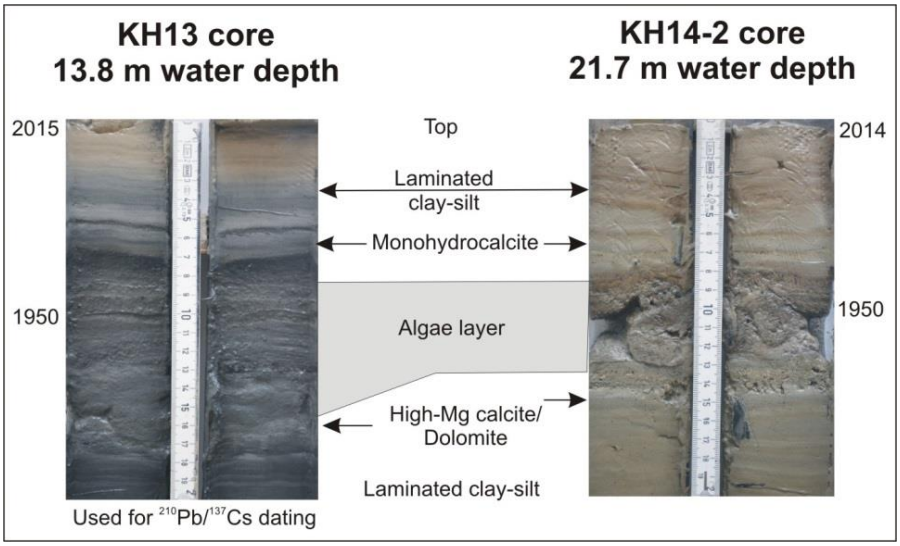

Fig. 8 Details of the top 20 cm of cores KH13 and KH14, showing similar sediment pattern.

KH13 in the south-east of the lake displayed organic-rich laminated clayey-silty mud with higher amounts of green algae until 60 cm depth. Laminated silty clay followed until 95 cm depth. From 95-133 cm depth organic-rich silty mud with thin sand layers with a distinct carbonate layer at 120 cm depth was recorded. Down-core until 200 cm depth, weakly layered clayey silt with intercalated carbonate bands were observed, followed by a nearly 10 cm thick layer of carbonate and plant-rich sandy silt from 210-219 cm core depth.

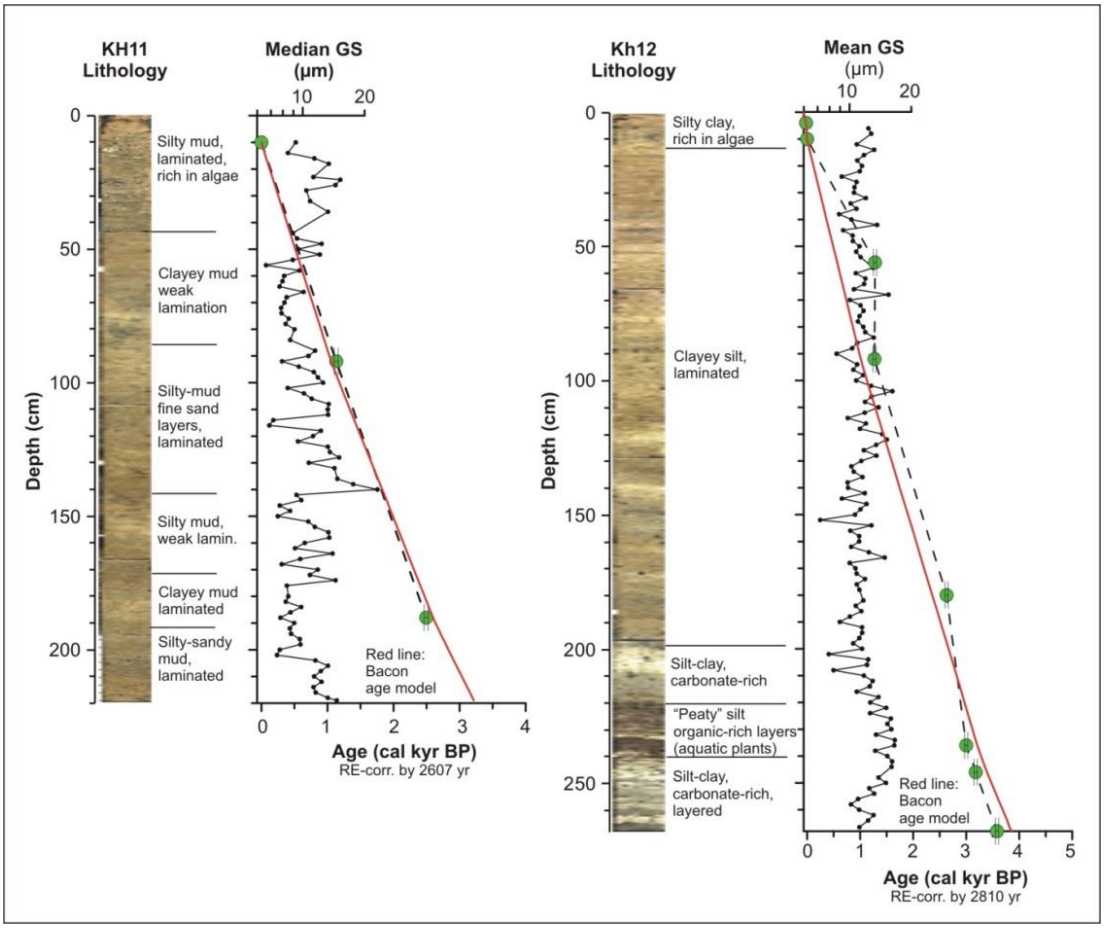

Fig. 9 A Lithology, median/mean grain size and age-depth models of cores KH11 and KH12. Green dots mark the original ^{14}C ages (bulk OM), corrected by RE; red lines show the respective Bacon age model.

KH14 in the center of the lake displayed the highest variety of visually recognizable sediment alternations from laminated clayey silt to sandy-silty mud, intercalated with thin carbonate layers until about 220 cm core depth. Down-core until 268 cm depth, finely laminated clay, silt, sandy-silt layers, carbonate bands and plenty of plant remains in individual layers occurred in between. Fig.10 shows this part of the core KH14 in comparison to core KH17 which was retrieved from the same site and thus displayed comparable lithologies. Thickness of the laminae varied, interrupted by cm-thick uniform layers mainly composed of clay and/or carbonates. The latter were identified as High-Mg calcite and Dolomite or Monohydrocalcite (see chapter 5.3.3).

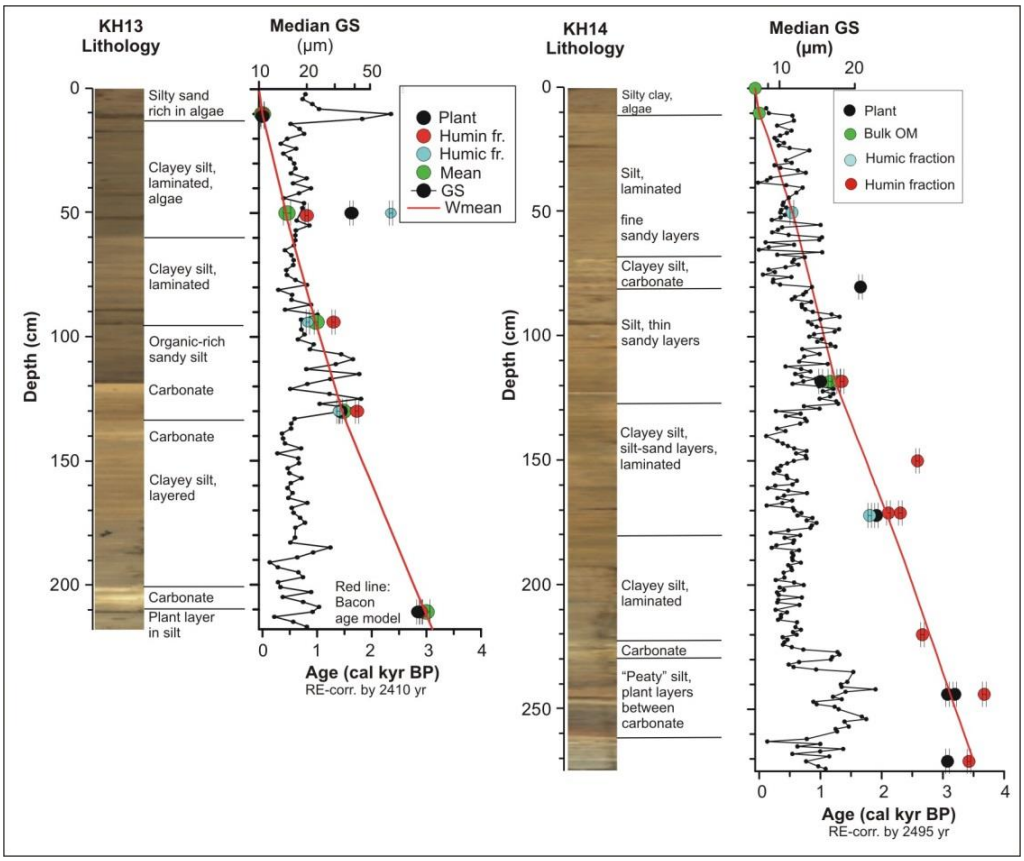

Fig. 9 B Lithology, median grain size and age-depth models of cores KH13 and KH14. Coloured dots mark the original ^{14}C ages, corrected by RE; red lines show the respective Bacon age model.

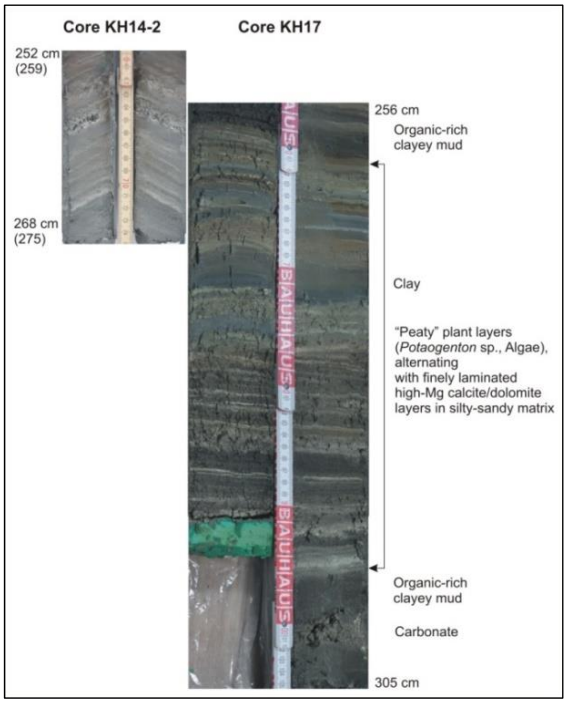

Fig. 10 Detail of cores KH14-2 and 17 between 256 and 305 cm depth. Left and right core halves show optimal matching between overlapping core sequences of KH17. KH14 (left photo) had a similar pattern but ended at 268 cm depth.

5.2.2 Chronological framework of cores KH11-KH14 and sections

The chronological framework of this study is based on three different absolute dating methods, which are commonly applied for dating organic-bearing sediments and carbonates from fossil remains as well (e.g., An et al., 2012; Hou et al., 2012; Yan et al., 2017). Aeolian sediments however, are commonly lacking dateable organic matter but are prone to optically stimulated luminescence dating methods (e.g., Lehmkuhl et al., 2000; Yu and Lai, 2012; Long et al., 2014; Stauch, 2015).

Due to the relatively high dating uncertainty of lacustrine sediments from lakes on the Tibetan Plateau and adjacent areas which frequently yield high reservoir errors (Zhang et al., 2005; Wu et al., 2009; Hou et al., 2012, Mischke et al., 2013), dating by $^{210}Pb/^{137}Cs$ method is increasingly applied in order to estimate the sedimentation rate and timing of the uppermost sediments in sections and lake records by preserved ^{137}Cs radioactive isotopes in sediments, resulting from nuclear tests (Wu et al, 1998; Wang et al., 2011; Liu. et al., 2009, Henderson et al., 2010; Yan et al., 2017). Apart from dating living plant material and other organisms in lakes as a base for defining a potential reservoir effect in lacustrine records, radionuclide dating ($^{210}Pb/^{137}Cs$) can provide a reasonable calculation of sedimentation rates (Beniot and Rozan, 2001) and thus a continuous and reliable age model for the upper 15 to 25 cm sediment sequence from the time of sampling until the onset of nuclear tests at around 1950 AD. Based on this chronology, radiocarbon ages from down-core sequences can be reservoir-corrected and partly adjusted to a longer age-depth model. In this study, the upper 25 cm of sediment core KH13 was dated by this method enabling the inference of likely reservoir errors through sediment depth. The entire chronology used in this study is based on calculations and detailed descriptions by Wünnemann et al. (in prep.).

5.2.2.1 $^{210}Pb/^{137}Cs$ dating results

KH13 sediment core was retrieved in 2015 which indicates that the topmost sample at 0 cm depth is equal to this age. According to Fig. 5 increasing values of ^{137}Cs peak at 6 cm depth and decline afterwards, reaching zero Bq/kg at 10 cm sediment depth. The highest value most likely represents the maximum caesium fallout which occurred in 1963 AD, according to Henderson et al. (2010), while the first zero value is considered to represent the time before the nuclear test at 1950 AD. According to the equation $y=-2.63*\ln(x)+20$ (Fig.5) the mean sediment accumulation rate (SAR) accounts for 12 yr/cm between 0 and 24 cm sediment depth in core KH13.

As all sediment cores KH11-KH14 showed similar sediment composition within the upper 20 cm, this age-depth model was also applied to cores KH11, 12 and 14.

Surface samples taken at various locations within the lake refer to the upper 0.5 and 2 cm sediment and thus represent accumulation within the last 6-ca. 15 years.

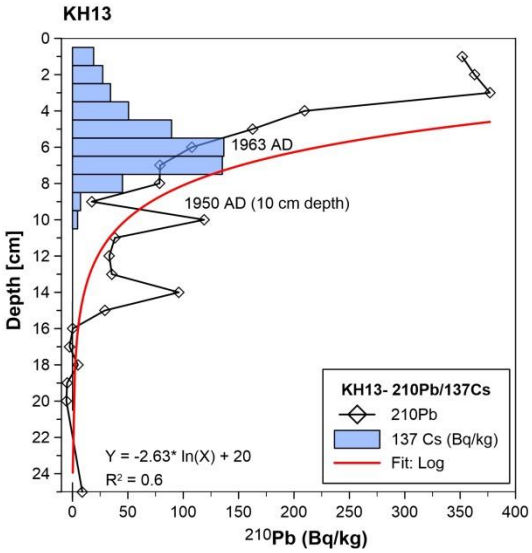

Fig.11 Radionuclide (^{210}Pb/^{137}Cs) dating results from core KH13, Kuhai Lake (for location see Fig. 4).

5.2.2.2 AMS radiocarbon dating results

Fifty-one AMs ages provide the chronological frame for all sediment cores. Ages from KH17 are reported here too, as they were used to establish the chronology of KH14 and KH17, both taken close to each other. In order to define the reservoir error for every individual core, ^{210}Pb/^{137}Cs dating results from KH13 were added. In addition, 17 AMS dates refer to the sections KH9, KHS1, 14, 27 and 29 (Tab.2). They were not RE-corrected as reference ages for estimating any RE were not available and could not be reliably calculated from REs of the lake cores, although a certain RE of maximum some hundred years might have been affected the ages at onshore sites too.

According to the Fig.9 A, B. every core provided an individual chronology, taking changes of grain size compositions into account, where possible.

Cores KH11 and KH12 were dated by using bulk organic matter (Fig.9 A). Linear interpolation to 10 cm depth which was considered to represent the year 1950 AD (= 0 BP) yielded mean reservoir errors (RE) of 2607 years for KH11 and 2810 years for KH12. These REs were subtracted from the original dates and then calibrated to calendar years BP.

For cores KH13 and KH14, samples were dated on plant remains, insoluble (humin), soluble (humic) fractions and bulk organic matter. Due to larger variations of ages from the same sample in both cores (see Fig.9 B, Tab.2), mean ages were used for estimating the mean REs. KH13 yielded a mean RE of 2410 years, while the mean RE for KH14 was calculated to 2495 years.

Radiocarbon dated sections (KH9, KHS1, KHS14, KHS27 and KHS29, see Figs.22-26, Tab.2) were based on bulk organic matter and plant remains from fluvio-lacustrine and/or shoreline deposits.

Tab. 2 Radiocarbon-AMS dating results from cores KH11-KH14/17 and KHS sections (A-C). Shaded ages were discarded from individual age models of cores KH11-KH14.

A)

Sample ID	Lab ID	Depth (cm)	Dated material	14C age yr BP				δ13C (‰)	RE years	RE-corr 14C-age	Cal.yr BP 2 sig. wmean	Cal. yr BP (Bacon)	Remarks
				Bulk OM, Mean	Plant	Humin (insol. fr.)	Humic (sol. fr)						
KH9-0 Plant	beta396861		Plant		350 ± 30			-24.2			403 ± 44		terr.plant
KH9-0	beta396020		Bulk OM	1020 ± 30				-24.5			938 ± 37		
KH11-0	NIGLAS	0	Lac.sed.									-64	210Pb/137Cs
KH11-1	NIGLAS	10	Lac.sed.									0	210Pb/137Cs
KH11-2	beta 398568	90-92	Bulk OM	3740 ± 30				-24.9	2607	1133	1040 ± 58		
KH11-3	beta 398569	186-188	Bulk OM	5100 ± 30				-25.3	2607	2493	2597 ± 133		
KH12-7	beta 398573	3-4	Bulk OM	2730 ± 30				-24.2	2750			-20	210Pb/137Cs
KH12-0	NIGLAS	10	Lac.sed.									0	210Pb/137Cs
KH12-6	beta 398572	55-56	Bulk OM	4090 ± 30				-25.1					discarded
KH12-5	beta 398571	91-92	Bulk OM	4080 ± 30				-25.4	2810	1270	1227 ± 55		
KH12-4	beta 398570	179-180	Bulk OM	5440 ± 30				-24.9					discarded
KH12-3	beta 395424	235-236	Bulk OM	5810 ± 30				-27.2	2810	3000	3173 ± 84		
KH12-2	beta 395423	245-246	Bulk OM	5990 ± 30				-24.1	2810	3180	3406 ± 49		
KH12-1	beta 395422	267-268	Bulk OM	6390 ± 30				-18.1	2810	3580	3900 ± 73		
KH13-0-1	NIGLAS	0	Lac.sed.									-65	210Pb/137Cs
KH13-1 9-10	beta 417204	9-10	Humin fr.			2580 ± 30		-24.8	2580	0	0	0	210Pb/137Cs
KH13.1.8-11 / 19631 Suppl.	beta 421961	8-11	Plant		2410 ± 30			-28.6	2410	0	0	0	
		10	mean	2495 ± 30					2495	0	0	0	
KH13-1 49-50	beta 417700	49-50	Humic fr.				2350 ± 30	-24.5					
KH13-1 49-50	beta 417699	49-50	Plant		1630 ± 30			-26.6					
KH13-1 49-51	beta 417205	49-51	Humin fr.			3220 ± 30		-22.7					
		50	mean	2785 ± 30					2410	375	449 ± 67	492	
KH13-1 93-94	beta 417701	93-94	Humic fr.			3240 ± 30		-25.1					
KH13-1 93-94	beta 417206	93-94	Humin fr.			3710 ± 30		-23.8					
		94	mean			3475 ± 30			2410	1065	981 ± 35	1040	
KH13-1 129-130	beta 417703	129-130	Humic fr.				3800 ± 30	-24.5					
KH13-1 129-130	beta 417702	129-130	Plant		3840 ± 30			-12,0					
KH13-1 129-130	beta 417207	129-130	Humin fr.			4140 ± 30		-23.9					
		130	mean	3990 ± 30					2410	1580	1472 ± 68	1594	
KH13-1 210-211	beta 417704	210-211	Plant		5260 ± 30			-14.5					
KH13-1 210-211	beta 417208	210-211	Humin fr.	5310 ± 30				-24.1					
		211	mean	5285 ± 30					2410	2875	2994 ± 74	2850	

B)

Sample ID	Lab ID	Depth (cm)	Dated material	14C age yr BP				δ13C (‰)	RE years	RE-corr 14C-age	Cal.yr BP 2 sig. wmean	Cal. yr BP (Bacon)	Remarks
				Bulk OM, Mean	Plant	Humin (insol. fr.)	Humic (sol. fr)						
KH14-2 49-50	beta 417705	49-50	Humic fr.				3030 ± 30	-25.1	2495	535	556 ± 22	547	
KH14-2 117-118	beta 417707	117-118	Humic fr.	3650 ± 30				-25,0					
KH14-2 117-118	beta 417706	117-118	Plant		3500 ± 30			-27.8					
KH14-2 117-118	beta 417210	117-118	Humin fr.			3940 ± 30		-25.1					
		118	mean	3795 ± 30					2495	1300	1236 ± 29	1249	
KH14.2-169-172	beta 421963	169-172	Humic fr.				4300 ± 30	-26.3					
KH14.2-169-172	beta 421961	169-172	Plant		4410 ± 30			-15.4					
KH14-2 170-171	beta 417211	170-171	Humin fr.			4800 ± 30		-26.5					
		171	mean	4605 ± 30					2495	2110	2074 ± 78	2076	
KH14-2.1	beta 417711	234-244	Plant		5770 ± 30			-26.5					discarded
KH14-2-2	beta 417214	244	Plant		5690 ± 30			-26.1					discarded
KH14-2-1 243-244	beta 417213	243-244	Humin fr.			6170 ± 30		-21.7					discarded
KH14-2 270-271	beta 417710	270-271	Plant		5570 ± 30			-29.5					
KH14-2 270-271	beta 417212	270-271	Humin fr.			5920 ± 30		-28.3					
		271	mean		5745 ± 30				2495	3250	3487 ± 55	3514	
KH17-79-80	beta 437797	79-80	Humin fr.	4150 ± 30				-27.6					discarded
KH17-149-150	beta 437798	149-150	Humin fr.			5080 ± 30		-28.3					discarded
KH17-219-220	beta 437799	219-220	Humin fr.			5160 ± 30		-25.2	2495	2665	2784 ± 29	2784	
KH17-309-310	beta 437800	309-310	Humic fr.			6740 ± 30		-25,2	2495	4245	4813 ± 25	4766	
KH17-370	beta 441471	369-370	Bulk OM	7950 ± 40				-25,0	2495	5455	6249 ± 63	6254	
KH7-401-402	beta 437802	401-402	Humin fr.			9160 ± 30		-24.2				7524	
KH17-431-432	beta 438792	431-432	Plant		9760 ± 40			-26.6					
KH17-431-432	beta 437803	431-432	Humin fr.			10,180 ± 40		-24.3					
		432	mean		9970 ± 30				2495	7475	8290 ± 42	8289	
KH17-486-487	beta 438793	486-487	Bulk OM	11710 ± 50				-22.7	2495	9215	10,379 ± 131	10,204	
KH17-486-487	beta 437804	486-487	Plant		12,240 ± 40			-26.9					discarded
KH17-487-488	beta 437805	487-488	Humin fr.			12,400 ± 40		-24.7					discarded
KH17-539-540	beta 438794	539-540	Plant		13,070 ± 60			-23.5					discarded
KH17-539-540	beta 437806	539-540	Humin fr.			13,830 ± 50		-22.3					discarded
KH17-580	beta 441472	579-580	Bulk OM	14,770 ± 60				-20.5					discarded
KH17-609-610	beta 437807	609-610	Humin fr.			12750 ± 50		-21.3	2495	10,255	11,972 ± 199	12,071	
KH17- 643	beta 441473	642-643	Bulk OM	13,190 ± 40				-22.9	2495	10,695	12,648 ± 70	12,660	
KH17-679-680	beta 437808	679-680	Humin fr.			18,220 ± 60		-19.9					discarded

C)

Sample ID	Lab ID	Depth (cm)	Dated material	14C age yr BP				δ13C (‰)	RE years	RE-corr 14C-age	Cal.yr BP 2 sig. wmean	Cal. yr BP (Bacon)	Remarks
				Bulk OM, Mean	Plant	Humin (insol. fr.)	Humic (sol. fr)						
KHS1 81-82	beta 417692	81-82	Plant		740 ± 30			-23,2		740	687 ± 24		
KHS1 81-82	beta 417693	81-82	Humic fr.				1530 ± 30	-24,2	790				discarded
KHS1 81-82	beta 417200	81-82	Humin fr.			2060 ± 30		-23,6	1320				discarded
KHS1 135	beta 417201	134-135	Humin fr.			1610 ± 30		-23,6		1610	1485 ± 72		
KHS1 157	beta 417202	156-157	Humin fr.			2680 ± 30		-21,2		2680	2798 ± 47		
KHS14 39-42	beta 417203	39-42	Humin fr.			210 ± 30		-24,4			193 ± 27		
KHS27-16/18	beta 423156	105-130	Plant		2410 ± 30			-15,1					discarded
		105-110											
KHS27-16/18	beta 421945	120-130	Humic fr.				2900 ± 20	-22					discarded
KHS27-17	beta 419593	110-120	Plant		1490 ± 30			-14,4		1490	1365 ± 53		
KHS27-12 89-90	beta 419592	89-90	Humic fr.				2420 ± 30	-22,5					
KHS27-12 85-90	beta 419591	85-90	Plant		2430 ± 30			-15,5		2430	2497 ± 67		
KHS27-1 0-10	beta 419590	0-10	Humic fr.				3600 ± 30	-24,5					discarded
KHS27-1 0-10	beta 419589	0-10	Plant		3170 ± 30			-14,2			3399 ± 53		
KHS29-4	beta 419599	174-178	Plant		1500 ± 30			-13,8		1500	1377 ± 48		
KHS29-3	beta 421947	130-135	Humic fr.		3070 ± 30			-24,3		3070	3285 ± 76		
KHS29-2	beta 421946	80-85	Humic fr.		4180 ± 30			-23,9		4180	4717 ± 64		
KHS29-1	beta 419596	55-60	Humic fr.		4340 ± 30			-24,7		4340	4909 ± 63		

The upper soil in section KHS14 was dated to 0.193 cal. ka BP. Fluvio-lacustrine (riverine) deposits at KHS1 site, located between ca. 1 and 3 m above the modern lake shore, were dated to between 2.8 (bottom) and 0.69 (top) cal. ka BP.

KHS27 in the south-west of the lake, up to 2 m above the modern lake level, provided ages between 3.4 and 1.38 cal. ka BP.

KHS29 clayey-silty sediments at the north-eastern site of the lake, 3 m higher than the modern shoreline, were dated to between 4.9 (bottom) to 3.28 cal. ka BP. Seagrass (*Potamogenton* sp.), washed ashore and deposited as distinct layer above the lacustrine sequences provided an age of 1.38 cal. ka BP).

5.2.2.3 OSL dating results

Twenty-five OSL ages from eight sections were determined in Kuhai Lake catchment (Tab.3, for locations see Fig.4). The ages of 21 samples from seven sections (Tab.3) were calculated based on both ICP and NAA data, and the age of four samples from section KH4 were determined by NAA data. Both sets of dates derived from ICP and NAA show little differences within errors (see appendix II 2). In order to compare the timing of wind-blown sediment deposition of all dated sections, NAA based ages were used for discussion in this study.

Two OSL ages were obtained from loess deposits in section KHS 17 (Fig.12) and range from 4.5 ka to 9.2 ka with errors of 0.63 ka and 0.57 ka (Tab.3). The section KHS 15, which contained sandy loess, was dated to 0.52± 0.05 ka, 0.41± 0.03 ka and 1.81± 0.17 ka. All other sections contained pure aeolian sand and showed two different time phases of deposition: during the early Holocene (8-11 ka), dated in sections KHS 25 and KHS 26, and during the late Holocene (0.2-4 ka) based on data from sections KHS 6, KHS 7, KHS13 and KH 4 (Tab.3, Fig.12).

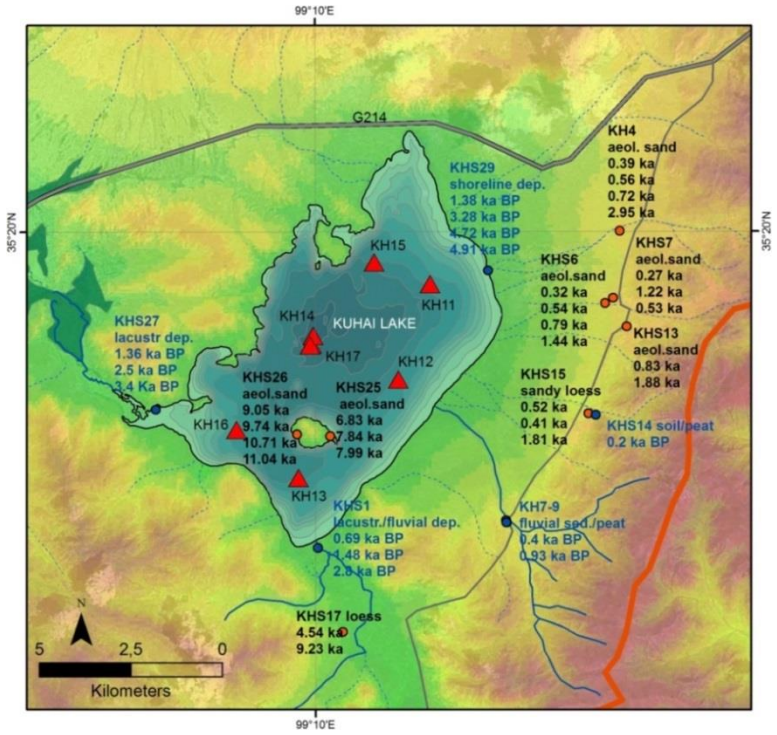

Fig. 12 Overview map of dated onshore sites in Kuhai Lake catchment.

Tab. 3 OSL dating results of sections in Kuhai Lake catchment. WC= water content.

Lab ID	Sample ID	Section No.	Height (cm)	Depth (cm)	U/ppm	Th/ppm	K/%	Dose rate (Gy/ka)	De (Gy)	Aliqouts Num.	WC%	Age (ka)
NL-904	KHO1-1	KHS6	400	125	2.94±0.11	7.33±0.23	1.15±0.05	3.43±0.26	1.09±0.04	8	2.50	0.32±0.03
NL-905	KHO1-2			180-185	2.83±0.1	6.96±0.23	1.15±0.05	3.27±0.24	1.77±0.03	8	5.04	0.54±0.04
NL-906	KHO1-3			245-250	2.23±0.09	6.46±0.21	1.16±0.05	3.07±0.24	2.42±0.01	8	4.98	0.79±0.06
NL-907	KHO1-4			320	1.95±0.08	6.15±0.21	1.07±0.05	2.89±0.24	4.15±0.06	8	3.64	1.44±0.12
NL-908	KHO2-1	KHS7	165	70-75	1.87±0.08	7.15±0.23	1.13±0.05	3.19±0.25	0.86±0.02	8	1.91	0.27±0.02
NL-909	KHO2-2			145-150	1.84±0.08	6.34±0.21	1.14±0.05	3.00±0.23	3.66±0.07	8	5.41	1.22±0.10
NL-910	KHO2-3			125-130	2.26±0.09	7.39±0.24	1.27±0.05	3.24±0.23	1.71±0.03	8	7.84	0.53±0.04
NL-911	KHO3-1	KHS15	190	75-80	2.05±0.09	7.45±0.24	1.27±0.05	3.27±0.23	1.70±0.11	8	6.09	0.52±0.05
NL-912	KHO3-2			110-115	2.33±0.09	7.20±0.23	1.22±0.05	3.21±0.23	1.31±0.03	8	7.78	0.41±0.03
NL-913	KHO3-3			160-165	2.30±0.09	7.45±0.24	1.16±0.05	3.10±0.22	5.62±0.33	8	9.27	1.81±0.17
NL-914	KHO4-1	KHS13	200	140-145	2.07±0.09	6.76±0.22	1.18±0.05	3.16±0.24	2.61±0	8	3.81	0.83±0.06
NL-915	KHO4-2			170-175	1.98±0.08	7.32±0.23	1.27±0.05	3.17±0.23	5.96±0.08	8	6.51	1.88±0.14
NL-916	KHO5-1	KHS17	60	25-30	2.70±0.10	10.90±0.31	1.68±0.06	3.77±0.21	17.12±2.16	8	16.24	4.54±0.63
NL-917	KHO5-2			45-50	2.68±0.10	10.30±0.29	1.78±0.06	3.89±0.22	35.86±0.92	8	13.13	9.23±0.57
NL-918	KHO6-1	KHS25	115	50-55	2.34±0.09	9.28±0.27	1.50±0.05	3.55±0.22	24.24±0.12	8	11.45	6.83±0.42
NL-919	KHO6-2			73-76	2.25±0.09	8.00±0.24	1.31±0.05	3.39±0.23	26.55±0.08	8	6.51	7.84±0.54
NL-920	KHO6-3			105-110	1.92±0.08	5.63±0.20	0.99±0.05	2.86±0.23	22.84±2.1	8	5.21	7.99±0.98
NL-921	KHO7-1	KHS26	320	38-43	2.18±0.09	7.21±0.23	1.37±0.05	3.55±0.26	32.17±0.4	8	0.77	9.05±0.67
NL-922	KHO7-2			137-142	2.12±0.09	7.00±0.22	1.36±0.05	3.44±0.26	33.53±1.14	8	0.68	9.74±0.80
NL-923	KHO7-3			240-245	2.24±0.09	6.84±0.23	1.30±0.05	3.20±0.23	34.31±0.52	8	5.85	10.71±0.80
NL-924	KHO7-4			300-305	2.10±0.09	7.61±0.24	1.46±0.05	3.21±0.21	35.37±1.06	8	11.20	11.04±0.80
NJU-1995	KH4-1	KH4	300	240	1.56±0.07	5.45±0.19	1.34±0.05	2.15±-0.15	6.34±0.21	10/11	5.14	2.95±0.23
NJU-1996	KH4-2			160	1.99±0.08	6.82±0.22	1.66±0.05	2.58±0.16	1.7±0.03	10/6	4.88	0.66±0.04
NJU-1997	KH4-3			70	2.14±0.09	6.21±0.2	1.54±0.05	2.58±0.16	0.98±0.03	9/9	2.41	0.38±0.03
NJU-1998	KH4-4			20	1.96±0.08	7.5±0.24	1.46±0.05	2.68±0.16	0.64±0.02	8/9	2.84	0.24±0.02

However, ‘quartz ages’ yielded generally older ages in comparison to ‘feldspar ages’, showing differences between 60 and 150 years, except for the age at 240 cm depth (bottom) which was almost 1.43 ka younger than the corresponding feldspar age.

5.3 Modern (last 15 yr) spatial distribution pattern of sediments in Kuhai Lake

Sediments from the lake surface of Kuhai were taken from 58 locations (see Fig.4). In this study only the upper 0.5-2 cm sediment was subject to mineral analyses by XRD on powdered samples, geochemical analyses and grain size, comprising the last 10-15 years of accumulation. According to the Figs.14-18 all data point to a high spatial diversity which will be presented below:

5.3.1 Spatial mineral and element distribution

Selected minerals refer to the identified carbonates (Calcite, Monohydrocalcite, Aragonite, High-Mg-Calcite and Dolomite) and sulfate (Gypsum). All other minerals such as clay minerals and other typical detrital components (Quartz, Feldspars and Amphibole) contributed in relatively high amounts to the overall sediment budget, but are excluded for further consideration, but presented in the appendix II 3. Halite was always present in all samples with slightly varying amounts (calculated by % cps), according to the saline nature of the lake.

XRD diagrams from selected samples are shown in Fig.14 A-D and demonstrate that identified Gypsum did not occur in several samples (Fig.14 A) or only in low amounts (mean: 3% cps, Fig.14 C). Conversely, Mischke et al. (2010b) reported extreme values for Gypsum in their record (green triangle in Fig.14) and thus may be a unique finding in this lake or subject to unclear identification. The same applies to Aragonite, which was generally not found in the surface samples, except for few which may have been traced from the XRD plots but showed no clear peaks next to the Quartz main reflex (d-value 3.34; 26.62 °2Theta) and identification remained doubtful.

Conversely, Monohydrocalcite (MHC) in expense of calcite occurred in most of the surface samples with variable amounts (Fig.14 B, D). High-Mg-Calcite and Dolomite were present in all samples with low amounts (1-3% cps) in general, except for few samples with extreme values exceeding 43% for High-Mg calcite and up to 10% for Dolomite.
The spatial distribution pattern of those minerals show that high calcite concentrations occur in the center and western part of the lake, whereas very low amounts were found in samples close to the inflowing drainages along the eastern and northern shore of the lake (Fig.14 A).

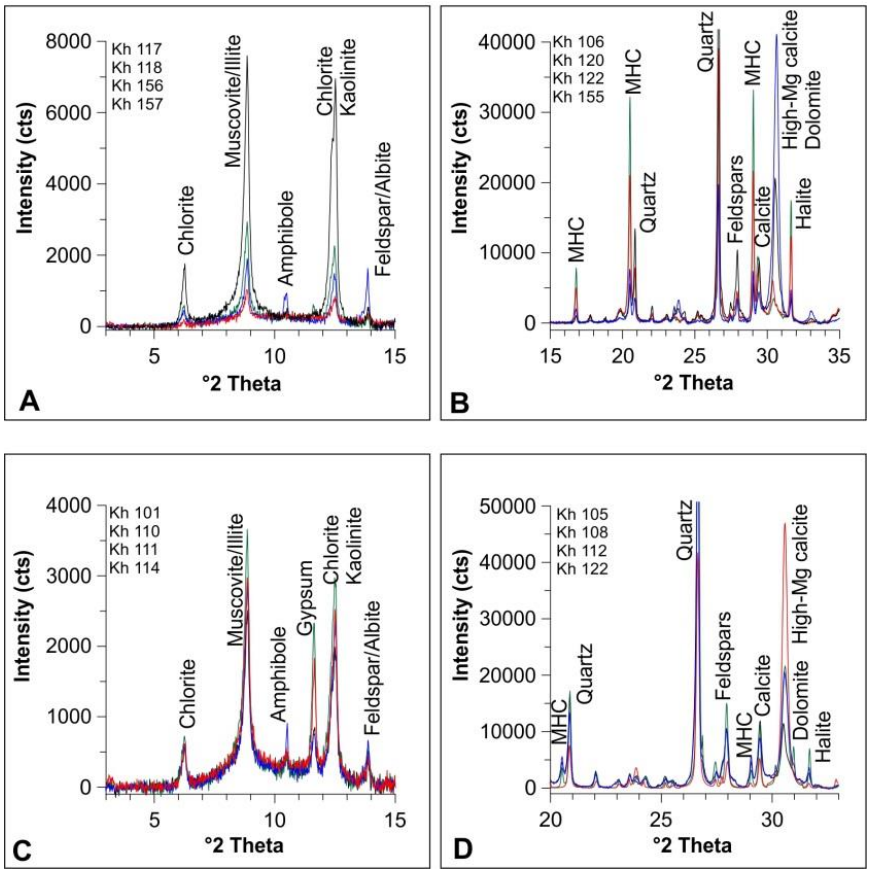

Fig. 13 Selected XRD diagrams from surface samples of Kuhai Lake. A, C: XRD peaks at 0-15 °2Theta showing the occurrence of clay minerals, Amphibole and Gypsum (the latter only in C). B, D: XRD peaks between 15 and 35 °2Theata, showing Monohydrocalcite (MHC), Quartz, Feldspar, Carbonates and Halite in different amounts.

MHC displays a similar pattern as Calcite (Fig.14 B) with highest concentrations (up to 30 % cps) around the island (southern part of the lake) and in the northwest of the lake at water depth below 8~10 m. Samples with lowest values and even disappearance of MHC are mainly located along the eastern shore of the lake, very similar to the calcite distribution pattern.

Highest concentration of calcium of up to 180 mg/g, measured by ICP-OES, were found in samples on the southern part of the lake, mainly confirming the XRD values for Calcite and MHC. Lower values (<100 -22 mg/g) were found in the northern part of the lake with lowest values close to the perennial river inflow region at the eastern and north-eastern shores (Fig.14 C).

High-Mg-Calcite and Dolomite show a very similar pattern with high concentrations only in the northern and south-eastern near-shore regions with water depth above 10 m (Fig.14 D, E). Conversely, in the deeper parts of the lake below 10 m both minerals occur with lowest values of <5% XRD cps and even are not present. Mg-Ca molar ratios, derived from the ICP values show a similar pattern as the XRD distribution maps with higher ratios of up to 10 at places with high amounts of High-Mg-Calcite and Dolomite (Fig.14 F), but also occur at near-shore-locations along the southern and southwestern shore and

in a small shallow bay in the west of the lake as well. Strontium-calcium molar ratios (Fig.14 H) show a similar pattern as the Mg-Ca ratio with highest values (up to 0.23) in the south-eastern and northern part of the lake and occur mainly above 10 m water depth. Higher values also occurred locally in two small bays at the western side of the lake and at a near-shore-location in the south.

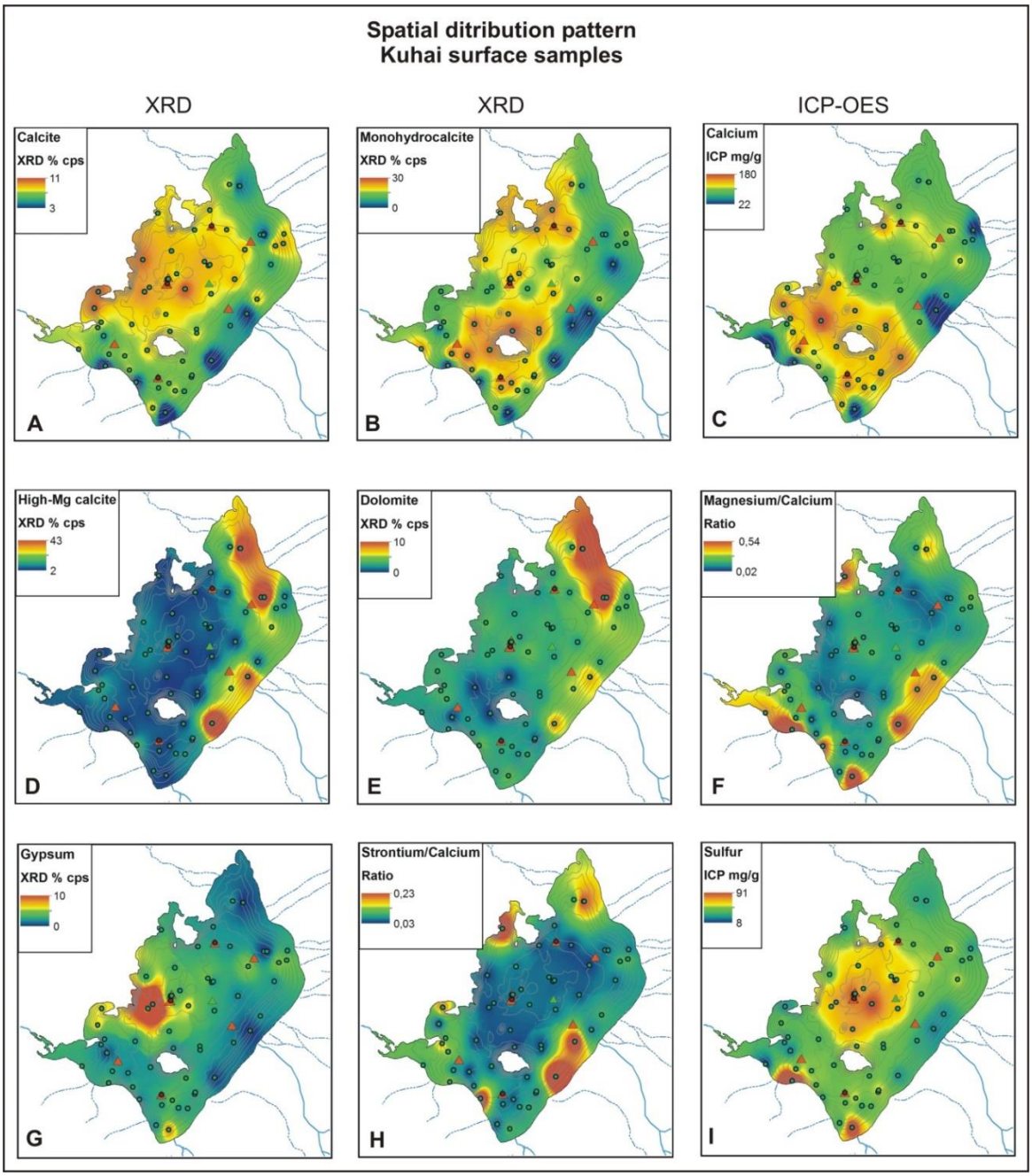

Fig. 14 Spatial distribution pattern of selected minerals, elements and their ratios in surface samples of Kuhai Lake. Spatial distribution maps refer to Inverse Distance Weighted Interpolation (IDW) method derived from ArcGIS10.

As already mentioned before, Gypsum is also unevenly distributed and displays highest XRD values (up to 10 % cps, Fig.14 G) in the south-western part of the lake while in the northern and eastern part of the lake Gypsum could not be found. This distribution pattern can be confirmed by sulphur values, which also display higher concentrations of up to 91 mg/g in the center of the lake basin (Fig.14 I) and much lesser amounts (<20 mg/g) in all other parts of the lake.

5.3.2 Spatial grain size and endmembers distribution

Sediments in Kuhai Lake are composed of clastic components, organic material (algae and higher aquatic plants), chemical precipitates (carbonates, sulphates, halites) and fossil remains (e.g., carbonate shells from ostracod) which together form the overall lake bottom deposits. The clastic components were analysed by means of grain size analyses providing 70 granulometric classes between ca. 0.02 and 2000 µm grain diameter. These fractions were grouped to grain size classes according to the international standard classification (Doeglas, 1965) into clay (<2 µm), silt (2-65 µm) and sand (65-2000 µm) components. The spatial distribution pattern of the fine components in the clay and silt fraction (<65 µm, clay-silt, Fig.15 C) shows a relatively wide and homogenous distribution pattern within Kuhai Lake, except for the northern bay region and along the shorelines on the western and south-western parts of the lake basin. Coarser grain size components (>65 µm, sand fraction, Fig.15 E) are concentrated at local places in near-shore regions along the northern, western and south-western parts of the lake.

The original grain-size distributions were transferred into an endmember modelling analysis (EMMA, Fig.15) – an eigen-space decomposition with different scaling procedures that extract genetically meaningful end-member grain-size distributions (i.e., loadings) and their percentages in each sample (endmember composition, i.e., scores; Dietze et al., 2012). As a result, three different endmembers (EMs) could be extracted from all surface samples which could explain 95% of variance with contribution of 84% (EM1), 8% (EM2) and 3% (EM3).

Notably the EMs 1 and 3 mirror the grain size components of the clay-silt fractions very well and show that the silt fraction (EM1, Fig.15 A) is mainly concentrated in the southern part of the lake. Conversely, the finest fraction (clay, EM3, Fig.15 B) is enriched in the north-eastern part of the lake as well as in spot-like patterns in the center and south-west, confirming that both EMs monitor the spatial distribution pattern of the grain size classes < 65 µm.

EM 2 (Fig.15 D) displays a distribution pattern similar to the grain size fractions >65 µm and explains the contribution of dominantly sand fractions to the overall sediment budget.

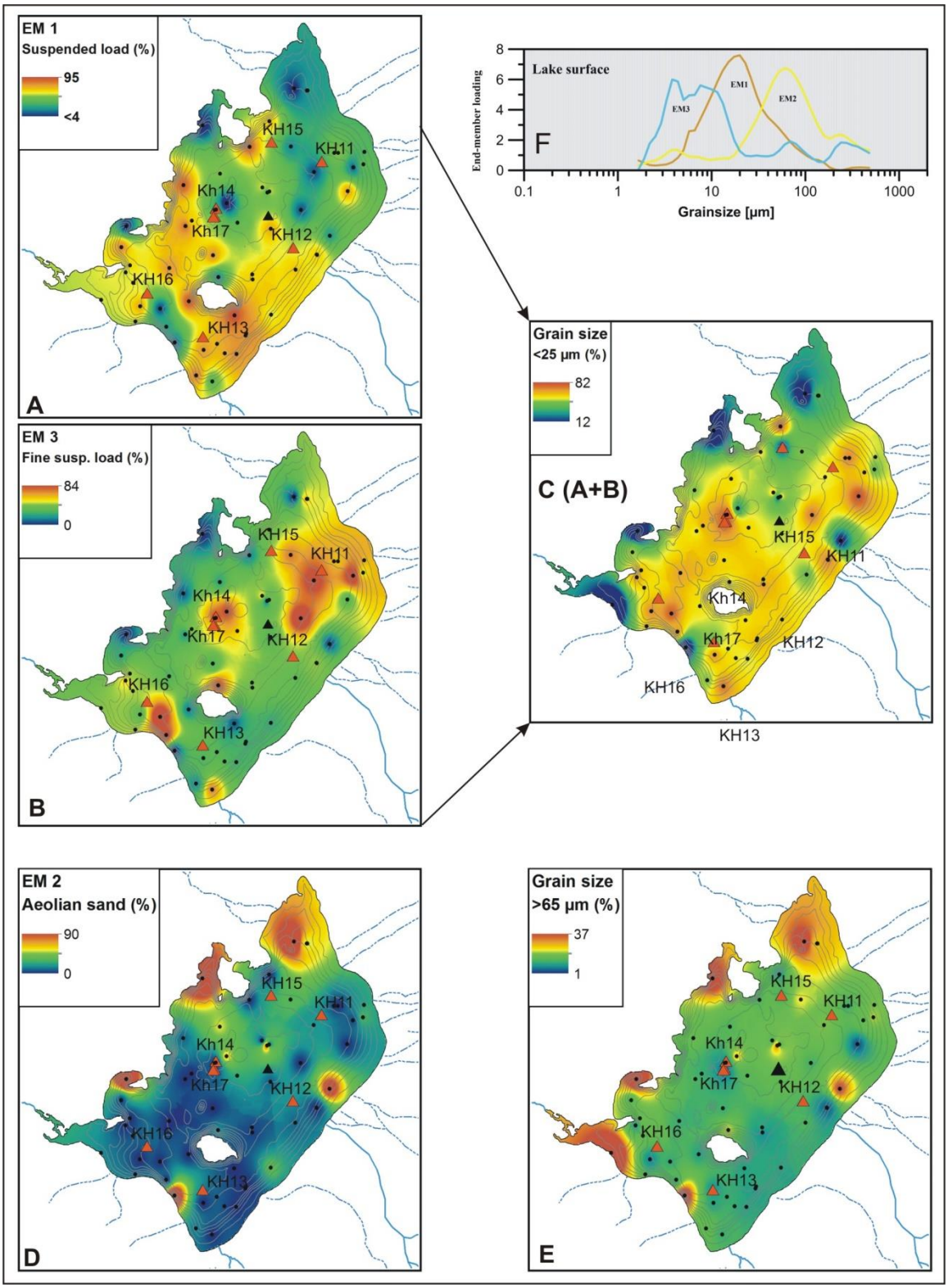

Fig. 15 Spatial distribution pattern of grain size components and respective endmembers (EMs) in Kuhai Lake, based on surface samples covering the last 15 years of accumulation. Spatial distribution maps refer to Inverse Distance Weighted Interpolation (IDW) method derived from ArcGIS10.

5.3.3 Ostracods in lake surface samples

5.3.3.1 Taxonomy of Recent ostracods in Kuhai

Two species of ostracod were identified in surface samples from Kuhai Lake (Fig.16), which were assigned to *Eucypris mareotica* (Fischer, 1855) and *Limnocythere inopinata* (Baird, 1843).

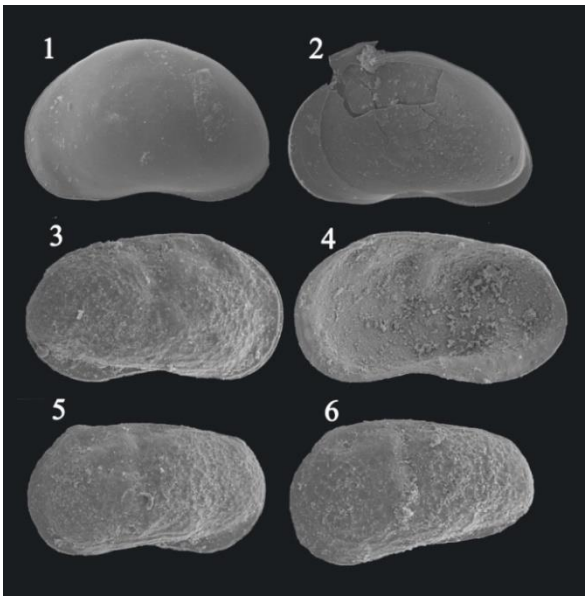

Fig. 16 SEM photographs from ostracod shells in Kuhai Lake. **(1-2) *Eucypris mareotica*:** (1) LV ext. length 984.4 μm (2) RV int. length 1.00mm **(3-6) *Limnocythere inopinata*:** (3) female RV ext. length 521.8μm (4) female RV int. length 508.4μm (5) female LV ext. length 490.1μm (6) juvenile LV ext. length 401.7μm. Abbreviations: RV, right valve; LV, left valve; int., internal view; ext., external view. Specimens housed in the Institute of Geological Sciences, Freie Universitaet Berlin, Germany. All samples are stored in Nanjing University, China.

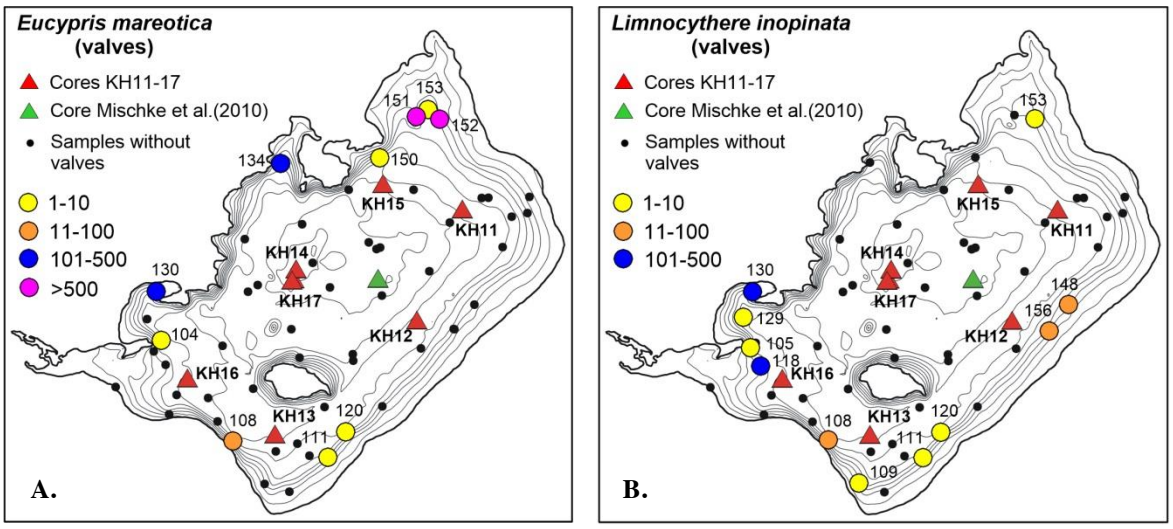

Fig. 17 Spatial distribution of ostracod in Kuhai Lake. Numbers of coloured samples indicate the number of surface sample. **A.** *Eucypris mareotica*; **B.** *Limnocythere inopinata*.

5.3.3.2 Spatial ostracod distribution

Among all investigated lake surface samples, *Eucypris mareotica* was found in 10 samples, of which 4 samples contained more than 100 valves, which can be considered as 'abundant'. They were found in the northern bay and in two bays on the west side of the lake (Fig.17 A). Lower amounts (< 100 valves per sample) only occurred in the northern (two samples) south to southwestern (three samples), southwestern part of the lake (1 sample). They always occurred at water depth above 10 m.

Nine of 54 lake surface samples contained *L. inopinata* (Fig.17 B), while only two of them contained abundant valves (>200), located in the south-western bay of the lake. Lower amounts occurred in the southern and eastern part of the lake. Few valves were recorded in one sample from the northern bay of the lake. Conversely, Mischke et al. (2010b) reported higher abundances of *L. inopinata* in one sample at the north-eastern side of the shallow lake. In general, *L. inopinata* was only found in the littoral zone of the lake with water depth not exceeding 9 m.

5.3.4 Spatial distribution of stable isotopes ($\delta^{18}O$, $\delta^{13}C$)

The spatial distribution pattern of stable oxygen and carbon isotopes ($\delta^{18}O$ and $\delta^{13}C$, ‰ VPDB) on carbonates in surface samples provided a similar picture for both isotopes (Fig.18) ranging between -9.3 and +2.54 ‰ (oxygen isotopes) and -2.8-+2.82 ‰ (carbon isotopes), respectively. These are relatively high magnitudes in the order of >11‰ for oxygen isotopes and 5.6‰ for carbon in comparison to variations in carbonates from Qinghai Lake (<1.5 ‰, Henderson et al., 2010).

Lightest values of both isotopes are distributed close to inflowing river mouths with an increasing trend (heavier values) towards the lake center and to areas without direct contact to inflowing rivers. Highest (heaviest) values are found in the southern and north-central part as well as in the northern bay of the lake, all apart from direct inflow regime during the last 15 years.

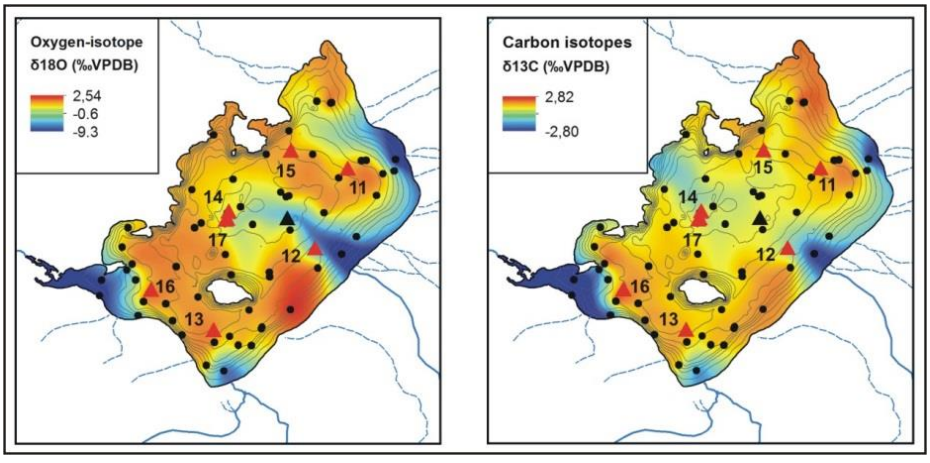

Fig. 18 Spatial distribution pattern of stable isotopes ($\delta^{18}O$ and $\delta^{13}C$, ‰VPDB) on carbonates in Kuhai Lake. Data processing is based on Topo-to-Raster Interpolation derived from ArcGIS10.

5.4 Spatio-temporal patterns in sediment cores of Kuhai Lake

5.4.1 Mineral composition in cores KH 11-14

In all seven sediment cores from Kuhai Lake, here only the cores KH11-KH14 are presented, a total of 12 minerals were identified and reported as percent counts per second (cps) from the total sum of all identified minerals against depth (appendix II 3) and calibrated age for the last 3.8 cal. ka BP. They include Quartz, Feldspars (Alkali-Feldspars and Plagioclases), Clay minerals (Chlorite, Illite/Muscovite and Kaolinite), Amphibole, Gypsum, Monohydrocalcite, Aragonite, Calcite, Mg-Calcite (High-Mg-Calcite), Dolomite, Halite and Pyrite. Their distribution pattern for each core is shown in the appendix II 3, where clay minerals and Feldspars are shown as sum graphs. Temporal distribution of carbonate facies are shown in Fig.19 and are described below:

In core KH11 (13.3 m water depth) Quartz contributed constantly about 40-60% to the entire mineral composition, except at 30-40 cm depth (ca. 0.25-0.45 cal. ka BP in Fig.19) with values of 28-36%. Feldspars contributed ca. 10% without strong changes throughout the core. Clayminerals fluctuated at around 6%, and Amphibole occurred occasionally in the core with an amount of 1-2%. Halite remained constant at a ~5% level, while Gypsum was only present with values below 3% (both not shown in figures).

Stoichiometric Calcite in core KH11 occurred in relatively continuous proportions ranging between 10% and 15%. High-Mg-Calcite varied between <3% and 28% with highest values at around 35 cm depth (0.35 cal. ka BP). Increased levels also occurred in 85-105 cm depth (1-1.3 cal. ka BP), at 160 cm depth (ca. 2.15 cal. ka BP) and at 190 cm depth (2.6-2.7 cal. ka BP). Aragonite and Dolomite occurred only occasionally with low values not exceeding 3%, while missing in the upper 40 cm (until ca 0.5 cal. ka BP) of the core. Monohydrocalcite (MHC) showed a clear increase until 136 cm (ca 1.65 cal. ka BP), with maximum value of 19% at 28 cm depth (0.45 cal. ka BP), followed by a slight decrease down to the core, with average values of 8 %.

In core KH12 (13.7 m water depth), Quartz ranged between 32-58%, with low values between 205 and 235 cm depth (appendix II 3, ca 2.75-3.3 cal. ka BP in Fig.19) in the lower part of the core. Feldspars ranged with 10% throughout the core and displayed slight fluctuations in the lower part. Clay-minerals slightly increased from the top of the core down to 200 cm depth with ranges of 4-8%. Halite was present throughput the core with mean values of 5% and higher values of up to 10% between 215-235 cm depth (ca. 2.8-3.3 cal. ka BP). Amphibole only occurred occasionally at 32 cm, 60 cm, 134 cm, 174 cm and 192 cm with ranges of 0.5%-1.2%. Pyrite was observed only in four samples in the upper part of the core with average of 1%. Gypsum was present with maximum values of 3%. MHC was present in most parts of the core with slightly increasing trend down-core and highest values between 215 and 235 cm depth (2.8-3.3 cal. ka PB), followed by relatively low values of 0-2% at 240-264 cm depth (3.3-3.8 cal. ka BP). Calcite showed constant distribution with range of 10% through the entire core except higher values of 36 % at 256 cm depth (3.65 cal. ka BP). High-Mg-Calcite remained more or less constant

with average values of 10%, except for some extreme values over 30% in the lower part of the core, coupled with very low values (<2-0%) at the neighboring depths. Aragonite and Dolomite only occurred occasionally (<5% mean) and did not exist together at a certain depth.

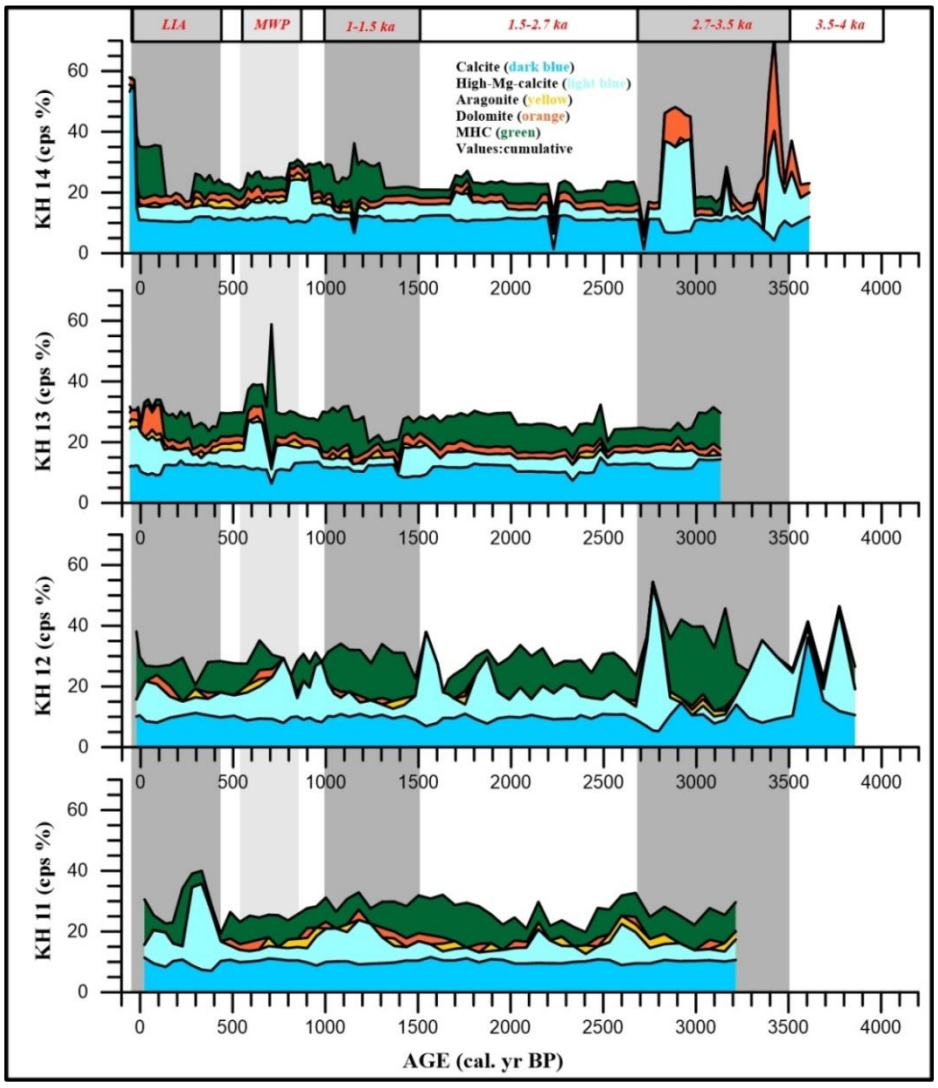

Fig. 19 Carbonate mineral distribution in cores KH11-KH14, Kuhai Lake, against age (cal. yr BP).

In core KH13 (13.7 m water depth), Quartz was dominant with up to ca 60% without strong fluctuations. The same applied to feldspars, clay-minerals and amphibole. They fluctuated on levels of 12 %, 10% and <1%, respectively. Gypsum fluctuated at around 1%.

MHC remained relatively constant throughout the core, except for one higher value at 70 cm core depth (40%, appendix II 3, 0.7 ka cal. BP, Fig.19). Calcite fluctuated between 6-12%. High-Mg-Calcite decreased down-core from ca.15% to nearly 0%, with slightly higher values at upper 25 cm (until ca 0.2 cal. ka BP), 60-70 cm (0.6-0.7 cal. ka BP) and 120-130 cm depth (ca 1.4-1.6 cal. ka BP). Aragonite occurred not continuously with

values <4%, while generally low amounts of Dolomite (<5%) had higher occurrences of up to 10%, Gypsum did not exceed 1%.

In core KH 14 (21.7 m water depth), Quartz, mainly constant throughout the core (appendix II 3), dominated the sediments with up to ca. 70% of all minerals, higher than observed in all other cores. Feldspars and Clay-minerals fluctuated irregularly within ranges of 5%. Gypsum and Amphibole ranged between zero and 1% with low values of Amphibole in the upper core (0-115 cm: <0.5%) and higher values down-core (~1%).

MHC fluctuated between 0% to 25%. High amounts of MHC occurred at 5-15 cm (0-1.5 cal. ka BP) and 85-125 cm depth (0.8-1.35 cal. ka BP, Fig.19). Calcite provided only high values in the upper 10 cm of the core (>50%) and remained more or less constant on a 10 % level until the end of the core. High-Mg-Calcite fluctuated within 0-15 % until 220 cm depth. High values of up to ca. 40% occurred at 215-230 cm and 260-270 cm depth, respectively (ca. 2.8-3.0 and 3.4-3.6 cal. ka BP). Aragonite occurred not continuously with values <3%. The same applied to Dolomite (max. 3%), except at 215-230 cm and 260-270 cm depth, contemporarily with High-Mg-Calcite.

5.4.2 Sedimentary characteristics in cores KH 11-14

5.4.2.1 Grainsize composition in cores KH 11-14

Grain size variations in catchment sections showed a wide range of grain size components with dominance of coarser fractions larger than clay-fine silt (11-500 µm), including medium silt, coarse silt, fine sand and medium sand in catchment sections (Tab.4, see also chapter 5.5). Coarse silt and fine to medium/coarse sand occurred more frequently in sections than in lake deposits. Conversely, in lake surface sediments and sediment cores KH11-KH14, the finer components contributed considerable amounts to the overall sediment budget (see also chapter 5.3.2, surface samples).

Tab. 4 Comparisons of EMMA results of cores and surface samples in Kuhai Lake.

Core ID	EMs No.	Explaining rate (%)	Modes of EMs (µm)			Descriptions of EMs			Interpretation of EMs		
			EM 1	EM 2	EM 3	EM 1	EM 2	EM 3	EM 1	EM 2	EM 3
KH 11	3	95	8	25	60	Bimode	Unimode, broad	Bimode	Lacustrine	Susp. load	Fluvial
KH 12	3	98	5	50	11	Multimode	Multimode	Broad mode	Lacustrine	Fluvial	Susp. load
KH 13	3	96	11	80	22	Bimode	Unimode	Multimode	Lacustrine	Fluvial	Susp. load
KH 14	3	97	10	35	60	Unimode	Unimode	Bimode	Lacustrine	Aeolian	Fluvial
Surface	3	95	20	60	4	Unimode	Multimode	Multimode	Susp. load	Aeolian Sa	Fine Susp.load

Note: Susp.= Suspended load; Aeolian Sa=Aeolian sand.

In general, clay fractions (<2 µm) occurred with no more than 10% in most of the samples from the Kuhai catchment, in lake surface samples and also in the sediment cores (see also chapter 5.3.2). Exceptionally low clay content was measured in core KH13, not exceeding 0.2%.

Silt, including fine silt (2-6.3 µm), medium silt (6.3-25µm) and coarse silt (25-63 µm) was almost the dominant grain size class in all sediment cores and in some catchment sections as well. However, different fractions within the silt class varied strongly through sediment depths of the cores.

Sand, including fine sand (250-630 µm), medium sand (250-630 µm) and coarse sand (>630 µm) mainly occurred in the fine sand fraction, while coarse sand was either completely absent or contributed in a very low amount to the sediments within the lake basin. Only few samples contained up to 5-6% coarse sand. Medium sand ranged between 0-10% in respective core samples.

Grain size variations in cores KH11-KH14 (Fig.20 A-D, Tab.4) differed among each other and are described as follows:

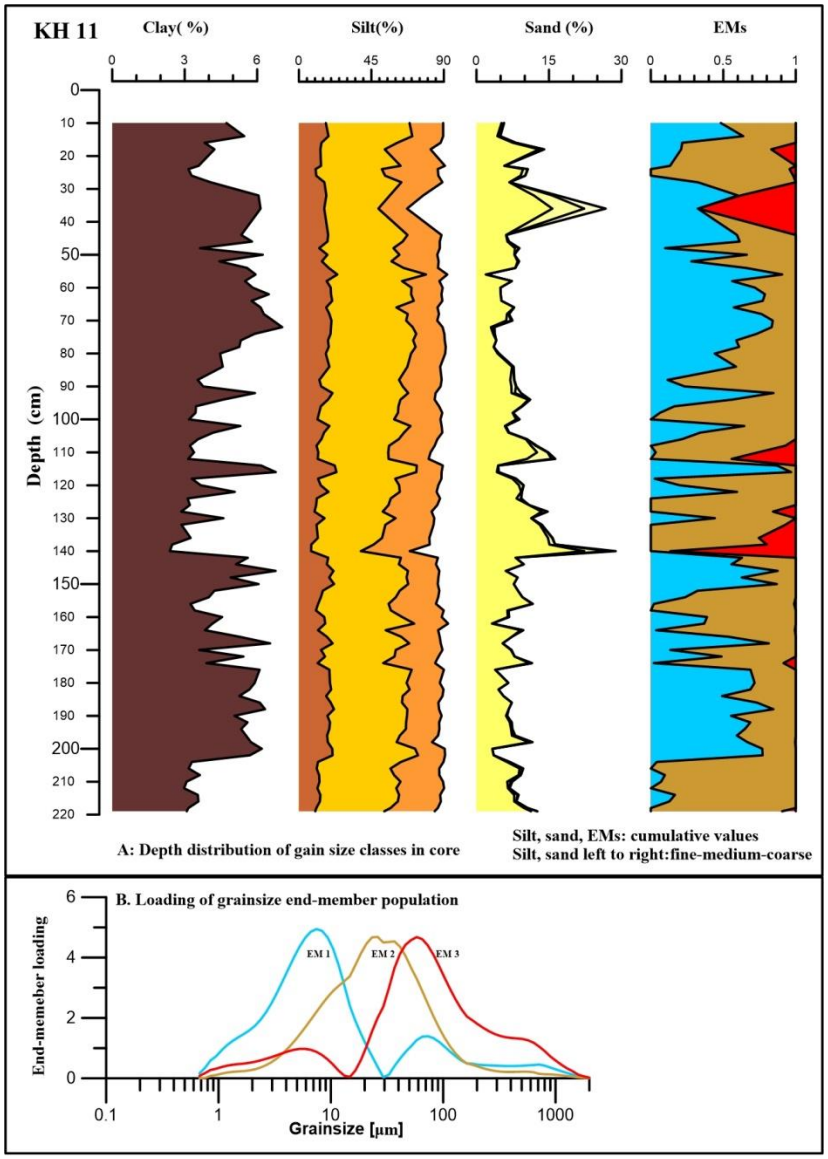

Fig. 20A Grain size distribution and endmembers of core KH11 through depth.

In core KH 11 (Fig.20 A), clay fluctuated between 3-6% on average, higher clay content was present at 30-70 cm, but deceased to less than 3% at 140 cm, followed by a sudden increase up to >6% with some fluctuations. After 200 cm, clay decreased again to about 3% until the end of core. Silt content kept almost constant with maximum amounts of ca. 90% except at ca. 35 cm and 145 cm with lower values of 60%. Medium silt was the major fraction throughout the entire core sequence. Sand (5-10%) fluctuated strongly throughout core KH 11 with considerable higher amounts of up to 20% at 35 cm and 140 cm depth.

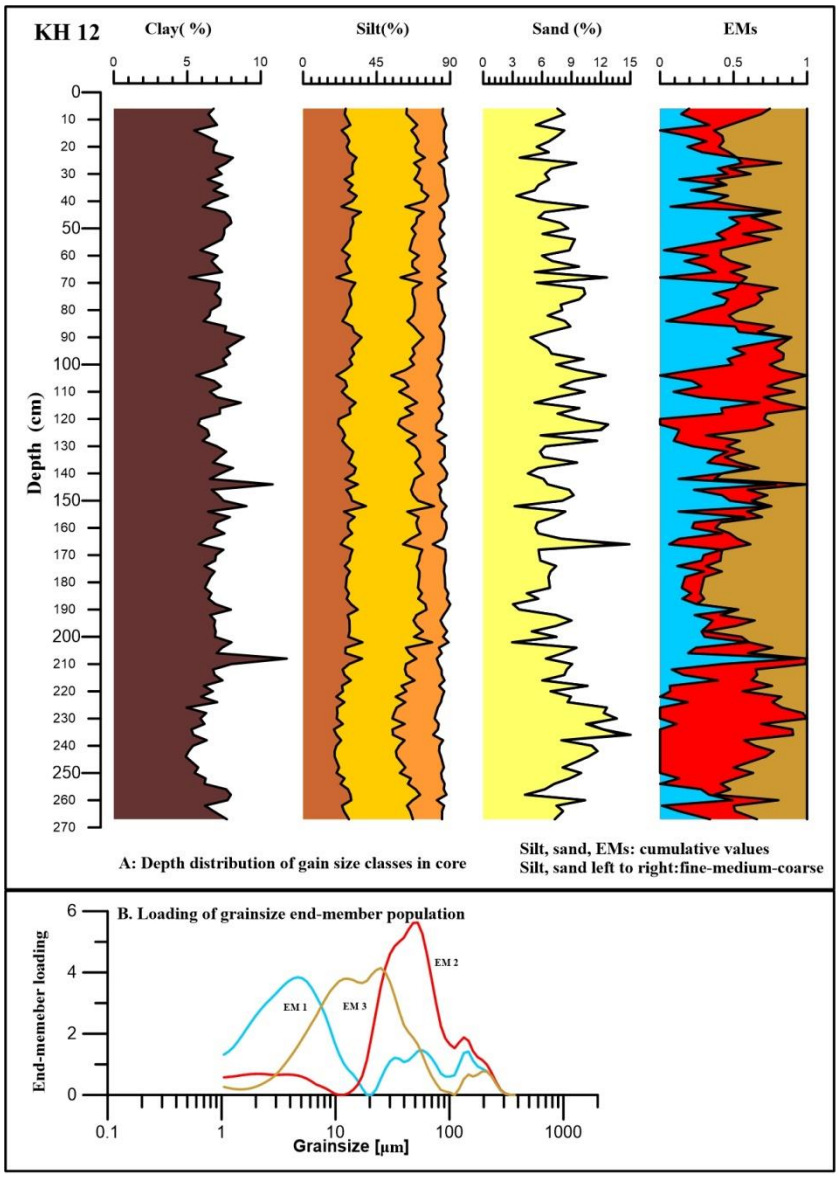

Fig. 20B Grain size distribution and endmembers of core KH12 through depth.

In core KH 12 (Fig.20 B), clay fluctuated between 5 and 8%, with slightly higher values (>9%) at 144 cm, 152 cm and 218 cm depth. Silt fractions showed a constant distribution pattern and fluctuated slightly between 80-90%. Similar to core KH11, medium silt was the dominant fraction, although fine silt contributed more to the overall silt components than in core KH11. Sand mainly occurred as fine sand and ranged between 3 and 15%,

but fluctuated considerably with a magnitude of up to 7%. Highest values were recorded at 230-240 cm sediment depth, lowest at 40 and 190 cm depth. Medium sand only appeared occasionally with very low amounts while coarse sand was lacking in the core.

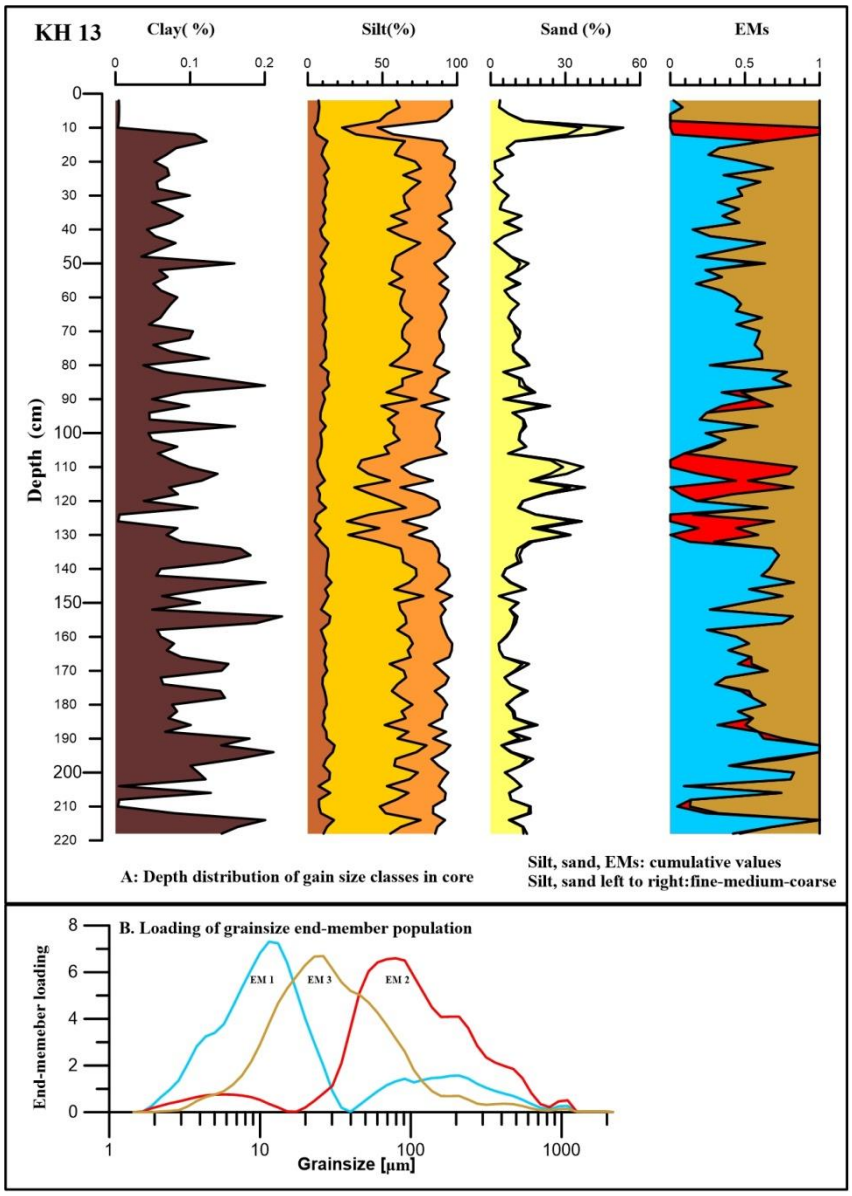

Fig. 20C Grain size distribution and endmembers of core KH13 through depth.

In core KH 13 (Fig.20 B), clay fluctuated strongly between 0-0.2% with slightly increasing trend down-core. These were the lowest values for clay, compared with all other sediment cores. Silt, especially medium silt, was the dominant grain size class and ranged between 80-98%, except for some samples in the upper (at 10-12 cm) and middle parts (105-120 cm) of the core. Sand fluctuated within 15% throughout the core, mainly consisting of fine sand. Higher content, exceeding 30% occurred at the depths with lowest silt values.

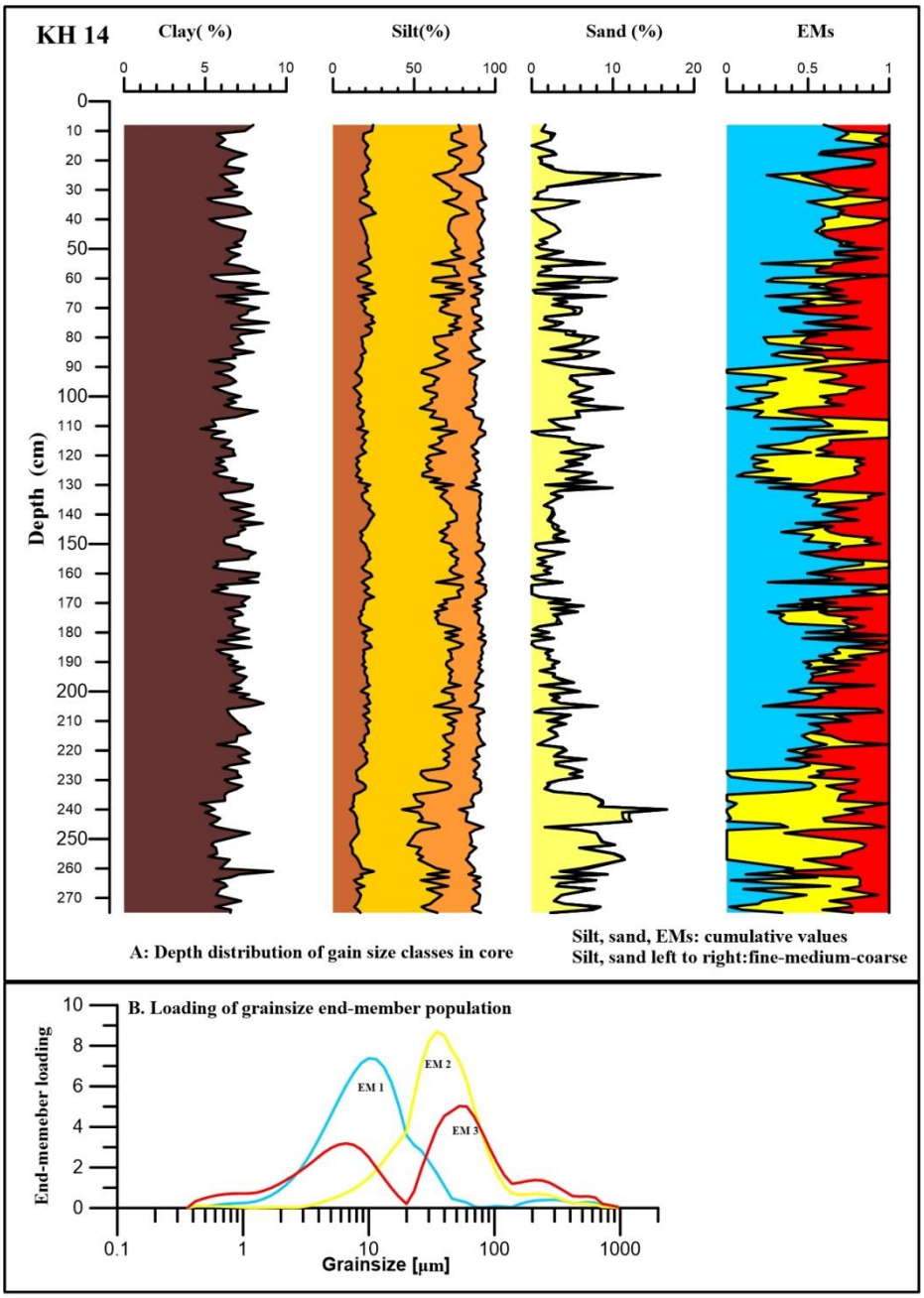

Fig. 20D Grain size distribution and endmembers of core KH14 through depth.

In core KH 14 (Fig.20 B), the clay fraction fluctuated at around 6-7% down to the end of the core. Highest clay value of 9.2% occurred in the lower part of the core (at 261 cm depth). Fine silt varied similar to the clay fraction (11-25%), while medium silt was also here the dominant fraction (32-61%). Coarse silt (8-39%) contributed in a wider range to the overall silt fraction. Sand, mainly fine sand, fluctuated stronger than the other fractions and contributed to the budget between 0-11%. Highest amounts of up to 16% were recorded at 25 cm and between 240 and 255 cm sediment depth.

5.4.2.2 Endmember distributions in cores KH11-KH14

Endmember modelling analysis (EMMA) was applied to lake surface samples (see chapter 5.3.2) and four lake sediment cores (KH 11-14) in this study. Three endmembers (EMs) apply to all sections, surface samples and cores with explanation rates of 90-98%. Different grain size components apply to EM1 (5-25 µm), EM2 (25-150 µm) and EM3 (4-400 µm, see Tab.4). EMs 1-3 in different sections and cores occurred in modes either with narrow peak, bimodal and/or in multi-modes, accordingly. Each end-member varied in different scale within the cores (Fig.20 A-D).

In KH 11 (Fig.20 A, Tab.4), EM1 (mean: 0.4, bi-modal curve at 8 µm and 70 µm) and EM2 (mean: 0.56, broad unimodal curve at 25-40 µm) were dominant throughout the core, while EM3 (mean: 0.04, bi-modal curve at 6 µm and 60 µm) only occurred occasionally. Lowest values of EM1 were always replaced by EM2, except for samples at 30 cm, 112 cm and 130-140 cm depth where EM3 contributed higher loadings to the overall sediments. Generally low but fluctuating loadings of EM1 at 15-25 cm and between 90 and 140 cm, 155-175 and 205-220 cm depth correspond inversely with highest loadings of EM2 with full loadings (1) at 100 cm, 124 cm, 126 cm, 158 cm, 206 cm, 212 cm and 218 cm depth.

In KH 12 (Fig.20 B, Tab.4), high frequency fluctuations from high loadings (up to 1) to extreme low values, even zero, were characteristic for this core EM1 (mean: 0.33, unimode at 5µm) representing the finest fractions, occurred as a multi-modal curve and ranged between 0-0.92. This EM showed a higher temporal diversity than in core KH 11. Larger sequences with very low loadings occurred between 104 and 130 cm and after 210-265 cm depth down-core Highest loadings showed a single peak at 90 cm depth (loading of 1) and at 208 cm depth (0.92). EM2 with the coarsest populations (mean: 0.3, multimodal with narrow main peak at ca. 50 µm) showed opposite trends to EM1. Both endmembers contributed roughly 63% to the total clastic sediment input. EM3 (mean: 0.36, broad modes between 11 µm and 25 µm), comprising the finer populations, fluctuated too and displayed highest loadings in the upper part of core KH 12 (15-42 cm), middle part (127-190 cm) and close to the end of the core (255-260 cm).

In KH 13 (Fig.20 C, Tab.4), EM 1 (mean loading: 0.42, bi-modal at 11 µm and 80-200 µm) increased from 0 to 0.6 at 2-14 cm depth, then fluctuated between 0.3-0.8 until 86 cm depth and experienced low values, followed by a sharp decrease down to 0 until 130 cm. a sharp rise to values of up to 0.8 followed afterwards until 144 cm depth, followed by stronger fluctuations between 0.2 and 1 down-core. EM2 (mean: 0.08, multimodes at ca-65-90 µm, 200 µm and 400 µm) occurred only occasionally at few depths but with higher amounts between ca. 110-130 cm depth Very low loadings are recorded for the lower part of the core. EM3 (mean 0.3, broad unimode, peaking at 25 µm fluctuated with decreasing trend from the upper part down to 86 cm depth, followed by a slight increase to 0.9 at 106 cm depth and remained on a relatively high level down-core with peaking values up to 0.9 at 205 and 209-212 cm depth.

In KH 14 (Fig.20 D, Tab.4), EM1 (mean: 0.46, unimode at 10µm) displayed a general decreasing trend from high values near the top (loading 1) to 0.6 at ca 85 cm depth, followed by lowest values (<0.4-0) at 95-110 and 120-131. Afterwards fluctuations on a higher loading level occurred until 220 cm depth, followed by a second strong decrease, even to zero values between 240 and 260 cm depth. EM2 (mean: 0.24, unimode at 35 µm) generally showed less contribution but with significantly higher values at depth where EM1 experience lowest loadings Highest amount were recorded in the lower part of the core. EM3 (mean: 0.3, bimodal at 5 µm and 60 µm) varied between 0-0.7 through the core. Zero values occurred at different parts of the core.

5.4.3 Ostracod associations and their distribution in cores KH 11-17 and sections

Five species of ostracod were identified in sediment cores from Kuhai Lake and catchment locations (Fig.16, Tab.5, appedndix II 4), which are *Eucypris mareotica* (Fischer, 1855), *Limnocythere inopinata* (Baird, 1843), *Fabaeformiscandona rawsoni* (Tressler, 1957), *Ilyocypris* spec. and *Tonnacypris edlundi* (Van der Meeren et al., 2009). However, *Eucypris mareotica* and *Limnocythere inopinata* are the most abundant ones.

Eucypris mareotica occurred only in lake sediment samples and some section samples (KHS 1 and KHS 27, 1 fragment in KHS 29, also see chapter 5.5, Figs.23-24, 26) with generally low amounts. This species was not found in the seven investigated ponds and near-shoreline wetlands.

E. mareotica was almost the dominant species in lake sediment cores. However, its occurrence within the cores varied considerably through depth (Fig.21, Tab.5). In KH 11, *E. mareotica* was uniquely dominant at 10-58 cm, 150 cm, 154 cm, 186 cm and 218 cm, while not found at 62-134 cm, 158-178 cm and 190- 214 cm (Fig.21 A).

In KH 12, this species was recorded as dominant species with some fluctuations at the upper 82 cm sediment depth, followed by alternations between appearance and disappearance between 86 cm- 216 cm. From 220 cm down-core it occurred as a unique species, interrupted by ostracod-free sequences at 252 cm, 256 cm and 264 cm depth (Fig.21 A).

In core KH 13, the higher resolution of 1 cm records show distinct distribution phases (Fig.21 A). *E. mareotica* occurred from 9 cm on with abundance until 80 cm depth. From 81 cm onward, it alternated from high abundances to no-occurrence until the end of the core.

In KH 14 (Fig.21 A), *E. mareotica* did not occur as frequently as in KH 13, despite a lower resolution (2 cm intervals). It only occurred in few samples between 7 and 17 cm core depth, followed by the high abundances until 50 cm). Afterwards, *E. mareotica* was occasionally present in very low amounts until 229 cm depth (<100 valves), except for depths between 121 cm and 123 cm depth. Higher, but variable abundances were recorded

for the sequence between 231 and 265 cm depth, while no ostracod were found in the last 10 cm of the core.

Although the cores KH15-KH17 are not in the focus of this study, ostracod analyses were also performed to demonstrate differences in occurrence and abundance at these sites (Fig.21 B). In core KH15 (Fig.21 B), *E. mareotica* occurred continuously from 8 to 18 cm, while from 24 cm on, it alternated between dominance and disappearance down to 134 cm depth and disappeared afterwards and showed highest abundance in the last sample of the core at 232 cm depth.

In KH 16 (Fig.21 B), *E. mareotica* showed higher abundance from 1-63 cm, followed by strong fluctuations (between 0- 100 %) until 171 cm depth, followed by continuously high abundances until the end of the core in 217 cm depth.

Low frequency and abundances of *E. mareotica* in KH 17 (1 cm resolution; Fig.21 B) are recorded for the upper part of the core until 236 cm depth, followed by a continuous dominance until 261 cm. No ostrcods however, were found between 247-249 cm depth. From 262 cm to 288 cm depth *E. mareotica* occurred in the range of 15-70%, disappeared afterwards until 421 cm (except for 406 cm depth with low relative abundance), and displayed highest frequencies until 578 cm depth. In the lowermost part of the core *E. mareotica* was not present, except for low rel. abundances (less than 100 valves) at 601, 606, 617 and 672 cm depth).

Limnocythere inopinata was found in different types of samples (pond/wetland and core sediment samples) with strong differences. In lake sediment cores KH 12, KH 13, KH 16 and KH 17 (Fig.21 A, B), several samples at different sediment depths contained *L. inopinata*, while only found in one sample in the upper parts of cores of KH 14 and 15. *L. inopinata* was the dominant species but in low amounts in cores KH11 and KH12 at around 102, 118, 138 and 182 cm core depth (KH11) and at 70, 78, 96, and 176 cm core depth (KH12), respectively. This species occurred only partly together with *E. mareotica* (Fig.21 A, Tab.5). High abundances of *L. inopiniata* were recorded in core KH12 at 192 cm and 212 cm. In core KH13 only nineteen samples contained *L. inopinata* with dominance only in the lower part (206-218 cm) of the core. Interestingly, only one sample containing *L. inopinata* was found in cores KH14 (14 cm depth) and KH15 (17 cm depth), both occurring together together with *E. mareotica*.

In KH 16, *L. inopinata* occurred more frequently throughout the core. Between 1-3 and 31-37 cm depth it was found together with *E.mareotica*. Higher abundances with discontinuous distribution were recorded from 37 cm down to 179 cm core depth and disappeared afterwards.

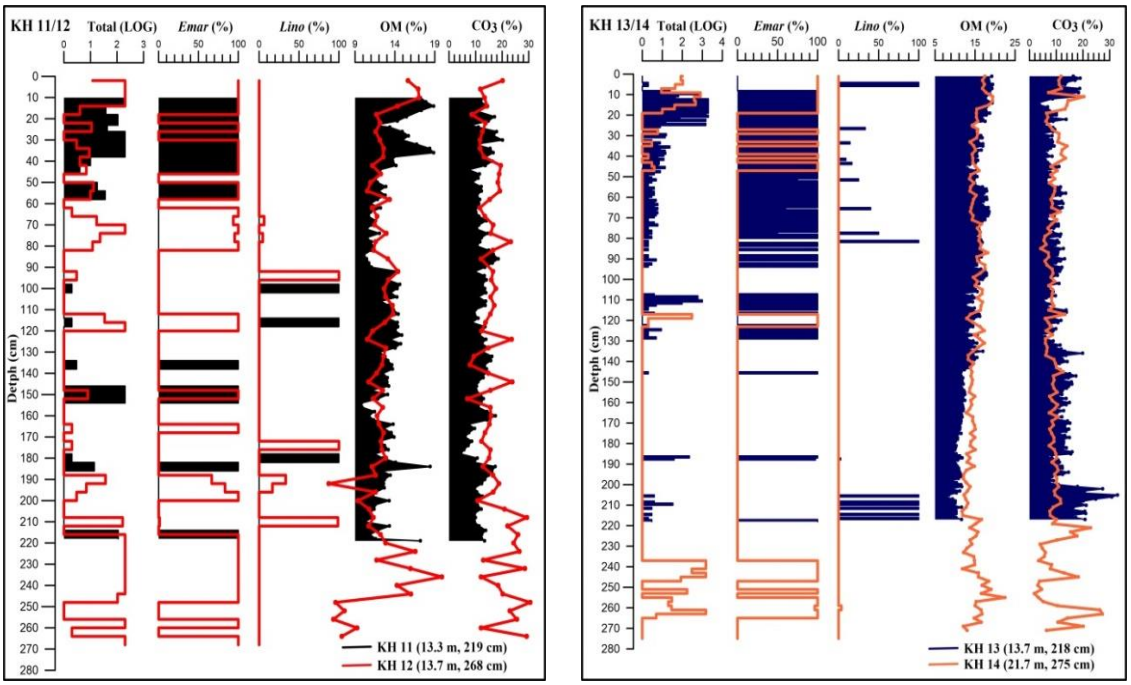

Fig. 21A Ostracod distribution, organic matter (OM) and carbonate (CO_3) content in cores KH11, KH12, KH13 and KH14, Kuhai Lake. *Emar= Eucypris mareotica*; *Lino= Limnocythere inopinata*.

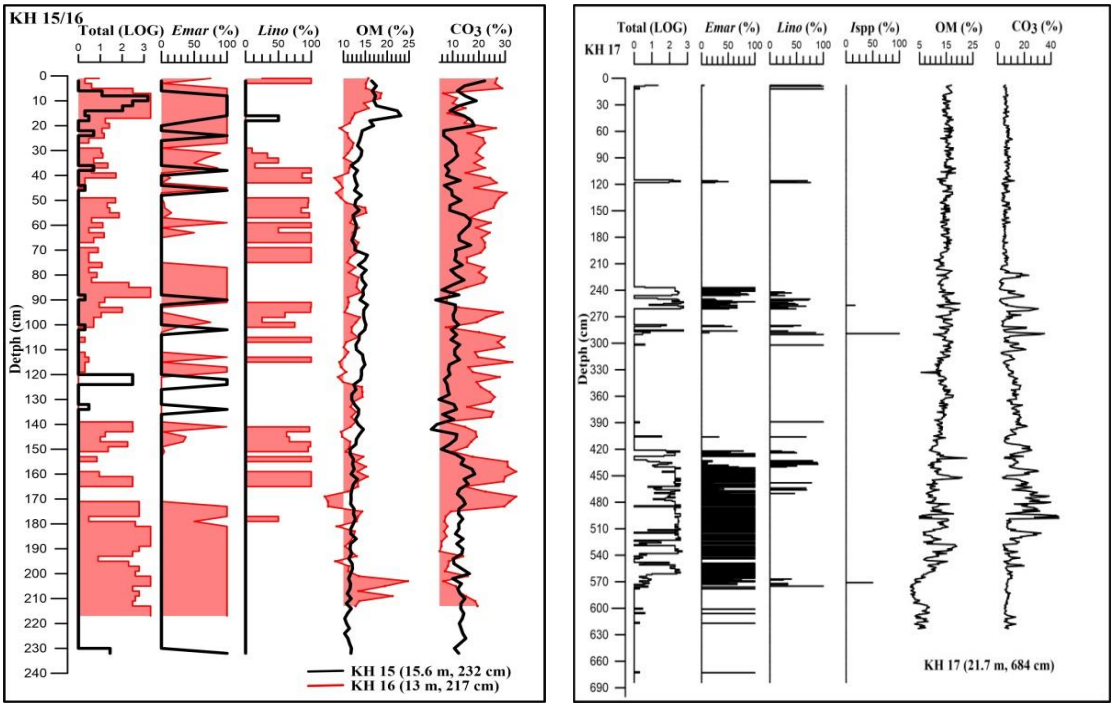

Fig. 21B Ostracod distribution, organic matter (OM) and carbonate (CO_3) content in cores KH15, KH16 and KH17, Kuhai Lake. *Emar= Eucypris mareotica*; *Lino= Limnocythere inopinata; I*spp= *Ilyocypris* spec.

Tab. 5 Occurrences of ostracods in samples in Kuhai Lake basin. **A.** cores; **B.** sections; **C.** ponds/wetlands.

A.

Core ID	*Eucypris mareotica* Depth of occurrence	*Limnocythere inopinata* Depth of occurrence
KH 11	10--58	102/118
	138	138
	150--154	
	186	182
	218	
KH 12	2--18	
	26	
	34--46	
	54--58	70
	66--82	78
	116-120	96
	152	
	168	
	176	
	192-200	192-196
	212	212
	220-248	
	260	
	268	
KH 13		5--6
	9--31	27
	33--46	34
	48--80	42/44/52/66/78
	83--84	82
	86	
	89--91	
	93--94	94
	108--115	110
	117	
	123	
	125--129	
	146	
	187--188	188
	218	206/209/210/212/215/217
KH 14	7--17	17
	23/37/45/89	
	101/121/123/133	
	231	
	239--247	
	253	
	257--265	
	Occurred with *E. mareotica*	

Sample ID	Depth (cm)	*Emar*	*Lino*	*Ispp*	*Fraw*
KHS1-1	6-10	0	0	0	0
KHS1-2	25-28	0	0	0	0
KHS1-3	31-35	0	5	0	0
KHS1-4	40-45	2	9	0	0
KHS1-5	48-50	0	0	0	0
KHS1-6	52-54	0	0	0	0
KHS1-7	54-56	1	1	0	0
KHS1-8	56-58	1	0	0	0
KHS1-9	60-66	1	1	0	0
KHS1-11	70-75	1	15	0	0
KHS1-13	93-97	0	4	0	0
KHS1-14	130-135	0	20	0	0
KHS1-16	151-156	0	48	0	0
KHS27-1	0-10	0	2	0	0
KHS27-3	20-30	0	18	0	0
KHS27-5	40-50	3	29	1	23
KHS27-6	50-60	0	10	3	45
KHS27-7	60-65	0	0	0	0
KHS27-8	65-70	0	1	0	0
KHS27-9	70-75	0	1	0	0
KHS27-10	75-80	0	72	0	0
KHS27-11	80-85	0	4	0	0
KHS27-12	85-90	0	2	0	0
KHS27-13	90-95	0	38	2	0
KHS27-14	95-100	0	36	17	44
KHS27-15	100-105	0	13	16	18
KHS27-16	105-110	0	1	2	8
KHS27-17	110-120	0	22	6	26
KHS27-18	120-130	0	0	0	1
KHS29-1	0-10	0	0	0	0
KHS29-2	15-20	0	0	0	0
KHS29-3	25-30	0	0	0	0
KHS29-4	35-40	0	0	0	0
KHS29-5	45-50	0	0	0	0
KHS29-6	55-60	0	0	14	0
KHS29-7	65-70	0	0	0	0
KHS29-8	75-80	0	0	12	0
KHS29-9	80-85	0	0	0	0
KHS29-10	85-90	0	0	0	0
KHS29-11	95-100	0	0	0	0
KHS29-12	105-110	0	0	0	0
KHS29-13	120-125	0	0	0	0
KHS29-14	130-135	0	4	6	0
KHS29-15	135-140	0	0	0	0
KHS29-16	145-150	0	0	1	0
KHS29-17	150-155	0	0	4	0
KHS29-18	158-166	1(f.)	2	1	0
KHS29-19	166-170	0	0	0	0
KHS29-20	170-174	0	0	2	0
KHS29-21	174-178	0	0	0	0
KHS29-22	190-195	0	0	0	0
KHS29-23	195-200	0	18	0	0
KHS29-24	215-220	0	0	0	0

B. *Emar=E. mareotica; Lino=L.inopinata; Ispp= Ilyocypris spec.; Fraw=F.rawsoni*

C.

Sample ID	Latitude (N)	Longitude (E)	*Ilyocypris* sp.	*Fabaeformiscandona rawsoni*	*Limnocythere inopinata*	*Tonnacypris edlundi*	Notes	Other organisms
KHPS1	35°19.622'	99°13.055'	8	2	1	1		
KHPS2	35°15.441'	99°09.551'	0	1	0	0		
KHPS3	35°15.373'	99°09.619'	0	0	8	0		
KHPS4	35°15.438'	99°09.580'	0	0	0	0		
KHP5-S1	35°15.299'	99°09.735'	0	0	0	0	0-8 cm	
KHP5-S2	35°15.299'	99°09.735'	0	0	0	0	0-1 cm	
KHP6-S1	35°16.275'	99°07.954	42	16	4	0	0-0.5 cm	*Pisidium* sp.
KHP6-S2	35°16.275'	99°07.954	144	42	7	0	0.5-6 cm	*Potamogeton* sp.; *Pisidium* sp.
KHP7-S1	35°15.700'	99°09.375	0	0	0	0	0-0.5 cm	*Chenopodiacea* sp. and other plant fruits
KHP7-S3	35°15.700'	99°09.375	0	2	0	0	0-5 cm	*Chenopodiacea* sp. and other plant fruits

In core KH 17(Fig.21 B), *L. inopinata* occurred in the upper part of the core between 8 and 12 cm depth, again at 116-118 cm and discontinuously between 242-261 cm core depths, generally with low relative abundances. Similar occurrences were found between 390 and 575 cm core depth. No ostracod were recorded in the lower part of the core until

684 cm final depth. *Fabaeformiscandona rawsoni* was only found in five pond samples and in the section of KHS 27(see chapter 5.5, Figs.23, 25, 26; Tab.5).

Ilyocypris spec. was identified in 3 pond/wetland samples, sections samples (KHS 27 and KHS 29, see chapter 5.5, Figs.25, 26, Tab.5) and in the middle part of the long sediment core KH 17 (at 263 and unique at 295 cm with low amount).
Tonnacypris edlundi was only found (one valve) in a sample from the near-shore wetland (lagoon) at site KHPS 1 (Fig.4, Tab.5).

5.4.4 Organic matter and carbonate distribution in cores KH11-14

Organic matter (OM) and total carbonate (shown as CO_3) were measured for all sediment cores KH11-KH14, The data are presented in Fig.21 A (chapter 5.4.3) to which the following description is referred to:

In KH 11, a distinct decrease (from 19% to 11 %) of OM in the upper part of the core (0-85 cm depth) followed by a sudden increase to around 14% and remained on this level with slight fluctuations and a general decreasing trend core downwards. Total carbonate (CO_3) fluctuated between 6% and 20%, with peaking values of up to 20% in the upper 40 cm of the core. Lowest values (down to 7%) were recorded in the lower part of the core at 165-180 cm depth. Carbonate showed a partly opposite trend compared with OM.

OM in core KH12 revealed a comparable trend as in core KH11 but with stronger fluctuations and relatively low values (<10%) between 20 and 85 cm depth, at 192 cm (6%) and at the end of the core between 250 and 270 cm depth (<6%). Total carbonate (CO_3) fluctuated on a level between 7 and 20%, until 205 cm depth similar to core KH11 and largely opposite to OM. Afterwards carbonate increased to higher levels, reaching 30% as maximum value at 250 cm depth.

Differently from the previous cores, OM in core KH 13 showed a more distinct decreasing trend from high values at the top (19%) down-core to ca. 11% at the base of core KH13. Slight fluctuations with a generally higher level (15-18%) occurred between 55 and 140 cm depth, followed by a relatively abrupt change to 12% OM with continuing decrease afterwards. Total carbonate ($CO_{3)}$ values changed within a range of 3-19%. High values at the top 15 cm (up to 19%) followed an abrupt decline to 4% and afterwards a general increase until 129 cm depth to 10%. A sudden higher level (mean: 14%), until 202 cm depth could be recognized, followed by a sequence of increased values down-core to >30% (mean: 27%, 202-220 cm depth).

In KH 14, similar trends of OM as in core KH13 were recorded. Abrupt increasing values up to 24% after 215 cm depth followed until the end of core KH14. Total carbonate (CO_3) showed similar changes to OM, while repeatedly distinct fluctuations between from 3% to 27% occurred in the lower part of the core from 250 cm down to the end.

5.5 Stable isotopes in lacustrine sediments and modern water

5.5.1 Distribution of stable isotopes $\delta^{18}O$ and $\delta^{13}C$ in cores KH11-KH14

Stable oxygen and carbon isotopes were measured on authigenic carbonate, as revealed by XRD analyses (see chapter 5.3.4 and chapter 5.4.1) Due to different carbonate facies in all cores, reaction time for ICP-MS measurements at Leibniz Laboratory for stable isotope research; University of Kiel, was adapted to the different minerals, such as MHC, Aragonite and Dolomite/High-Mg calcite. Oxygen isotopes ($\delta^{18}O$, reported in VPDB) of lake carbonate in core KH 11 ranged between -4.9 to1.7‰, while -4.0 to 2.0‰ in KH 12, -5.9 to 2.0‰ in KH 13 and -6.4‰ to 2.7‰ in KH 14. Fluctuations of values among each core were surprisingly high, compared with other isotope records in adjacent regions of the Tibetan Plateau (Lister et al., 1991; Henderson et al., 2010; Zhang and Mischke, 2009; An et al., 2012; Yan and Wünnemann, 2014). Maximum differences were recorded in core KH14, accounting for 9.16‰, lowest occurred in core KH12 (6‰). Compared with mean values in surface samples (the last 15 years) isotopic values in cores varied considerably through time (Tab.6)

Values of $\delta^{13}C$ (reported in VPDB) in KH 11 and KH 12 varied with 0.04 - 3.4 ‰ and 0.2 -6.4‰, respectively, while -0.7‰ - 2.5‰ and -4.0‰ - 2.7‰ were recorded in cores KH 13 and KH 14. Similar to $\delta^{18}O$ values, larger differences among the $\delta^{13}C$ values of each core were notable. They ranged between 3.2‰ in KH13 and 6.7‰ in KH14 as the minimum and maximum values (Tab.6).

Tab.6 Isotope values in surface samples and cores, Kuhai Lake.

Site	$\delta^{18}O$ (‰ VPDB)				$\delta^{13}C$ (‰ VPDB)			
	Mean	Max.	Min.	Range	Mean	Max.	Min.	Range
Surface sed. around KH11	0.51				2.00			
Surface sed. around KH12	0.29				1.46			
Surface sed. around KH13	-2.53				1.85			
Surface sed. around KH14	-0.92				1.39			
KH11	-1.86	1.69	-4.88	6.57	1.43	3.44	0.039	3.48
KH12	-0.64	2.01	-4.00	-6.01	1.75	6.39	-0.18	-6.56
KH13	-1.57	2.02	-5.93	-7.95	1.29	2.54	-0.67	-3.21
KH14	-2.09	2.74	-6.42	-9.16	0.03	2.70	-4.01	-6.70

The distribution of stable oxygen and carbon isotopes for each core against depth (Fig.36) is described below:

In KH 11, $\delta^{18}O$ values in the upper 40 cm ranged around +2‰ with a very low value of -3.4‰ at 23 cm depth. A sequence of low values (around -2‰) occurred between 40 and 80 cm depth, followed by heavier values (ca. 0‰) until 110 cm depth. Down-core, all values remained below 0‰ with more negative peaks (-4.7‰ and -3.7‰) at 178 and 210 cm depth.

$\delta^{13}C$ fluctuated in the upper part of the sediment core (0-120 cm) between 3‰ and 1‰, followed by relatively constant values around 2‰ until the end of the core.220 cm depth and a strong increase towards heavier values (up to 7‰) until 230 cm depth. Towards the end of the core, $\delta^{13}C$ returned back towards low values down to 0‰.

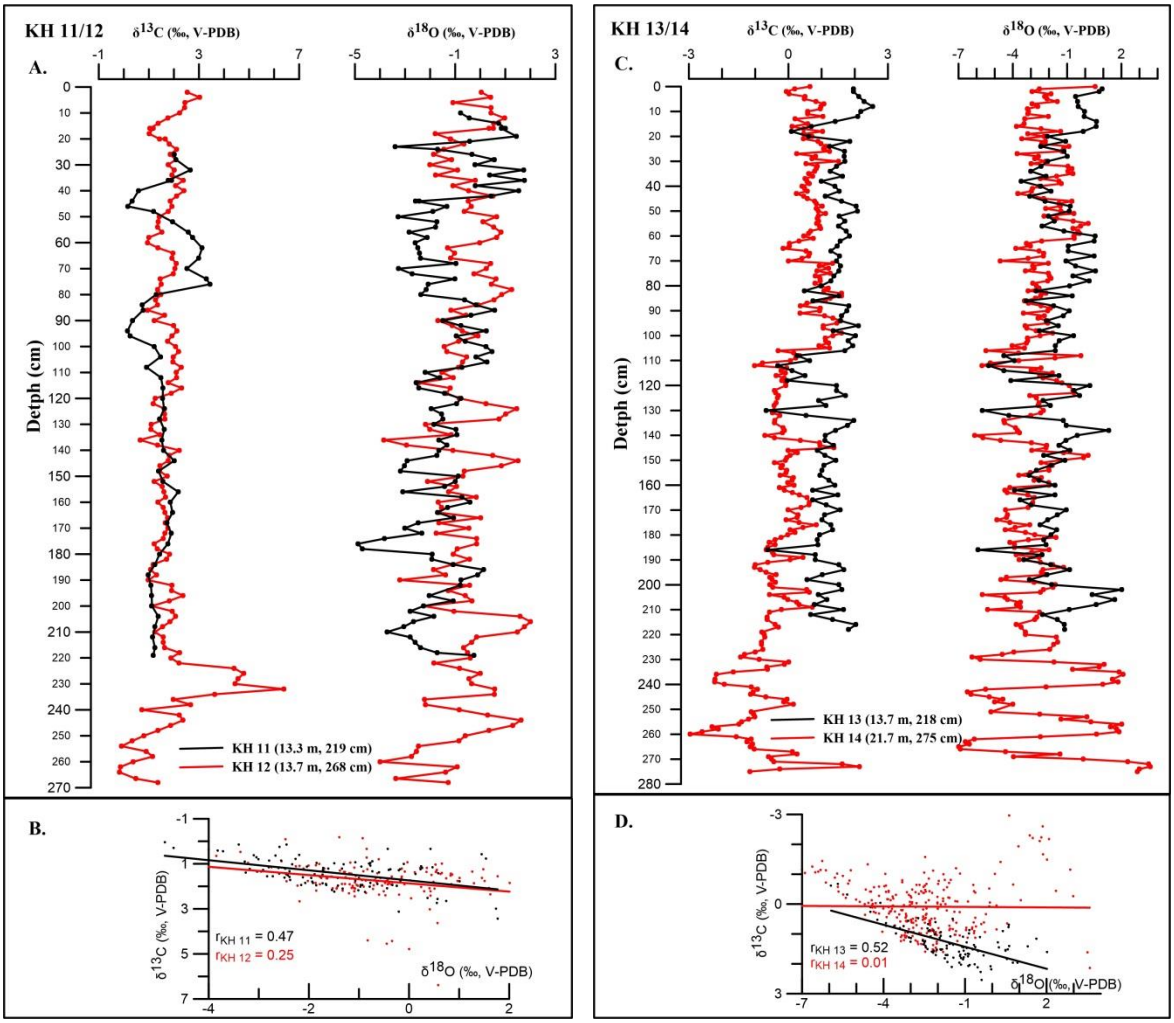

Fig. 22 Stable isotopes ($\delta^{18}O$, $\delta^{13}C$) in sediment cores KH11/KH12 (A) and KH13/14 (C) against depth. Correlations between carbon and oxygen isotopes for all cores are shown below (B, D).

Oxygen isotopes in KH 12 fluctuated differently, partly opposite to those in KH11 and ranged between -4‰ and 2‰. Heavier values of up to 2‰ occurred in 80, 120, 145, 210 and 240 cm depth. Most negative values were recorded for the lower part of the sediment core at 260 cm depth (-4‰).

Carbon isotopes of sediments in core KH12 fluctuated much less than those in core KH11 and remained almost constant (1-2‰) until about 220 cm depth. Afterwards a strong increase towards heavier values (up to 7‰) until 230 cm depth was recorded, followed by a return towards low values down to 0‰.

In KH 13, $\delta^{18}O$ and $\delta^{13}C$ displayed two distinct stages of changes. The first one showed a decreasing trend from top to 112 cm depth and ranged between -5.4 and 1 ‰ ($\delta^{18}O$) and -0.3 -2.5 ‰ in $\delta^{13}C$. The second stage showed a general slight increase of both values.

Oxygen isotopes in core KH14 showed comparable variations as in core KH13, although slight differences were visible. In general $\delta^{18}O$ decreased slightly from top down to 220 cm depth with an excursion of lower values (-3.7‰ to -5.2‰) between 130 and 140 cm depth, similar to KH 13. Afterwards (200-275 cm depth) strong fluctuations from very heavy values (up to +3‰) to lowest values (-6.4‰) occurred frequently.

Variations in $\delta^{13}C$ followed the trends described for core KH13. Stronger fluctuations within a range of >7‰ for $\delta^{18}O$ and ca 5‰ for $\delta^{13}C$ could be observed in the lower part of core KH14.

Correlation coefficients between $\delta^{18}O$ and $\delta^{13}C$ in KH 11 and KH 12 were r=0.47 and r=0.25, while in KH13 highest coefficient of r=0.52 was recorded. In KH 14 the values scattered in a very wide range, resulting in almost no correlation (Fig.22 B, D).

5.5.2 Stable isotopes $\delta^{18}O$ and δD in water samples

Rain/snow, river and lake water (including a vertical water profile in the center of the lake at 20 m water depth) was applied to isotope analysis too (values are reported in VSMOW). $\delta^{18}O$ values of rain (in late June 2016) varied between -0.3‰ and -4.6‰, with δD values of -12.2‰ to -24.9‰. In early June, snow isotope values reached -11.4‰ (-78.9‰ δD). Meanwhile, values of river water in Kuhai catchment varied between -10.28 and -11.46‰ ($\delta^{18}O$), and -66.9‰ to -78.9‰ for δD (early June 2015).

Values of lake water taken in early June 2015 reached values of -0.95‰ and -1.41‰ in late June 2016 between -0.1‰ and -0.27‰ (both $\delta^{18}O$). Corresponding δD values were -22.49- -23.98‰ and -23.31-24.09‰, respectively. Lake water down to the bottom of the lake ranged between -0.1‰ and -1.1‰ and thus showed minor variations throughout the water column (Fig.23). Water isotopes in near-shore locations and isolated ponds ranged in early June 2015 between -4.38‰ and -9.05‰ (-30.23 to -52.68‰ in δD). As comparison, isotope data from Donggi Cona adjacent to Kuhai Lake were added in Fig. 23, consisting of lake, river and near-shore pond waters as well as rainfall, all from late June-early July 2016.

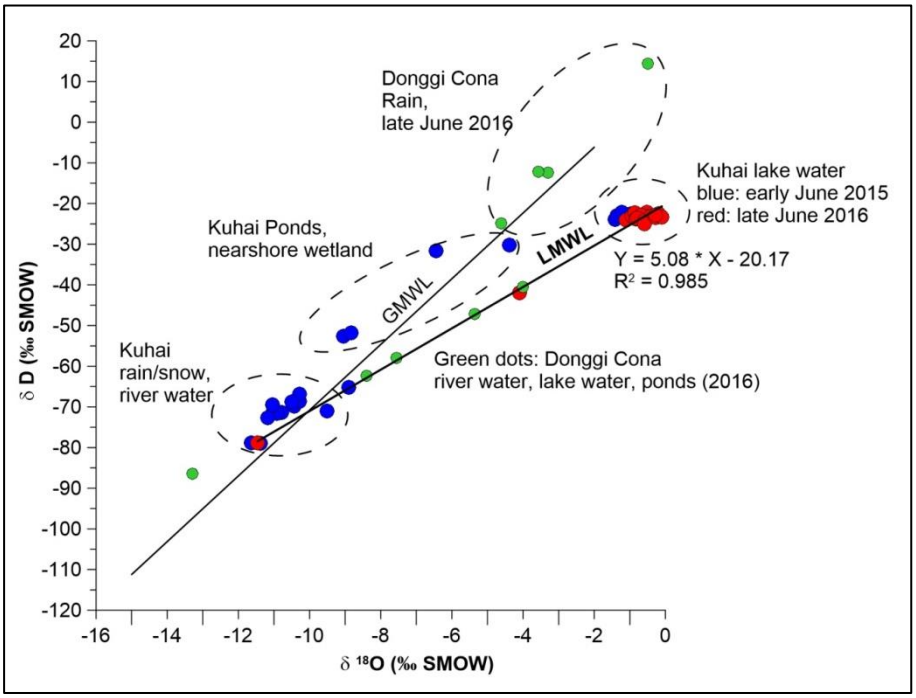

Fig. 23 Stable isotopes ($\delta^{18}O$, δD) in water samples of Kuhai Lake area.

5.6 Sediments in onshore regions of Kuhai Lake catchment

In total 30 sections were investigated for catchment studies. Twenty-nine of them were analyzed in detail, separated into three groups (Figs.24-37, Tab.7):
i) sections containing lacustrine and/or nearshore-deposits, dated by AMS-^{14}C (KHS1, KHS27, KHS29),

ii) sections containing aeolian deposits dated by OSL (KH 4, KHS 6, KHS7, KHS13, KHS15, KHS17, KHS25 and KHS 2) and

iii) sections without chronological control are presented in the appendix II 5, but grain size distribution curves were included in individual appendix II 5.

5.6.1 Sections with lacustrine/near-shore deposits

5.6.1.1 Section KHS 1

This section was dug across the 2.24 m high lower terrace down to the modern river bed of the perennial river, located southeast of lake. It consisted of lacustrine/floodplain and fluvial sediments. Well-sorted fine sand (Fig.4; Fig.24) with ripple structures was distributed in one branch of the modern river bed (ca. 1 m above the modern lake shore), indicative of material that could be transported as suspended load together with finer components during turbulent flow periods, contributing to the lake's sediment budget.

Sampling from top to bottom refers to the sequences below the 30 cm thick soil layer on top of the section (Fig.25). Detailed description from top to bottom in KHS 1 is as follows:
Top of section to surface: 30cm;

0-23 cm:	brownish sandy clay, homogenous, modern roots
23-30 cm:	clay, grayish; homogenous, modern roots
30-48 cm:	brownish fine sand, homogenous; modern roots
48-51cm:	grayish clay with oxidation dots, homogenous, modern roots
51-54 cm:	brownish fine sand, oxidation dots, homogenous, modern roots
54-56 cm:	grayish clay
56-58 cm:	grayish clay, oxidation dots
58-66 cm:	brownish fine sand, oxidation dots
66-70 cm:	gravel flat-sized, up to 1 cm in diameter, fine brownish sand, modern roots
70-93 cm:	brownish sand, grayish clay, layered, 2 cm thickness for each 70-78 cm: permafrost boundary; 78-81~82 cm: organic-rich clay
93-97 cm:	clay, oxidized features
97-118 cm:	gravels flat-sized, up to 3 cm in diameter, finer in the lower part
118-124 cm:	fine sand and fine gravels up to 3 mm in diameter
124-143 cm:	grayish clay, homogenous, plenty of organic remains
143-144 cm:	gravel, 4 mm in size
144-151 cm:	grayish clay, homogenous

151-156 cm: brownish fine sand
156-163 cm: grayish clay, organic-rich
163-164 cm: brownish clay, oxidation features
164-194 cm: coarse gravels, 5 cm in diameter

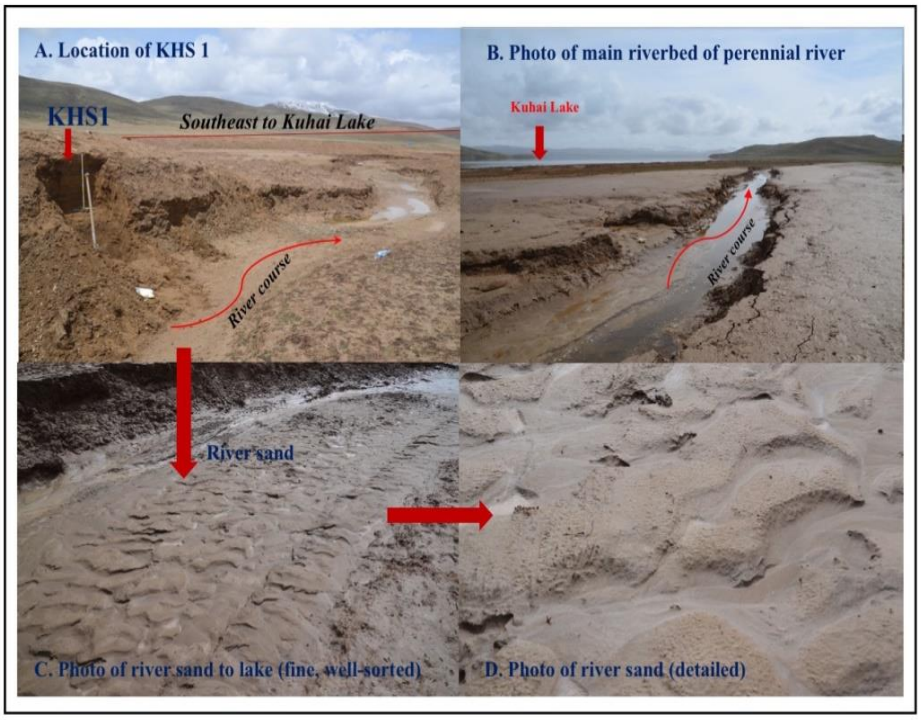

Fig. 24 Photos of sediment in the perennial river where section KHS 1 is located.

Two ostracod species (*Eucypris mareotica* and *Limnocythere inopinata*) were found in several parts of the section (see chapter 5.4.3).

Grain size of sediment in KHS 1 ranges from silt (modes between 15 and 35 µm) to fine sand mean mode: 105 µm, Fig.25 A). Organic matter and carbonate ($CaCO_3$) range between 2-15% and 9-14 %, respectively (Fig.25). High values of organic matter and low value of carbonate both occur at 135 cm depth in the lower part of the section. Three selected lacustrine sediment samples from 81-82 cm, 135 cm and 157 cm were dated to 687±24 cal. yr BP, 11485±72 cal. yr BP and 2798±47 cal. yr BP, respectively (Fig.25, Tab.2).

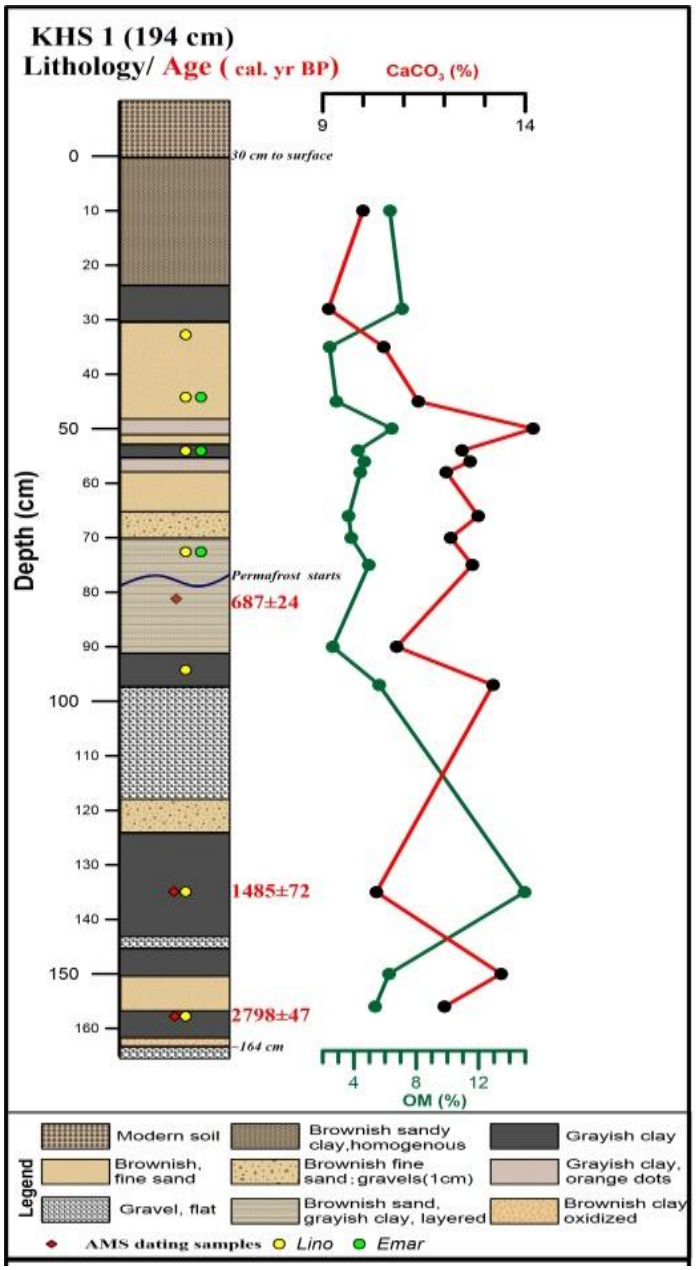

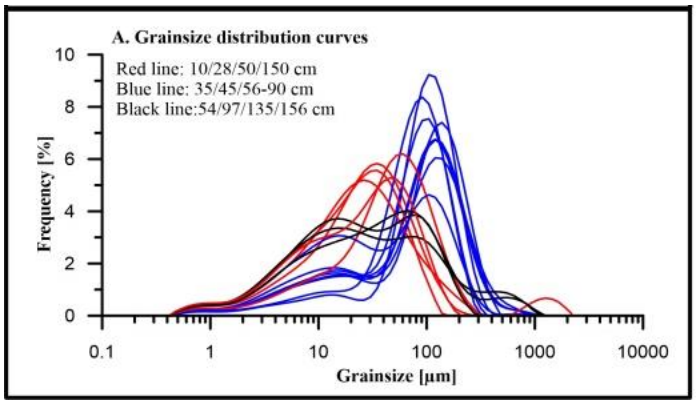

Fig. 25 Photo of KHS 1 (left) and its lithology, chronology, geo-chemical and sedimentological characteristics (right).

5.6.1.2 Section KHS 27

This section was located in the south-eastern bay of Kuhai lake within the inflow of a drainage from the wetland farther west (Fig.4). Lacustrine sediments were exposed here reaching up to 2 m above the modern lake level (see also Fig.2). The total height of KHS 27 was 1.3 m with frozen sediments (permafrost) at the bottom, 50 cm above the water level (Fig.26).

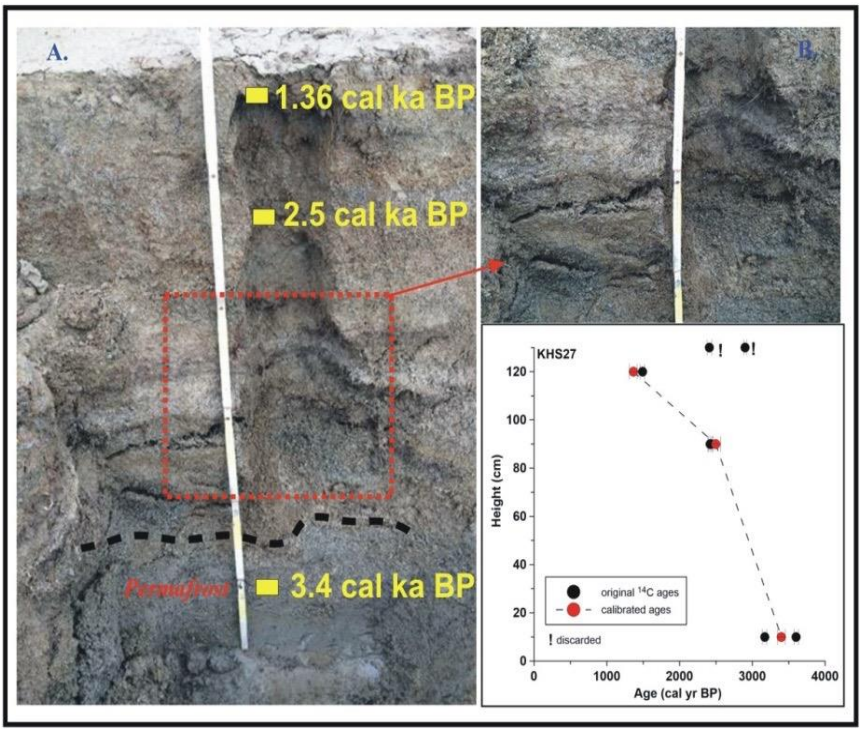

Fig. 26 Section KHS27, south-east of Kuhai Lake. Lacustrine sequences (A) with detail (B) containing high organic matter (plant remains) and age-depth model (lower right). Permafrost boundary to annually unfrozen mollisol is at ca. 30 cm height (from bottom).

The section completely consisted of lacustrine clayey to silty mud, intercalated by numerous layers of plant remains (mainly seagrass). Totally 4 species of ostracod (*L. inopinata*, *Eucypris mareotica*, *Ilyocypris* sp. *Fabaeformiscandona rawsoni*) were found in this section (see chapter 5.4.3). The topmost part consisted of several desiccation cracks and a thin salt crust on the surface. Lithology described from top to bottom is as follows:

112-130 cm: light gray clayey silt, occasionally sand lenses, desiccation crack, salt (halite) on top
110-112 cm: silty clay, dry with some seagrass on top;
85-110 cm: brownish grey silty clay;
75-85 cm: grayish brown silty clay, few organic remains
70-75 cm: dark brown silty clay rich in organic matter harder material
65-70 cm: light gray silty clay, crumbly, some organic matter, thin carbonate layers)
60-65 cm: light brownish crumbly silty clay, organic material
50-60 cm: dark brownish silty clay, plenty of organic material, crumbly structure

45-50 cm: brownish silty clay, crumbly, plant remains
30-45 cm: grayish silty clay, crumbly, plant remains, lower part contains ice lenses (30-35cm)
0-30 cm: grey clay-silt, sand lenses, black dots (organic matter), frozen (permafrost).

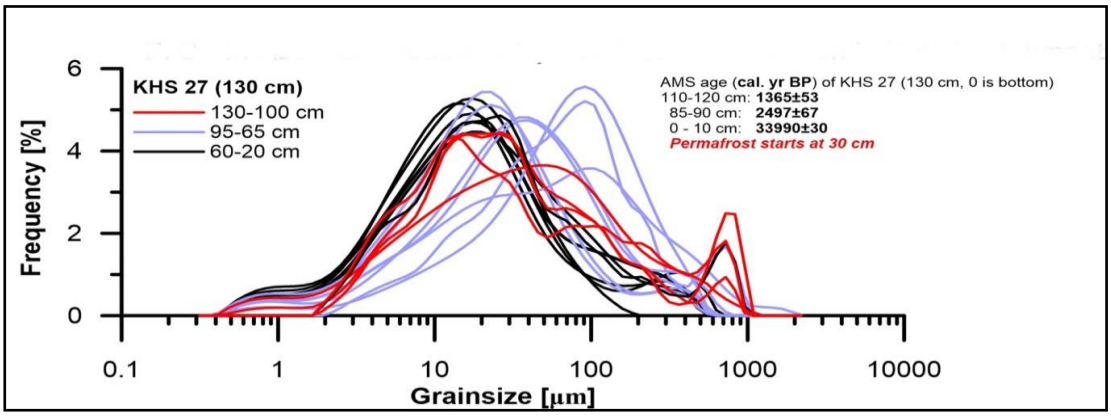

Fig. 27 Grain size distribution curves of samples from section KHS27.

In general, organic matter varied between 8-20 %, but was considerably higher within layers of plant remains, while carbonate ranged from 10 to 45 %. Modes of grain size in KHS 27 ranged from 10 µm (silt fraction) to 150 µm (fine sand fraction). Some samples in the lower section mainly consisted of silt but also coarse sand (mode > 630 µm, Fig.27). Four samples from different depth were dated by different fractions (Tab.2), three of them were used for the age model (Fig.26) without applying a potential reservoir error (RE), as references ages as a base for assuming a RE could not be achieved. According to Tab.2 and Fig.24, the used three samples dated to 1365 ± 53 cal. yr BP (110-120 cm), 2497 ± 67 cal. yr BP (85-89 cm) and 3399 ± 53 cal. yr BP (0-10 cm).

5.6.1.3 Section KHS 29

This naturally exposed section with 225 cm in height was located at the river bank (terrace) closed to the river mouth of an episodic river at the northeastern part of the lake (Fig.4; Fig.2). The top of KHS 29 was 300 cm higher than the present lake level, measured by tachymeter in 2016. Detailed description from top to bottom is as follows (Figs.28, 29):

Top: grassland
210-225 cm: mixed layer of sand, silt, gravel (surface), soil
200-210cm: sandy gravel (190-top modern roots)
190-200 cm: gray clayey-silty sand
178-190cm: gravelly sand poorly sorted, gravels up to 3cm in diameter, loose
174-178cm: gravelly sand mixed with sea grass, layered
166-174cm: gray sandy silt with clay lenses
156-166cm: coarse gravel (<1 cm in diameter), partly flattened, well sorted
140-156cm: layered mainly fine sand, silt partly crossed-bedded (fluvial)

130-140 cm: sand, gravel, angular to sub-rounded (fluvial)
116-130 cm: gray clayey silt and yellow-red fine sand (boundary is oxidized)
110-116 cm: gravelly sand
85-110 cm: silty-sandy clay
52-85 cm: sand, silt-lay layers, slightly deformed, not continuous (58-72 cm sandier)
0-52 cm: sand, gravel mixed with gray clay
Bottom: very coarse and angular-shaped metamorphic rock fragments

Organic matter ranges within 4-15 %, while carbonate ($CaCO_3$) reached values between 10 and 20 %. Highest organic matter occurred at the layer of seagrass (aquatic plant, Fig.26 B). Two ostracod species (*Limnocythere inopinata* and *Ilyocypris* sp.) were found in several sequences, as shown in Fig.16 (see also chapter 5.4.3).

Grain size ranged from 6-600 µm, with differentiation of 3 EMs through the whole section. Four organic-rich lacustrine sediment samples were dated to 1377 ± 48, 3285 ± 76, 4717 ± 64 and 4909 ± 63 cal. yr BP at 174-178 cm, 130-135 cm, 80-85 cm and 55-60 cm, respectively (Fig.29). Cryoturbation features occur at 85 cm height in KHS 29 but more obvious in a river bank section opposite of KHS29 (Fig.28 B).

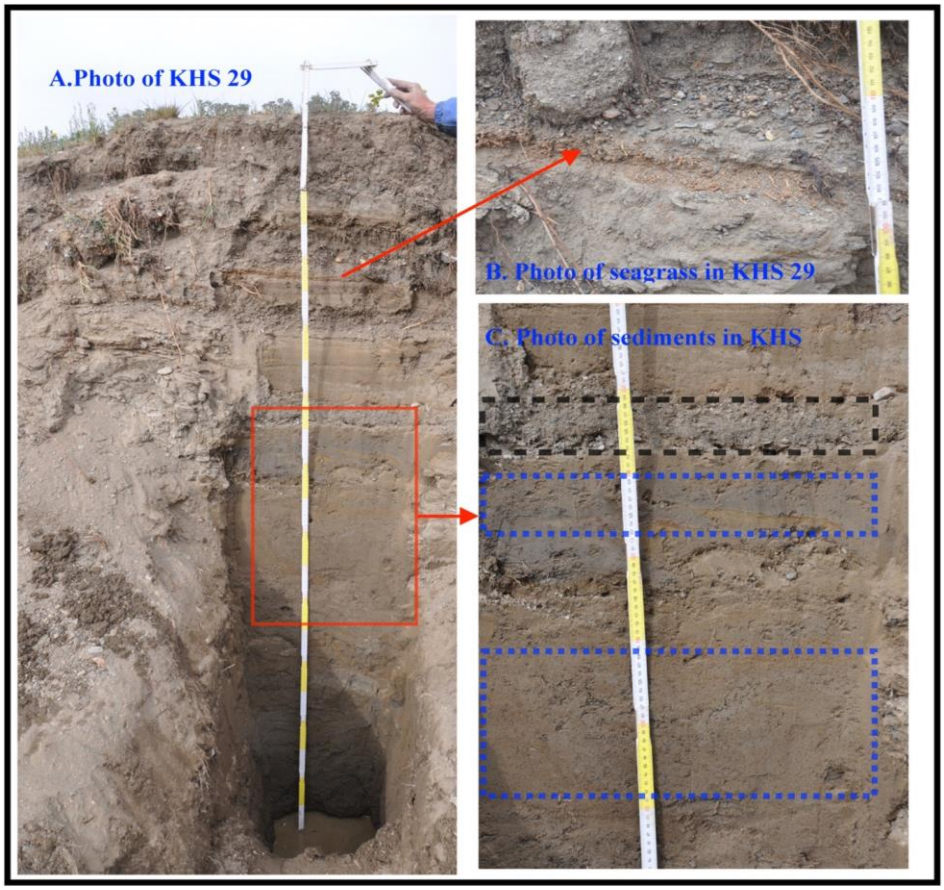

Fig. 28 Section KHS29, north-east of Kuhai Lake at near-shore location, 3 m above the present lake level. A: overview photo of the sction; B: Detail of the upper sequence with former shoreline grass layer (*Potamogeton* sp.) at the lower boundary of shoreline pebbles; C: details of the middle part of the section showing layers of different sediment composition.

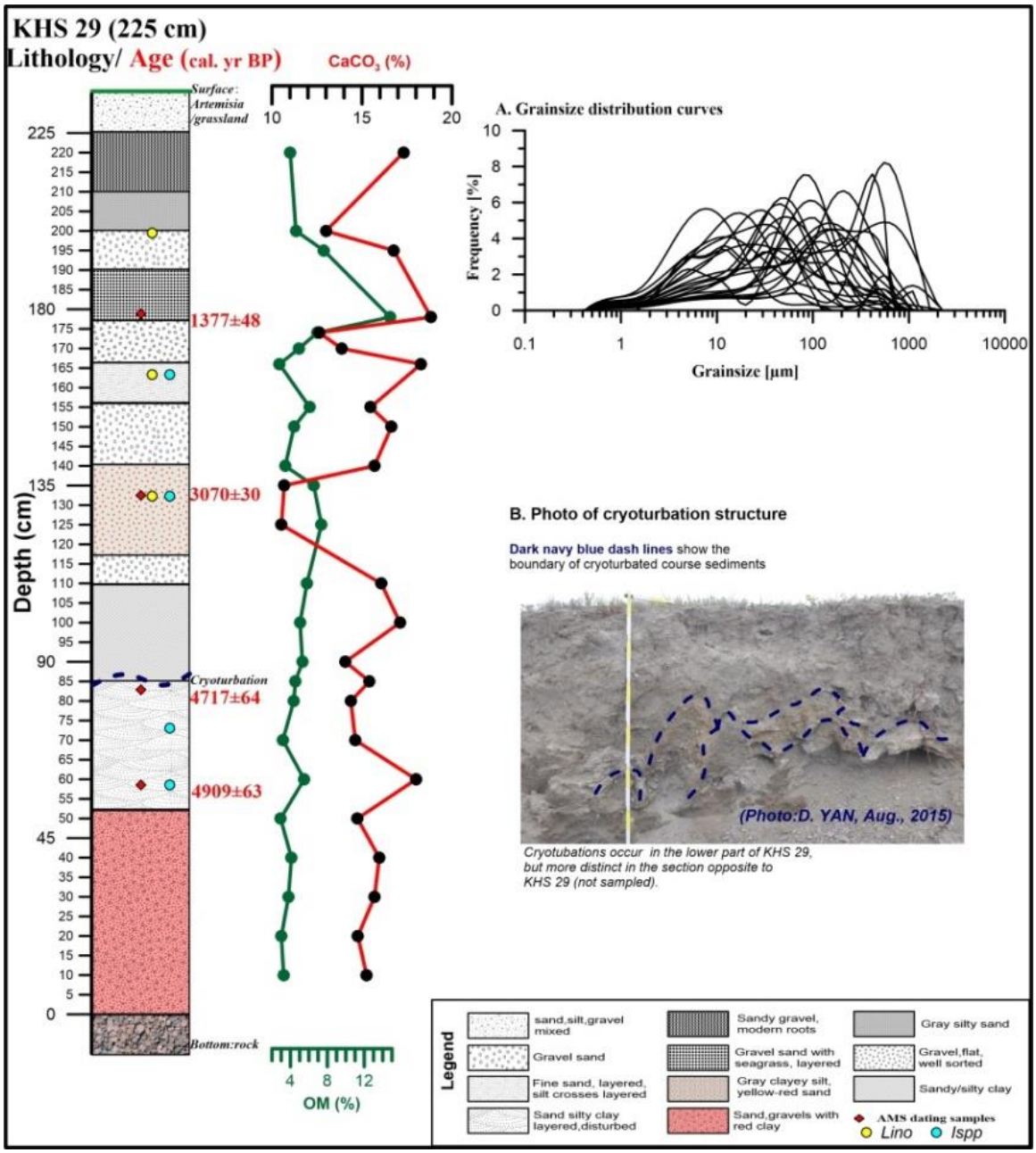

Fig. 29 Section KHS29 at the river bank of an episodic drainage at the north-eastern side of Kuhai Lake, showing lithology with location of identified ostracod, AMS dated samples and OM/$CaCO_3$ content throughout the section. A: grainsize distribution curves of all analyzed samples; B: photo showing cryoturbation features in a section opposite of KH29.

5.6.2 Sections with aeolian deposits

In total 26 onshore sections within the Kuhai catchment and one section few hundred meters east of the south-eastern catchment boundary contained aeolian deposits (Fig.4) which were all subject to grain size analyses in this study (Tab.7). Two sections (KHS 2 and KHS 17) in the south-eastern lake catchment contained loess. Eight small sections were taken from tophill locations in the eastern (KHS 13-21) and southern (KHS 3-5) catchment. They all contained silty to sandy aeolian deposits with variable grainsize between 35 and 250 µm (Tab.2). Three short sections (KHS 22-24) and two longer sections (KHS 25-26) located on the southern island in Kuhai Lake were used for aeolian sediment references in terms of grain size composition. Nine sections containing aeolian sand are from riverside locations (KHS1, 7-12, 14,16) and three from near-shore (KHS 28) and eastern fan locations (KHS 6, 15). Sections which were dated by OSL are described in more detail as follows:

Tab. 7 Comparison of grain size results of sections in Kuhai catchment.

Type of sections	Sections ID	No. of analyzed samples	Grain size modes		Classes	Marks
			Range (µm)	Depths at (cm)		
Loess	KHS 17	6	11	40	MSi	*4.5-9.2 ka*
			32-50	10/20/30/50/60	CSi	
Tophill	KHS 3	1	50	15-20		
	KHS 4	1	35	15-20		
	KHS 5	1	55	15-20		
	KHS 13	4	150--250	30/80/130/180	FSa	*0.8-1.8 ka*
	KHS 18	1	35		Csi	
	KHS 20	1	72		FSa	
	KHS 21	1	50		CSi	
Island	KHS 22	3	30-60	5/10/15/20	CSi	
	KHS 23	1	40	13		
	KHS 24	2	35--50	10--20		
	KHS 25	11	30--40	20/30/40		*6-8 ka*
			90--200	10/50--105	Fsa	
	KHS 26	6	90--200	43--305		*9-11 ka*
Riverside	KHS 1	16	25--60	10/28/50/54/97-150	Csi	
			70--150	35/45/56-90/156	FSa	
	KHS 7	7	150--290	15-160		*0.2-1.2 ka*
	KHS 8	3	55	50	CSi	
			100-120	15/35	Fsa	
	KHS 9	1	190			
	KHS 10	1	150			
	KHS 11	1	45		CSi	
	KHS 12	1	110		FSa	
	KHS 14	5	30-40	43/130	Csi	
			150-170	20-39	FSa	
	KHS 16	3	20	40	MSi	
			30	70	Csi	
			120	100	Fsa	
	KHS 29	23	8--25	20/60/80/110/174/195	MSi	
			30--63	30/40/85/135/150/166	CSi	
			90--250	10/50/70/90/125/155/190/200	FSa	
			250-630	150/178/220	MSa	
Paleo-lacustrine	KHS 27	17	15--25	20-60/75/80/105/130/***120***	MSi	
			25--60	70/80/100/110/***120***	CSi	
			90--100	65/90/95	FSa	
Lakeside/fan	KHS 6	18	120--250	25-285/350	FSa	*0.3-1.4 ka*
			250--500	325/385	MSa	
	KHS 15	20	50--60	40/90/100/120/160	CSi	*0.4-1.8 ka*
			70--200	10-30/50-80/110/130-150/170-190	FSa	
	KHS 28	9	17-20	50/60	MSi	
			90-190	35/70-140	Fsa	

Notes: 1. Fine silt (Fsi); medium silt (MSi); oarse silt(CSi); fine sand (FSa); medium sand(MSa) 2.KHS27:120 cm bi-modes

	OSL dated (BP)		Permafrost				
	AMS dated		Cryoturbation				

5.6.2.1 Section KH 4 (dune, 4237 m a.s.l)

This section located within the northeastern dune field was dug in September, 2014 (Fig.4) and reached 300 cm in height. Based on the visual inspection, the dune sand could be divided into two generations, separated by a thin band of coarser material. Four samples were dated by OSL with Quartz and K-Feldspar (Fig.30, Tab.3). Ages dated by two different minerals show differences, which would be related to different bleaching conditions of Quartz and K-Feldspar. Here the younger ages are based on determinations by K-feldspars while the older age refers to Quartz, perhaps better bleached than K-Feldspar (pers. comm. Prof. Manfred Frechen). Hence, K-Fs-ages revealed 0.24 ± 0.02 ka, 0.38 ± 0.03 ka and 0.66 ± 0.04 ka, respectively for the upper dune sand at 20 cm, 70 cm and 160 cm depth, while the sample at 240 cm depth in the lower part of the dune sand was Quartz-dated to 2.95±0.23 ka. These ages in general confirm the two generations of dune formation.

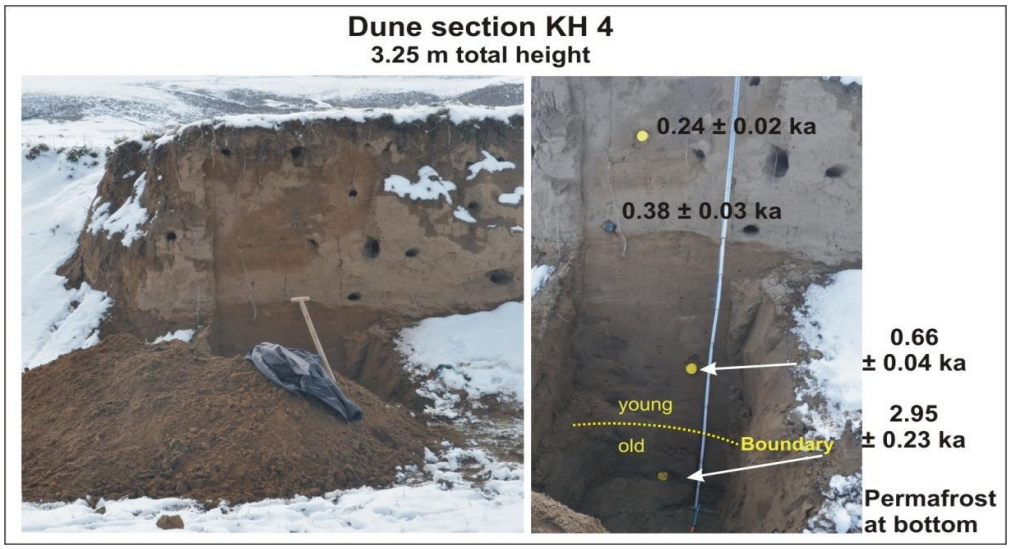

Fig. 30 Photo (left) and chronology (right) of KH 4.

5.6.2.2 KHS 6 (4228 m a.s.l.)

Section KHS 6 with a height of 400 cm is a dune body located at the eastern side of the lake, ca. 2 km south of KH 4 (Fig.4). Compared with the dune sediments at KH4 frequent alternations between finer and coarser aeolian components were obvious. The lithology can be described from the top to bottom as follows:

0-129 cm: brownish fine sand alternating with medium sand layers, modern roots until 170cm;
129-130 cm: grayish silty clay
130-160 cm: silty fine sand
160-200 cm: fine sand
200-210 cm: medium sand

210-218 cm: fine sand
218-224 cm: silt
224-260 cm: fine sand alternating with medium sand layers
260-270 cm: medium sand, 0.5 cm layer of fine sand to silt
270-300 cm: fine and medium sand layers
300-305 cm: fine sand, pockets of coarse sand, cryoturbated
305-375 cm: fine sand to medium sand (signs of cryoturbation)
375-385 cm: coarse sand, oxidation features
385-400 cm: fine to medium sand.

Organic matter was relatively low (<5 %), carbonate content ($CaCO_3$) changed within 10-13% (Fig.31). Grain size of selected dune sands showed a unimodal pattern ranging from 200 to 500 µm, mainly between fine to medium sand fractions. Clay (1-2%) and silt fractions (10-30%) however, were present in all samples with peaking values between 120-140 cm and 220-270 cm depth.

Four samples were OSL dated, covering the period from 1.44 ka to 0.32 ka (Fig.31). According to the ages, generally coarser aeolian sand was deposited at around 1.44 ka and 0.54 ka, while finer components were likely deposited around 0.79 and 0.32 ka.

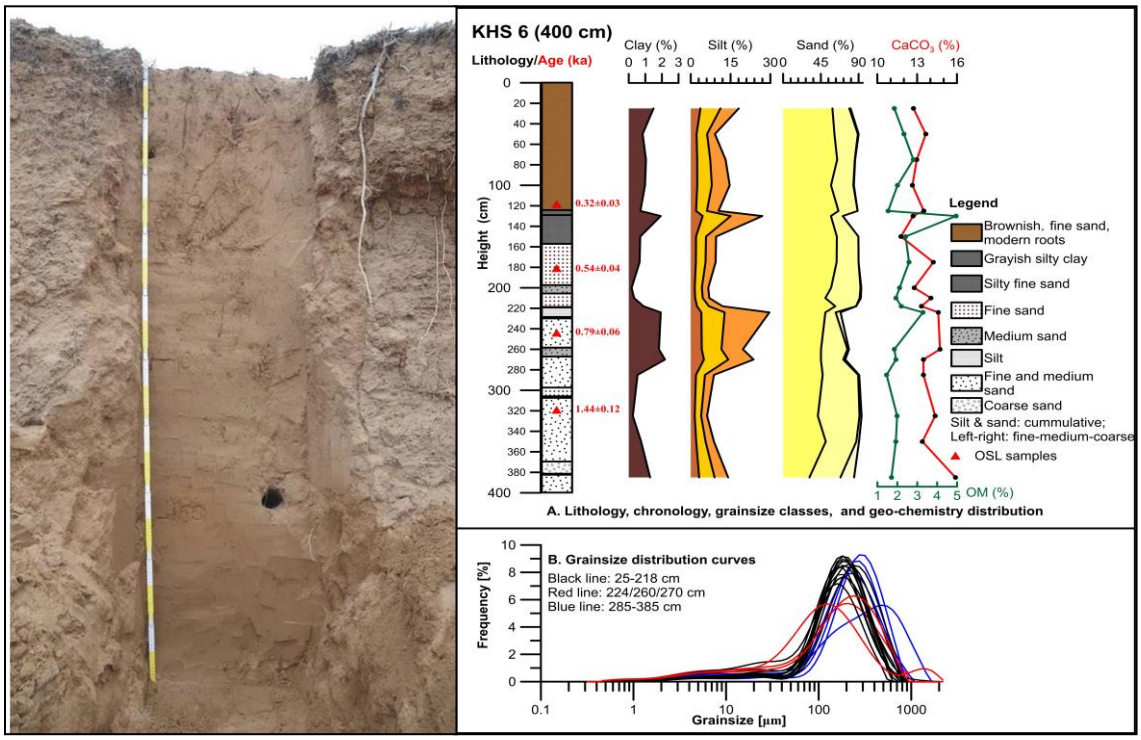

Fig. 31 Photo of KHS 6, upper 2 m (left) and lithology, chronology, geo-chemical and sedimentological characteristics (right).

5.6.2.3 Section KHS 7 (4237 m a.s.l.)

This 165 cm high section KHS 7 was located at a river side of an episodic drainage at the northeastern side of the lake (Fig.32). The lithology can be described from top to bottom as follows:

0-95 cm: light brown medium sand, modern roots;
95-160 cm: fine sand, black dots (organic matter), modern vertical root traces (138-159 cm: silty fine sand), from 110 cm downward brownish-red (oxidized) fine sand
160-165 cm: reddish-brown coarse sand, flat gravels up to 5 cm in diameter.

Organic matter in KHS 7 is very low (<3 %), while carbonate ($CaCO_3$) decreased from 20% (bottom to 16.5% (top) with a lowest value at 135 cm depth (Fig.32). OM varied between 1 and 3%. Grain size data show an increase of clay (2%, Fig.32, B) in the lower part of the section. Silt occupied about 10% of the sediment and increased parallel to the clay content to 30% at 145 cm depth. Fine to medium sand ranged between 85 and 90%, while the fine sand component was always the dominant fraction. The grain size distribution curves therefore show a unimodal pattern with a mean mode at 200 µm, except for two samples in the lower part of the section with a wider range and modes between 250 and 300 µm.

Three samples were selected for OSL dating and revealed ages of 1.22 ± 0.1 ka, 0.53 ± 0.04 ka and 0.27 ± 0.01 ka, respectively (Fig.32). The latter age seems to be problematic due to a very low error. Aeolian deposits contained more silt during the time interval centering at 1.22 ka (at 145 cm depth) compared with the other time intervals.

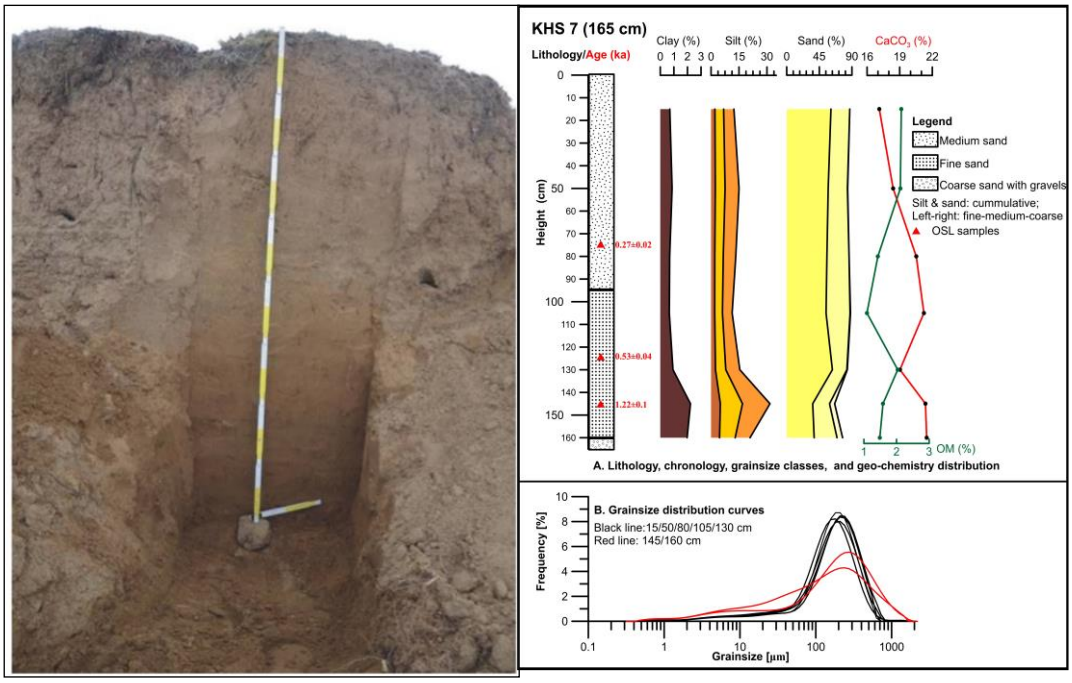

Fig. 32 Photo lithology (left), geo-chemical and sedimentological characteristic in KHS 7 (right).

5.6.2.4 Section KHS 13 (4286 m a.s.l.)

This section was located at the northeastern part of the catchment on the upper stream region of an episodic river (Fig.33). The 2 m high section provided more homogenous light brown fine sand within the whole section Fig.33 A).

Low organic matter (2-3%) and carbonate ($CaCO_3$, 10-13%) in four samples characterize the geochemical composition in KHS13. Generally low amount of clay, 10-14% silt and about 85-90% sand fractions are comparable with section KHS 7. All analyzed samples show a unimodal distribution with a mean mode at 250 µm. (Fig.33 B). Two OSL ages of 1.88 ± 0.14 ka and 0.83 ± 0.06 ka indicate that the lower part of the Aeolian sands were deposited during a 1000-year period.

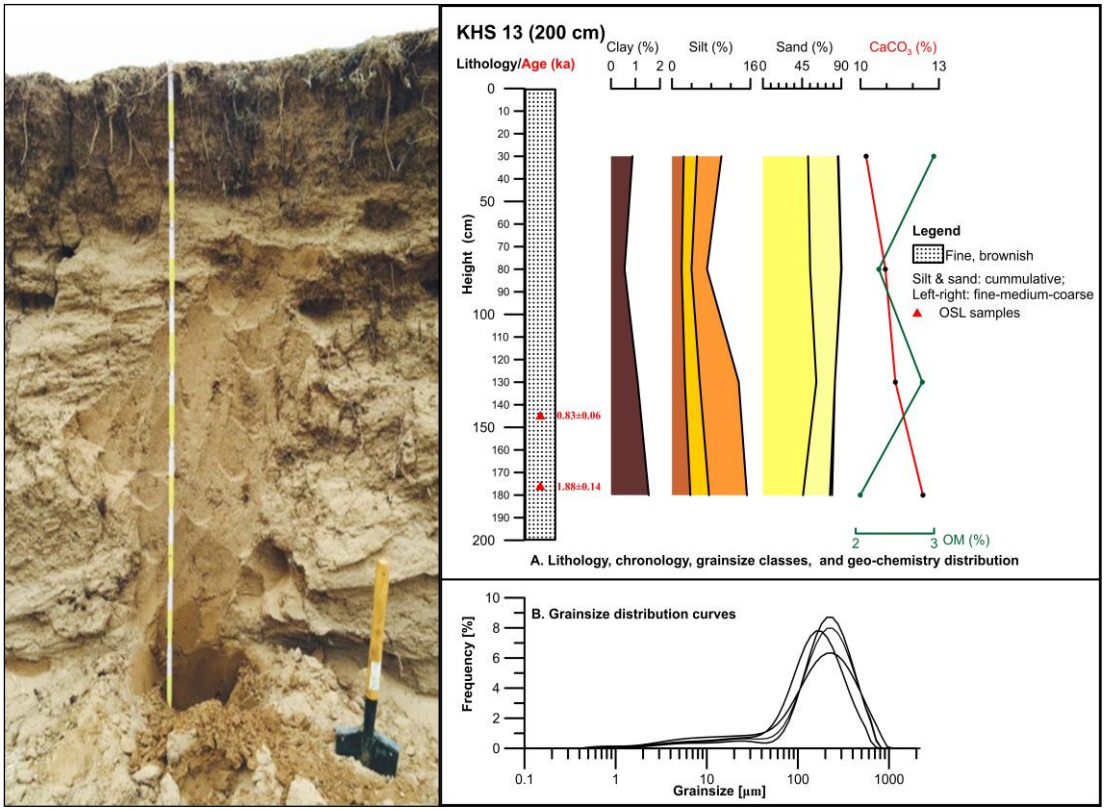

Fig. 33 Photo lithology (left), geo-chemical and sedimentological characteristic in KHS 13 (right).

5.6.2.5 Section KHS 15 (4245 m a.s.l.)

This naturally exposed 200 cm high section was located on the eastern side of the lake at a river bank of an episodic river (Fig.4, Fig.34). Changes in lithology were easily visible and are described from the top to bottom as follows:

0-10 cm: brownish fine sand, modern soil with roots
10-25 cm: light brown fine sand
25-40 cm: dark brown, fine sand, rich in organic matter; paleosol
40-60 cm: brown, fine sand, roots, black dots
60-70 cm: fine and medium sand, roots, black dots
70-90 cm: fine sand, silty sand in lower part, black dots with 1 cm medium sand at 77-78cm; cemented at 80cm
90-104 cm: dark brown silty sand on the left section, rich in organic, weak paleosol
104-190 cm: silty sand, 1 piece of flat 12 cm gravel at 110-120cm
Bottom: gravels >5 cm in size.

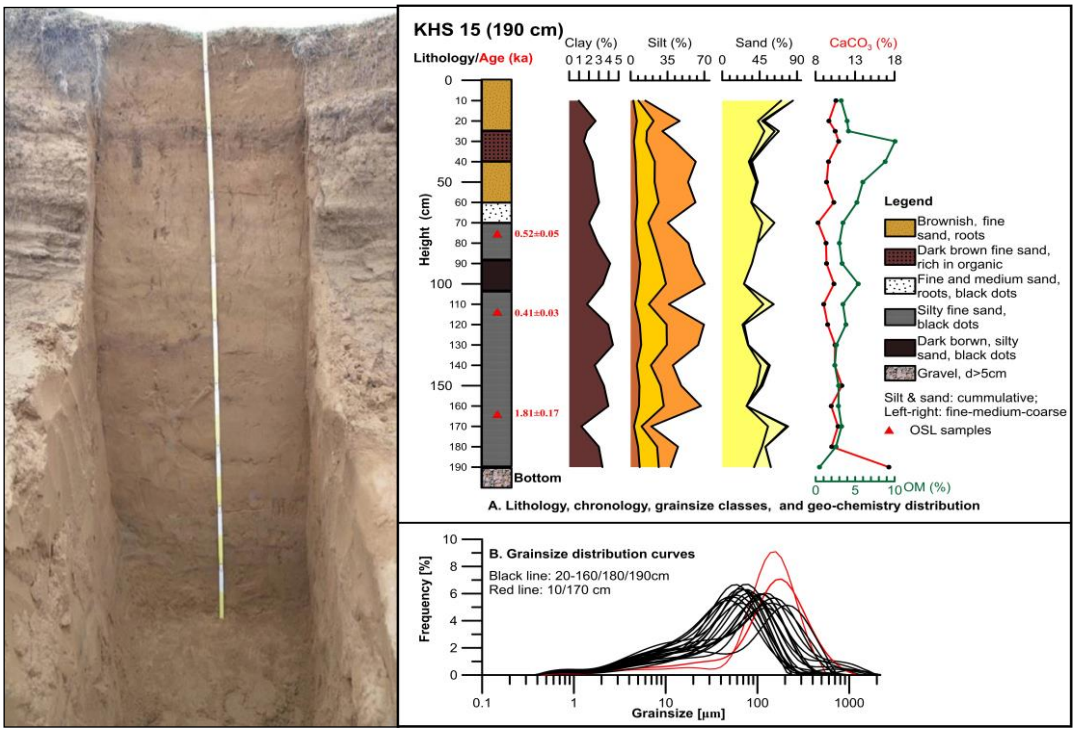

Fig. 34 Photo lithology (left), geo-chemical and sedimentological characteristic in KHS 15 (right).

Except for the sample at 25 cm with 10% organic matter (paleosol) all other samples vary between 0-5% OM in KHS 15. Carbonate ($CaCO_3$) content ranges at around 10%, expect for 18% in the sample at the bottom of section. Grain size distribution curves show three different groups of sediments: i) with broad mode at 45-70 µm, covering more the silt fractions, assigned to sandy loess; ii) a broad mode at 100-150 and at 250 µm, typically for a mixed fine dune sand with silt components and iii) a sharp mode at180-200 µm assigned to pure fine aeolian sand. Highest content of well-sorted sand was found at 10 cm and 170 cm. Samples with higher sand components at 75 cm and 115 cm were OSL-

dated to 0.52 ka and 0.41 ka, while the sample at 165 cm with more finer particles was dated to 1.81 ka.

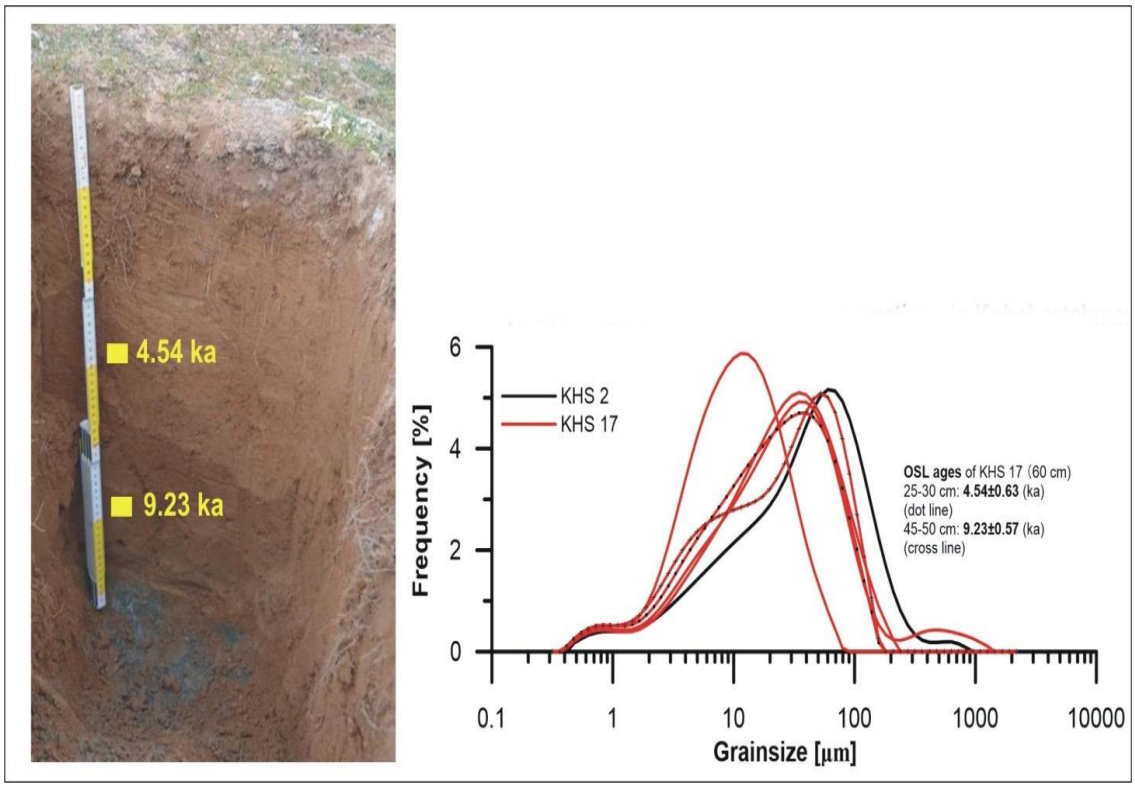

Fig. 35 Photo of KHS17 section with location of OSL ages (left) and grainsize distribution curves (right).

5.6.2.6 Section KHS 17 (loess section, 4164 m a.s.l.)

Section KHS 17 dug on a hill position in the eastern lake catchment was identified as a loess section (Fig.4, Fig.35), consisting of 60 cm homogenous silt above bedrock, displaying following lithostratigraphy:

0-5 cm: brownish silty soil, grass
5-56 cm: light brownish-red homogenous silt
56-57 cm: reddish-gray clayey silt, signs of ground water influence
57-60 cm: grayish clay (weathering rocks) and gray bedrock below.

Samples with 10 cm in resolution were taken for grain size analysis and two samples were dated by OSL (Fig.35; Tab.3). Most of the samples have modes at 32-50 µm, similar to grain size in loess sediments from the neighboring lake Donggi Cona catchment (Stauch et al., 2012). However, a sample from 40 cm depth reveals a mode at 11 µm which is considered to be too fine for classical loess deposits and thus could represent suspended sediments deposited in a temporarily existing small water body. Two samples at 25-30 and 45-50 cm depth were OSL-dated to 4.5 ± 0.63 ka and 9.23 ± 0.57 ka and indicate two phases of loess accumulation.

5.6.2.7 Section KHS 25 (island, 4161 m a.s.l.)

This section was located on the eastern hill of the island in the southern part of Lake Kuhai (Fig.4), where bedrock is covered by up to 3 m thick sandy sediments of aeolian origin. Section KHS25 was dug on a gentle slope near the eastern top of the island and reached 115 cm thickness. The lithostratigraphy can be described as follows:

0-25 cm: dark brown fine sand, modern roots, modern soil
25-60 cm: light brown silty fine sand, modern roots
60-115 cm: brown fine sand
Bottom: weathered rock fragments, 2cm in size.

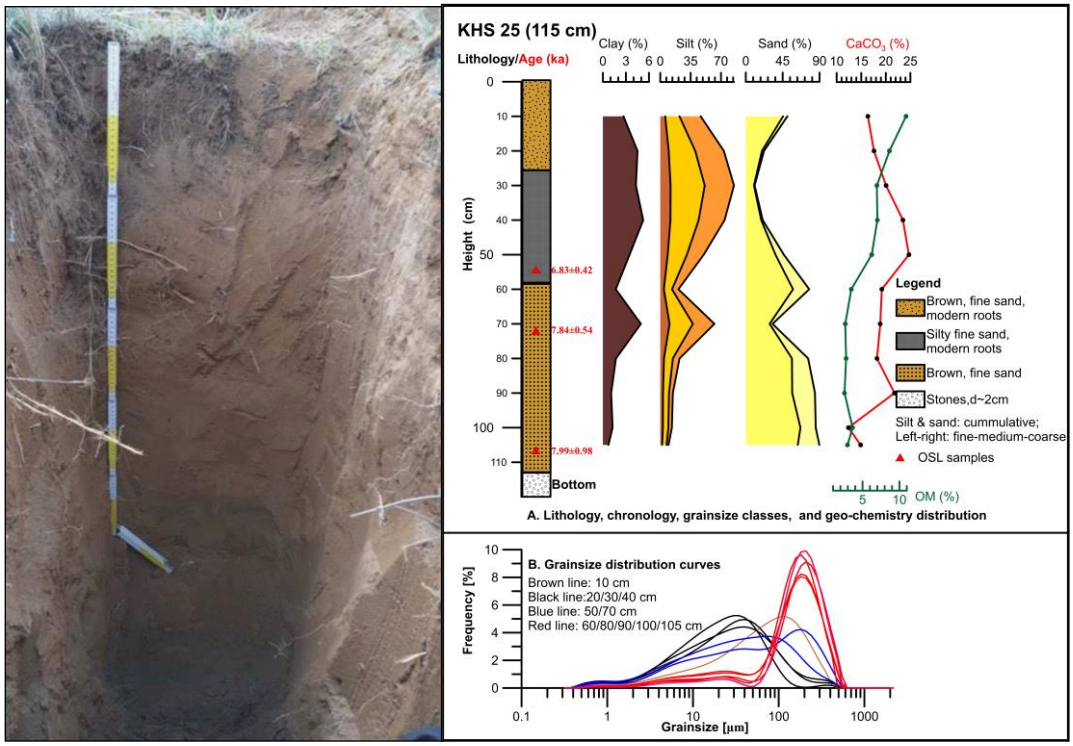

Fig. 36 Photo lithology (left), geo-chemical and sedimentological characteristic in KHS 25 (right).

Organic matter in KHS 25 decreased slightly from 10 % (upper soil) to 2 %, while carbonate ($CaCO_3$) content increased from 10 % to 25 % from top to bottom. Grain size data show two different types of aeolian sediments: finer components with up to 70 % in the silt fraction (ca 25-50 cm depth) and a more sandy component with 55-90% fine to medium sand (ca. 50-105 cm depth, Fig.36). Grainsize distribution curves show these two different components too. Broad modes between 30 and 100 µm characterize the upper loess/sandy loess sequence, while narrow modes at around 200 µm are dominant in the lower part of this section (Fig.36). These two different groups of grain size modes can be likely assigned to different energy transport mechanisms (e.g., different wind speeds).

The lower part between 105 and 75 cm depth was OSL-dated to between 7.99 and 7.84 ka, while for the upper sequence only an age of 6.83 ka at during 55 cm depth indicates a younger generation of aeolian deposition. Considering the homogenous sandy sediment and accepted error of OSL dating, this more than half meter-thick fine sand in the lower part of the section could have been deposited at a similar time (ca. 8 ka).

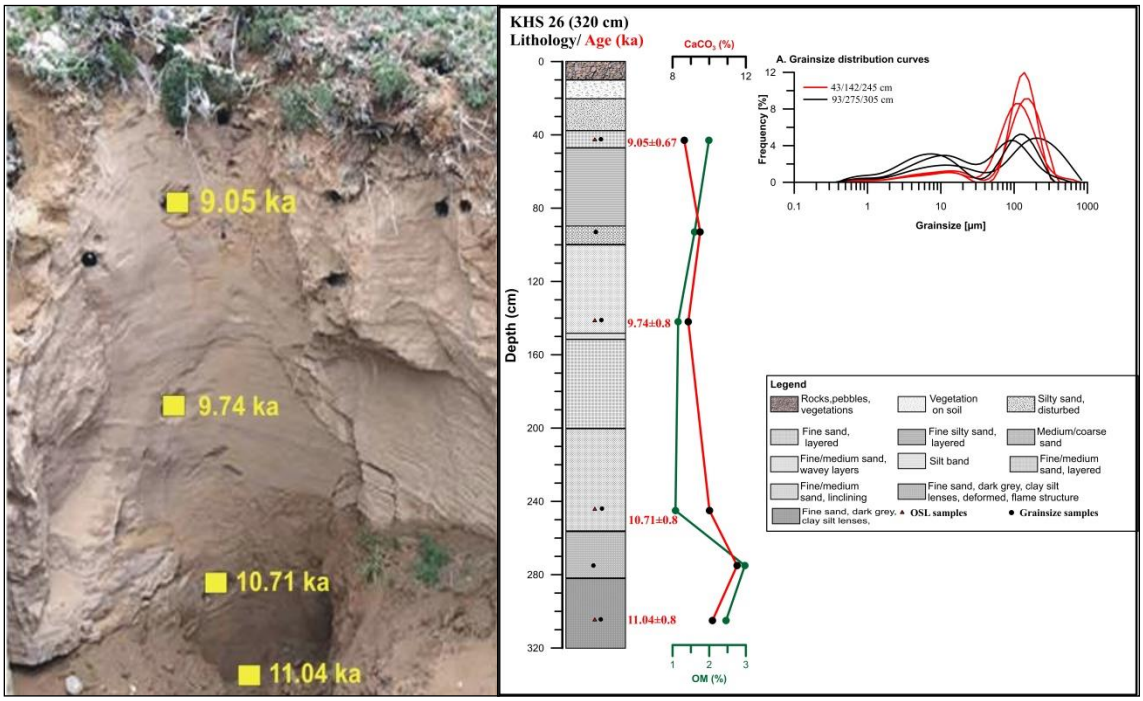

Fig. 37 Photo of section KHS 26 with OSL ages (left), lithology, geochemical data (OM, $CaCO_3$) and grainsize distribution curves (right).

5.6.2.8 Section KHS 26 (island, 4142 m a.s.l.)

This section was dug in a gentle slope position close to the center part of the island and provided a 320 cm long section (Fig.37). The lithostratigraphy showed following sequences from top to bottom:

0-10 cm: rocks fragments, pebbles, vegetation
10-20cm: vegetation on soil
20-39 cm: silty sand, disturbed
39-47 cm: fine sand, layered
47-96 cm: fine/silty sand, layered
96-100 cm: medium/coarse sand
100-149 cm: layered fine/medium sand, wavy structures
from 100 cm downward layers slightly dip SE direction
149-151 cm: silt band
151-200 cm: medium/fine sand, layered
200-258 cm: as before, inclining
258-282 cm: dark gray fine sand, clay silt layers (lenses), deformed, flame structure
282-320 cm: fine sand, clay-silt lenses
245-320 cm: gray silty layers intercalated with silty sand lenses.

Organic matter remained low (1-3%) in section KHS 26. Carbonate ($CaCO_3$) changed within 8-12% (Fig.37). Grain size distribution curves can be divided into two groups of aeolian sediments which show bimodal curves with broad modes at 6-9 µm and 100-200 µm at 90, 275 and 305 cm depth, respectively (black curves in Fig.37 A). A second group displays unimodal curves with sharp modes at 110-180 µm in 45, 142 and 245 cm depth, respectively (red curves in Fig.37 A).

Four samples at 305, 245,140 and 40 cm sediment depth were OSL-dated to between 11 and 9 ka, placing aeolian deposition into the early phase of the Holocene.

6. Discussion

6.1 Processes and spatio-temporal diversity of sediments in Kuhai Lake Basin

Environmental and climate reconstructions based on a variety of proxy data from lake basins on the Tibetan Plateau and adjacent areas were increasingly utilized (chapter 2). Comparison of these results indicates a quite heterogeneous picture of climate-controlled hydrological variations in lakes throughout the Late Glacial and Holocene periods. The overwhelming majority of published records from various lakes were mainly based on sediment geochemistry or bio-proxies from single sediment cores, preferably obtained from center parts of the respective lake basins. It was always an unspoken assumption that those records reflect the overall dynamic processes within a lake basin reasonably well and hence, are prone to regional and global climate teleconnections. Research that combined lake records with related catchment dynamics was very seldom utilized, except for more recent studies on the northeastern Tibetan Plateau which were conducted within a Sino-German collaborative research program (DFG priority program 1372: TiP '*Landscape and lake system response to Late Quaternary Monsoon dynamics on the Tibetan Plateau-Northern transect'*) during the last years. It focused on the analysis of sediment cascades from the sources to the sinks, combining catchment investigations with lake research (e.g., Dietze et al., 2010; Ijmker et al., 2012; Stauch et al., 2012; Opitz et al., 2012; Wrozyna et al., 2012; Kasper et al., 2012, 2013; Ramisch et al., 2016; Lockot et al., 2015). Moreover, it could be demonstrated that individual catchment processes played an important role for variations in lake development during the Late Pleistocene/Holocene time as revealed by lake-catchment studies at Tso Kar, India (Wünnemann et al., 2010) and Paiku Lake (Paiku Co), southern Tibetan Plateau (Wünnemann et al., 2015), which strongly controlled variations in lake hydrology there, partly independent of climate influence. Furthermore, Wünnemann et al. (2012) and Yan and Wünnemann (2014) could show that lake records from different water depth and locations within a single lake basin revealed a high diversity of sedimentological and biological patterns which would have resulted in different interpretations of climate signals, if only one record was used for reconstructions. Research considering sedimentary processes in lakes in relationship to catchment processes remain less investigated.

In this study, information from the catchment as well as multiple sediment cores from Kuhai Lake at different locations and water depth were combined, in order to decipher interrelationships between onshore and offshore processes during the last 4 ka BP, which certainly depended on climate impact but also on local influences, such as potential tectonic activity and diverse runoff behavior of drainages around the catchment.

All presented high-resolution proxy data from the catchment and lake were subject to various processes through time that contributed to the overall development of the lake basin and are discussed within individual paragraphs.

6.1.1 Catchment dynamics and related geomorphology

6.1.1.1 Fluvial drainages

The spatial distribution pattern of drainages around the lake basin is considered to be an important aspect for variations in the hydrological balances of the relatively small lake (ca. 50 km^2). Only three of the numerous rivers around the lake provide water and sediments all year round (Fig.4), except for few months during the freezing period in winter. Conversely, all other drainages only contribute to the lake during the rainy season in summertime, according to the climate data which indicate summer monsoon influence nowadays. As a result, the north-eastern, northern and northwestern parts of the lake basin only receive water and sediments episodically.

Moreover, it is noteworthy to mention that none of the inflowing rivers formed deltas at the margin of the lake, probably due to limited sediment transport and the wide and flat wetland area along the eastern shoreline of the lake where a certain proportion of sediment load could be deposited already outside the lake before reaching the water body (e.g., Wright, 1977; Pettijohn et al., 1987). Hence, deposition of coarser fluvial/alluvial material, mixed with soil wasting processes at the surface, seem to be responsible for the lack of coarse sediments in the lake bottom. The area outside the lake basin is affected by permafrost, which could be found in several sections ca. 1.4 m below the surface.

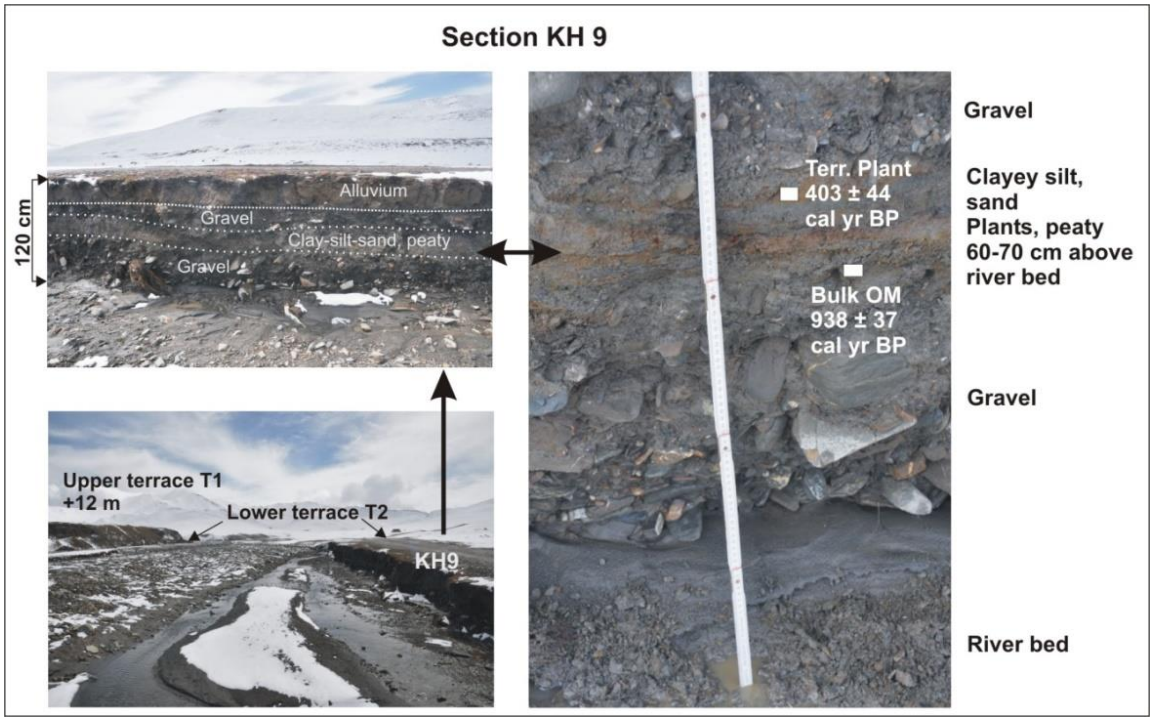

Fig. 38 Section KH9, lower terrace T2, river bank of the perennial river in the eastern catchment. Upper left: T2 sequences; lower left, overview of the terraces T1 and T2, view to east; right side: detail of section KH9.

Two distinct terrace systems developed at the eastern side of the lake as a result of sequential incision of the rivers into the alluvial/fluvial fans. The higher one, (T1 in Fig.2

A, Fig.38), ca. 10-12 m above the modern river beds, consisted of coarse fluvial gravels, mainly with angular shape, indicating short-distance transport with coarsening-up towards the upper catchment. Lithology of the material confirms local provenance mainly composed of metamorphic rocks of Permian age and to a lesser extent, Triassic components (sandstone, limestone). The latter components were only observed in the terrace systems of the perennial river, while all others provided Permian and Proterozoic facies, in agreement with the geological map (Fig.3). The formation of the upper terrace sediments most likely falls into a period of fluvial activity, probably during the last glacial time, although glacial remains such as moraines and other morphological features (e.g., cirques) could not be observed. The incision however, happened afterwards and may fall into the period of stronger erosional activity at the end of the glacial period. Two different processes may be responsible for this development: i) a very low or temporarily non-existing lake, which would increase the flow gradient between the upper catchment and the lake basin, resulting in enhanced erosion by high-energy flow. Mischke et al. (2010) reported that Kuhai Lake experienced very low lake level during the Last Glacial Maximum (LGM) and may have consisted of partly isolated small ponds or was even dry. Another explanation could be that the driving factor for terrace formation was ii) tectonically induced uplift of the mountains which resulted in the same effect as mentioned before. The active Kunlun fault, tangential to Kuhai catchment in the south that induced the push-up structure of the Anyemaqen Mts. (Van den Woerd et al., 2002; Fu et al., 2005), resulting in transverse faults crossing Kuhai Lake, could be a likely mechanism to explain uplift of the eastern Kuhai catchment. However, it is most probable that both processes acted together and enabled terrace formation. Ice-wedge casts in this terrace body, combined with other periglacial features, such as cryoturbation, indicate permafrost conditions during and after deposition of the thick gravel layers in terrace T1.).

The lower terrace (T2, Fig.2 A) also consisting of mainly angular-shaped coarse gravels of local provenance, interrupted by organic-rich fine material (Fig.38) indicates a second erosional phase which was dated to the period of the Little Ice Age (<400 cal. yr BP) and may indicate stronger effect of a lowered lake level at that period. The same terrace level was also observed along the second perennial river in the south-east of the lake. However, gravels were not found there but instead almost sandy-silty material which was deposited under lower energy flow or perhaps during phases of overbank flow along the flat near-shore regions of the meandering river bed, mixed with sands of aeolian origin (see Fig.2).

Along the western side of the lake, inflowing rivers are lacking due to the steep morphology of smaller and partly isolated mountain hills that border the lake there (Fig.4). However, the western catchment of Kuhai includes several drainages in the north-west that drain along fluvial-alluvial fans via a shallow sub-basin (wetland) toward the south-western part of the lake. This sub-basin acts as the local sink for most of the drainages in the north-western and western part of Kuhai catchment, while only a limited contribution of water and sediments reach the main lake today, compared with discharges from the other parts of the catchment.

6.1.1.2 Shorelines and onshore sections with lacustrine deposits

Morphological field investigations in combination with remote sensing analyses and OSL dating reveal the existence of shoreline generations in Tibetan lakes (Yu et al., 2001; Liu et al., 2011, 2015; Liao et al., 2013) Accordingly, several shorelines were also observed in Kuhai Lake surrounding the lake of which the highest visible shoreline was found ca. 8-10 m above the present lake level, thus marking the highest lake level of Kuhai Lake. A higher level of this closed lake would have induced an outflow along the south-eastern valley system towards the Yellow River catchment (Fig.4). This shoreline is not visible everywhere around the lake due to its weak morphological shape, but can be traced along the eastern shore as a slight terrace-like landform crossing the fluvial-alluvial fans there. Along the western side of the lake, also surrounding the larger island, this shoreline level is connected with cliff-like features along the steep slopes of the hills (Fig.2 F, appendix II 5), hence better traceable there.

Lower shorelines, likely indicating younger lake levels, are well-developed around the lake and indicate numerous fluctuations of the lake (Fig.2 H). Notably these paleo-shorelines consist of sand and gravels, partly well rounded and flattened, overlain or mixed with sea grass as described in section KHS29 (Figs.28-29) at ca. 2.5m above the present lake level. According to the river bank profile opposite of section KHS29, deformation of sediments by freeze-thaw effects (cryoturbation) are indicative of periglacial environmental conditions during or after this period, as it happens today.

The fine-grained sediments below the identified shoreline sequence contained two ostracod species (*Limnocythere inopinata* and *Ilyocypris* sp.) which are indicative of a shallow aquatic environment, most likely within a littoral, near-shore setting, as layered sediments with changes in sediment grain-size composition indicate (Fig.28). They were deposited during a period between roughly 4.9 and >1.3 cal. ka BP, after deposition of fluvial sand and gravels which occurred below the lacustrine sequence.

According to the dated aquatic plants in the shoreline sequence which point to a higher lake level during the Medieval Warm Period (MWP), it can be assumed that all other shorelines (at least three) below this level are much younger and may represent lake level fluctuations of the last few hundred years. Until now however, literature about the origin, timing and nature of these shoreline generations is lacking.

Higher lake levels are also documented in onshore sections KHS27 and KHS1 (Figs.24-27), which both display different sedimentary processes. Comparable sections at Qinghai Lake were recently OSL-dated by Liu et al. (2015), based on near-shore sandy deposits or lacustrine sequences. In Kuhai Lake, fine-grained and carbonate-rich sediments with plenty of aquatic plant remains and intercalated fine sand layers are evidence of deposition in a shallow lacustrine environment close to the inflow region at the south-western part of the lake. The exposed sediments occurred up to 1.3 m above the present lake level and are thus a clear signal for a higher lake stage. In addition, ostracod associations indicate a shallow lake/pond environment (*Limnocythere inopinata*, *Eucypris*

mareotica, *Ilyocypris* sp., *Fabaeformiscandona rawsoni*), that existed from ca >3.4-1.38 cal. ka BP, according to the dated sediments, similar in timing to the sequences in section KHS29.

Sediments in sections KHS1 however, showed layers between ostracod-bearing fine-clastic components and very well-sorted fine sand, not found in the other sections. Ostracod communities (*Eucypris mareotica* and *Limnocythere inopinata*) in general testify the deposition under a shallow aquatic environment with potential contribution of slightly flowing water as indicated by *L. inopinata* and *Ilyocypris* sp. They can tolerate lentic and also slightly flowing water conditions (Meisch, 2000; Frenzel et al., 2010; Mischke, 2012; Akita et al., 2016; Yan et al., 2017), perhaps with temporarily higher salinities (*Eucypris mareotica*, Mischke et al., 2007, 2010b; Yan and Wünnemann, 2014). These conditions may have occurred in phases of lake level rise with ingression into the valley. On the other hand, the high proportion of well-sorted sand points to the incorporation of sediments primarily transported by aeolian activity and deposited within the river valley. It is likely that these sediments were re-mobilized during temporary flooding events. The latter may have induced overbank flow and the deposition of these sediments as well, being then assigned to fluvial components. The current situation shows that the majority of the well-sorted fine sands in the modern river bed point to a mixture of sediments from the local catchment sources including air-transported components as well. According to the dated sediments from this section, these processes occurred between 2.8 cal. ka BP and the modern time.

6.1.1.3 Aeolian deposits in Kuhai catchment

Analyses of the onshore sections containing aeolian deposits (see chapter 5.5) confirm the wide-spread distribution of aeolian deposits within the Kuhai catchment. Notably north-east of the lake basin, dune fields are associated with the episodically active drainage systems. These relatively small dune bodies of maximum 4 m individual height are semi-fixed by vegetation, except on their lakeward sides (west to north-west direction) which indicate reactivation of sand transport due to grazing impact by sheep and goats. Although most of the investigated sections were located within the eastern catchment, aeolian sediments were also found in the western part, especially along the hillslopes facing towards the lake (Fig.4, appendix II 5) and on the larger island located in the southern part of the lake (see also chapter 5.6.2).

Grain size data confirm that the dune sands and aeolian deposits in sections outside the dune field mainly consist of fine to medium sand (modes at 200-300 µm, mean: 250 µm), deposited at different times (Fig.39, see also chapter 5.6.2). Dune sands at the neighbouring Donggi Cona Lake basin provided similar grain size ranges (~210 µm, Stauch et al., 2012). It seems likely that the source area for sand transportation was restricted to the catchment itself, namely along the drainages crossing the dune field, but also along the shoreline regions of the lake and the fluvial-alluvial fans (mainly sparsely vegetated) in the north-western and southwestern sub-catchments. According to the prevailing wind directions (mainly N, NW and W) in Kuhai lake area, erodible material

was transported eastward resulting in higher accumulations on the eastern side of the lake or on the wind-shadow side of the hills along the western lake margin.

Interestingly, thick aeolian deposits were found on the southern island but not in the lake sediments. It remains an open question how these aeolian sands could reach the island without affecting the lake bottom sediments. Yan et al. (2017) found that the lack of eaolian deposits in Daotanghe Pond close to Qinghai Lake was likely the result of a frozen water body, preventing aeolian sands from deposition in the pond during a period of the LIA. A similar situation may have occurred in Kuhai Lake, enabling the transport of sand across the closed ice cover from the western shore region to the rocky island during the frozen status of the lake.

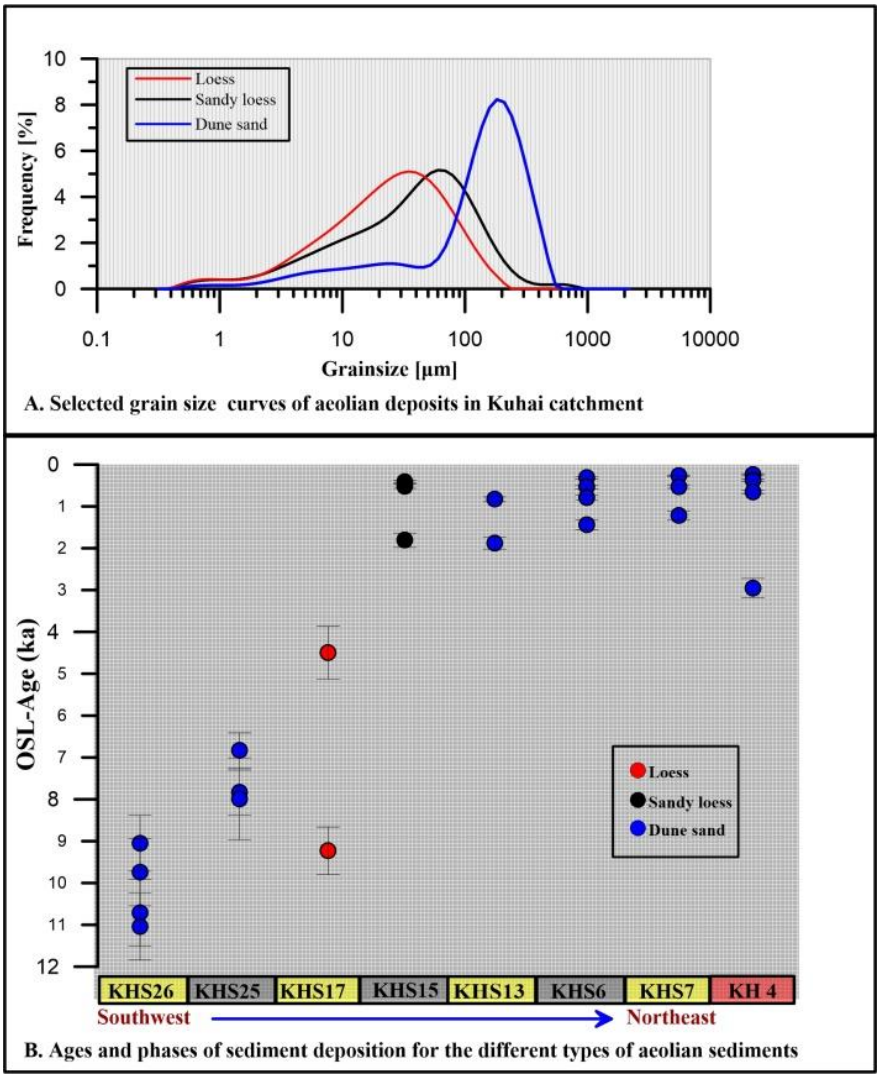

Fig. 39 Selected grain size curves for loess, sandy loess and dune sand in Kuhai catchment (**A**) and OSL dating results from sections containing aeolian deposits (**B**).

Two sections in higher locations above the present Kuhai Lake (KHS15, KHS17, Figs.34-35, chapter 5.6.2) provided up to 2 m-thick loess deposits of significantly finer grain size fractions than at all other sites. Sandy loess with grain size modes between 60 and 150 µm

dominated the section KHS15 in an uphill position, while the second site KHS17 consisted of pure loess with a mean grain size mode of 35µm (~50% of the grain size components <2-35µm), very similar to loess deposits in Donggi Cona region (Stauch et al., 2012). The contribution of fine components <6.3 µm accounts for 17% (mean) in this section.

Loess deposits were not found in the lower parts of the Kuhai catchment, supporting the assumption of Stauch et al. (2012) and Stauch (2016) that loess deposits are preferably located in higher positions of lake catchments, due to larger distance transport of these grain size components as suspended load in air mass and deposited at places where loess could be trapped by vegetation cover, for example, or at lee-side positions protected against wind strengths. However, it can be assumed that the source for the loess in Kuhai catchment is of local origin rather than far distance transport, although not proved. Potential sources are the flat and temporarily dry shoreline regions and fine-grained sediments on top of alluvial fans, as well as the exposed lacustrine sediments after a high lake stay that are susceptible to deflation during dry seasons, anyhow. Similar assumptions were reported in neighbouring Lake Donggi Cona by Stauch et al. (2014).

The timing of aeolian mobility and deposition can be inferred from OSL-dated sections (see chapter 5.5.2 and figures/table therein). Dune sands on the island were likely deposited during the early Holocene and early mid-Holocene between 11 and 9 ka and 8-6.8 ka, respectively (Fig.39). They are the oldest aeolian sand deposits only found on the island so far, covering bedrock there. Also, one age from the loess deposits in section KHS 17 falls into this period (9.2 ka), while a younger age (ca. 4.5 ka) towards the top of the section indicates a quite long phase of about 60 cm thick loess deposition at that site. If this age range is correct, the mean annual sediment accumulation rate (SAR) for loess accounts for 0.423 mm $year^{-1}$.

All other dated aeolian sands were deposited during the late Holocene. The ages of the dune field in the north-eastern catchment indicate deposition during two phases: an earlier phase, dated to about 3 ka and a young phase covering the last 600 years. Aeolian sands and sandy loess in all other sections indicate depositional phases between 1.9 and 0.3 ka, suggesting that the last 2000 years provided preferable conditions for sand transport and deposition. This period of aeolian sand accumulation was also reported from Qinghai Lake region (Liu et al., 2011, 2015) and from sites adjacent to Kuhai catchment (Stauch et al., 2012; IJmker et al, 2012, Stauch et al.,2014; Stauch, 2015). Stauch (2016) distinguished between six phases of enhanced aeolian activity during the LIA (1630-1725 CE, 1450-1530 CE and 1250-1350 CE) and Dark Age Cold Period (DACP, 750-950 CE, 390-540 CE and 50-225 CE) in the north-eastern Tibetan Plateau during the last 2 ka. OSL data in this study match several of these phases but due to limited data they cannot be convincingly assigned the specific phases mentioned above. However, due to the lack of G-values and fading results, all respective OSL data remain tentative.

Furthermore, from the available data it cannot be inferred that during the older periods of the early Holocene/mid Holocene eaolian sand transport and subsequent deposition in Kuhai catchment did not take place. It seems plausible to argue that older aeolian deposits (dune sands) were re-mobilized and lost their older OSL signal due to repeated sunlight exposure during transport. However, mid-Holocene ages of dune deposits remain less reported in this larger region and may indicate that climatic and/or geomorphological conditions for sand transport were limited.

Two paleosol layers between aeolian sediments in section KHS15 (Fig.40, see also Fig.34, chapter 5.6.2) were formed within fine sand of aeolian origin. OSL ages between the relative weakly developed lower paleosol indicate its formation between 0.4.and 0.5 ka. The age reversal in this sequence does not allow a better estimation for the time of soil formation. The well-developed paleosol in the upper part buried by aeolian deposits of unknown age seem to be formed after 0.4 ka, indicating a break in aeolian deposition at that time before further aeolian sands were accumulated again. Compared with the relatively weak paleosol below and above (modern soil on top of the profile), this soil appears to be formed during favourable moisture conditions or its formation lasted longer, although the timing of soil development falls into the period of the relatively cold LIA.

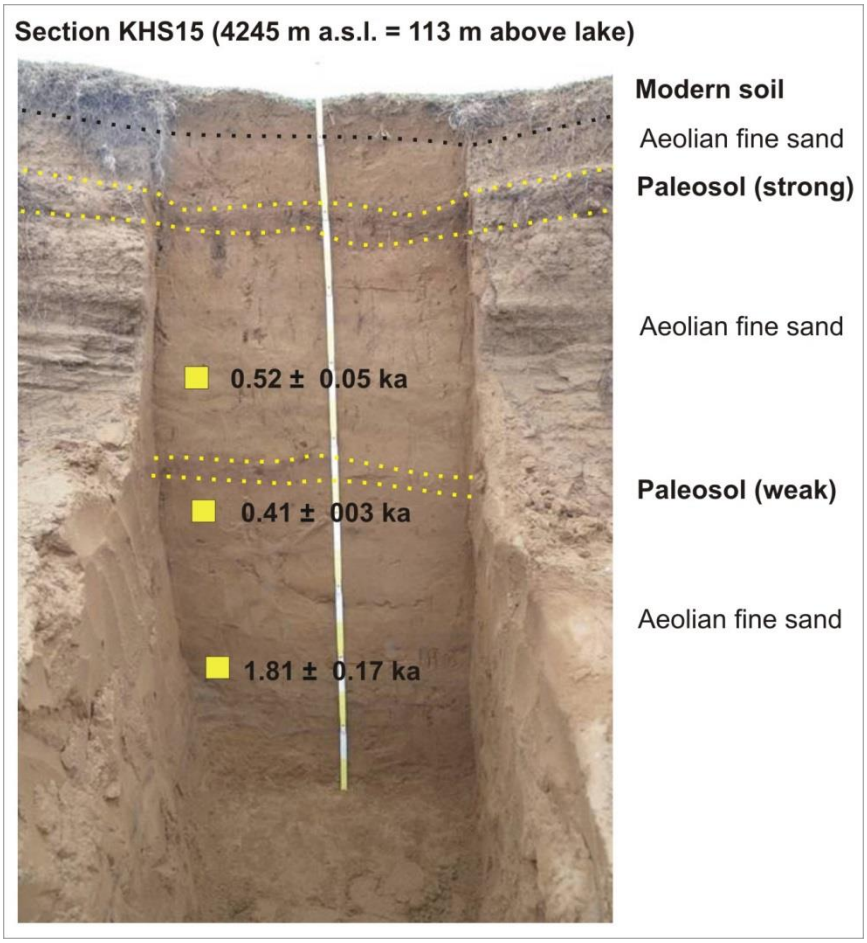

Fig. 40 Section KHS15 aeolian sand section with OSL ages and marked (paleo) soil layers.

Similar conditions can be inferred from the organic-rich (peaty) layers in the terrace T2 section KH9 (Fig.38) which were formed at around 193±27 cal. yr BP (Tab.2), at least requiring favourable hygric conditions for wetland development there (Bullock and Acreman, 2003).

6.1.2 Sedimentary processes in Kuhai Lake

It is well-known that lake basins are complex systems with general diverse limnological, geochemical and sedimentary patterns (e.g., Håkanson and Peters, 1995; Last, 2002), depending on lake size, basin morphology, water quality and water depth as well as geological and climate settings. Despite tectonic influence on many lake basins of the Tibetan Plateau, the interrelationship between catchment processes and the lake basin plays an important role with respect to sediment and water flux towards the lake.

Commonly, sediment records from the central part of lakes were used for paleoclimate studies, implying that they best monitor hydrological and climate-related variations through time. Catchment influence was not considered or in some cases indirectly inferred from the used proxy records (e.g., Lister et al., 1991; Wei and Gasse, 1999; Shen et al., 1995; Zhang and Mischke, 2009; Mischke et al., 2010a; An et al, 2012). In general, it can be assumed that records from central parts of lakes in far distance from inflowing rivers and other catchment-related processes, such as mass flows or changes in river courses and locally restricted sediment transport, for example, cannot be traced in those records, as long as fluctuations in water budget (notably lake level declines) remain on moderate levels. Instead, they only can reflect the mean of many lake-internal and –external processes which commonly lead to the underestimation of locally relevant processes related to sediment flux and water resources. Conversely, multiple sediment records from different locations within a lake system enable the recognition of sedimentary processes and water resources much more precisely. They allow the identification of individual processes that can reflect influences of local and regional/global climatic significance (Rickets et al., 2001; Wünnemann et al., 2012; Yan and Wünnemann, 2014).

Kuhai Lake serves as an example to demonstrate the high spatio-temporal diversity of lake deposits, which encompass the last 4000 years.

6.1.2.1 Modern processes derived from lake surface sediments in Kuhai Lake

The spatially diverse distribution pattern of chemical precipitates, grain size components and aquatic organisms (ostracod, organic carbon) in lake surface samples of the saline Kuhai Lake are likely attributed to five major processes:

i) local different sediment and water influx from the catchment in relation to nearshore morphology,

ii) lake-internal currents by wind fetch and pathways of inflowing water,

iii) lake basin morphology with respect to water depth and related vertical temperature gradients,

iv) light penetration as a function of water transparency and
v) catchment topography in combination with seasonality of climate parameters, influencing aeolian transport and depositional processes.

These influencing processes are discussed in light of the different proxy data obtained from the surface samples that represent the deposition during the last 15 years.

6.1.2.1.1 Aquatic plants and organic matter (OM)

Nearly all surface samples contained plenty of algae (mainly green algae, not identified in detail) in all water depth. Higher aquatic plants, such as *Potamogeton sp*. only occurred in the photic shallow littoral zone of the lake above 6 m water depth with water temperatures >10°C in summer time. The abrupt disappearance below this water depth indicates insufficient light penetration for photosynthesis of these plants, due to lowered transparency by increased suspended particles in the water column, including algae (Håkanson and Peters, 1995). However, dissolved oxygen existed in all water depth enabling biological life, even at water depth exceeding 20 m, thus indicating ventilated lake bottom waters in the profundal zone. According to systematic echo sounding results which enabled the visual inspection of the lake-bottom sediments and water column above, a higher density of aquatic plants close to the inflowing rivers was observed, despite low values of OM preserved in surface sediments (Fig.41). It may indicate that freshwater flux and slightly coarser sediments could have a positive influence on aquatic plant growth. With respect to the spatial distribution pattern (Fig.41) however, highest values of OM mainly occurred in sediments of the profundal zone (deeper parts of the lake), except for some areas in the south-southeast and a north-western bay of the lake, indicating that aquatic algae were the main contributors of OM in the surface sediments.

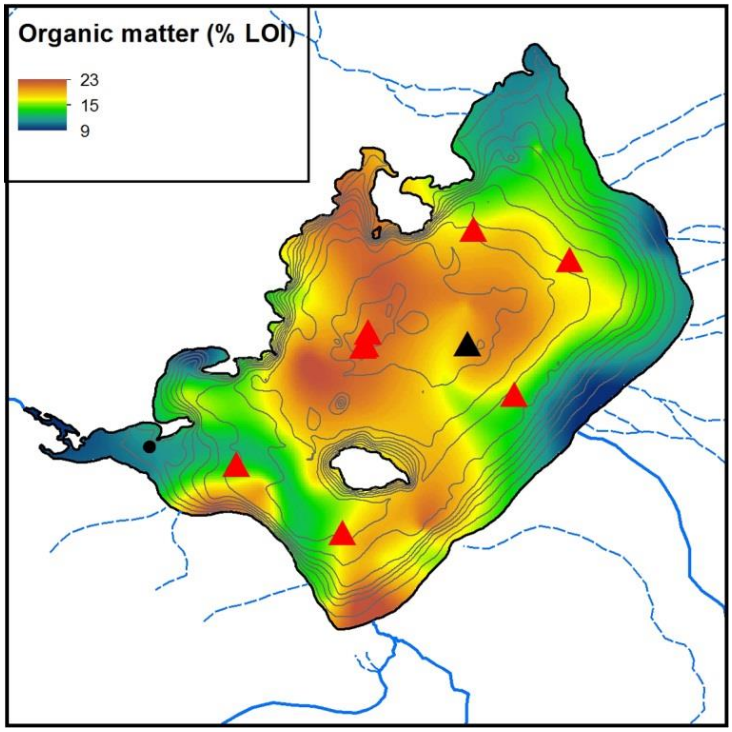

Fig. 41 Spatial distribution of organic matter in lake surface sediments of Kuhai Lake. Red triangles mark the locations of cores KH11-KH17; black triangle the core published by Mischke et al. (2010).

Variations in organic carbon/OM are frequently used in lake records to infer climate-dependent changes in bio-productivity through time based on the assumption that warm-wet climatic conditions would have enhanced vegetation development and thus increase in organic carbon, finally preserved in lake records (Zhao et al., 2011; Wu et al., 2006; Wünnemann et al., 2012; An et al., 2012; Hou et al., 2016; Yan et al., 2017). These inferences however, depend on the preservation ability in lake systems and, as documented in this study, on the location, where sediment cores were retrieved. Values at a certain site and a certain time can be high, while at a different site values can be very low for the same time period, as documented in Kuhai Lake. Variations through longer time periods therefore require the evaluation of lake-internal depositional conditions that affect the distribution of bio-remains.

6.1.2.1.2 Ostracod associations

Only two species of ostracod (*Eucypris mareotica, Limnocythere inopinata*) were found in surface samples at few locations along the littoral zones of the lake (Fig.17, chapter 5.4.3), whereas surface sediments from the deeper parts remained free of any ostracod. Species however, inhabiting the nearshore shallow ponds and wetlands close to the lake, included few more species, depending on their habitat preferences as discussed below:

Eucypris mareotica (Fischer, 1855) also known as *Eucypris inflate* (Sars, 1930) is abundant in Qinghai Lake (ca.14 ‰ salinity). This species is found in brackish to saline waters with a very wide salinity range, but more as a saline water indicator (Meisch, 2000; Mischke, 2012; Li et al., 2010; Yan and Wünnemann, 2014). The preferred water depth is

<23 m, with an optimum of ca. 5 m in Lake Donggi Cona (Mischke et al., 2010a). *E. mareotica* was also reported in sediment cores of Hala Lake with salinity ranges of 17-18 ‰ (Yan and Wuennemann, 2014).

E. mareotica was found as fossil forms in few lake surface samples but also in sections (KHS1, KHS27) and in cores (KH 11-KH17), assuming that the modern water chemistry of pH 7.2-8.7, conductivity 19.9-22.8 mS/cm, TDS 20.1 g/L. were tolerated by this species. Based on the surface samples, *E. mareotica* were only found at 7-11 water depth, with higher abundances at 7-8 m water depth, especially at locations closer to inflow. This species was not found at depth below 12 m.

Limnocythere inopinata (Baird, 1843) is a widely distributed species which is unable to swim in water bodies on the Tibetan Plateau, but is tolerant to a wide variety of environmental conditions and can live in the littoral zone of small water bodies, such as ponds, lakes and even wetlands (Smith and Delorme, 2010) and in running waters as well (Meisch, 2000; Li et al., 2010) but not in springs or streams in North American freshwater bodies (Smith and Delorme, 2010). *L. inopinata* can live in waters with EC of 1.4-2.0 mS/cm (Mischke et al., 2007), while the salinity optimum lies at of 3-9‰ (Holmes et al., 1999). *L.inopinata* prefers calm waters rich in macrophyte debris on the lake bottom (Meisch, 2000; Li et al., 2010). This species prefers a <10 m water depth, especially with the optimum depth between 1 and 2 m in Lake Donggi Cona, but also occurs there occasionally in 8-10 m water depth (Mischke et al., 2010a). Records from European lakes indicate an optimum water depth of around 6 m (Meisch, 2000). Zhai et al. (2010) described *L. inopinata* as an abundant species at 7-9 m water depths, less abundant at depths of 9-10 m and 1.5-7 m while scarce at depths of 10-11.5 m, based on a detailed study in Dali Lake, Inner Mongolia. However, this species is very seldom found in deeper environments (Savolainen and Valtonen, 1983, ref. in Mischke et al., 2010a). In Lake Tangra Yumco in southern Tibet, *L. inopinata* was even found at 235 m water depth, with 8.3 ‰ salinity of the host water (Akita et al., 2012). Li et al. (2010) found shells of *L. inopinata* in swamps and samples of Lake Qinghai, Lake Erhai and in the littoral zone of Lake Gahai, with salinity optima of 4.63-14.74‰ in this area.

In Kuhai lake area, *L. inopinata* is recorded in different kinds of samples. In addition to the living conditions in lake water, this species occurred frequently in nearby ponds with pH of 7.6-8.1, salinity of 0.65-2.35‰ (conductivity 1.3-6.3 mS/cm) and TDS of 0.9-5.1 g/L. Consequently, the pH and salinity ranges of *L. inopinata* are wider than those of *E. mareotica* in Kuhai Lake area. Fossils of *L. inopinata* were found at 5-8 water depth based on the recent distribution pattern in the lake (Fig.17, chapter 5.4.3), with higher abundances at 8 m water depth, right above the present thermocline and closer to inflowing freshwater . This species was not found in water depth below 8 m.

***Ilyocypris* spec.** in Kuhai was not identified in detail because of their similarity to other species in Tibetan lakes, which do not allow a clear species identification. *Ilyocypris bradyi*, *Ilyocypris echinata* and *Ilyocypris gibba* were reported in recent ostracod distribution patterns in the Qinghai Lake area (Li et al., 2010). The genus *Ilyocypris*

occurs in lakes, ponds, ditches and rivers etc. (Meisch, 2000). Yan et al. (2017) reported that *Ilyocypris* sp. occurred in all wetlands around Qinghai Lake and in Erhai Lake but not in Qinghai Lake itself, indicating a clear preference to fresh or slightly brackish water conditions.

In Kuhai Lake area, *Ilyocypris* sp. was only present in two ponds (KHP1 and KHP6), in the lower part of core KH17 (not focused in this study) and in sections (KHS27 and KHS29) but not in surface sediments of the lake. According to the abundant occurrence of this species in the nearby pond (KHP6) with influence of moving water, pH value of 7.6, salinity of 0.7 ‰ (conductivity 1.3 mS/cm) and TDS of 0.9 g/L. seem to be preferable living conditions for this species. Hence, the occurrence of *Ilyocypris* sp. in sediment cores could indicate similar ecological conditions.

Fabaeformiscandona rawsoni (Tressler, 1957) was only found in pond samples (KHP 1, KHP 2, KHP 6 and KHP 7) and some samples of section KHS 27 but not in lake surface sediments.

The majority of published records about ecological conditions of *F. rawsoni* indicate that this species prefers shallow lentic water bodies with variable water chemistry (e.g. Curry 1999; Griffiths and Holmes, 2000; Bunbury and Gajewski, 2005) and a wide range of water temperatures (Griffiths and Holmes, 2000; Smith and Delorme, 2010). It is known to survive drying out and freezing in smaller water bodies (Smith and Delorme, 2010). The same is reported for *Candona candida* in Europe (Meisch, 2000) and confirmed by preference for small water bodies on the Tibetan Plateau (Akita et al., 2016). It was also described as a lake and pond environment indicator based on the records from a section (P14) from the neighboring Donggi Cona Lake (Mischke et al., 2015). However, Mischke et al. (2003) reported that *Candona rawsoni* (a synonym for *Fabaeformiscandona rawsoni*, Griffiths, 1995) is abundant in the littoral zone of Lake Luanhaizi with some influence of moving water. This species was also frequently found in wetlands and ponds in the vicinity of Qinghai Lake, including Daotanghe wetland/pond region, where contact to fluvial activity of the attached Daotangh River was reported (Yan et al., 2017).

In Kuhai Lake area, *F. rawsoni* is present in relative freshwater environments of small ponds/wetlands close to the lake with pH values of 7.6-8.7, salinity 0.7-11.5‰ (conductivity 1.3-29.9 mS/cm) and TDS of 0.9-18.3 g/L. These values are generally lower than those of Kuhai Lake water and may explain why this species was not found in all lake surface samples.

Tonnacypris edlundi (Van der Meeren et al., 2009) was named after taxonomy studies in western Mongolia. It was found in a grassy outflow stream at Bakhlagiin spring and at several nearby sites as well. Reported water chemistry from nearby accounted for pH 7.9, conductivity 1222 µS/cm, TDS 876 mg/L, water temperature of 6.3 °C and DO of 11.5 mg/L (Van der Meeren et al., 2009). Compared with the type of waterbody, containing *T. edlundi* in Mogolia, the wetland conditions in Kuhai Lake area are similar, but due to only

1 valve found in sample KHP1, ecological conditions for this species could not be approved.

6.1.2.1.3 Carbonates in surface samples

According to the semi-quantitative results based on XRD analyses of minerals and the quantitative ICP analyses of selected major geochemical elements (Ca, Mg, Sr, S), carbonate minerals occurred as stoichiometric Calcite, Monohydrocalcite (MHC), Mg-rich Calcite (High-Mg-Calcite), Dolomite and Aragonite (see Fig.14, chapter 5.3.1). Apart from small amounts of detrital carbonate input (<3%), namely from the eastern catchment (Triassic limestone) and by aeolian transport from local sources, the majority of carbonates are considered to be precipitated from bi-carbonate-rich (HCO_3^-) lake water as authigenic carbonates mainly by the release of carbon dioxide (CO_2) under evaporative pressure and/or by CO_2 uptake of plants/algae during photosynthesis (Kelts and Talbot, 1990; Wei and Gasse, 1999; Last, 2002; Leng and Marshal, 2004). The latter is assigned to biogenically induced carbonate precipitation. Major cations (Ca^{2+}, Mg^{2+}) are delivered as weathering products from the bedrock catchment by river discharge and by dust transport across the lake basin as well. It can be assumed that carbonate precipitation mainly occurs during the summer period of increased biological activity and warmer surface waters . The latter reached higher temperatures (13°C, measured end of June 2016) than the air temperature (8°C, maximum in summer, according to meteorological data), due to strong radiation in high altitudes (<4100 m). According to the vertical temperature profiles (Fig.7) which show mixed surface waters with almost constant temperatures down to ca. 6 m depth, it can be assumed that carbonate precipitation preferably occurs in this part of the water body.

Water inflow with generally lower temperature (<6°C) and thus less ability to immediate carbonate precipitation and deposition, however, seem to be a controlling factor for the distribution of carbonate in the lake basin (Gierlowski-Kordesch and Kelts, 1994). Inflowing water in combination with moving surface water, the latter induced by wind fetch mainly from northern to north-western directions (see chapter 5.1), is responsible for the transport of water and suspended load far into the lake center and to generally southern directions (Fig.42). As a result, deposition of Calcite and MHC are highest in the central, north-western and southern part of the lake (Fig.17, chapter 5.3.1), comparable with the spatial distribution pattern of calcium concentrations in the lake basin (Fig.17, chapter 5.3.1). Interestingly, MHC, the hydrous form of calcite ($CaCO_3+H_2O$), was always found in association with calcite and exceeded the calcite values at several locations.

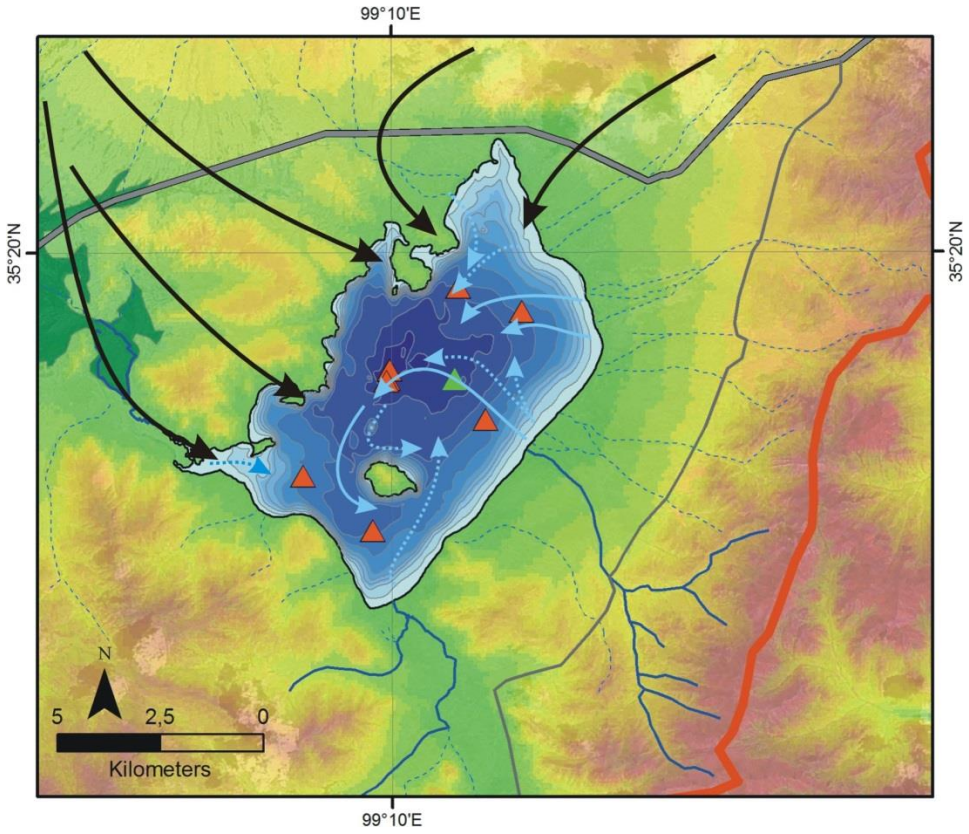

Fig. 42 Sketch showing the major surface wind trajectories in Kuhai catchment (black arrows) and surface water currents across the Kuhai Lake (blue arrows). Dotted blue lines indicate less influence on surface water movement.

MHC is considered to be a relatively rare and unstable carbonate mineral which does not occur in all lakes on the Tibetan Plateau. It was already described by Zhou et al. (2010) who found this mineral in few surface samples from Kuhai Lake. MHC was also reported from Nam Co, southern Tibet, as a distinct sequence in a sediment core, dated to 2.1 cal. yr BP (Li et al., 2008), but not found in surface samples so far. MHC in a short sequence of lake deposits from Heihai Lake, western Tibet, was described by Chen (2014, unpublished Master thesis, Nanjing University).

Several studies on this seldom mineral indicate that it is formed in saline water bodies and in presence of magnesium-containing solutions (Winland, 1969; Taylor, 1975; Fukushi et al., 2011) and converts to calcite or aragonite with increase in water temperature (Taylor, 1975; Bird et al, 1991) or under a dry state (Hull and Turnball, 1973). Dickens and Brown (1970) mentioned that MHC changes to Ikaite ($CaCO_3 + 6H_2O$) under aqueous solution near 0°C, accompanied by increase in volume, so that this hydrate will be more favoured by increased pressure (Hull and Turnbull, 1973). Fukushi et al. (2011) mentioned in their review paper that MHC forms in presence of high Mg/Ca ratio exceeding 4 and transforms to Aragonite under temperatures of 10, 25, 40 and 50°C within hours or few days, based on laboratory tests. The solubility of MHC however, decreases with temperature (Fukushi et al., 2011).

In sediments of Kuhai Lake highest values of MHC were only found at sites with Mg/Ca ratios below 4 and not simultaneously with non-detrital High-Mg-Calcite and Dolomite. With respect to the distribution pattern of MHC in Kuhai Lake, higher concentrations were found in sediments below 10 m water depth and thus below the summer thermocline reaching temperatures below 8°C and down to 0.8°C. It can be therefore assumed that MHC is preferably preserved under cold water conditions in the profundal zone of the lake and may be also preserved in sediments once sedimentation rates are high, as reported by Li et al. (2008). Low amounts and even the lack of MHC in the eastern and north-eastern shallower parts indicate the fast mixing of cold river water with warmer lake waters, hindering possible formation of MHC from preservation in surface sediments nowadays. However it is not yet clear whether MHC also forms before, after or parallel with precipitation of calcite in surface waters. MHC was observed under natural conditions as a precursor or intermediate product during calcite formation (Fukushi et al., 2011), while transformation of MHC is reduced once the minerals reached the cold water zones below the thermocline. From this study it cannot be decided whether faster sedimentation rates of lake-bottom sediments prevent MHC from transformation, as proposed by Li et al. (2008).

High-Mg-Calcite and Dolomite showed a very restricted distribution pattern in lake surface sediments of Kuhai Lake (Fig.17, chapter 5.3.1). Despite their minor lake-wide distribution as detrital components, high concentrations only occurred in the shallow littoral zones above 10 m water depth in the northern part of the lake and in the east, close to the inflowing perennial river. Higher Mg-Ca ratios were associated with the occurrence of these minerals but also along the southern/south-western lake shallow lake margin (Fig.17, chapter 5.3.1).

Marine and lacustrine carbonates are usually classified by Mg content in stoichiometric calcite, stoichiometric dolomite and excess-Ca Dolomite as well (Solotchina et al., 2009; Gierlowski-Kordesch et al., 2010), identifiable in XRD diagrams by the shift of peaks between stoichiometric Calcite and Dolomite reflections (Goldsmith et al., 1961). Based on the observational XRD data the mineral sequence Calcite-High-Mg-Calcite-Dolomite is considered to be mainly dependent on the Mg/Ca ratio of the water from which the minerals precipitated. Successive precipitation form Calcite to Dolomite is likely the result of shifts in water chemistry towards increased Mg content during ongoing precipitation, resulting in higher salinity, unless the water is constantly renewed by freshwater supply (Last, 2002).This general pattern can be confirmed by the co-occurrence of High-Mg-Calcite and Dolomite with increased Mg/Ca ratios in the respective samples from Kuhai Lake.

The formation mechanisms of dolomite formation however, are still controversially discussed, often referred to as the ‘dolomite problem’ (Hardie, 1987; Warren, 2000; Fenter, 2007). Despite the lack of convincing explanation how Dolomite was formed, most scientists agree that the majority of this mineral in sediments was formed secondarily by replacing pre-existing carbonates under individual settings (Machel, 2004).

According to Wright and Wacey (2005), Dolomite can also form directly from aqueous solutions in saline and evaporitic settings, as it may happen in Kuhai Lake today.

The reason for its locally restricted distribution remains an open question. Wünnemann et al. (2012) and Wagner (2012, unpublished diploma thesis, TU Berlin) reported the presence of non-detrital Dolomite and High-Mg-Calcite in Hala Lake only at two sites as a result of a tectonically induced mass flow layer from the very shallow northern littoral zone (<10 m water depth) down to the deeper parts of the lake which happened between 8 and 7 cal. ka BP.

Modern non-detrital Dolomite was reported form limited shallow water locations in Qinghai Lake (Yu et al., 2007), similar to the findings in Kuhai Lake, thus indicating its formation under high evaporative pressure in warmer waters of the littoral zone and likely mediated by microbial processes as well (Deng et al., 2010). Taking the above-mentioned aspects of Dolomite/High-Mg-Calcite formation into account, the finding of these minerals in Kuhai Lake suggests their in-situ formation, perhaps at places with less water exchange under local high evaporative pressure.

The occasional occurrence of Aragonite with low amounts (<3%) in surface samples of Kuhai Lake cannot be convincingly associated with the transformation of MHC to aragonite or to other formation processes and also do not show a specific spatial pattern. Hence, this mineral is not considered important related to a certain process. The same applies to Gypsum and the sulphur content in surface samples, which were only found in the central part of the lake basin (Fig.17, chapter 5.3.1) in amounts of <10%. It seems likely that this mineral was transported as a detrital component from the eastern catchment, where the Permian rock formation with locally limited Gypsum-bearing rocks was mined in the past decades. As a result, Gypsum was found in many surface samples but by no means in all. The higher concentration of this mineral in the central part of the lake may be related to transport processes as suspended load via the inflowing rivers and finally deposited there. This finding however contradicts the extreme high Gypsum values and Aragonite in the uppermost sequences of a sediment core close to the lake center, reported by Mischke et al. (2010b), as already mentioned before. The lack of any MHC in this core as well seems to be a unique finding within the entire lake basin and thus casts doubts on the identification of these mineral components.

6.1.2.1.4 Clastic sediments and grain size distribution

Clastic sediments from lake surface sediments were divided into several classes by means of grain size analyses followed by an endmember modelling analysis (EMMA). Single grain-size parameters such as sand, silt, and clay content, or the associated methods of moments (e.g., mean, skewness, kurtosis; Folk and Ward, 1957) however, are biased when applied to multi-modal distributions. Multivariate statistical methods however, such as principal component analysis, factor analysis, and end-member modelling, allow interpretation of all variables within the dataset for every sample (IJmker et al., 2012)

with respect to sediment transport processes and the characterization of typical depositional environments (Dietze et al., 2012; Wang et al., 2015).

As described in the results part (chapter 5.3.2), selected grain size components and the extracted endmembers (EMs) showed a quite diverse spatial pattern (Fig.15, chapter 5.3.2), comparable with the distribution pattern of major carbonate minerals and cations.

In an ideal case, an extracted EM can be assigned to a single process, responsible for the accumulation of a certain grain-size composition. In many cases however, extracted EMs show multi-modal compositions and thus need to be assigned to several involved processes (Wang et al., 2015; Yan et al., 2017). The interpretation of a single process or several processes behind a certain EM depends on the knowledge about the various influencing factors between the sources and the sinks that contributed to the overall sediment budget. In the case of Kuhai lake sediments all extracted three EMs showed multi-modal distributions (see chapter 5.3.2) and thus indicate at least two different processes involved in each EM:

EM1 with the highest score (84% explained variance), mainly derived from the grain size components 2-25µm (fine/medium silt, Fig.15 A, C) was assigned to the typical component for suspended load, transported by the rivers into the lake (ref. Fig.22, chapter 5.5.1). Aeolian sediments, especially wind-blown dust (loess) with a significantly coarser mode than EM1 (35-50 µm), also contained finer fractions in the order of 5-12% of the total loess fraction (ref. Fig.33, chapter 5.5.2). It can be assumed that a certain proportion of loess contributed to this suspended load too, but perhaps of minor importance as the spatial distribution of EM1 within Kuhai Lake indicates. Higher amounts of EM1 were found in the southern part of the lake basin. Taking the transport mechanisms of the rivers and the movement of surface water, affected by wind fetch into account (see above) higher depositional rates in the southern part of the lake seem plausible. Dominance of windblown fine material would result in a more evenly distributed depositional pattern.

EM2, mainly comprising the fractions >65 µm (Fig.15 D, E) only contributed low amounts to the overall sediment composition. It was assigned to the aeolian component, related to fine sand transport from nearby locations and partly trapped in ice, explaining the randomly scattered distribution pattern in the lake basin. Higher proportions of EM2 in the northern and western small bays however, are likely not only the result of wind-transported sand there. Two further processes might have contributed to this EM too:

i) locally transported fine sand during melting processes in early spring when the frozen ground and wetland started to thaw, resulting in surface flow and fluvial transport of silt/sand to the bay and

ii) near-shoreline turbulences induced by wave activity which resulted in disintegration of mixed sediments and better sorting towards coarser fractions (here fine sand), while the finer fractions were removed and transported as re-suspended load. This may have happened in the small bays on the western side of the lake.

On the other hand, the northern bay lies in the direct trajectory of the main wind direction (Fig.42) in late winter and early spring which is responsible for dune formation on the north-eastern side of the lake basin (Lu et al., 2004, 2011; Lai et al., 2009, An et al., 2012). It could be therefore possible that deflated material from the fluvial fan in the north-western catchment was transported westward crossing the lake bay and captured there. This is in general possible, as ice-melt starts from the shore regions in end of March at the same time when wind strength in that region is high. The same applies to the south-western part of the lake with high proportions of EM2 there. A similar process was considered and identified in Hala Lake and Daotanghe Wetland, Qinghai Lake area (Wang et al., 2015; Yan et al., 2017).

EM3 with very low contribution to the overall sediment mainly comprised the finest fraction (clay, Fig.15 B, chapter 5.3.2), assigned to fine suspended load transport. Its distribution with highest amounts in the northern part of the lake not far away from the inflow region of the episodically active drainages in the north east of the lake is surprising, on the first view, but can be convincingly explained. The contributing rivers are only active during the rainy season in summer time, while the rivers pass the very flat and muddy nearshore wetlands and uptake these fine components as suspended load which is then transported into the lake (Fig.2 J). As moving inflow waters from north-east meet with moving surface waters almost in opposite directions, a calm water zone not far from the inflow region may be responsible for sedimentation of the suspended load, even the finest fractions (e.g., Pettijohn et al., 1987). It even seems likely that the water masses and sediments from these rivers may not be always fully transported to the center of the lake and farther south (Fig.42). This specific behaviour is discussed in light of stable isotope distributions in carbonates later (chapter 5.3.4).

Combining both EM1 and EM3 together, their spatial distribution patterns match the pattern for grain size fractions <25 µm very well (Fig.15 C) This also confirms the major contribution of suspended load material to the lake basin, influenced by lake-internal near-surface currents (Fig.42), that are responsible for the spatially diverse distribution over the entire lake basin. Aeolian components may be likely included in the overall sediment budget, but remain at a lower level, perhaps.

6.1.2.2 Past processes derived from sediments in cores KH11-14 in Kuhai Lake

It is important to mention again that sediment cores KH 11, KH12, KH13 and KH 14 are from different locations in Kuhai Lake (Fig.4), reflecting local influences from the sub-catchments much stronger than those records from central parts of larger lakes in far distance from their sources and shores, such as Qinghai Lake (Shen et al., 2005; Liu et al., 2011; An et al., 2012), for example. As mentioned before, records there only represent the **mean** of potential influencing factors and processes archived in the respective sediments, rather than locally important effects.

Instead, the investigated sediment cores within the relatively small Kuhai Lake were much more susceptible to local catchment influences. Sediment core KH 11 was located

in the northeast, indicating stronger influence by the episodic river, entering the lake basin there. Core KH 12 in the east of the lake was strongly influenced by the perennial river with higher energy flow. Core KH 14 was located in lake's center with reduced influence by the perennial river and perhaps by episodic inflow from the north-east. Core KH 13 was obtained from the southeast of Kuhai Lake with direct influence of the other perennial river, mainly delivering sediments under low energy flow from a sub-catchment with different morphology, compared with the main perennial river farther north. As a result, the overall distribution of grain size composition in each core shows quite a lot of differences but also similarities among them. This implies that the contribution of individual processes at each site has changed through time, which could indicate changes in hydrological balances in Kuhai Lake.

The indicators of sedimentary grain size endmembers are usually integrated parts of sediment sources and dynamic processes under different depositional conditions and environments, including the lithology and proximity of sediment sources, transport regimes and/or lake current strength (Weltje, 1997; Dietze et al., 2012, 2013; Wang et al., 2015; Yan et al., 2017). Hence, the mixture of different grain size populations (based on EMMA) can be interpreted as the results of the interaction of different transportation and sedimentary processes. The major processes contributing to the sediment deposition in cores form Kuhai Lake were derived from the endmember algorithm provided by Dietze et al. (2012).

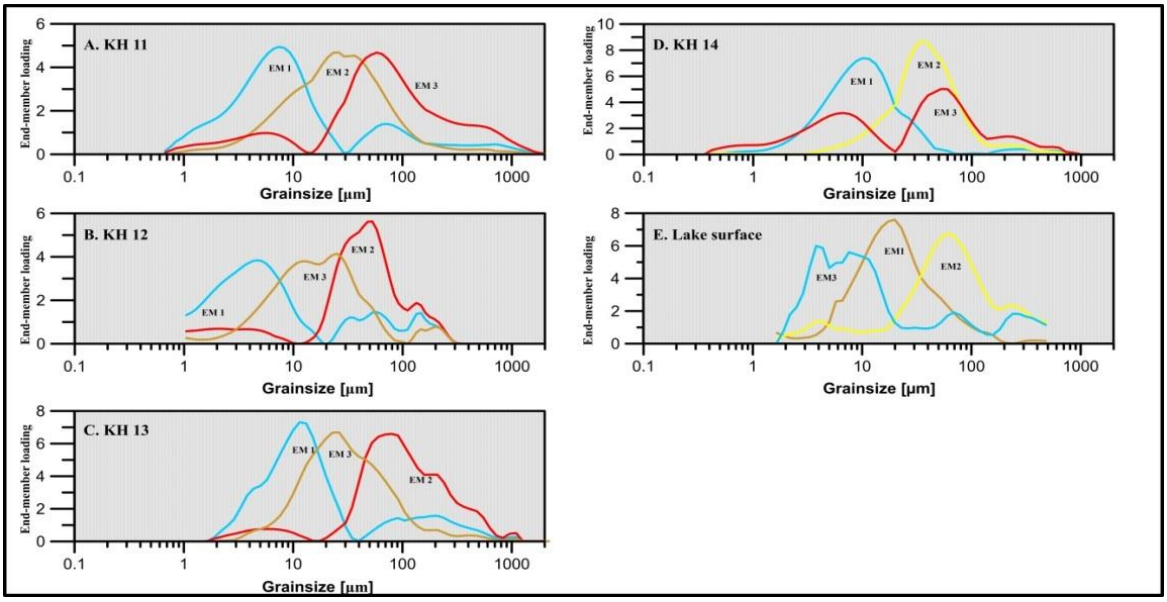

Fig. 43 Endmember distributions in cores KH11-KH14 (A-D), in comparison to lake surface samples (E).

As shown in Fig.43 and Tab.8, the major sediment components in sediment cores from Kuhai Lake are composed of clay and silt, demonstrating that slack water deposits, typical for lacustrine environments, dominated the overall sediment input under almost still water conditions (Wang et al., 2015). Coarser components (sand) in the cores occurred at different time periods in different amounts within the cores. Considering the fact that loess deposits in Kuhai catchment and the neighbouring lake catchment of Lake Donggi Cona showed grain size modes at 35 µm (see chapter 5.5.2 and Stauch et al., 2012), the typical loess component (Vriend et al., 2011) with a unimodal distribution curve could be only documented in core KH 14 from the lake center with deeper water conditions, but not in cores KH 11-13 from the littoral zones, because the latter were stronger affected by river inflow. Coarser grain-size components in coarse silt to fine sand fractions (50-80 µm) suggests stronger influence of fluvial activity, apart from the contribution of aeolian sand that was observed in surface samples with a random spatial distribution pattern as ice-trapped components. Compared with the sediment grain-sizes from riverside sections (100-400 µm, see chapter 5.5.2) and other records (Daotanghe: Yan et al., 2017; Hala Lake: Wang et al., 2015), the sandy sediments observed in respective cores are much finer, although fluvial activity may have been high enough to deliver coarser components to the drill sites as well. However it can be assumed that coarser grains were trapped in the littoral zone because of reduced flow velocity and the trapping effect the dense aquatic plant cover (e.g. *Potamogeton* sp., Fig.2 K) there. Sandy loess found in the section KHS15 outside the lake basin with a comparable grain size composition (50-80 µm and coarser) cannot be directly compared with the suspended load sediments in the lake, as the morphological settings and related onshore processes are stronger affected by near-surface aeolian transport. As a result, short-distance aeolian sand transport can be mixed with suspended air-born loess transport at certain sites along the fluvial-alluvial fans and are considered to be of locally limited processes.

The variable contribution of clastic sediments, delineated as their EMs in cores KH11-14, may not only show fluctuating sediment flux under current lake level conditions but more likely show changing distances between river inflow and the respective sites, dependent on water level changes as demonstrated by Wünnemann et al. (2006, 2010) and Hartmann and Wünnemann (2009), for example.

Owing to the fact that the sediment composition in the cores provided larger variations in grain size through time compared with lake surface samples (Fig.43), the three identified EMs needed to be re-interpreted according to differences in EMs with respect to grain size modes and contribution through sediment depth and time (see chapter 5.4.2). According to Fig.43, after comparing and combining the grain-size distribution in each sediment core, the environmental significances of individual endmembers (EMs) in the grain size distribution can be interpreted as follows:

Tab. 8 Comparisons of EMMA modelling results in Kuhai Lake.

Core ID	No. of EMs	Explaining rate (%)	Modes of EMs (µm)			Descriptions of EMs			Interpretations of EMs		
			EM 1	EM 2	EM 3	EM 1	EM 2	EM 3	EM 1	EM 2	EM 3
Surface	3	95	20	60	4	Unimode	Multimode	Multimode	Suspended load	Aeolian sand	Fine suspended load
KH 11	3	95	8	25	60	Bimode	Unimode	Bimode	Lacustrine	Suspended load	Fluvial
KH 12	3	98	5	50	11	Multimode	Multimode	Broad mode	Lacustrine	Fluvial	Suspended load
KH 13	3	96	11	80	22	Bimode	Unimode	Multimode	Lacustrine	Fluvial	Suspended load
KH 14	3	97	10	35	60	Unimode	Unimode	Bimode	Lacustrine	Aeolian	Fluvial

EM1 in all four cores (KH11-14) were assigned to lacustrine deposits, originally transported as fine suspended load to the core sites, as is happens today. The bi- to multi-modal curves in all four sediment cores have main modes at 5-11 µm, suggesting the deposition of fine to medium silt (see also Dietze et al., 2013). Additionally, coarse silt and fine sand fractions in EM1 curves in cores KH11, KH13 and KH14 would be related to coarser suspended load by enhanced river water supply. In KH12, EM1 also showed an additional mode at the coarse silt fraction, which could be assigned to stronger energy flow from the perennial river at certain periods.

EM2 in sediment core KH14 has a sharp unimodal peak 35 µm (medium silt), which presents the same grain-size distribution as the identified loess section KHS17 from southeast Kuhai Lake (chapter 5.6.2) and Donggi Cona (Stauch et al., 2012). It is therefore most likely that EM2 in KH14 represents the major aeolian component documented in the lake center.

Conversely, EM2 in core KH11 and EM 3 in KH 12 and KH13 were assigned to coarser suspended load with main broad bi-modes at 20-40 µm (fine to medium silt). Taking the locations of cores into account, KH11 is affected by the inflow of the nearby episodic rivers which only delivered suspended load during their active phases with stronger water supply. However, in addition to the episodic water supply, the aeolian components likely contributed certain amounts to the overall sediment budget (Nugteren et al., 2004; Vriend et al, 2011, An et al., 2012). Similar grain size fractions (fine silt and medium silt, ca. 35 µm) hamper the differentiation between fluvially transported suspended load and aeolian loess. Hence an overlapping of both processes can be assumed. Taking the observed loess deposits in the onshore sections and resulting SAR (0.4 mm yr^{-1} for the time period 9.2-4.5 cal. yr BP) into account, the contribution of the loess component would have been much less than the fluvial (suspended load) one. Similar processes apply to EM3 in KH12 and KH13. KH12 however, is influenced by the perennial river discharge with higher energy flow, so that EM3 in this core has a main mode in the fine silt fraction (15-25 µm) together with a right-tailed mode of fine to medium sand, while EM3 in KH 13 has a more clear mode at 25 µm (fine to medium silt), which is more likely produced by

the constant water and sediment supply via the meandering river in the south-east of Kuhai Lake, indicating perennial lower energy flow as it happens today.

EM3 in KH 11 and KH 14, together with EM2 in KH 12 and KH 13 can be assigned to a typical fluvial process of relative higher energy flow with multi-modes between <10 and 400 µm (Fig.43). The main modes of EM3 in KH11 and 14 and EM2 in KH12 and KH13 represent the coarse silt/fine sand fractions (60-100 µm) and modes with coarser components underline the potential fluvial origin. Due to the location of KH14 in the lake center, less river influence can be assumed, resulting in finer grain size fractions (25 µm) of EM 3 too.

Variations of these two EMs suggest alternations in lake level and thus more (less) influence of fluvially transported grain size populations (EM3/EM2) to the respective sites. For example: a deceasing lake level and/or increased flow energy of the eastern perennial river would result in coarser components delivered to the lake center, where finer suspended load material can be contemporaneously deposited (Vandenberghe, 2002). In locations closer to the shore, coarser material would be deposited as well, while finer components are lacking due to continued transport as fine suspended load towards the center. During higher lake levels and /or reduced river flow, coarser components cannot reach the center, except for the finer suspended load, while coarser material in nearshore regions may consist of both, coarser and finer components.

The spatially diverse distribution pattern of sediments and related EMs, observed in lake surface samples, can be also recognized in the cores for the last 4000 years. Based on the outlined processes and behaviour of transportation mechanisms, changes in sediment composition of cores KH11-KH14 with reference to the EMs and stable oxygen isotopes are discussed, following consecutive time periods marked in Fig.44. Slight differences in chronology of probably 100 years between the records need to be considered, as each core is based on an individual chronology but with reference to the so-called master chronology of core KH14. However, taking the existing spatial diversity of modern sediments in Kuhai Lake into account (chapter 5.3), simple Wiggle matching cannot be applied for a realistic core comparison.

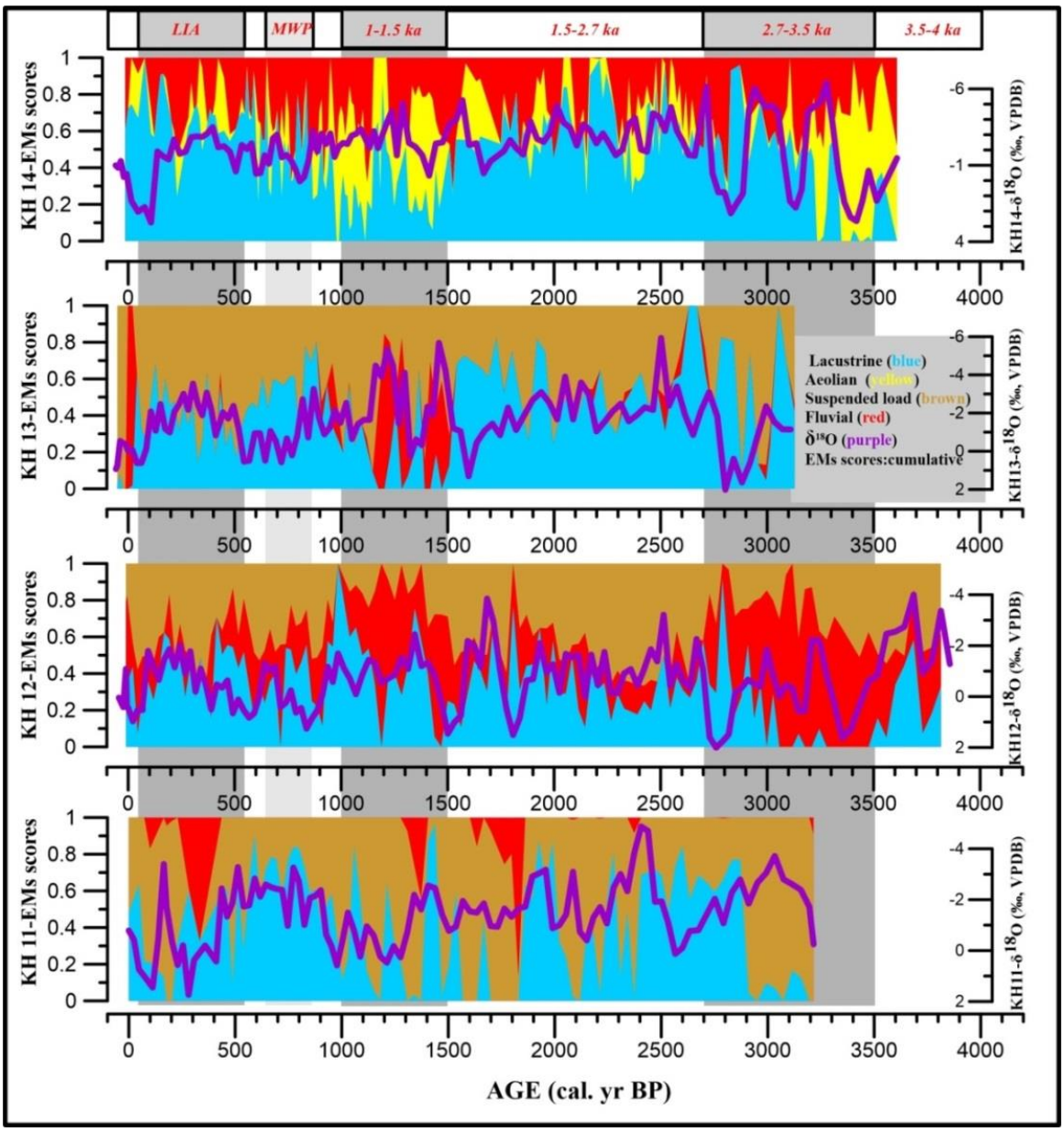

Fig. 44 Endmembers (EMs) grain size and oxygen stable isotope distributions in cores KH11-KH14 through time.

The period 4.0-2.7 cal. ka BP is not fully represented by all sediment cores. Only core KH12 covers this period completely. In core KH11, lacustrine sediments (blue colour in Fig.44) were absent or showed very low amounts in expense of coarser suspended load components (brown colour in Fig.44) between 3.2 and 2.9 cal. ka BP with reverse conditions afterwards. Comparable conditions could be observed in core KH12 with low or even absent lacustrine facies between 3.9 and 2.8 cal. ka BP. Differently from KH11, high amounts of fluvial sediments (red colour in Fig.44) and variable suspended load replaced the fine-grained sediments at that time. In core KH13, fluctuating proportions of lacustrine and suspended load sediments occurred at 3.2-2.7 cal. ka BP, while in core KH14 very low to absent lacustrine facies was replaced by eolian sediments (yellow

colour in Fig.44), alternating with fluvial components between 3.65 and 3.2 cal ka BP, but with considerably higher amounts of lacustrine components after 3.2 cal. ka BP.

In general, the spatio-temporal distribution pattern of the three EMs suggests unfavourable hydrologic conditions for the deposition of EM1 (fine-grained lacustrine facies) during this time period. Even in the central part (KH14), this component was lacking for certain periods. Instead, fluvial (coarser) and coarser suspended load sediments at sites KH11 and KH12 and to a certain extent also at KH13 indicate that the influence of moving water at the respective core sites was considerably higher than nowadays. The input of aeolian sediments (loess) at site KH14 indicates that this component also contributed to the other core sites but was mixed there with suspended load and/or coarser fluvial sediments. Corresponding loess deposits are preserved in the upper part of the loess section KHS17 (see Fig.35). Hence, it can be inferred from this distribution pattern that the lake most likely experienced a low stage with slightly fluctuating lake levels. The sites KH11, 12 and 13 may have even temporarily fallen dry or they hosted very shallow water environments, similar to ponds and wetlands, episodically flooded by river activity, as it happens today. Such conditions were observed at the onshore section KHS1 and in the flat wetland regions along the eastern and north-eastern shore. Furthermore, aeolian activity occurred contemporaneously with the deposition of loess in core KH14 and KHS17 between 3.6 and 3.0 cal. ka BP, as evidenced by the OSL- dated dune sand at the bottom of section KH4 (Fig.30, chapter 5.6.2), which provided a similar age. Stable oxygen isotopes fluctuated within high amplitudes of up to 9‰, almost similar in all cores, indicating highly variable isotopic composition of the host water and perhaps different moisture sources.

During the **period 2.7-1.5 cal. ka BP** lacustrine deposits (fine suspended load, slack water) dominated the sediments in KH 13 and 14, accompanied by suspended load (KH13) and fluvial/aeolian components in KH14. Conversely highly variable amounts of lacustrine and suspended load components were recorded in cores KH11 and KH12 for the same time span. It can be assumed that the hydrological conditions in the lake center and also in the southern part of the lake (KH13) were relatively stable in terms of favourable conditions for the continuous deposition of fine-grained lacustrine components (EM1) and lake water conditions, although fluctuations were visible by the contribution of the other two EMs as a result of moderate changes in the hydrological balance of the lake without phases of desiccation. The high-amplitude fluctuations in cores KH11 and KH12 can be explained by variable river water discharge and energy flow. From KH11 it can be assumed that lower lake levels and/or enhanced energy flow from the episodically flowing rivers in the north-east induced up to 100% of suspended load deposition during the time intervals 2.2-2.0 and 1.7-1.5 cal. yr BP. Stable oxygen isotopes in cores KH13 and KH14 fluctuated with relatively low amplitudes and a trend towards heavier values at around 1.6 cal. ka BP. Higher fluctuations were recorded in the cores KH11 and KH12, due to variable water flux along the two different drainages systems and likely also at different times: only summer period for the drainage mainly supplying sediments in KH11 and all year round supply from the perennial system mainly influencing cores KH12 and KH14.

A period of mainly negative water balances seem to have occurred at **1.5-1.0 cal. ka BP.** This can be observed in all cores, although the contribution of EMs varied considerably, similar to the time period 3.5-3.0 cal. ka BP. Hence, it can be assumed, that the lake experienced a negative water balance with low lake levels again, resulting in low deposition of the lacustrine facies in expense of suspended load (KH11), fluvially dominated sediments (KH12, KH13) and aeolian (loess) deposits, as well as fluvial components in KH14. Stable oxygen isotopes show comparable fluctuations among the cores but partly with opposite trends in core KH11. They are also not associated with the same EMs. Stronger negative values coincide with enhanced fluvial signals in the cores KH13 and KH14 while associations with lacustrine fine-grained deposits occurred in KH12 and only partly in KH11. Strong positive oxygen values in core KH11 are opposite to strong negative values in KH12, 13 and partly KH14, indicating water supply from different water sources with likely seasonal character, similar to the older periods.

The period between 1.0 and 0.5 cal. ka BP, encompassing the Medieval Warm Period (MWP), is characterized by high amounts of lacustrine deposits in access of suspended load that dominated cores KH11 and 13 and, to a lesser extent, the other two cores KH12 and 14, which also contained fluvial components and loess (KH14). Stable oxygen isotopes were quite different among the cores with lighter values in core KH11, almost heavier values in core KH12, and variable values in cores KH13 and KH14. These strong differences in isotopic composition may show that in addition to slight changes in water budget, the contribution of water towards the core sites followed the pathways of the different fluvial systems and their timing of discharge but also the distribution of water masses on the lake itself by the local current system, as discussed above.

The last **period 0.5 cal. ka BP-Present**, including the Little Ice Age (LIA), again shows differences in the contribution of the EMs in cores with generally medium to high proportions of the lacustrine facies but again opposite distribution patterns between core KH11 and the other cores. The same applies to the stable oxygen isotopes which showed generally heavy values in core KH11 and light values in all other cores. An exception is the period of the last ca. 150 years, where the isotopic composition showed heavier values in all cores.

This anomalous distribution patterns of stable oxygen isotopic composition in the cores KH11-KH14 seem to be closely linked not only to the timing of water input but also to the catchment characteristics and the sources of moisture availability (Talbot, 1990; Leng and Marshall, 2004; Henderson et al., 2010; Yan et al., 2017). This aspect is discussed in chapter 6.3 in more detail.

6.2 Water depth changes during the late Holocene (4000 years)

Changes in the hydrological balances of Kuhai Lake result in the loss (increase) of water volume and area. Commonly, lake records can be used to infer such variations by selected proxies derived from lake sediments (e.g., Zhang et al., 2002; Zhang and Mischke, 2009; Mischke et al. 2010b; this study), although quantitative calculations of volume and area remain speculative in most cases. Yan and Wünnemann (2014) could show that quantitative estimations of water depth changes can be successful, if several sediment cores in combination with limnological conditions and ecological preferences of ostracod associations are taken into account, as demonstrated for Hala Lake. Paleo-shorelines surrounding lake basins are suitable indicators at least for higher lake levels during certain periods, as they commonly mark the former boundaries of a lake (e.g., Wünnemann et al., 1998, 2015; Liu et al., 2011, 2015), preserved as morphological features and respective sediments of a typical shoreline facies, often consisting of well-rounded-to flattened pebbles, for example (Pachur et al. 1995; Lehmkuhl and Haselein 2000; Wünnemann et al., 2007; Reinhardt et al., 2007). Remote sensing analyses of shorelines were frequently applied to identify several generations of them (Li et al., 2010; Zhou et al., 2010; Liu et al., 2011; Liao et al., 2013; Li et al., 2014; Wünnemann et al., 2015) but in general without a defined chronostratigraphy, as long as the individual shorelines were not dated. Water balance changes were also derived from hydrological modelling approaches, taking past shorelines and other parameters into account (Kasper et al., 2015).

Quantitative estimations of water depth changes and related lake level variations in Kuhai Lake however, are based on the following factors (see also Tab.9):

i) occurrence of massive aquatic plant (*Potamogeton* sp.) only at water depth <6 m;
ii) abundant presence of *L. inopinata* and *E. mareotica* at 7-8 m water; few abundance at <3 m and lack of ostracod >11 m in water depth (Fig.17);
iii) elevation differences between dated paleo-lacustrine and palaeoshorline sediments and the present lake level;
iv) high concentration of non-detrital Dolomite and High-Mg-Calcite (HMC) at <8-10 m water depth and the dominance of Monohydrocalcite (MHC) in sediments <10 m for cold water condition and/or supply (Fig.14).

Given the premise that limnological conditions during phases of comparable water level as it is today did not change throughout the late Holocene, then the sediment records from cores and catchment sections can be used to estimate water depth changes. Considering successive sedimentation over time, water depth changes could be transferred to lake level changes for certain time windows, based on the individual chronology models of each sediment core and sections with age uncertainties of 100-150 years for the cores, at most.

6.2.1 Periods of lower-than-Present water depths

During **4-2.7 cal. ka BP**, water depth in Kuhai Lake was estimated to have dropped by about 6-16 m compared with the present lake level during different time intervals, divided into two phases: i) 4-3.4 cal. ka BP and ii) 3.4-2.7 cal. ka BP. This inference was already discussed on the base of sedimentary processes (see above), which confirm lowest contribution of lacustrine deposits and even absence at all sites during this period.

The older period was only documented in core KH12 and partly in core KH14. Important is that organic-rich layers composed of plant communities including sea grass (e.g., *Potamogeton* sp., similar to the modern time) were found in the bottom of cores KH12 and KH14, covering the time ~after 3.8 -3.4 cal. ka BP. These plants only occur today in the littoral zone of the lake above 6 m water depth and in shallow pond-like environments close to the lake. Taking into account that these communities (not identified in detail) were also found in core KH14 at a modern water depth of ~22 m, it can be assumed that the lake shrank at least by about 14-16 m to enable plant growth there. This would also indicate that the sites at KH11-K13 were temporarily dry and/or experienced pond/wetland conditions (Fig.45). The occurrence of abundant ostracod (*Eucypris mareotica*, Fig.46) at site KH12 is evidence of a shallow, perhaps episodically existing brackish water body, isolated from the lake. Highest values of High-Mg-Calcite and Dolomite in cores KH12 at 3.8 ka BP and at 3.5 ka BP in KH14 (Fig.19) is a further indicator of a shallow water body and high evaporative pressure, even in the lake center and could indicate a water depth of 8-10 m. Hence, a minimum lake level decline of about 6 m at 3.8 ka BP and ca. 14-16 m at 3.5 ka BP was estimated.

Tab. 9 Estimated water depth changes and related factors in Kuhai Lake during late Holocene.

Period			Lake status (m)		Catchment signals				Lake signals													
			Higher than present	*Lower than present*	*Lakeside sections*			*Dune sections*	**Organic-rich layer**				**Ostracods**				**Minerals**				**Sediment**			
Time	**Major Events/ *Dynasties***	**Age (ka BP)**	+	—	**Sediment**			**Aeolian activity**	*Littoral zone (13-14 m)*			*Lake center (~22 m)*	*Littoral zone (13-14 m)*			*Lake center (~22 m)*	*Littoral zone (13-14 m)*			*Lake center (~22 m)*	*Littoral zone (13-14 m)*			*Lake center (~22 m)*
					KHS1 *SE*	KHS29 *NE*	KHS27 *SW*		KH11	KH12	KH13	KH14/KH17	KH11	KH12	KH13	KH14	KH11	KH12	KH13	KH14/ KH17	KH11	KH12	KH13	KH14/KH17
Late Holocene	Dry interlude																							
	Xia/Shang	4~3.4		6-16	—	F	—	A	—	OM	—	OM	—	A	—	A-N	—	HMC(3.8 ka)	—	HMC(3.5 ka)	—	S	—	A
		3.4~3.3		6-14	—	L	L						—	A	—	F-A	—	HMC	—		—	F	—	A
	West Zhou	3.3~2.8		~14	F	F	F	A						A	F	A		MHC		HMC (2.9 ka)	S	F	S	L
		2.8	~ 1.2	~11-14	L	F	F?											HMC			L	L	L	F
		2.8~2.7		~11	F	F	F?											HMC			L	F	S	F
	East Zhou	2.7~2.5		~9	F?	F	F?						F	F							L	S	S	F
		2.5	~ 1.4	~6	L?	F	L						F	F	A			MHC			L	S	S	L
	Qin/Han/Era of disunity	2.5~1.5	~1.5?		L?	F	L	A (2-1.8 ka)					F	F			MHC	MHC	MHC	MHC	S	S	L	L
		1.5	~ 1.4	~2	L	F	L						F	A			MHC	HMC			S	F	F	F
	East Jin Cold Event	1.5~1.4	~ 1.4	~4	L?	F	L	A					F	A	F						S	F	F	A
	Era of disunity	1.4	~2.5?	~6	F?	L*?	L?						F	A	F			MHC			L	F	S	A
	Tang	1.4~1 ka		~14-8	F	F	—						F	F	A (1.2ka)	A (1.3 ka)		MHC		MHC	S	F	S	F
	MWP	0.95~0.65	~2.5?-1.9		L*	L*?	—	A (830-800 yr)					F	F	F				MHC		L	S	L	L
	LIA	0.55~0.05	1.1?	~3-14	—	F?	—	A (530-200 yr)					F-A	F-A	F-A	F-A	HMC(0.3-0.4 ka			MHC	S	S	S	L
20th Century	Warm /cold events	Since 1990 AD		>4	F	F	—		OM	OM	OM	OM	N-A	N-A	N-A	N-A					—	F	F	L

Notes:

Organic-rich layer	OM	Living aquatic plants limit: <6 m	Minerals	HMC	High concentration High-Mg-Calcite: ~8 m;	SE/NE/SW	Locations in Kuhai lake
Ostracods	A	Abundant ostracod (>100 valves) in lake;~7-8 m; pond: *Lino /Ispp*: <1 m; numbers are ages of occurrence		MHC	High concentration Monoydrocalcite: >12 m; and/ or cold water supply	F-A	Ostracod changed from few to abundant
	F	Few ostracod (<10 valves):6,~10-11 m; pond/wetland	Other symbols	—	No information due to core age limit or not dated/calibrated ages	N-A/N-A	Ostracod changed from zero to abundant; vice verse
		No ostracod: >12 m or <3 m		*/?	*: paleaoshorelines; ?: not dated	F+A	Fluvial and aeolian processes
Sediment *(major sedimentary processes)*	L	Lacustrine/ slack water ;		S	Suspended load (low fluvial energy)		
	A	Aeolian; Numbers are part of OSL dated ages		F	Fluvial (high fluvial energy); in sections it's described by gravel & sand		

The possible area of the lake during the shallow stages in comparison to its present and maximum stages is outlined in Fig.45 and shows that the cores KH11-KH13 were located close to the margin of the water body.

Also during the subsequent period 3.4-2.7 cal. ka BP, the lake still experienced a shallow status but water depth may have fluctuated more frequently, and flooded the sites KH11-H13 irregularly. However, abundant and continuously occurring ostracod in all cores, except KH11 until 3.0 cal. ka BP indicate relatively favorable conditions for them to exist. After about 3.0 cal. ka BP, ostracod disappeared in core KH14, indicating water depth rise beyond the living conditions of *E. mareotica* in this lake. However, highest Dolomite and High-Mg-Calcite occurred between 3.0 and 2.8 cal. ka BP in core KH14 and in cores KH12 (within the uncertainty of timing) but not in the other ones, confirming the locally restricted occurrence of these minerals only at certain places and at water depth comparable with the modern time. The presence of MHC between peaking values of High-Mg-Calcite in core KH12 (ca. 3.2-2.9 cal. ka BP) may point to special conditions for the preservation of MHC under intermittent higher lake level/greater water depth. The relative proximity to inflowing cold water from the perennial river under fluctuating lake levels and increased lacustrine sediment deposition (Li et al., 2008) both may have fostered MHC formation and preservation at this site. This low water depth with some fluctuation existed until 2.8 cal. ka BP.

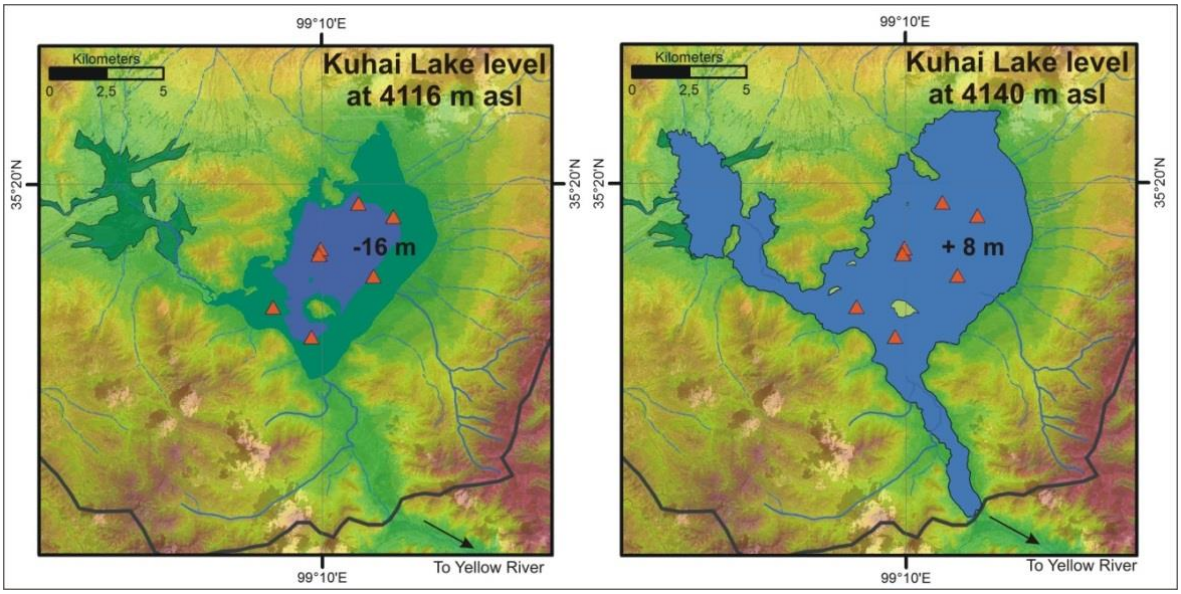

Fig. 45 The possible extent of the lake during the shallow stages (left) in comparison to its present (left) and maximum stages (right).

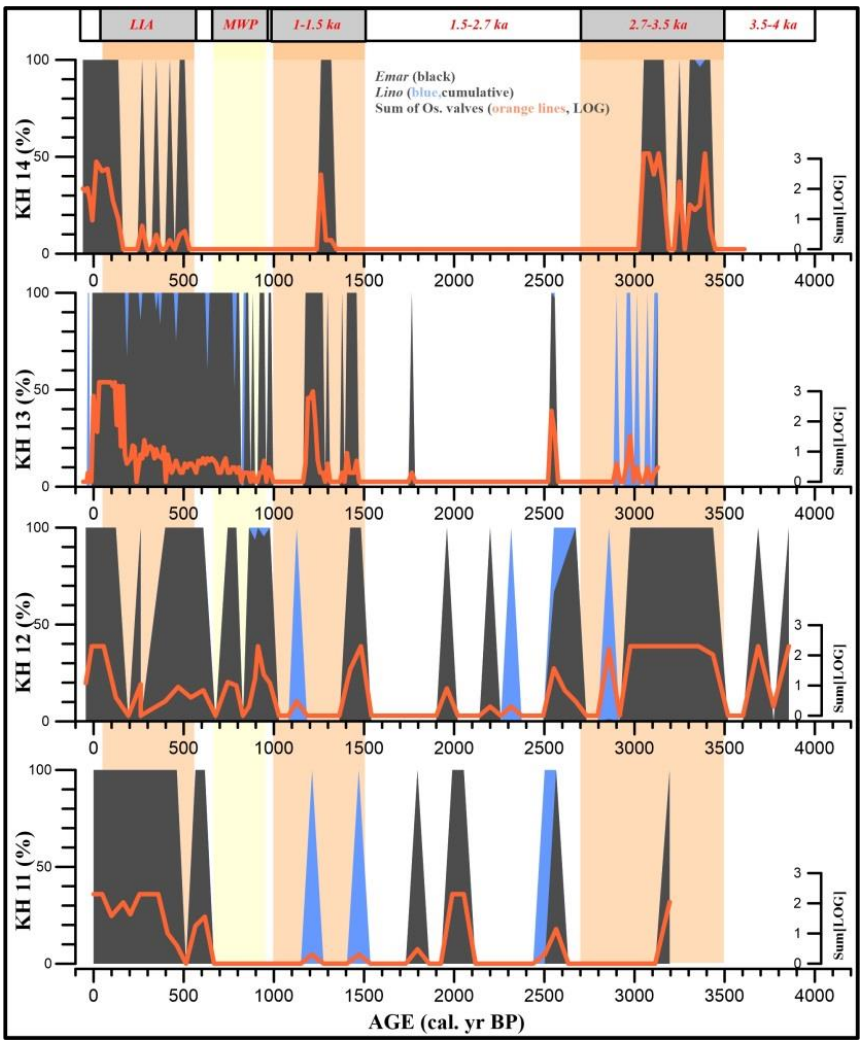

Fig. 46 Ostracod occurrences in sediment cores KH11-KH14 in Kuhai Lake, during the last 4000 years.

A short-term increase of water depth seems to have occurred afterwards, evidenced by ostracod (48 valves *L.inopinata)* found in lacustrine deposits of sections KHS1 (chapter 5.6.1) indicating either a lake level rise up to 1.2 m above the modern lake level within a very short period of roughly 100 years or pond-like conditions separated from the lake. The preferred living conditions of this species and high amounts of lacustrine deposits in cores KH11-13 however, may indicate the former inference.

Despite short-term irregular fluctuations of the water depth, the overall conditions during this time period point to very negative water balances. Comparable conditions were reported from Qinghai Lake (An et al., 2012; Hou et al., 2015) and from Tso Moriri Lake in north-western Indian Himalaya (Gupta et al., in rev.), assigned to a dry climatic phase with clear signals of negative hydrological balances (dry interlude) in both regions, although of slightly shorter duration.

Still lower water depth until **2.5 cal. ka BP** but with a clear signal of rising trend was recorded by the increase of suspended sediment supply in all cores and the lack of ostracod in core KH14, while variable amounts of the two identified species varied

between few and abundant in the other cores. They notably indicate water depth that did not exceed 9-10 m at that time interval. A summer thermocline similar to that of today may have existed at all sites. It can be furthermore assumed that higher amounts of MHC in all cores, preferably formed and preserved in colder water below the thermocline, are indicative of at least this greater water depth (Tab.9).

A longer period (~500 years) of variable water depths below the present lake level occurred between **1.5 and 1.0 cal. ka BP**, similar to the older period of low water depth (3.6-3.0 cal. ka BP). This period however was less punctuated, as the sediments in the cores and the onshore sections displayed partly different patterns. Recorded variable amounts of ostracod at different times between the cores indicate more unstable living conditions at the core sites, perhaps related to stronger fluctuations in water depth and ecology. However, the occurrence of *E. mareotica* in core KH14 at around 1.3 cal. ka BP (Fig.46) may point to the shallowest phase (ca. 14 m lowered water depth in the lake center) during this time interval. Higher amounts of non-detrital High-Mg-Calcite and the lack of MHC, only recorded in core KH12 at around 1.5 cal. ka BP may point to locally favorable conditions for its formation in shallower water. The same applies to the site KH11 but at different time (1.3-1.0 cal. ka BP), matching at least the low water depth at site KH14.

This inference however, is opposite to the dated lacustrine sediments in sections KHS1 and KHS29 which indicate higher-than-present lake levels at around 1.3 cal. ka BP. A reason for this contradiction could be the unclear time of the respective deposits, as their ages were not RE-corrected due to unknown reference ages. It can be therefore assumed that this time of deposition in the respective sections could be also younger in age.

The youngest period of lower water depth of about 3-14 m below the present lake level was recorded for **the Little Ice Age** (LIA, ca. 0.55-0.05 cal. ka BP), characterized by different abundances of ostracod in all cores, with stronger variations in core KH14 (Fig.46). Significantly higher amounts of non-detrital High-Mg-Calcite (Fig.19) was only recorded in core KH11 at 0.4-0.3 cal. ka BP, indicative of local formation during estimated water depth lower than 7 m at that site. It remains unclear, why this mineral was not formed at sites KH12-13, although the water depth was similar.

During the 20th century water level might have been still lower than at the present time, inferred from abundant algae in all cores, which did not occur in such high amounts before. Furthermore, all cores contained abundant ostracod (*E. mareotica*) until the mid of the last century, which indicates more favorable ecological conditions for this species to exist. Reduced water depth might be one factor among unknown others, especially for the massive occurrence of algae at all sites. Changes in water chemistry (e.g., phosphorus, derived from intensified pasture activity around the lake) could be a further factor for increased algae blooms. This aspect however, was not investigated in this study. Higher non-detrital Dolomite and High-Mg-Calcite in core KH13 could be a further signal for lowered water depth although not recorded at other sites.

6.2.2 Periods of equal and higher-than-Present water depths

Positive water balances that induced increasing water depth in Kuhai Lake were recorded for a possible very short period at around **2.8 cal. ka BP** (see above) and much more distinct at **2.5-1.5 cal. ka BP**. Sediment characteristics revealed high amounts of lacustrine deposits in finest fractions and of coarser suspended load (see above). The lack of any ostracod in KH14 and only their occasional occurrence in generally low abundances in other cores indicate larger water depth, similar of today, but with slight fluctuations around this depth towards lower (occurrence of ostracod at core sites) or equal/higher (disappearance of ostracod), taking the modern conditions for ostracod as reference. Lacustrine sediments in onshore sections (KHS1 and KHS27) above the modern lake level, containing the same species, are evidence of temporary higher lake levels (>1.5 m, equal to 1.5 m greater water depth) during this time interval. The lack of non-detrital High-Mg-Calcite and continuous occurrence of MHC at the core sites support this assumption. The marked highest lake level of Kuhai Lake however (Fig.45), has occurred during an earlier period, probably of Mid-Holocene age. This time of results were excluded from this study and will be published elsewhere.

Slightly higher lake stages (~1.4 m) may have also occurred at around **1.4 cal. ka BP**, if the ages obtained from exposed lake sediments in section KHS27 is correct. Stronger fluvial activity of the perennial river that delivered slightly coarser sediments to core site KH12 could be a further indicator, if higher energy flow of the river and not the distance between the inflow region and the core site is considered. This inference however, remains speculative.

Nevertheless, a clear signal for increased water depth during **the Medieval Warm Period** (MWP, 0.95-0.65 cal. ka BP) can be inferred from high deposition of lacustrine fine-grained components in all cores and the only irregular occurrence of ostracod at that time, while they were completely lacking in cores KH11 and KH14.

6.3 Climate inferences

In is widely accepted that the Asian Summer Monsoon (ASM), divided into the branches of the Indian Summer Monsoon (ISM) and the East-Asian Summer Monsoon (EASM) played the major roles for effective moisture transport across the Chinese territory during the Late Pleistocene and Holocene. Their influences with respect to the large region of the Tibetan Plateau and their interplay with the mid-latitude Westerlies crossing the Plateau region as well, is still a matter of debate (Boos and Kuang, 2010; Herzschuh, 2006; Chen et al., 2008; Zhang et al., 2011; An et al., 2012; Yao et al., 2012; Liu et al., 2014). Especially these interplays along the modern boundary of summer monsoon influence have been frequently discussed in many papers. For example, Ramisch et al. (2016) argued that the Kunlun Mountains formed an important barrier for the northward migration of the ISM during the Holocene. An et al. (2012) postulated on the base of a sediment record from Qinghai Lake that alternations between stronger summer monsoon influence (higher moisture supply) and Westerly-derived climate conditions (increased dust flux) happened frequently during the last 30 ka BP. Dominance of westerly climate and weak monsoon influence during the LGM, Younger Dryas (YD) and the late Holocene Little Ice Age (LIA) were considered as the most important ones (An et al., 2012).

Research results based on stable oxygen isotope records from the same lake (Lister et al., 1991; Liu et al., 2009; An et al., 2012) indicate a very similar pattern with speleothem records (Dongge Cave: Wang et al., 2005, Dykoski et al., 2006), confirming the validity of isotopic records from lake sediments in terms of summer monsoon impact (Zhang et al., 2011). Hence, speleothem records became classical archives for identifying monsoon-related climate signals in many other records (Li et al., 2014). Henderson et al. (2010) however, pointed out for the first time, that isotope records can be also differently interpreted, not only confirming effective summer monsoon moisture supply.

With respect to the neighboring Donggi Cona Lake, strong EASM influence with minor fluctuations during the entire Holocene was reported on the base of onshore records (Dietze et al., 2012, 2013), lake deposits (Opitz et al., 2012; Mischke et al., 2010a), biomarkers (Aichner et al., 2012) and water stable oxygen isotopes (Weynell et al., 2016). An extent of the summer monsoon influence to about 1000 km farther west during the Holocene climatic optimum was recently assumed by Stauch et al. (2015), based on loess deposits in Heihai Lake region.

It was also pointed out by many authors (e.g., Herzschuh, 2006; Wünnemann et al., 2003, 2007; Chen et al., 2008) that lakes on the Tibetan Plateau and adjacent regions experienced a general desiccation trend from the early to the late Holocene, following the weakening pattern of monsoon influence due to the southward shift of the intertropical convergence zone (ITCZ) that resulted in a weakening of the pressure gradients between the Pacific Ocean and the Asian continent as the main drivers for monsoonal moisture transport (Haug et al., 2001; Sirocko et al., 1993; Gupta et al., 2003; Fleitmann et al., 2007; Herzschuh, 2006; Wünnemann et al., 2007, 2010).

Taking these numerous research results into consideration, it could be expected that information from Kuhai Lake should confirm this already existing knowledge. Notably the reconstructed variations in water balance throughout the last 4000 years should monitor this weakening and/or strengthening effects by the EASM.

In addition to the already discussed inferences on hydrological variations in Kuhai Lake, derived from water/sediment flux and related catchment-lake interactions, combined with some bio-indicators, it is important to discuss the contribution of stable oxygen isotopes in light of climate-induced water sources for a more detailed understanding of the EASM influence at this site during the last 4000 years.

As outlined above it seems to be (still) common sense that oxygen isotopes in carbonates from speleothems, fossil remains and lake sediments and also from isotopes trapped in glacier ice (Thompson et al., 1997; Tian et al., 2003; Yao et al., 2012) are considered very good recorders of changes in effective moisture supply and possible temperature changes, delivered by the summer monsoon over Asia.

In general, more negative (depleted) isotopic values in speleothem records are considered to monitor increased effective moisture supply from the summer monsoon, while more positive values reflect weaker summer monsoon influence at respective sites (e.g., Fleitmann et al., 2007; Wang et al., 2005). Hence, heavier oxygen isotopes were reported in terms of stronger influence by Westerly-derived climate parameters (An et al., 2012) resulting in a relatively weak monsoon signal. Conversely, Henderson et al. (2010) discussed the isotopic signals in their record from Qinghai Lake partly in an opposite way for the period of the LIA, which could much better explain the relationship with sedimentary processes at the neighboring Daotanghe pond/wetland (Yan et al., 2017). All other existing lake records however, are based on this inference, although it is under debate whether speleothem records solely monitor the parameter effective moisture in all regions.

Oxygen isotopes from authigenic carbonate in sediment cores from Kuhai do not show this general pattern mentioned above, although it can be assured that they were extracted from carbonate formed in situ, such as MHC, while possible detrital components, such as limestone, did not affect the isotopic signals significantly. Hence, this dataset cannot confirm high comparability with other oxygen isotope records (e.g., Zhang et al. 2011) from the monsoon realm. Moreover, the isotope records from cores KH11-KH14 do not show a consistent pattern through space and time, underlining their high diversity too, as already demonstrated and discussed for the other sediment parameters (see chapters 6.1 and 6.2).

In agreement with the transportation processes derived from sediments in Kuhai Lake, likely monitoring the different influence from the two types of river systems, oxygen isotope data show this relationship too and even more pronounced (Fig.47) when compared with data from Wanxiang cave record. Wanxiang cave is located about 570 km south-east of Kuhai Lake, close to the eastern border of the Tibetan Plateau at 1930 m

a.s.l. It is therefore currently the nearest site that recorded the summer monsoon moisture supply for the last 1600 years (Zhang et al., 2008).

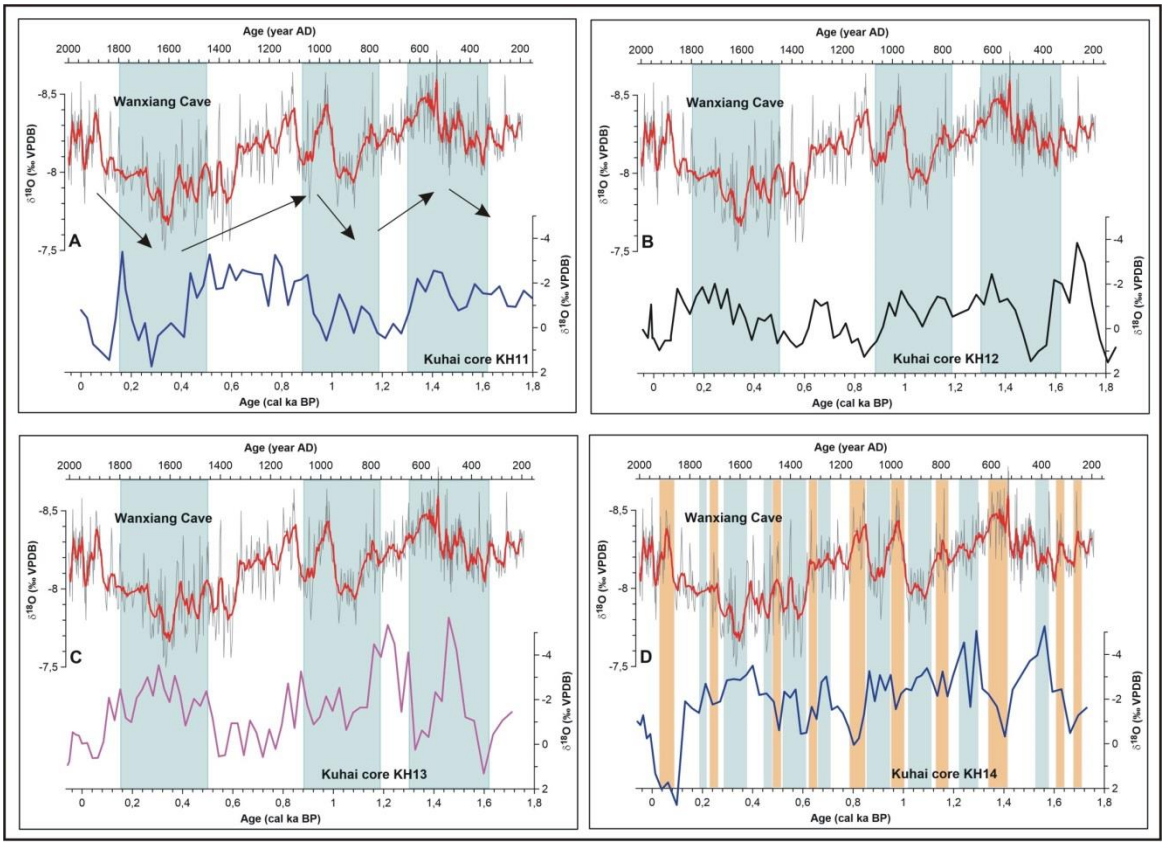

Fig. 47 Oxygen isotope variations of lake carbonates in cores KH11-KH14, Kuhai Lake, for the last 1800 years in comparison with speleothem record from Wanxiang cave. Shaded areas mark periods of certain importance.

It can be seen from Fig.47 A that oxygen isotopes in core KH11 mainly match with variations of summer monsoon influence at Wanxiang cave. This suggests that the water supply along the episodically flowing rivers in Kuhai catchment mainly occurred during the summer period of strongest rainfall, when summer monsoon influence was highest there. Conversely, isotopic values in the other cores show increasing opposite trends (Fig.47 B-D) in comparison to the Wanxiang record, with almost complete opposite signals in core KH14 (Fig.47 A). Hence, it can be assumed that the isotopic signals are much stronger affected by water supply from the perennial rivers that also contribute water during off-monsoon periods. As a result, isotopic signatures are significantly different. It suggests that isotopically light values in the Wanxiang Cave record, (stronger monsoon influence) correspond with heavier isotopic signals in the lake records and vice versa (Fig.47 D, for example). This strong difference can be explained by the assumption that rainfall during the summer time, although perhaps isotopically light (in Maduo County, Ren et al., 2013), becomes heavier during the transport from the sources to the lake basin (evaporative effect) and is mixed there with relatively warm and isotopically heavier lake water (see chapter 5.5.2, Fig.23). The resulting heavier values from which

finally the carbonates precipitate however, vary spatially, as seen in Fig.23 for the modern time. In addition to this likely process, isotopically lighter water from rain and snow, including molten near-surface ground ice (annually frozen ground and permafrost), during the off-monsoon period between autumn (late September) and spring (early June) also contribute to the lake via the perennial rivers at periods with lower air temperatures and colder lake water. These waters favor the precipitation of isotopically much lighter carbonates and may even enhance the formation of MHC and Calcium-Hexahydrite ($CaCO_3$+$6H_2O$) towards more stable minerals (Hull and Turnbull, 1973).

The proportion of these two different waters with a clear seasonal effect influences the isotopic signals of the lake carbonates in cores KH12-KH14 significantly, but not in core KH11. In other words: Reduced rainfall during summer time (monsoon season) increases the relative proportion of water from the off-monsoon season, mainly supplied by the perennial rivers and to a much lesser extent by the episodic ones.

Based on this specific relationship between inflowing waters and the isotopic composition of carbonates in lake deposits, it can be assumed that seasonal effects on the contribution of effective moisture played a dominant role, at least for the last 1.6 cal. ka BP, but likely also for the older periods. It also shows that short-term variations (decadal scale) in water supply have direct influence on the isotopic signals in lake sediments, really different from records in other lakes such as Qinghai Lake, where only mean values could be recorded (An et al., 2012). Consequently, heavy oxygen isotopes in Kuhai Lake are associated with rainfall during the summer time (opposite to isotope signals in cave records), while lighter values represent water supply during the off-monsoon period with significantly reduced supply in summer seasons.

Those lighter values were reported from river waters around Donggi Cona, all representing runoff during April and October (Weynell et al., 2016). Both periods definitely do not belong to the summer monsoon season. The same applies to river water and local snow/rainfall in early June 2015 at Kuhai Lake, which indicate water supply before or close to the onset of monsoon season (Fig.23). Oxygen isotopes of the lake water at that time were significantly heavier, due to mixed water body and the evaporative effect on the isotopic composition (Talbot, 1990; Leng and Marshall, 2004, Fig.37, chapter 5.5.2). Monsoon-related rain water in Donggi Cona, that fell end of June 2016 provided heavier $\delta^{18}O$ values, close to the mean of the lake water (Fig.23, chapter 5.5.2), although perhaps not representative for the entire monsoon season (Ren et al., 2013).

Commonly, stable oxygen isotopes and carbon isotopes in lakes correspond to each other with a positive significant correlation ($r \geq 0.6$), if the lake is a hydrologically closed system (Talbot, 1990; Fontes et al., 1996; Leng and Marshall, 2004). Although Kuhai Lake is considered to be a closed system without any subaerial outflow, correlation between both isotopes are lower or even non-existing (e.g., at site KH14, lake-center, see Fig.22). As already mentioned by Talbot (1990) and Leng and Marshall (2004), this relationship is not always a simple mechanism of oxygen and carbon isotope fractionation processes and depends on many additional factors such as the contribution of detrital carbonate and/or

the composition of different carbonates within the sediments, for example. Influence of carbon-13 by detrital components seems to be of minor importance in Kuhai Lake with respect to old limestone. The different types of carbonates were already considered during isotope extraction processes (see methods part). A more important factor might be that reworked material containing carbon-13 isotopes from organic matter, transported back to the lake via the drainages, could have resulted in lower correlation coefficients in some of the cores. High reservoir errors of dated organic matter indicate this potential influence. The reason for this anti correlation, however, remains an open question and was not considered in more detail within this study.

Taking these unexpected and surprising results of stable oxygen isotope composition in lake records of Kuhai Lake together with all other research results into account, the following climate-affected hydrological variations of Kuhai Lake and catchment can be outlined as follows:

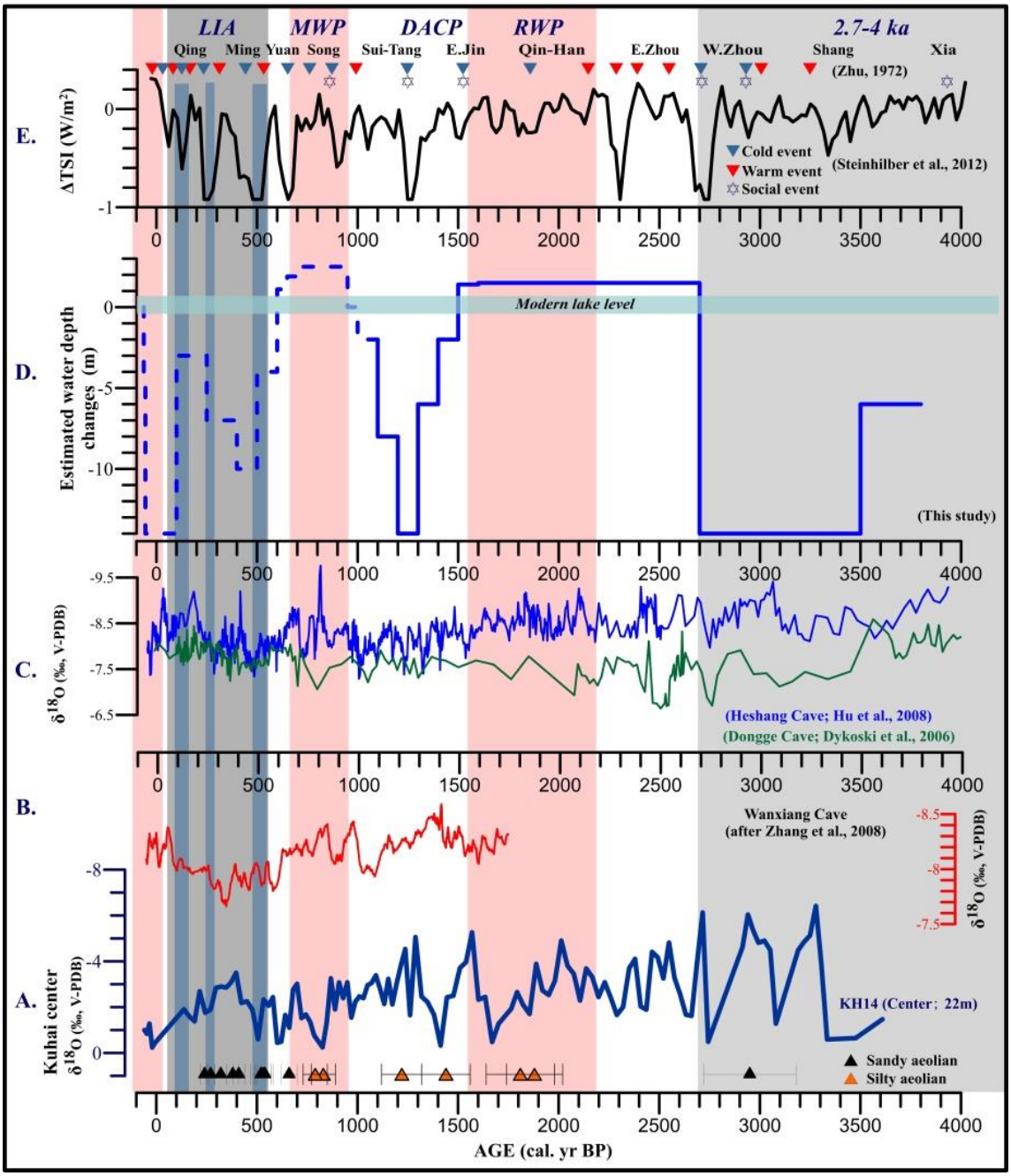

Fig. 48 Comparison of estimated water depth variations, reconstructed from sediment proxies and ostracod in Kuhai Lake and variations in stable oxygen isotopes in core KH14 for the last 4000 years (**A, D**), compared with records from Dongge Cave (Dykoski et al., 2006), Heshang Cave (Hu et al., 2008), both (**C**), Wanxiang Cave (Zhang et al., 2008) (**B**), and with Total Solar Irradiance (TSI, Steinhilber et al., 2012) (**E**). Red and black triangles (bottom) mark dated aeolian deposits; red and blue triangles (top) mark cold, warm or social events, reported by Zhu (1972). Shaded areas (rose, gray, blue) mark certain time intervals of importance. Social events with relation to climate are marked here but not discussed in detail. They belong to the collapses of Xia, Shang, West Zhou and East Jin dynasties, An Shi Rebellion and 'Yi Guan Nan Du' in Song Dynasty, which indicated that the population and economy center in China started to shift to south of the Yangtze River.

A dry Late Holocene interlude

The most severe anomaly in Kuhai lake basin and catchment was recorded for the time period between 4 and 2.7 cal. ka BP, corresponding to the Xia, Shang and Western Zhou dynasties in China, known as a relatively unstable period of cultural and social conflicts (Zhu, 1972). The same author summarized temperature changes during the last 5 ka in China, based on archeological and historical records. Air temperature in China, mainly in lowland regions, fluctuated at around 2°C higher than present (1970s) during the first 2000 years (3-5 ka BP). As revealed from the lake records, all data point to a lake shrinkage by about 16 m in maximum that resulted in partly isolated swamp/wetland/pond environments at sites KH11-13 and a low water depth in the lake center. This phase was accompanied by aeolian activity in the catchment, although not completely preserved in all investigated sections.

The inferred extreme negative water budget was attributed to a strong reduction in water supply. As the rainy season in the past may have also occurred during summers, mainly derived from the EASM, it can be assumed that local rainfall was very limited, indicating a weak summer monsoon influence in the Kuhai region at that time. Strong fluctuations of oxygen stable isotopes from extreme heavy to periodically very light values can be interpreted as low contribution of water into a shallow lake during summertime, favoring the higher proportion of isotopically light values from the off-monsoon seasons. This water supply however, was generally less than that during the rainy season in summer, according to the modern climate data.

Although heavier isotopic values were interpreted as higher contribution of summer rainfall (see above), this assumption may have been not valid for periods of low lake level. Negative water balances that caused low lake level/low water depths were associated with heavier isotopic values due to increased evaporative pressure und warm water (≥13°C in modern time) during the summer season. Reduced water supply by isotopically lighter rain water (Ren et al., 2013) would not be able to change the isotopic composition in lake water dramatically but instead would lead to slight shifts towards lighter values (see modern distribution of stable isotopes in surface samples, chapter 5.3.4), as also observed in records from Qinghai Lake (Henderson et al., 2010). The same effect applies to phases of high lake level/greater water depth (more water volume), because the ratio of water input to water volume could be the same: low lake level/less inflow versus high lake level/high inflow, taking the loss of water by evaporation into account (e.g., Wünnemann et al., 2006) In so far, changes in isotopic composition of lake water and precipitates from it cannot explain variations in water volume/lake level alone without considering other factors such as sediment supply and composition.

On the other hand, extreme light isotopic values, associated with off-monsoon colder water supply as recorded here for this time period, become more pronounced under shallow water conditions than in phases of increased water volume, because the mixing of these waters with isotopically heavier lake water towards heavier values is reduced.

This period of weak monsoon influence in Kuhai Lake region is also recorded in cave records (Dongge Cave: Dykoski et al., 2006; Heshang Cave: Hu et al., 2008, Fig.48 C) from the monsoon realm by heavier oxygen isotopes in both records with some differences in timing, but in general comprising the same time period. Following the general interpretation of these records, a weaker summer monsoon can be inferred, supporting the assumption of weak summer monsoon impact in Kuhai Lake as well. Hou et al. (2015) found in the lake record provided by An et al. (2012) a period of sustained summer temperature decline by about 4°C between 5 and 3.5 ka, based on alkenone data. Their inference however, only partly accords in timing with the reduction of water supply in the Kuhai record. Short-term warm events (~2°C higher than present) for the time windows at 3.3 and 3.0 ka were reported in historical records related to the development of Shang Dynasty, summarized by Zhu (1972). Based on these data it seems possible that summer temperature changes may not have played a major role for variations in moisture supply in Kuhai Lake are.

Dry climatic conditions with reduction in water supply towards the populated regions of the former Harappan culture (India) were also reported from a lake record in NW India (Tso Moriri), which perhaps fostered the collapse of this Indus valley civilization there (Wünnemann et al., 2010; Leipe et al., 2014; Gupta et al., in review). It seems therefore likely that this dry interlude affected a larger region in Asia and also other regions as well (e.g., Haug et al., 2001), pointing to a global-scale phenomenon, probably governed by the southward shift of the ITCZ at that time. However, severe changes in solar radiation (Total Solar Irradiance, Steinhilber et al., 2012, Fig.48 E) during this period did not occur and thus may not have been an important driver, except for the periods between 3.0-2.9 and 2.8-2.7 cal. ka BP, where lowest TSI match with a very weak summer monsoon signal in cave records and in the Kuhai lake record as well. The cold event at that time, reported as one of the documented coldest periods in China at 1000 BC (2950 yr BP), was accompanied by the collapse of the Shang Dynasty and during the other period by the collapse of the West Zhou Dynasty (Zhu, 1972), coincident with solar minima and low water flux to the Kuhai lake basin.

A millennium of warm-wet climate stability (2.7-1.5 ka BP)

The period of ameliorated climatic conditions between 2.7 and 1.5 cal. ka BP comprises the Eastern Zhou, Han- and Qin Dynasties in China, contemporaneous with the so-called Roman Warm Period (RWP) in Europe of favorable climatic conditions. In Kuhai Lake region, all records indicate a strengthening of the summer monsoon effective moisture supply that favored the rise in lake level/water depth, similar to the present situation. This can be confirmed by the cave records (Dykoski et al., 2006; Hu et al., 2008) and also by data from Qinghai Lake (An et al., 2012; Hou et al., 2015). An up to 10 m higher lake level based on OSL-dated paleo-shorelines around the lake, was reported by Liu et al. (2011, 2015). Data from Kuhai Lake also point to slightly higher lake levels than at present as a result of generally increased discharge along the rivers (episodic and perennial) during the summer seasons. Fluctuations in the isotopic records from lake

carbonates however, indicate variable contribution of water during summers and during the off-monsoon seasons too. A short-term period of less water supply from the catchment under reduced summer monsoon activity may have occurred at 1.7-1.5 cal. ka BP, indicated by the stable oxygen isotope records from Wanxiang Cave (Zhang et al., 2008) and from core KH14, displaying similar but opposite isotopic variations as mentioned before. This colder period of relative short duration coincides with the reported collapse of the East Jin Dynasty so that it was considered as a distinct cold event (1-2℃ lower than present) denoted as 'East Jin Cold Event' in China (Zhu, 1972). Slightly reduced solar radiation (TSI values, Steinhilber et al., 2012), occurred contemporaneously, although not very pronounced. A further reported cold event during the Han Dynasty (ca. 1.8 ka, Zhu，1972), coincident with slight reduction in TSI may have been too short or only of local significance and thus cannot be connected with environmental changes in Kuhai Lake region.

Aeolian activity in the catchment with respect to sand transport and deposition in dune bodies was probably low during the entire period, based on the available records, supporting the argument of general wetter and perhaps warmer climatic conditions resulting in reduced deflation processes and aeolian sand deposition around the lake basin, except for the deposition of loess in higher regions of the catchment, perhaps due to denser vegetation cover that could trap loess sediments there (Stauch et al., 2015, 2016).

A period of short-term climate instability (1.5 cal. ka BP - Present)

Many paleoclimate records covering the last 1500 years were subject to controversial discussions about the climate impact, especially along the modern transition zone between EASM and Westerlies influence (Liu et al., 2006; Henderson et al., 2010; Tan et al., 2008, 2011; Yang et al. 2014; Chen et al., 2014). This period of climate instability, also denoted to the Dark Ages Cold Period (DACP, e.g., Liu et al., 2011), MWP (or Medieval Climate Anomaly, MCA; IPCC, 2007; Fig.48) and the LIA covered the time of the Sui, Tang, several short-lived kingdoms, Song, Yuan, Ming and Qing Dynasties in China until 1912 AD, prior to the foundation of the Peoples Republic of China (e.g., Zhu, 1972; Yu, 1986).

The entire period of the last 1500 years showed opposite trends of stable oxygen isotopes between Wanxian Cave and Kuhai KH14 record in a nearly perfect pattern as outlined above (see Fig.47). Therefore, it can be used to identify short-term fluctuations of summer monsoon rainfall in this region.

For the period of the DACP, higher summer monsoon influence in Wanxiang Cave (Fig.47 B) corresponds to a still higher lake level at Kuhai Lake but with shrinking trend between 1.5 and 1.4 cal. ka BP, culminating in the lowest lake level/water depth and a strong negative (light) isotopic signal in core KH14 at about 1.3-1.4 cal. ka BP. It marks the relatively fast turn from a strong to a weak monsoon signal with respect to water supply during the summer season. Hence, the colder period of the DACP in China (Liu et al., 2011) can be also characterized as a drier period in Kuhai Lake region, coincident

with gradual lake level declines at Qinghai Lake (Liu et al., 2011) and increased aeolian mobility in the catchment of Kuhai Lake, both matching the solar minimum in the TSI record (Fig.47 E) for this time period. It coincided with a social event called An Shi Rebellion (Zhu, 1972), which resulted in the division of the Tang dynasty into a North and a South Branch and induced the immigration from north to south China. Based on the Kuhai records it can be inferred that the summer monsoon influence became weaker and was replaced by stronger influence of the Westerlies.

An opposite trend towards increasing water depth/lake level at Kuhai Lake and thus increased water supply encompasses the MWP (MCA) which was generally considered to be warmer and wetter in this larger region (Yang et al., 2014; Liu et al., 2015; Yan et al., 2017), as also inferred from more negative isotope values in the Wanxiang Cave record (Fig.47 B). The change from lighter to more heavier isotopic values in the KH14 record suggests increased higher proportions of water supply during the summer season (monsoon signal) as also inferred from increased fine suspended material input at all core sites under a water level close or even slightly above the present one. The dated exposed sediments of section KHS27 (Fig.26) as well as the plant layers in section KHS29 (Fig.29) indicate this assumption, if the respective ages would have been biased by a RE of about 500-600 years.

In contrast to the MWP, the LIA experienced again water level/water depth decline as revealed by the stronger influence of isotopically lighter values from the off-monsoon season. Also the isotope record from Wanxiang Cave suggests a period of weak monsoon influence (Fig.48 B), comparable with the other cave records (Fig.48 C). From the ostracod records in cores KH11-KH14 it can be assumed that the water depth at all sites was reduced by about 10 m (mean). This would accord with strong negative isotopic signals in the KH14 record. It implies the lack of water supply during the summer season, enabling such water decline under colder and drier climate conditions with reduced evaporative power (Henderson et al., 2010). Yan et al. (2017) discussed the climatic conditions during the three-partite LIA based on wetland/pond formation near Qinghai Lake and found that a prolonged freezing period (ice cover) may have influenced depositional processes in the pond area, resulting in reduced aeolian input. The same may have happened at Kuhai Lake, as aeolian sediments in the respective sequences of the cores remained less pronounced. However, aeolian activity during this period was probably strong because OSL-dated dune formation and deposition of aeolian sands in several sections are clear evidence. Based on the paleosol layers in section KHS15, some short-term phases of higher effective moisture supply during the LIA (0.4-0.5 and 0.2-0.4 cal. ka BP) were recorded, accompanied by presumably less aeolian activity. After 0.2 cal. ka BP however, aeolian activity was enhanced and favored the accumulation of respective sandy sediments in dune bodies and in slope regions of Kuhai catchment (Fig.40, chapter 6.1.1). The inference of weak summer monsoon influence in favor to westerly derived climate accords with records from Qinghai Lake (Henderson et al., 2010; Liu et al., 2011; An et al. 2012), with a flood-draught index from the adjacent region (Tian et al., 2007) and reconstructed precipitation patterns in Longxi region, NE Tibetan Plateau (Tan et al.,

2008, 2011) as well as with tree-ring-based precipitation reconstructions from the Dulan area (Yang et al., 2014). Theses evidences likely correspond to the grand solar minima (Steinhilber et al., 2012, Fig.48 E), although only partly recognizable in the Kuhai records.

The last 150-200 years show a short-term decrease of the lake until the mid-20th century, according to ostracod results, extreme high algae production even in the lake center. Isotopic signatures showed heavier values than nowadays, likely the result of high evaporation of a smaller water body despite possible water contribution during the summer periods as the Wanxiang cave record indicates (Fig.48 B). A fast lake level rise afterwards and increasing water depth close to its present level by much stronger water supply can be assumed, likely in response to increased summer monsoon activity. This time period however, is not well documented in the core records due to low resolution of the proxy data. An increased water supply may also result from higher discharges along all drainage systems at the end of the monsoon season (September) as observed in 2015, similar to the meteorological records of the last 50 years. It remains a general question whether these water masses are still related to the monsoon influence or already an effect of local water vapor recycling processes while the monsoon front already left this region, assumed for pre-monsoon rainfall in Maduo region ca. 100 km farther south (Ren et al., 2013).

A comparison between records over China for the time periods of the MWP and LIA was discussed by Chen et al. (2014). Their results indicate that during the MWP dry climate conditions occurred west of the modern monsoon boundary while wet conditions existed in the east. During the LIA this relationship was just opposite. The data from Kuhai Lake and adjacent regions along the modern monsoon boundary cannot confirm this inference. Considering the combined research results from Kuhai Lake and its catchment it can be demonstrated that a single record from the lake can provide quite different results, if comparison with other lake records from the same system including the catchment is not generated into value. Hence, many of the reported sites selected for this comparative study for calculating climate conditions during the MWP and LIA lack this comprehensive consideration and therefore may be also open for other interpretation.

Reported climate variations within the Kuhai Lake region derived from a pollen record (Wischnewski et al., 2011) were not considered in this study because inferred climate changes were based on a likely incorrect chronology, at least too different from the chronology used in this study, disabling reliable comparisons for certain time intervals.

7. Conclusions

Based on the analyses of four well-dated sediment cores from different locations in Kuhai Lake in combination with sediment records from the catchment, the afore-mentioned scientific questions could be answered reasonably well.

Major results show that there exists a very high spatial diverse sediment pattern in lake surface samples (last 15 years of accumulation) with respect to all investigated parameters (grain size distribution and endmembers, minerals and geochemical components, including stable isotopes from sediments, and ostracod distributions). This pronounced spatial diversity is also recorded in sediment cores KH11-KH14 for the last 4000 years and confirm a temporal diversity as well. This diversity strongly depended on the sediment and water supply from the catchment. Fluvially transported material (mainly as suspended load) and aeolian sediments of local origin contributed to the overall budget quite differently in space and time. Hence, a sediment record and resulting proxy data from a single site was considered not representative for the understanding of climate-influenced transportation and depositional processes. Linkages between depositional processes in the lake basin and catchment dynamics (fluvial/aeolian activity) strongly depended on

i) the location of sediment cores with respect to the inflowing river systems,
ii) the seasonality of river discharge with respect to episodically active drainages versus perennial systems,
iii) the distribution pattern of sediment/water influx with respect to lake-internal currents and
iv) temporal different phases of aeolian mobility and resulting spatial distribution patterns of aeolian sand/loess within the lake and catchment.

Surprisingly, stable oxygen isotopes from authigenic carbonate in sediments of cores KH12-KH14 displayed inverse signals in comparison with speleothem records, except for the core KH11 and thus required a different interpretation of the isotopic signatures in terms of summer monsoon effective moisture supply. These data also showed that water/sediment contribution during off-monsoon seasons became very pronounced, generally not visible in lake records which only provided mean values, far away from local sources. Hence, the seasonally different discharge behaviors of the river systems in Kuhai catchment could be more clearly identified. They provided both, the summer monsoon signal and the off-monsoon signal with variable magnitude and amplitude, and with different effects on the local core sites.

Resulting climate influences by the EASM and Westerlies for the last 4000 year reveal a very weak EASM in favor of Westerly influence during a dry and presumably colder period between 4.0 and 2.7 cal. ka BP, corresponding with lowest lake level/lowest water depth during the entire period under consideration. A more stable and moister climate of

approximately 1200 years duration resulted in positive water balances with increased water depth/lake level, but with intermediate fluctuations until around 1.5 cal. ka BP. These conditions were attributed to stronger summer monsoon impact in expense of westerly-derived climate signatures, while aeolian activity was probably less pronounced.

Highly unstable climate conditions during the last 1500 years that resulted in frequent alternations between stronger/weaker influences of the EASM were recorded at all investigated sites but again with different magnitude and signatures. Comparison among the sites show that the most prominent alternations corresponded with the DACP (weaker monsoon, stronger Westerly impact), MWP (intensified monsoon signal, weak Westerly influence) and the LIA, dominated by Westerly climate signatures, all in agreement with published records from adjacent sites.

The mechanisms of these climate alternations remain less discussed in this study but they seem to be related to external forces, such as the southward migration of the ITCZ and possible solar influence, for example, without excluding other potential drivers reported in the available literature.

References

Aichner, B., Herzschuh, U., Wilkes, H., Schulz, H.-M., Wang, Y., Plessen, B., Mischke, S., Diekmann, B., Zhang, C., 2012. Ecological development of Lake Donggi Cona, north-eastern Tibetan Plateau, since the late glacial on basis of organic geochemical proxies and non-pollen palynomorphs. Palaeogeography, Palaeoclimatology, Palaeoecology 313-314,140-149.

Akita, L.G., Frenzel, P., Börner, N., Wang, J., Peng P., 2012. Distribution of recent ostracoda and their use in palaeoenvironmental reconstruction of Tangra Yumco, Central Tibetan Plateau. Geological Society of America Abstracts with Programs 44(7), 40.

Akita, L., Frenzel, P, Wang, J.B., Börner, N., Peng, P., 2016. Spatial distribution and ecology of the Recent Ostracoda from Tangra Yumco and adjacent waters on the southern Tibetan Plateau: a key to palaeoenvironmental reconstruction. Limnologica-Ecology and Management of Inland Waters 59, 21-43.

An, Z., Colman, S., Zhou, W., Li ,X., Brown, E., Timothy Jull, A., Cai, Y., Huang, Y., Lu, X., Chang, H., Song, Y., Xu, H., Liu, W., Jin, Z., Liu, X., Cheng, P., Liu, Y., Ai, L., Li, X., Liu, X., Yan, L., Shi, Z., Wang, X., Wu, F., Qiang, X., Dong, Z., Lu, F., Xu, X., 2012. Interplay between the Westerlies and Asian monsoon recorded in Lake Qinghai sediments since 32 ka. Scientific Report 2(8), 619.

Benoit, G., Rozan, T.F. 2001. 210Pb and 137Cs dating methods in lakes: A retrospective study. J. of Paleolimnology 25 (4), 455-465.

Bird, M., Chivas, A., Radnell, C., Burton, H., 1991. Sedimentological and stable isotope evolutionof lakes in theVestfold Hills, Antarctica.Palaeogeography, Palaeoclimatology, Palaeoecology 84(14), 109-130.

Bird, B.W., Polisar, P.J., Lei, Y., Thompson, L.G., Yao, T., Finney, B.P., Bain, D.J., Pompeani, D.P., Steinman, B.A., 2014.A Tibetan lake sediment record of Holocene Indian summer monsoon variability. Earth and Planetary Science Letters 399, 92-102.

Blaauw, M., Christen, J.A., 2011. Flexible paleoclimate age-depth models using an autoregressive gamma process. Bayesian Analysis 6, 457-474.

Boos, W.R., Kuang, Z., 2010. Dominant control of the South Asian Monsoon by orographic insulation versus plateau heating. Nature 463, 218-222.

Böhner, J., 2006. General climatic controls and topoclimatic variations in Central and High Asia. Boreas 35 (2), 279-295.

Bullock, A., Acreman, M., 2003. The role of wetlands in the hydrological cycle. Hydrol. Earth Syst. Sci. 7 (3), 358-389.

Chen, F., Yu, Z., Yang, M., Ito, E., Wang, S., Madsen, D.B., Huang, X., Zhao, Y., Sato, T., Birks, J.B., Boomer, I., Chen, J. An, C., Wünnemann, B., 2008. Holocene Moisture Evolution in Arid Central Asia and its Out-of-Phase Relationship with Asian Monsoon History. Quaternary Science Reviews, 27, 351-364.

Chen, H., 2014.Geochemical records of lacustrine sediments in Heihai Lake, NE Tibetan Plateau. Master thesis, Nanjing University, China.

Chen, F., Q. Xu, J. Chen, H.J.B. Birks, J. Liu, S. Zhang, L. Jin, C. An, R.J. Telford, X. Cao, Z. Wang, X. Zhang, K. Selvaraj, H. Lu, Y. Li, Z. Zheng, H. Wang, A. Zhou, G. Dong, J. Zhang, X. Huang, J. Bloemendal, Z. Rao, 2014. East Asian summer monsoon precipitation variability since the last deglaciate. Scientific Reports 5, p.11186.

Chen, F., Wu, D., Chen, J., Zhou, A., Yu, J., Shen, J., Wang, S., Huang, X., 2016. Holocene moisture and East Asian summer monsoon evolution in the northeastern Tibetan Plateau recorded by Lake Qinghai and its environs: A review of conflicting proxies. Quaternary Science Reviews 154, 111-129.

Curry, B.B., 1999. An environmental tolerance index for ostracodes as indicators of physical and chemical factors in aquatic habitats. Palaeogeography. Palaeoclimatology, Palaeoecology 148, 51-63.

Dean, W.E., 1974. Determination of carbonate and organic matter in calcareous sediments and sedimentary rocks by loss on ignition: comparison with other methods. Journal of Sedimentary Research 44(1): 242-248.

Dearing, J.A., 1997. Sedimentary indicators of lake level changes in the humid temperate zone: a critical review. Journal of Paleolimnology 18, 1-44.

Deng, S., Dong, H., Lv, G., Jiang, H., Yu, B., Bishop, M.E., 2010. Microbial dolomite precipitation using sulfate reducing and halophilic bacteria: Results from Qinghai Lake, Tibetan Plateau, NW China. Chemical Geology 278 (3-4), 151-159.

Dickens, B., Brown, W.E., 1970. The crystal structure of calcium carbonate hexahaydrate at approximately -120°C. Inorganic Chemistry 9, 480-5.

Dietze, E., Diekmann, B., Wünnemann, B., Aichner, B., Hartmann, K., Herzschuh, U., IJmker, J., Jin, H., Kopsch, C., Lehmkuhl, F., Li, S., Mischke, S., Niessen, F., Opitz, S., Stauch, G., 2010. Basin morphology and seismic stratigraphy of Lake Donggi Cona, north-eastern Tibetan Plateau, China. Quaternary International 218, 131–142.

Dietze, E., Diekmann, B., Wünnemann, B., Aichner, B., Hartmann, K., Herzschuh, U., IJmker, J., Jin, H., Kopsch, C., Lehmkuhl, F., Li, S., Mischke, S., Niessen, F., Opitz, S., Stauch, G., 2012. An end-member algorithm for deciphering modern detrital pro- cesses from lake sediments of Lake Donggi Cona, NE Tibetan Plateau, China. Sedimentary Geology 243–244, 169–180.

Dietze, E., Wünnemann, B., Hartmann, K., Diekmann, B., Jin, H., Stauch, G., Yang, S., Lehmkuhl, F., 2013. Early to mid-Holocene lake high-stand sediments at Lake Donggi Cona, northeastern Tibetan Plateau, China. Quaternary Research 79 (3), 325-336.

Doeglas D. J., 1968. Grain-size indices, classification and environment. Sedimentology 10 (2), 83-100.

Domroes, M, Peng, G., 1988. The climate of China. Berlin: Springer

Duller, G., 1994. Luminescence dating using feldspars: A test case from southern North Island, New Zealand. Quaternary Science Reviews 13, 423–427.

Dykoski, C.A., Edwards, R.L., Cheng, H., Yuan, D.X., Cai, Y.J., Zhang, M.L., Lin, Y.S., Qing, J.M., An, Z.S., Revenaugh, J., 2006. A high-resolution, absolute-dated Holocene and deglacial Asian monsoon record from Dongge Cave, China. Earth and Planetary Science Letters 233, 71-86.

Fan, Q., Ma, H., Cao, G., Chen, Z., Cao, S., 2012. Geomorphic and chronometric evidence for high lake level history in Gahai lake and Toson Lake of north-eastern Qaidam Basin, north-eastern Qinghai-Tibetan Plateau. Jpirnaö of Quaternary Science 27 (8), 819-827.

Fenter, P., Zhang, Z., Park, C., Sturchio, N., Hu, X., Higgins, S., 2007. Structure and reactivity of the dolomite (104)-water interface: New insights into the dolomite problem. Geochimica et Cosmochimica Acta 71 (3), 566-579.

Fleitmann, D., Burns, S.J., Mangini, A., Mudelsee, M., Kramers, J., Villa, I., Neff, U., Al- Subbarye, A.A., Buettner, A., Hippler, D., Matter, A., 2007. Holocene ITCZ and Indian monsoon dynamics recorded in stalagmites from Oman and Yemen (Socotra). Quaternary Science Reviews 26, 170-188.

Folk, R.L., Ward, W.C., 1957. Brazos river bar: a study in the significance of grain size parameters. Journal of Sedimentary Petrology 27, 3-26.

Fontes, J-C., Gasse,. F., Gibert, E., 1996. Holocene environmental changes in Lake Bangong basin (Western Tibet). Part 1: Chronology and stable isotopes of carbonates of a Holocene lacustrine core. Palaeogeography Palaeoclimatology Palaeoecology 120, 25-47.

Frenzel, P., Wrozyna, C., Xie, M. P., Zhu, L. P., Schwalb, A., 2010. Palaeo-water depth estimation for a 600-year record from Nam Co (Tibet) using an ostracod-based transfer function. Quaterna- ry International 218, 157-165.

Fu, B., Awata, Y., Du, J., He, W., 2005. Late Quaternary systematic stream offsets caused by repeated large seismic events along the Kunlun fault, northern Tibet. Geomorphology 71, 278–292.

Fukushi, K., Munemoto, T., Sakai, M., Yagi, S., 2011. Monohydrocalcite: a promising remediation material for hazardous anions. Science and Techonology of Advanced Material 12, 1-12.

Gierlowski-Kordesch, E., Kelts, K., 1994. Global Geological Record of Lake Basins, Vol 1, World and Regional Geology 4. Cambridge University Press.

Gierlowski-Kordesch, E.H., Alonso-Zara, A., Tanner, L., 2010. Chapter 1: Lacustrine Carbonates. In: Carbonates in Continental Settings: Facies, Environments, and Processes. 61, 1-101, Elsevier.

Goldsmith, J.R., Graf, D.L. Haer, H.C., 1961. Lattice constants of the calcium-magnesium carbonates. The American Mineralogist 46, 453-457.

Griffiths, H.I., 1995. European Quaternary freshwater Ostracoda: a biostratigraphic and palaeobiogeographic primer. Scopolia, 34, 1-168.

Griffiths, H.I., Holmes, J.A., 2000. Non-marine ostracods and Quaternary palaeoenvironments. Quaternary Research Association, London.

Gupta, A.K., Anderson, D.K., Overpack, J.T., 2003, Abrupt changes in the Asian southwest monsoon during the Holocene and their links to the North Atlantic Ocean, Nature,421, 354–357.

Gupta, A., Dutt, S., Wünnemann,B., Yan, D.,2017. A long arid interlude in the NW Himalaya during ~4350-3450 cal. yrs BP and collapse of the Indus Valley civilization. Geophysical Research Letters (In review).

Günther, F., Mügler, I., Mäusbacher, R., Daut, G., Leopold, K., Gerstmann, U.C., Xu, B., Yao, T., Gleixner, G., 2011. Response of dD values of sedimentary n-alkanes to variations in source water isotope signals and climate proxies at lake Nam Co, Tibetan Plateau. Quaternary International 236, 82-90.

Håkanson, L., Peters, R. 1995. Predictive Limnology. SPB Academic Publishing, Amsterdam, 464 pp.

Hardie, L.A., 1987. Dolomitization, a critical view of some current views. Journal of Sedimentary Research 57 (1), 166-183

Hartmann, K., Wünnemann, B., 2009. Hydrological changes and Holocene climate varia- tions in NW China, inferred from lake sediments of Juyanze palaeolake by factor ana- lyses. Quaternary International 194, 28–44.

Haug, G. H., K. A. Hughen, M. Sigman, L. C. Peterson and U. Rohl (2001), Southward Migration of the Intertropical Convergence Zone Through the Holocene, Science, 293, 1304-1308..

Heiri, O., Lotter, A.F., Lemcke, G., 2001. Loss on ignition as a method for estimating organic and carbonate content in sediments: reproducibility and comparability of results. Journal of Paleolimnology 25, 101-110.

Henderson, A.C.G., Holmes, J.A., Leng, M.J., 2010. Late Holocene isotope hydrology of Lake Qinghai, NE Tibetan Plateau: effective moisture variability and atmo- spheric circulation changes. Quaternary Science Reviews 29, 2215-2223.

Herzschuh, U., 2006. Palaeo-moisture evolution in monsoonal Central Asia during the last 50,000 years. Quaternary Science Reviews 25, 163-178.

Herzschuh, U., Winter, K., Wuennemann, B., Li, S., 2006. A general cooling trend on the Tibetan Plateau throughout the Holocene recorded by the Zigetang pollen spectra. Quaternary International 154-155, 113-121.

Herzschuh, U., Birks, HJ., Liu, X., Kubatzki, C., Lohmann, G., 2010. What caused the mid-Holocene forest declineon the eastern Tibet-Qinghai Plateau? Global Ecology and Biogeography 19 (2), 278-286

Holmes, J. A., M. J. Allen, F. A. Street-Perrott, M. Ivanovich, R. A. Perrott, M. P. Waller, 1999. Late Holocene palaeolimnology of Bal Lake, Northern Nigeria, a multidisciplinary study. Palaeogeography Palaeoclimatology Palaeoecology 148, 169-185.

Holmes, J.A., Cook, E.R., Yang, B., 2009. Climate change over the past 2000 years in Western China. Quaternary International 194, 91-107.

Hong, Y., Hong, B., Lin, Q., Zhu, Y., Shibata, Y., Hirota, M., Uchida, M., Leng, X., Jiang, H., Xu, H., Wang, H., Yi, L., 2003. Correlation between Indian Ocean summer monsoon and North Atlantic climate during the Holocene. Earth and Planetary Science Letters 211, 371-380.

Hong, Y.T., Hong, B., Lin, Q.H., Shibata, Y., Hirota, M., Zhu, Y.X., Leng, X.T., Wang, Y., Wang, H., Yi, L., 2005. Inverse phase oscillations between the East Asian and Indian summer monsoons during the last 12,000 years and paleo-El Niño. Earth and Planetary Science Letters 231, 337-346.

Hou, X. (Ed.), 2001. Vegetation Atlas of China. Science Press, Beijing.

Hou, J., Andrea, WJD, Liu, Z., 2012. The influence of 14C reservoir age on interpretation of paleolimnological records from the Tibetan Plateau. Quaternary Science Reviews 48, 67-79.

Hou, J., Huang, Y., Zhao, J., Liu, Z., Colman, S., An, Z., 2016. Large Holocene summer temperature oscillations and impact on the peopling of the northeastern Tibetan Plateau. Geophisical Research Letters 43(3), 1-8.

Hu, C., Henderson, G., Huang, J., Xie, S., Sun, Y., Johnson, K., 2008. Quatitifacation of Holocene Asican monsoon rainfall from spatially seperated cave records. Earth and Planetary Science Letters 266, 221-232.

Hudson, A.M., Quade, J., 2013. Long term east-west asymmetry in monsoon climate on the Tibetan Plateau. Geology 41, 351-354.

Hull, H., Turnbull, A.G., 1973. A thermochemical study of monohydrocalcite. Geochimica et Cosmochimica Acta 37, 685-694.

Huth, T., Hudson, A.M., Quade, J., 2012. A paleohydrologic model of Baqan Tso, Tibet, based on lake shorelines. AGU Fall meeting 2012, Abstracts PP41A-1987.

IJmker, J., Stauch, G., Hartmann, K., Diekmann, B., Dietze, E., Opitz, S., Wünnemann, B., Lehmkuhl, F., 2012. Environmental conditions in the Donggi Cona lake catchment, NE Tibetan Plateau, based on factor analysis of geochemical data. Journal of Asian Earth Sciences 44, 176–188.

Immerzeel, W., van Beek, L., Bierkens, M., 2010. Climate change will affect the Asian water towers. Science 328, 1382-1385.

Jin, L., Chen, F., Morrill, C., Otto-Bliesner, B.L., Rosenbloom, N., 2012. Causes of early Holocene desertification in arid central Asia. Climate Dynamics 38, 1577-1591.

Kasper, T., Haberzettl, T., Doberschütz, S., Daut, G. Wang, J., Zhu, L., Nowaczyk, N., Mäusbacher, R., 2012. Indian Ocean Summer Monsoon (IOSM)-dynamics within the past 4 ka recorded in the sediments of Lake Nam Co, central Tibetan Plateau (China). Quaternary Science Reviews 39, 83-85.

Kasper, T., Frenzel, P., Haberzettl, T., Schwarz, A., Daut, G., Meschner, S., Wang, J., Zhu, L., Mäusbacher, R. 2013. Interplay between redox conditions and hydrological changes in sediments from Lake Nam Co (Tibetan Plateau) during the past 4000 cal BP inferred from geochemical and micropaleontological analyses.Palaeogeography, Palaeoclimatology, Palaeoecology 392, 261–271.

Kasper, T., Haberzettl, T., Wang, J., Daut, G., Zhu, L., Mausbacher, R., 2015. Hydrological variations on the Central Tibetan Plateau since the Last Glacial Maximum and their tele- connection to inter-regional and hemispheric climate variations. Journal of Quaternary Science 30, 70–78.

Kelts, K., Talbot, M., 1990. Lacustrine carbonates as geochemical archives of environmental change and biotic/abiotic interactions. In: Tilzer, M.M., Serruya, C. (Eds.), Large Lakes. Springer, Berlin, pp. 288–315.

Kramer, A., Herzschuh, U., Mischke, S., Zhang, C., 2010. Holocene treeline shifts and monsoon variability in the Hengduan Mountains (southeastern Tibetan Plateau), implications from palynological investigations. Palaeogeography, Palaeoclimatology, Palaeoecology 286, 23-41.

Krause, P., Biskop, S., Helmschrot, J., Flügel, W.A., Kang, S., Gao, T., 2010. Hydrological system analysis and modelling of the Nam Co basin in Tibet. Advances in Geosciences 27, 29-36.

Kürschner, H., Herzschuh, U., Wagner, D., 2005. Phytosociological studies in the north-eastern Tibetan Plateau (NW China)—a first contribution to the subalpine scrub and alpine meadow vegetation. Botanische Jahrbücher der Systematik 126, 273-315.

Lai, Z., Kaiser, K., Brückner, H., 2009. Luminescence-dated aeolian deposits of late Quaternary age in the southern Tibetan Plateau and their implications for landscape history. Quaternary Research 72, 421-430.

Lai, Z.P., Mischke, S., Madsen, D., 2014. Paleoenvironmental implications of new OSL dates on the formation of the “Shell Bar” in the Qaidam Basin, northeastern Qinghai-Tibetan Plateau. Journal of Paleolimnology 51, 197-210.

Last, W.M., 2002. Geolimnology of salt lakes. Geosci. J. 6, 347-369.

Lee, J., Li, S-H., Aitchison, J.C., 2012. OSL dating of paleoshorelines at Lagkor Tso, western Tibet. Quaternary Geochronology, doi 10.1016/quageo2012.11.003.

Lehmkuhl, F., Haselein, F., 2000. Quaternary palaeoenvironmental change on the Tibetan Plateau and adjacent areas (Western China and Mongolia). Quaternary International 65 (66), 121–145.

Leipe, C., Demske, D., Tarasov, P.E., HIMPAC Project Members, 2014. A Holocene pollen record from the northwestern Himalayan lake Tso Moriri: implications for palaeoclimatic and archaeological research. Quaternary International 348, 93-112.

Leng, M., Marshall, J., 2004. Palaeoclimate interpretation of stable isotope data from lake sediment archives. Quaternary Science Reviews 23, 811-831.

Li, M., Zhu, L., Kang, S., You, Q., Wang, J., Zhang, Q., Xie, M., 2008. The occurrence of genesis of Monohydrocalcite in the Nam Co, Tibet. Journal of Mineral Petrol 1(28), 1-7. (In Chinsed with English abstract)

Li, X.Z., Liu, W.G., Zhang, L., Sun, Z.C., 2010. Distribution of recent ostracod species in the Lake Qinghai area in northwestern China and its ecological significance. Ecological Indicators 10, 880-890.

Li, Y., Morrill, C., 2010. Multiple factors causing Holocene lake level change in monsoonal and arid central Asia as identified by model experiments. Climate Dynamics 35, 1119-1132.

Li, X., Liu, W., Xu, L., 2012. Stable oxygen isotope of ostracods in recent sediments of Lake Gahai in the Qaidam Basin, northwest China: The implications for paleoclimatic reconstruction. Globla and Planetary Change 94-95, 13-19.

Li, Y., Wang, N., Chen, H., Li, Z., Zhou, X., Zhang, C., 2012. Tracking millennial-scale climate change by analysis of the modern summer precipitation in the marginal regions of the Asian monsoon. Journal of Asian Earth Sciences 58, 78-87.

Li, Y., Liao, J., Guo, H., Liu, Z., Shen, G., 2014. Patterns and Potential Drivers of Dramatic Changes in Tibetan Lakes, 1972–2010. PLoS ONE 9(11), 111890.

Liao, J.J., Shen, G.Z., Li, Y.K., 2013. Response of lake variations to climate change in the Ti- betan Plateau in the past 40 years. Int. J. Digital Earth 6 (6), 534–549.

Lin L., Chen, F., Morrill, C., Otto-Bliesner,B., Rodenbloom, N., 2011. Causes of early Holocene desertification in arid central Asia. Climat Dynamics , doi 10.1007/s00382-011-1086-1

Lister, G., Kelts, K., Zao, C., Yu, J., Niessen, F., 1991. Lake Qinghai, China: closed-basin lake levels and the oxygen isotope record for ostracoda since the latest Pleistocene. Palaeogeography Palaeoclimatology Palaeoecology 84, 141-162.

Liu, X., Liu, Z., Kutzbach, J.E., Clemens, S.C., Prell, W.L., 2006. Hemispheric insolation forcing of the Indian Ocean and Asian monsoon: Local versus remote impacts. Journal of Climate 19, 6195-6208.

Liu, X., Shen, J., Wang, S., Wang, Y.B., Liu, W.G., 2007. Southwest monsoon changes indicated by oxygen isotope of ostracode shells from sediments in Qinghai Lake since the late Glacial. Chinese Science Bulletin 52 (4), 539-544.

Liu, X., Dong, H., Yang, X., Herzschuh, U., Zhang, E., Stuut, J.W., Wang, Y., 2009. Late Holocene forcing of the Asian winter and summer monsoon as evidenced by proxy records from the northern Qinghai-Tibetan Plateau. Earth Planetary Science Letters 280, 276-284.

Liu, X., Lai, Z., Madsen, D., Yu, L., Liu, K., Zhang, J., 2011. Lake level variations of Qinghai Lake in northeastern Qinghai–Tibetan Plateau since 3.7 ka based on OSL dating. Quaternary International 236, 57-64.

Liu, X.J, Lai, Z., Zeng, F.M., Madsen, D.B., E, CY, 2013. Holocene lake level variations on the Qinghai-Tibetan Plateau. Inernational Journal of Earth Science 102, 2007-2016.

Liu, Z., Wen, X., Brady, E.C., Otto-Bliesner, B., Yu, G., Lu, H., Cheng, H., Wang, Y., Zheng, W., Yihui Ding, Edwards, R.L., Cheng, J., Liu, W., Yang, H., 2014. Chinese cave records and the East Asia Summer Monsoon. Quaternary Science Reviews 83, 115-128.

Liu, X.J., Lai, Z.P., Madsen, D., Zeng, F.M., 2015. Last Deglacial and Holocene lake level variations of Lake Qinghai, northeastern Qinghai-Tibetan Plateau. Journal of Quaternary Science 30, 245-257.

Lockot, G., Ramisch, A., Wuennemann, B., Hartmann, K., Haberzettl, T., Chen, H. und B., D.,2015. A process- and provenance-based attempt to unravel inconsistent radiocarbon chronologies in lake sediments – an example from Lake Heihai, North Tibetan Plateau (China).Radiocarbon 57, 1003-1019.

Long, H., Lai, Z., Frenzel, P., Fuchs, M., Haberzettl, T., 2012. Holocene moist period recorded by the chronostratigraphy of a lake sedimentary sequence from Lake Tangra Yumco on the south Tibetan Plateau. Quaternary Geochronology 10, 136-142.

Long, H., Shen, J., Tsukamoto, S., Chen, J., Yang, L., Frenchen, M., 2014. Dry early Holocene revealed by sand dune accumulation chronology in Bayanbulak Basin (Xinjiang, NW China). Holocene. 24, 612–624.

Long, H., Shen, J., Wang, Y., Gao, L.,Frechen, M., 2015. High resolution OSL dating of a lateQuaternary sequence from Xingkai Lake (NE Asia): Chronological challenge of the “MIS3a ega-paleolake” hypothesis in China. Earth Planet. Sci. Lett. 428, 281-292.

Lu, H., Wang, X., Ma, H., Tan, H., Vandenberghe, J., Miao, X., Li, Z., Sun, Y., An, Z., Cao, G., 2004. The Plateau Monsoon variation during the past 130 kyr revealed by loess deposit at northeast Qinghai-Tibet (China). Global and Planetary Change 41, 207-214.

Lu, H., Zhao, C., Mason, J., Yi, S., Zhao, H., Zhou, Y., Junfeng, J., Swinehart, J.,Wang, C., 2011. Holocene climatic changes revealed by aeolian deposits from the Qinghai Lake area (northeastern Qinghai-Tibetan Plateau) and possible forcing mechanisms. The Holocene 21, 297-304.

Lu, H., Yi, S., Lu, Z., Mason, J.A., Jiang, D., Cheng, J., Stevens T.,Xu, Z., Zhang, E., Jin, L., Zhang, Z., Guo, Z., Wang, Y., Otto-Bliesner, B., 2013. Variation of East Asian monsoon precipitation during the past 21 k.y. and potential CO2 forcing. Geology 41 (9), 1023-1026.

Machel, H.G., 2004. Concepts and models of dolomitization: a critical reappraisal. Geological Society, London, Special Publications 235 (1), 7-63.

Madsen, A., Buylaert, J., Murray, A., 2011. Lunimescence dating of young coastal deposits from New Zealand using feldspar. Geochronometria 38, 378-390.

Meisch, C., 2000. Freshwater ostracoda of western and central Europe. Spektrum Akademischer Verlag, Heidelberg.

Mischke, S., Herzschuh, U., Kürschner, H., Fuchs, D., Chen, F., Fei, M., Sun, Z., 2003. Sub-recent ostracoda from Qilian Mountains (NW China) and their ecological significance. Journal of Limologica 33, 280-292.

Mischke, S., Herzschuh, U., Massmann, G.,Zhang, C., 2007. An ostracod-conductivity transfer function for Tibetan lakes. Journal of Paleolimnology 38, 509-524.

Mischke, S.,Zhang, C., 2010. Holocene cold events on the Tibetan Plateau. Global and Planetary Change 72, 155-163.

Mischke, S., Bößneck, U., Diekmann, B., Herzschuh, U., Jin, H., Kramer, A., Wünnemann, B., Zhang, C., 2010a. Quantitative relationship between water-depth and sub-fossil ostracod assemblages in Lake Donggi Cona, Qinghai Province, China. Journal of Paleolimnology 43, 589–609.

Mischke, S., 2012. Quaternary ostracods from the Tibetan Plateau and their significance for envi- ronmental and climate-change studies. Developments in Quaternary Sciences 17, 263-279.

Mischke, S., Zhang, C., Börner, A., Herzschuh, U., 2010b. Lateglacial and Holocene variation in aeolian sediment flux over the northeastern Tibetan Plateau recorded by laminated sediments of a saline meromictic lake. Journal of Quaternary Science 25, 162-177.

Mischke, S., Weynell, M., Zhang, C., Wiechert, U., 2013. Spatial variability of 14C reservoir effects in Tibetan Plateau lakes. Quaternary International 313-314, 147-155.

Mischke S., Zhang C., Fan R., 2015. Early to mid-Holocene lake high-stand sediments at Lake Donggi Cona, northeastern Tibetan Plateau, China—Comment to the paper published by Dietze et al., Quaternary Research 79(2013), 325-336. Quaternary Research 83, 256-258.

Molnar, P., 1989. The geological evolution of the Tibetan Plateau: American Scientist, 77, 350-359.

Nugteren, G., Vandenberghe, J., Van Huissteden, J. and An, Z., 2004 A Quaternary climate record based on grain size analysis from the Luochuan loess section on the Central Loess Plateau, China. Global and Planetary Change 41, 167-183.

Opitz, S., Wünnemann, B., Aichner, B., Dietze, E., Hartmann, K., Herzschuh, U., IJmker, J., Lehmkuhl, F., Li, S., Mischke, S., Plotzki, A., Stauch, G., Diekmann, B., 2012. Late glacial and Holocene development of Lake Donggi Cona, north-eastern Tibetan Plateau, inferred from sedimentological analysis. Palaeogeography, Palaeoecology, Palaeoclimatology 337-338, 159-176.

Opitz, S. , Ramisch, A. , Mischke, S. and Diekmann, B., 2013. Holocene lake stages and thermokarst dynamics in a discontinuous permafrost affected region, north-eastern Tibetan Plateau.. Journal of Asian Earth Sciences 76, 85-94.

Pachur, H., Wuennemann, B., and Zhang, H., 1995. Lake evolution in the Tengger Desert, Northwestern China, during the last 40,000 years. Quaternary Research, 44, 171-180.

Pang, H., Hou, s., Kaspari, S., and Mayewski, P., 2014. Influence of regional precipitation patterns on stable isotopes in ice cores from the central Himalayas. The Cryosphere 8, 289-301. doi:10.5194/tc-8-289-2014.

Pettijohn, F.J., Potter, P.E., Siever, R., 1987. Sand and sandstone. Springer New York, Berlin, Heidelberg, 553pp.

Qiu, J., 2008. China: the third pole. Nature 454, 393-396.

Ramisch, A., Lockot,G., Haberzettl, T., Hartmann, K.,Kuhn, G., Lehmkuhl, F.,Schimpf, S., Schulte, P., Stauch, G., Wang, R., Wünnemann,B., Yan, D., Zhang, Y.,Diekmann B., 2016. A persistent northern boundary of Indian Summer Monsoon precipitation over Central Asia during the Holocene. Scientific Report 6, 25791.

Reimann, T., Tsukamoto, S., Naumann, M.,Frenchen, M., 2011. The potential of using K-rich feldspars for optical dating of young coastal sediments- A test case from Darsse Zingst pennisula (southern Baltic Sea coast). Quaternary Geochronology 6, 207-222.

Reimer, J.P., Bard, E., Bayliss, A., Beck, J.W., Blackwell, P.G., Ramsey, C.B., Brown, D.M., Guil- derson, T.P., Haflidason, H., Hajdas, I., Hatté, C., Heaton, T.J., Hogg, A.G., Hughen, K.A., Kai- ser, K.F., Kromer, B., Manning, S.W., Reimer, R.W., Richards, D.A., Scott, E.M., Southon, J.R., Turney, C.S.M., Van Der Plicht, J., 2013. Intcal13 and Marine13 Radio- carbon Age Calibration Curves 0–50,000 Years Cal Bp. Radiocarbon 55, 1869-1887.

Reinhardt, C., Wünnemann,B., Krivonogov, S., 2007. Geomorphological evidence for lake level fluctuations of the Aral Sea during the last millennia. Geomorphology 93, 302-315.

Ren, W., Yao, T., Yang, X., Joswiak, D., 2013. Implications of variations in d18O and dD in precipitation at Madoi in the eastern Tibetan Plateau.Quaternary International, 313-314.

Ricketts, R.D., Johnson, T.C., Brown, E.T., Rasmussen, K.A., Romanovsky, V.V., 2001. The Holocene paleolimnology of Lake Issyk-Kul, Kyrgyzstan: trace element and stable isotope composition of ostracodes. Palaeogeography, Palaeoclimatology, Palaeoecology 176, 207–227.

Shen, J., Liu, X., Wang, S., Ryo, M., 2005. Palaeoclimatic changes in the Qinghai Lake area during the last 18,000 years. Quaternary International 136, 131–140.

Sirocko, F., Sarntheim, M., Erlenkeuser, H., Lange, H., Arnold, M., Duplessy, J.C., 1993. Century-scale events in monsoonal climate over the past 24,000 years. Nature 364, 322–324.

Smith A.G., Delorme L.D., 2010. Chapter 19: Ostracoda. Ecology and classification of North American freshwater invertebrates (Third Edition), 725-771.

Solotchina, E.P., Prokopenko, A.A., Kuzmin, M. I., Solotchin, P.A., Zhadanova, A.N., 2009. Climate signals in sediment mineralogy of Lake Baikal and Lake Hovsgol during the LGM-Holocene transition and the 1-Ma carbonate record from HDP-04 drill core. Quaternary International 205 (1-2), 38-52.

Stauch, G., IJmker, J., Pötsch, S., Zhao, H., Hilgers, A., Diekmann, B., Dietze, E., Hartmann, K., Opitz, S., Wünnemann, B., Lehmkuhl F., 2012. Aeolian sediments on the north-eastern Tibetan Plateau. Quaternary Science Reviews 57, 71-84.

Stauch, G., Poetsch, S., Zhao, H., Lehmkuhl, F., 2014. Interaction of geomorphological processes on The North-eastern Tibetan Plateau during the Holocene, an example from a sub-catchment of Lake Donggi Cona. Geomorphology 210, 23-35.

Stauch, G., 2015. Geomorphological and palaeoclimate dynamics recorded by the formation of aeolian archives on the Tibetan Plateau. Earth Science Review 150, 393-408.

Stauch, G., 2016. Multi-decadal periods of enhanced aeolian activity on the northeastern Tibet Plteau during the last 2 ka. Quaternary Science Reviews 149, 91-101.

Steinhilber, F., Abreu, J.A., Beer, J., Brunner, I., Christl, M., Fischer, H., Heikkilä, U., Kubik, P.W., Mann, M., McCracken, K.G., Miller, H., Miyahara, H., Oerter, H., Wilhelms, F., 2012. 9,400 Years of cosmic radiation and solar activity from ice cores and tree rings. Proceedings of the National Academy of Sciences of the United States of America 109, 5967-5971.

Tabolt, M., 1990. A review of the palaeohydrological interpretation of carbon and oxygen isotopic ratios in primary lacustrine carbonates. Chemical Geology (Isotope Geoscience Section), 80, 261-279.

Tan, L., Cai, Y., Yi, L., An, Z., Ai, L, 2008. Precipitation variations of Longxi, northeast margin of Tibetan plateau since AD 960 and its relationship with solar activity. Climate of the Past 4, 19-28.

Tan, L., Cai, Y., An, Z., Yi, L., Zhang, H., Qin, S., 2011. Climate patterns in north central China during the last 1800 yr and their possible driving force. Clim. Past, 7, 685–692.

Taylor, G., 1975. The occurrenceof mnohydrocalcte in two small lakes in the southeast of South Australia. American Mineralogist 60, 690-697.

Thompson, L.G., Yao, T., Davis, M.E., Henderson, K.A., Mosley-Thompson, E., Lin, P.- N., Beer, J., Synal, H.-A., Cole-Dai, J., Bolzan, J.F., 1997. Tropical climate instability: the last glacial cycle from a Qinghai-Tibetan ice core. Science 276, 1821-1825.

Tian, L., Yao, T., Schuster, P.F., White, J.W.C., Ichiyanagi, K., Pendall, E., Pu, J., Yu, W., 2003. Oxygen-18 concentrations in recent precipitation and ice cores on the Tibetan Plateau. Journal of Geophysical Research 108, doi: 10.1029/2002JD002173.

Tian, L., Yao,T ., MacClune, K., White, J.W.C., Schilla, A. Vaughn, B., Vachon, R., Ichiyanagi, K., 2007. Stable isotopic variations in west China: A consideration of moisture sources. Journal of Geophysical Research 112, D10112, doi:10.1029/2006JD007718.

Vandenberghe, J., 2002 The relation between climate and river processes, landforms and deposits during the Quaternary. Quaternary International 91, 17-23.

Van der Meeren, J., Khand, Y., Martens, K., 2009. On Recent species of Tonnacypris Diebel & Pietrzeniuk, 1975 (Crustacea, Ostracoda), with new species descriptions from Mongolia. Zootaxa 2015, 1-41.

Van der Woerd, J., Tapponnier, P., Ryerson, F.J., Meriaux, A.-S., Meyer, B., Gaudemer, Y., Finkel, R.C., Caffee, M.W., Guoguang, Z., Zhiqin, X., 2002. Uniform postglacial slip- rate along the central 600 km of the Kunlun Fault (Tibet), from 26Al, 10Be, and 14C dating of riser offsets, and climatic origin of the regional morphology. Geophysical Journal International 148, 356–388.

Vriend, M., Prins, M.A., Buylaert, J.P., Vandenberghe, J. and Lu, H. 2011 Contrasting dust supply patterns across the north-western Chinese Loess Plateau during the last glacial-interglacial cycle. Quaternary International 240, 167-180.

Wagner J., 2012. Mineralogy and geochemistry of Hala Lake sediments, China. unpublished diploma thesis, Technology University Berlin, Germany.

Wang, X., Yang, H., Zhao, Q., Chen, Y., Chen, J., Wang, L., 2011. Modern sedimentation rates and dry-humid change inferred from grain size records in Dianchi Lake,Yunnan Province. Journal of Geographical Reseach 30(1), 161-171. (In Chinese with English abstract)

Wang, R., Zhang, Y.Z., Wünnemann, B., Biskaborn, B.K., Yin, H., Xia, F., Zhou, L.F., Diekmann, B., 2015. Linkages between Quaternary climate change and sedimentary processes in Hala Lake, northern Tibetan Plateau, China. Journal of Asian Earth Sciences 107, 140-150.

Wang,Y., Cheng, H., Edwards, R.L., He, Y., Kong, X., An, Z., Wu, J., Kelly, M., Dykoski, C., Li, X., 2005.The Holocene Asian Monsoon: Links to Solar Changes and North Atlantic Climate, Science,308, 854-857, doi: 10.1126/science.1106296.

Wang, Y., Liu, X., Herzschuh, U., 2010. Asynchronous evolution of the Indian and East Asian Summer Monsoon indicated by Holocene moisture patterns in monsoonal central Asia . Earth Science Reviews 103, 135-153.

Wang, T., Wag, H., Jiang, D., 2010. Mid-Holocene East Asian summer monsoon climate as simulated by the PMIP2 models. Palaeogeography, Palaeoclimatology, Palaeoecology 288, 93-102.

Wanner, H., Beer, J., Buetikofer, J., Crowley, T.J., Cubasch, U., Flueckiger, J., Goose, H., Grosjean, M., Joos, F., Kaplan, J.O., Kuettel, M., Mueller, S.A., Prentice, I.C., Solomina, O., Stocker, T.F., Tarasov, P., Wagner, M., Widmann, M., 2008. Mid- to Late Holocene climate change: an overview. Quaternary Science Reviews 27, 1791-1828.

Warren, J., 2000. Dolomite: occurrence, evolution, and economically important associations. Earth Science Reviews 52 (1-3), 1-81.

Wei, K., Gasse, F., 1999. Oxygen isotopes in lacustrine carbonates of West China revisited: mplications for post glacial changes in summer monsoon circulation. Quaternary Science Reviews 18, 1315–1334.

Weltje, G.J., 1997. End-member modeling of compositional data: numerical- statistical, algorithms for solving the explicit mixing problem. Journal of Mathematical Geology 29, 503-549.

Wen, R., Xiao, J., Chang, Z., Zhai, D., Xu, Q., Li, Y., Itoh, S., 2010. Holocene precipitation and temperature variations in the East Asian monsoonal margin from pollen data from Hulun Lake in northeastern Inner Mongolia, China. Boreas 39 (2), 262-272.

Weynell, M., Wiechert, U., Zhang, C., 2016. Chemical and isotopic (O, H, C) composition of surface waters in the catchment of Lake Donggi Cona (NW China) and implications for paleoenvironmental reconstructions. Chemical Geology 435, 92-107.

Winland, H.D., 1969. Stability of calcium carbonate polymorphs in warm, shallow seawater. Journal of Sedimentology and Petrology 39, 1579-1587.

Wischnewski, J., Mischke, S., Wang, Y.B., Herzschuh, U., 2011. Reconstructing climate variability on the northeastern Tibetan Plateau since the last Lateglacial — a multi-proxy, dual-site approach comparing terrestrial and aquatic signals. Quaternary Science Reviews 30, 82–97.

Wright, L.D., 1977. Sediment transport and deposition at river mouths, a synthesis. Geological Society of America Bull. 88, 857-868.

Wright, D.T., Wacey, D., 2005. Precipitation of dolomite using sulphate-reducing bacteria from Goorong Region, South Australia: significance and implications. Sedimentology 52 (5), 987-1008.

Wrozyna, C., Frenzel, P., Daut, G., Mäusbacher, R., Zhu, L., 2012. Holocene lake-level changes of Lake Nam Co, Tibetan Plateau, deduced from ostracod assemblages and d18O and d13C signatures of their valves. Ostracoda as Proxies for Quaternary Climate Change Chapter 16, 281-295.

Wu, Y., Wu, J., Xue, B., Qian, J., Xiao, J., 1998. Paleoenvironmental evolution in Dianchi Lake area since 13 ka BP.Journal of Lake Sciences 10(2), 5-9 (In Chinese with English abstract)

Wu, Y., Lücke, A., Jin, Z., Wang, S., Schleser, G.H., Battarbee, R.W., Weilan, X., 2006. Holocene climate development on the central Tibetan Plateau: a sedimentary record Cuoe Lake. Palaeogeography, Palaeoclimatology, Palaeoecology 234, 328–340.

Wu, Y., Li, S., Lücke, A., Wünnemann, B., Zhou, L., Reimer, P., Wang, S., 2009. Lacustrine radiocarbon reservoir ages in Co Ngoin and Zige Tangco, central Tibetan Plateau. Quaternary International 212, 21–25.

Wünnemann, B., Pachur, H., Zhang, H., 1998. Climatic and environmental changes in the deserts of Inner Mongolia, China, since the Late Pleistocene. In: Alsharhan, A.S., Glennie, K.W., Whittle, G.L., Kendall, C.G.St.C. (Eds.), Quaternary Deserts and Climatic Change. Balkeema Publishing House, Rotterdam, pp. 381–396.

Wünnemann, B., Mischke, S., Chen, F., 2006, A Holocene sdimentary record from Bosten Lake, China. Palaeogeography Palaeoclimatology Palaeoecology 234, 223-238.

Wünnemann, B., Hartmann, K., Janssen, M., Zhang, H.C, 2007. Responses of Chinese desert lakes to climate instability during the past 45,000 years In: Madsen, D.B., Chen, F.H., and Gao, X. (Eds.), Late

Quaternary Climate Change and Human Adaptation in Arid China, Developments in Quaternary Science 9, 11-24.

Wünnemann, B., Demske, D., Tarasov, P.E., Kotlia, B.S., Bloemendal, J., Diekmann, B., Hartmann, K., Reinhardt, C., Riedel, F., Arya, N., 2010. Hydrological evolution during the last 15 kyr in the Tso Kar lake basin (Ladakh, India), derived from geomorphological, sedimentological and palynological records. Quaternary Science Reviews 29 (9-10), 1138-1155.

Wünnemann, B., Wagner, J., Zhang, Y., Yan, D., Wang, R.,Yan, S., Fang, X., Zhang, J., 2012. Implications of diverse sedimentary patterns in Hala Lake, Qinghai Province, China for reconstructing Late Quaternary climate. Journal of Paleolimnology 48, 725-749.

Wünnemann, B., Yan, D., Ci, R., 2015. Morphodynamics and lake level variations at Paiku Co, southern Tibetan Plateau, China. Geomorphology. 246, 489-501.

Xu, Q., Xiao, J., Li, Y., Tian, F., Nakagawa, T., 2010. Pollen-Based Quantitative Reconstruction of Holocene Climate Changes in the Dahai Lake Area, Inner Mongolia, China. Journal of Climate 23 (11), 2856-2868.

Yan, D., Wünnemann, B., 2014. Late Quaternary Water Depth Changes in Hala Lake, Northeastern Tibetan Plateau, Derived from Ostracod Assemblages and Sediment Properties in Multiple Sediment Records. Quaternary Science Reviews 95, 95-114.

Yan D., Wuennemann, B., Hu, Y., Frenzel, P., Zhang, Y., Chen, K., 2017. Wetland evolution in the Qinghai Lake area, China, in response to hydrodynamic and eolian processes during the past 1100 year. Quaternary Science Reviews 162:42-59 .

Yang, B., Qin, C., Wang, J., He, M., Melvinb, T.M., Osbornb, T.J., Briffab, K.R.. 2014. A 3500-year tree-ring record of annual precipitation on the northeast Tibetan Plateau. Proceedings of the National Academy of Sciences of the United States of America 111(8), 2903-2908.

Yao, T., Thompson, L., Yang, W., Yu, W., Gao, Y., Guo, X., Yang, X., Duan, K., Zhao, H., Xu, B., Pu, J., Lu., A., Xiang, Y., Kattel, D.B., Joswiak, D., 2012. Different glacier status with atmospheric circulations in Tibetan Plateau and surroundings. Nature Climate Change 2, 663–667.

Yu, Y., 1986. Denis Twitchett; Michael Loewe, eds. Cambridge History of China: Volume I: the Ch'in and Han Empires, 221 B.C. – A.D. 220. University of Cambridge Press. pp. 455–458. *ISBN 978-0-5212-4327-8*.

Yu, G., Harrison, S.P., Xue, B., 2001. Lake Status Records from China. Data Base Documentation, Max-Planck-Institute for Biogeochemistry Jena.

Yu, B., Dong, H., Jiang, H., Li, S., Liu, Y., 2007. Discover of spheric Dolomite aggregations in sediments from bottom of Qinghai Lake and its significance for Dolomite problem. Geoscience 21(1), 66-70.

Yu, L., Lai, Z., 2012. OSL chronology and palaeoclimatic implications of aeolian sediments in the eastern Qaidam Basin of the northeastern Qinghai-Tibetan Plateau. Palaeogeogr. Palaeoclimatol. Palaeoecol. 337-338, 120-129.

Zhai, D., Xiao, J., Zhou, L., Wen, R., Chang, Z., Pang, Q., 2010. Similar distribution patter of different phenotypes of Limnocythere inopinata (Baird) in a brakish-water lake in Inner Mongolia. Hydrobiologia 651, 185-197.

Zhang Y.,Peng B.,Chen J., Lv, J., 2005. Evaluating amount of sediment accumulation of Dianchi Lake using 137 Cs dating. Acta Geographica Sinica 60 (1), 71-78. (In Chinese with English abstract)

Zhang, H., Wünnemann, B., Ma, Y.z., Peng, J., Pachur, H.-J., Li J., Qi, Y., Chen, G., Fang, H.& Feng Z., 2002. Lake Level and Climate Change between 40,000 and 18,000 14C Years BP in Tengger Desert, NW China. Quaternary Research 58, 62-72.

Zhang, P., Cheng, H., Edwards, R., Chen, F., Wang, Y., Yang, X., Liu, J., Tan, M., Wang, X., Liu, J., An, C., Dai, Z., Zhou, J., Zhang, D., Jia, J., Jin, L., Jonson, K., 2008. A test of climate, sun and culture relationships from an 1810-year Chinses Cave Record. Science 322, 940-942.

Zhang, C., Mischke, S., 2009.A Lategracial and Holocene lake record from the Nianbaoyeze Mountains and inferences of lake, glacier and climate evolution on the eatern Tibetan Plateau, Quaternary Science Reviews 28, 1970-1983.

Zhang, J., Chen, F., Holmes, J.A., Li, H., Guo, X., Wang, J., Li, S., Lü, Y., Zhao, Y., Qiang, M., 2011. Holocene monsoon climate documented by oxygen and carbon isotopes from lake sediments and peat bogs in China: a review and sysnthesis. Quaternary Science Reviews 30, 1973-1987.

Zhao, Y., Yu, Z., Zhao, W., 2011. Holocene vegetation and climate histories in the eastern Tibetan Plateau: controls by insolation-driven temperature or monsoon-derived precipitation changes? Quaternary Science Review 30, 1173-1184.

Zhou, J., Han, F., Pang, X., Luo, C., Yan, J., 2010. Preliminary investigation of Hajiang Salt Pond and Kuhai Lake in Yellow River Source Area. Journal of Salt Lake Research 18(3), 18-22. (In Chinsed with English abstract)

Zhou, W.J., Yu, S.Y., Kukla, G.B., Jull, G.J., Xian,F., Xiao, J.Y., Colman, S.M., Yu, H.G., Liu, Z.,Kong, X.H., 2010.Postglacial changesin the Asian summer monsoon system: a pollen recordfrom the eastern margin of the Tibetan Plateau, Boreas 39, 528-539.

Zhu, L.P., Peng, P., Xie, M.P., Wang, J.B., Frenzel, P., Wrozyna, C., Schwab, A., 2010. Ostracod-based environmental reconstruction over the last 8,400 years of Nam Co Lake on the Tibetan plateau. Hydrobiologia 648(1), 157-174.

Zhu, K., 1972. Study on climate changes during last 5000 years in China. Acta Archaeologica Sinica 1，168-189. (In Chinese)

Acknowledgements

I would like to express my special appreciation and many thanks to my PhD supervisors: Prof. Dr. Bernd Wuennemann and Prof. Dr. Brigitta Schuett. Prof. Dr. Wuennemann introduced to me what good science would be, always with full of passion. He taught me how to achieve materials and data, especially his presence during field work and lab work in person, as well as guided me to develop a more comprehensive way in lake-catchment research. Although we experienced very hard time due to this scientific working way, I enjoyed a lot. I am so appreciated that I would have this cherish opportunity to form my own thinking, which is helpful for my whole life.

I would also like to thank Dr. Zhang Yongzhan, Nanjing University, China, who supported me in all aspects all the time. As he said, we are family. I got a lot of energy from his encouragement. Thanks also to all my group members: Mr. Hu Yanbo, Miss. Mona Storms, Miss. Marielle Neyen, Mr. Tao Ran and Mr. Eric Runge, who shared very good memory with me in the field and lab works, I still remember how we encouraged each other under very harsh conditions on the Tibetan Plateau. Especially to Mr. Hu Yanbo, I am very proud that he supported me and developed a lot within the same project. Appreciations are also deserved to Mr. Liu Xuan, Nanjing University, China, for his help in field as well as in administration management; to Prof. Dr. Cao Guangchao, Prof. Dr. Chen Kelong, Prof. Dr. Hou Guangliang, Qinghai Normal University, China, for their full-support in coordinations with local minorities during field work; also to PD. Dr. Peter Frenzel and Mr. Mauro Alivernini, Jena, as well as Dr. Georg Stauch, RWTH, for their support in field and lab works. Especially to PD Dr. Peter Frenzel, I am so touched by his energetic support in ostracod sampling, identification and interpretations.

Thanks to all colleagues and cooperators from Germany and China: Dr. Kai Hartmann, Dr. Philipp Hoelzmann, Mr. Frank Kurtz, Prof. Dr. Achim Schulte, Dr. Jens Boelscher, Dr. Christian Reinhadt-Imjela, Ms. Maria von Bodecker, Prof. Dr. Frank Riedel, Mr. Ding Wei, Mr. Jan Evers, Prof. Dr. Margot Boese, Prof. Dr. Manfred Frechen, Dr. Nils Andersen, Dr. Long Hao, Mr. Gao Lei, Dr. Xia Weilan, Dr. Zeng Hai'ao, Dr. Gao Jianhua, Dr. Pang Hongxi, Dr. He Ting, Prof. Dr. Zheng Hongbo, Prof. Dr. Zhang Hucai and Prof. Dr. Jiang Zhilong. They all guided and supported me in sample measurement, data analysis and knowledge exchange and administration management.

Special thanks to my friends and family. Dear Mr. Zhai Yuhan, Miss Yan Chongchong, thank you very much to suffer high elevation and coldness in order to accompany me for field work. Dear Ms. Yan Huanhuan, you are so strong and optimistic struggling with diseases, which encouraged me to face all troubles and problems I met in work and find solutions to them. Ms. Li Yuanlan, Miss He Wenjie and Mr. Liu Song, I appreciate that you were always behind me, no matter what happened during this long time of hard work. Finally special thanks to my parents, who always supported me and it's very cherishing for me being educated to be honest and fair.

Appendix I——Methods: selected photos of work facilities

1. Field work

Fig. App.I 1 Photos of field work in Kuhai Lake. A, C. Catchment study; B. Lake water sampling; D. Lake drilling: double-A-drilling system.

2. Lab work

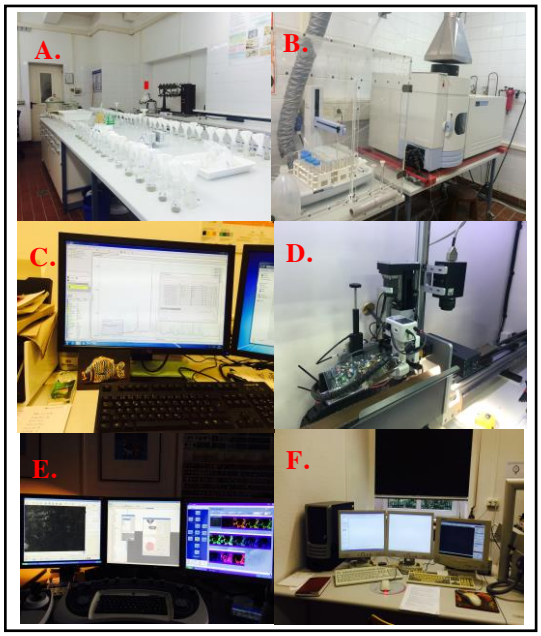

Fig. App.I 2 Photos of part lab work in Kuhai Lake. A. XRD data receiver; B. XRF detector C-D.ICP preparation and measurement; E. SEM for minerals; F. SEM for ostracod.

Appendix II——Results

1. Limnological parameter

Tab. App.II 1 Limnological parameter of water samples from Kuhai Lake.

Sample ID	PH	ORP(mv)	EC	TDS	Salinity	RES	δDV-SMOW(‰)	stdev (‰)	δ18OV-SMOW (‰)	stdev(‰)	Note
KHW1	8.12	193	988 µs	644 mg/L	0.49 ppt	1.05 kΩ	-78.91	0.8	-11.38	0.25	river
KHW2	8.04	201	1263 µs	892 mg/L	0.64 ppt	802 Ω	-71.41	0.31	-11.02	0.19	river
KHW3	8.24	202	988 µs	684 mg/L	0.49 ppt	1.00 kΩ	-71.33	0.23	-10.78	0.12	river
KHW4	8.04	201	825 µs	585 mg/L	0.40 ppt	1.15 kΩ	-71.58	0.26	-10.92	0.05	river
KHW5	8.56	225	22.5 ms	20.6 g/L	12.9 ppt	44.2 Ω	-22.49	0.34	-0.95	0.2	lake
KHW6	8.68	225	22.2 ms	20.6 g/L	12.6 ppt	45.0 Ω	-22.72	0.14	-1.06	0.01	lake
KHW7	8.74	222	22.2ms	20.9 g/L	13.0 ppt	44.2 Ω	-23.98	0.14	-1.41	0.09	lake
KHW100	7.94	197	995 µs	700 mg/L	0.51 ppt	993 Ω	-78.81	0.24	-11.63	0.09	river
KHW102	8.18	206	981 µs	682 mg/L	0.49 ppt	1.01 kΩ	-69.89	0.24	-10.43	0.17	river
KHW103	8.02	213	926 µs	645 mg/L	0.46 ppt	1.06 kΩ	-68.68	0.12	-10.28	0.07	river
KHW104	8.23	213	638 µs	438 mg/L	0.31 ppt	1.54 kΩ	-66.87	0.28	-10.28	0.05	river
KHW-0	8.67	220	20.9 ms	20.1 g/L	12.3 ppt	46.0 Ω	-22.94	0.01	-1.36	0.01	lake
KHW2-0	8.68	230	23.2 ms	21.6 g/L	13.4 ppt	42.7 Ω	-22.16	0.13	-1.22	0.09	lake
KHR1	7.24	127	81.0 µs	50.3 mg/L	0.03 ppt	15.1 kΩ	-31.64	0.01	-6.45	0.12	snow
KHR2	7.55	146	18.44 µs	11.8 mg/L	0.01 ppt	51.0 kΩ	-52.68	0.26	-9.05	0.11	snow
KHR3	7.21	160	22.60 µs	14.5 mg/L	0.01 ppt	43.8 kΩ	-51.82	0.48	-8.83	0.04	rain/snow
KHP2W	8.55	238	10.81 ms	10.0 g/L	5.88 ppt	91.4 Ω	-71.03	0.19	-9.51	0.04	pond
KHP3W	8.05	236	6.34 ms	5.10 g/L	3.47 ppt	153 Ω	-65.15	0.31	-8.9	0.21	pond
KHP4W	8.68	219	3.59 ms	2.77 g/L	1.90 ppt	272 Ω	-72.64	0.1	-11.18	0.16	pond
KHP5W	8.07	226	4.42 ms	3.40 g/L	2.35 ppt	222 Ω	-69.48	0.14	-11.04	0.14	pond
KHP6W	7.63	228	1305 µs	923 mg/L	0.65 ppt	758 Ω	-68.79	0.16	-10.5	0.02	pond
KHP7W	8.67	-269	19.87 ms	18.3 g/L	11.5 ppt	49.6 Ω	-30.23	0.16	-4.38	0.07	pond

2. Sample locations

Tab. App.II 2 Coordinates of samples from Kuhai Lake.

Locations	Lat	Long	Water depth (m)	Type	Time of sampling
KH4	35,31692	99,25621		Section	
KHS1	35,25549	99,16743		Section	
KHS2	35,16435	99,25650		Section	
KHS3	35,24866	99,13767		Section	
KHS4	35,25059	99,14418		Section	
KHS5	35,25396	99,15390		Section	
KHS6	35,31573	99,25386		Section	
KHS7	35,33348	99,25831		Section	
KHS8	35,33516	99,25762		Section	
KHS9	35,32938	99,24343		Section	
KHS10	35,32582	99,21799		Section	
KHS11	35,28673	99,26020		Section	
KHS12	35,24369	99,20327		Section	
KHS13	35,30991	99,26028		Section	
KHS14	35,28816	99,25095		Section	
KHS15	35,28847	99,24876		Section	
KHS16	35,29133	99,24393		Section	
KHS17	35,23470	99,17478		Section	
KHS18	35,28715	99,27337		Section	
KHS19	35,29250	99,28940		Section	
KHS20	35,29430	99,29356		Section	
KHS21	35,29292	99,28136		Section	
KHS22	35,28552	99,16292		Section	
KHS23	35,28396	99,16493		Section	
KHS24	35,28544	99,16733		Section	
KHS25	35,28297	99,17118		Section	
KHS26	35,28340	99,16122		Section	
KHS27	35,28963	99,11851		Section	
KHS28	35,29071	99,13251		Section	
KHS29	35,32374	99,21870		Section	
KH11	35,32042	99,20124		Core	
KH12	35,29688	99,19164		Core	
KH13	35,27271	99,16155		Core	
KH14	35,30559	99,16559		Core	
KH15	35,32578	99,18443		Core	
KH16	35,28459	99,14301		Core	
KH17	35,30534	99,16515		Core	
KHPS1	35,32703	99,21758		Pond	
KHPS2	35,25735	99,15918		Pond	
KHPS3	35,25622	99,16032		Pond	
KHPS4	35,25730	99,15967		Pond	
KHP5-S1	35,25498	99,16225		Pond	
KHP6-S1	35,27125	99,13257		Pond	
KHP7-S1	35,26167	99,15625		Pond	
KH100	35,26807	99,16887	-10,65	Lake surface samples	
KH101	35,27842	99,17208	-13,2	Lake surface samples	
KH102	35,28228	99,15692	-14,62	Lake surface samples	
KH103	35,29138	99,15046	-14,08	Lake surface samples	
KH104a	35,29209	99,13738	-11,29	Lake surface samples	

Continued

KH105a	35,29022	99,13587	-7,92	Lake surface samples	
KH106	35,28099	99,14073	-11,51	Lake surface samples	
KH107c	35,27686	99,13911	-3,88	Lake surface samples	
KH108	35,27104	99,15218	-8,7	Lake surface samples	
KH109	35,26209	99,15934	-6,2	Lake surface samples	
KH110b	35,26044	99,16463		Lake surface samples	
KH111	35,26794	99,17272	-8,66	Lake surface samples	
KH112	35,27856	99,18430	-6,81	Lake surface samples	
KH113a	35,28963	99,17805	-15,85	Lake surface samples	
KH114	35,30376	99,17318	-18,93	Lake surface samples	
KH115a	35,31715	99,16732	-18,8	Lake surface samples	
KH116a	35,26898	99,16173	-12,46	Lake surface samples	
KH117a	35,28825	99,17814	-15,58	Lake surface samples	
KH118a	35,28737	99,13840	-7,68	Lake surface samples	
KH119	35,27293	99,17572	-11,72	Lake surface samples	
KH120	35,27347	99,17595	-12,25	Lake surface samples	
KH121	35,29086	99,19248	-11,29	Lake surface samples	
KH122a	35,31232	99,20980	-12,56	Lake surface samples	
KH123	35,32296	99,21549	-3,04	Lake surface samples	
KH124	35,31192	99,18309	-19,07	Lake surface samples	
KH125a	35,31221	99,18383	-18,82	Lake surface samples	
KH126a	35,30427	99,15790	-17,43	Lake surface samples	
KH127a	35,30284	99,15586	-16,95	Lake surface samples	
KH128a	35,27062	99,16630	-13,70	Lake surface samples	
KH129a	35,29707	99,13446	-11,43	Lake surface samples	
KH130a	35,30284	99,13617	-8,31	Lake surface samples	
KH131a	35,29489	99,16501	-16,59	Lake surface samples	
KH132a	35,30206	99,18421	-17,96	Lake surface samples	
KH133	35,32446	99,17717	-16,58	Lake surface samples	
KH134	35,33030	99,16155	-9,83	Lake surface samples	
KH135	35,27534	99,14938	-12,30	Lake surface samples	
KH136	35,28267	99,12778	-1,87	Lake surface samples	
KH137a	35,30900	99,16956	-19,95	Lake surface samples	
KH138a	35,31333	99,18143	-18,41	Lake surface samples	
KH139	35,31753	99,19862	-15,42	Lake surface samples	
KH140	35,31877	99,21171	-10,76	Lake surface samples	
KH141	35,31956	99,21507	-5,99	Lake surface samples	
KH142a	35,28032	99,14739	-13,75	Lake surface samples	
KH143a	35,28890	99,16678	-14,92	Lake surface samples	
KH144	35,31402	99,15515	-16,18	Lake surface samples	
KH145	35,30722	99,16560	-20,08	Lake surface samples	
KH146a	35,30732	99,16595	-20,20	Lake surface samples	
KH147a	35,30719	99,19426	-16,87	Lake surface samples	
KH148a	35,30014	99,20383	-5,07	Lake surface samples	
KH149	35,32446	99,19092	-14,68	Lake surface samples	
KH150	35,33138	99,18387	-12,56	Lake surface samples	
KH151a	35,34032	99,19214	-7,99	Lake surface samples	
KH152	35,33978	99,19633	-6,75	Lake surface samples	
KH153a	35,33983	99,19655	-6,12	Lake surface samples	
KH154	35,32273	99,20539	-11,78	Lake surface samples	

Continued

KH155	35,32277	99,20677	-11,60	Lake surface samples	
KH156	35,29492	99,19958	-6,69	Lake surface samples	
KH157	35,29496	99,19945	-7,08	Lake surface samples	
WS1	35,2887	99,1796	-14,66	Lake water samples	Sep 14
WS2	35,2871	99,1810	-13,53	Lake water samples	Sep 14
WS3	35,2847	99,1824	-12,58	Lake water samples	Sep 14
WS4	35,3033	99,1733	-18,78	Lake water samples	Sep 14
KHW1R	35,33574	99,26353		Water samples	Sep 14
KHW2R	35,30528	99,25435		Water samples	Sep 14
KHW3R	35,29122	99,24419		Water samples	Sep 14
KHW4R	35,26221	99,22397		Water samples	Sep 14
KHW5R	35,27938	99,17226		Water samples	Sep 14
KHW6R	35,31489	99,15250		Water samples	Sep 14
KHW7R	35,34019	99,18829		Water samples	Sep 14
KHW1W	35,16448	99,25690		Water samples	early June 2015
KHW2W	35,28949	99,25021		Water samples	early June 2015
KHW3	35,29121	99,24350		Water samples	early June 2015
KHW4	35,26218	99,22390		Water samples	early June 2015
KHW-0	35,31096	99,17125		Water samples	early June 2015
KHW2-0	35,26044	99,16463		Water samples	early June 2015
KHR1	35,26604	99,15280		Water samples	early June 2015
KHR2	35,26604	99,15280		Water samples	early June 2015
KHR2	35,26604	99,15280		Water samples	early June 2015
KHP2W	35,25735	99,15918		Water samples	early June 2015
KHP3W	35,25622	99,16032		Water samples	early June 2015
KHP4W	35,25730	99,15967		Water samples	early June 2015
KHP5W	35,25498	99,16225		Water samples	early June 2015
KHP6W	35,27125	99,13257		Water samples	early June 2015
KHP7W	35,26167	99,15625		Water samples	early June 2015
Khsection 0	35,31116	99,1647		Water samples	end June 2016
Khsection 1	35,31116	99,1647		Water samples	end June 2016
Khsection 2	35,31116	99,1647		Water samples	end June 2016
Khsection 3	35,31116	99,1647		Water samples	end June 2016
Khsection 4	35,31116	99,1647		Water samples	end June 2016
Khsection 5	35,31116	99,1647		Water samples	end June 2016
Khsection 6	35,31116	99,1647		Water samples	end June 2016
Khsection 7	35,31116	99,1647		Water samples	end June 2016
Khsection 8	35,31116	99,1647		Water samples	end June 2016
Khsection 8-2	35,31116	99,1647		Water samples	end June 2016
Khsection 9	35,31116	99,1647		Water samples	end June 2016
Khsection 10	35,31116	99,1647		Water samples	end June 2016
Khsection 11	35,31116	99,1647		Water samples	end June 2016
Khsection 12	35,31116	99,1647		Water samples	end June 2016
Khsection 13	35,31116	99,1647		Water samples	end June 2016
Khsection 14	35,31116	99,1647		Water samples	end June 2016
Khsection 15	35,31116	99,1647		Water samples	end June 2016
Khsection 16	35,31116	99,1647		Water samples	end June 2016
Khsection 17	35,31116	99,1647		Water samples	end June 2016
Khsection 18	35,31116	99,1647		Water samples	end June 2016
Khsection 19	35,31116	99,1647		Water samples	end June 2016
Khsection 20	35,31116	99,1647		Water samples	end June 2016
KHSW113	35,30199	99,16873		Water samples	end June 2016
Temp1	35,2887	99,1796	-14,66	Temp./Oxy measure	early June 2015
Temp2	35,2871	99,1810	-13,53	Temp./Oxy measure	early June 2015
Temp3	35,2847	99,1824	-12,58	Temp./Oxy measure	early June 2015
Temp4	35,3033	99,1733	-18,78	Temp./Oxy measure	early June 2015
Temp5	35,29409	99,17612	17,85	Temp./Oxy measure	end June 2016

3. Chronology frame

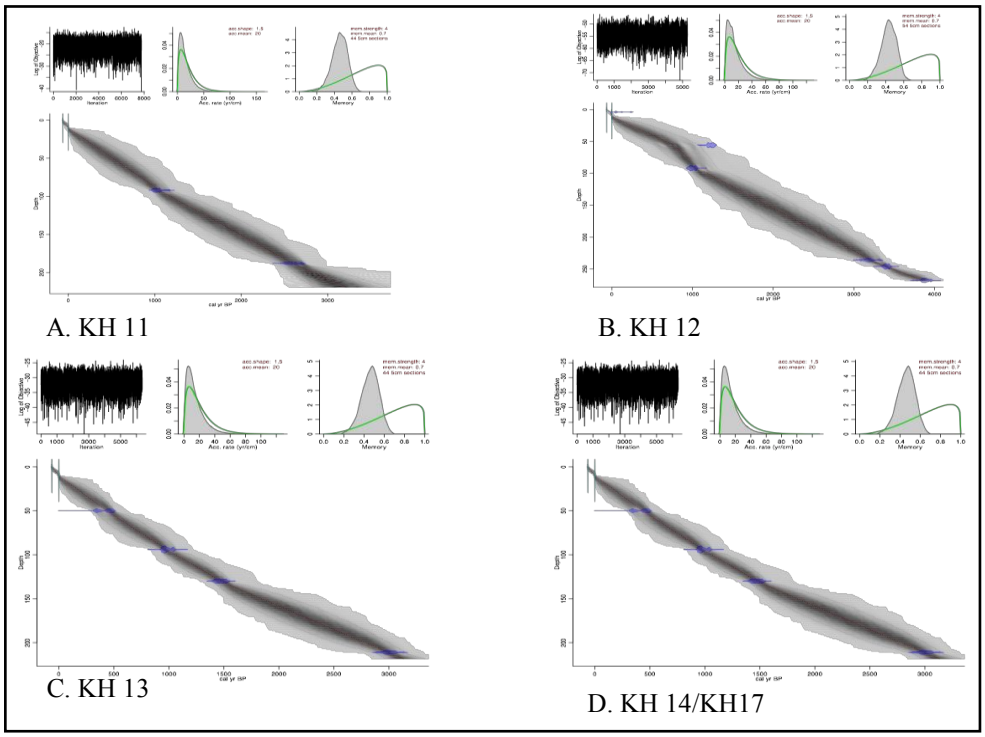

Fig. App.II 1 Age-depth model of sediment cores KH11-14/17, Kuhai Lake. Bacon output graph refers to R [version 2.2] (Blaauw and Christen 2011). Upper panels depict the MCMC iterations (left: stationary distribution among neighboring iterations). The prior (green curves) and posterior (grey histograms) distributions for the accumulation rate (middle panel) and memory (right panel). Bottom panel shows the calibrated ^{14}C dates (transparent blue) and the age-depth model (darker greys indicate more likely calendar ages; grey dotted lines show 95% confidence intervals; red dotted line shows the single best model based on the weighted mean age for each depth.

Tab. App.II 2 Full set of OSL results at Kuhai catchment based on ICP and NAA.

Lab ID	Sample ID	Section No.	Height (cm)	Depth (cm)	U/ppm	Th/ppm	K/%	Dose rate (Gy/ka)		De (Gy)		Aliquots Num.	WC%	Age (ka)	
								Qz	K-Fs	Qz	K-Fs			Qz	K-Fs
ICP obtained															
NL-904	KHO1-1	KHS6	400	125	3.05±0.03	7.82±0.12	1.44±0		3.77±0.25		1.09±0.04	8	2.50		0.29±0.02
NL-905	KHO1-2			180-185	2.98±0.03	7.92±0.04	1.42±0.03		3.62±0.24		1.77±0.03	8	5.04		0.49±0.03
NL-906	KHO1-3			245-250	2.36±0.03	7.05±0.1	1.33±0.02		3.29±0.24		2.42±0.01	8	4.98		0.74±0.05
NL-907	KHO1-4			320	2.03±0.01	6.44±0.02	1.26±0.06		3.11±0.24		4.15±0.06	8	3.64		1.34±0.11
NL-908	KHO2-1	KHS7	165	70-75	2.15±0.03	7.67±0.09	1.42±0.04		3.57±0.25		0.86±0.02	8	1.91		0.24±0.02
NL-909	KHO2-2			145-150	1.97±0.01	7.13±0.06	1.43±0.02		3.35±0.23		3.66±0.07	8	5.41		1.09±0.08
NL-910	KHO2-3			125-130	2.28±0.03	8.23±0.08	1.56±0.01		3.56±0.23		1.71±0.03	8	7.84		0.48±0.03
NL-911	KHO3-1	KHS15	190	75-80	2.01±0.01	6.98±0.1	1.56±0.05		3.50±0.23		1.70±0.11	8	6.09		0.49±0.04
NL-912	KHO3-2			110-115	2.33±0.02	7.99±0.15	1.44±0.03		3.46±0.23		1.31±0.03	8	7.78		0.38±0.03
NL-913	KHO3-3			160-165	2.38±0.03	8.08±0.07	1.47±0.02		3.44±0.22		5.62±0.33	8	9.27		1.63±0.14
NL-914	KHO4-1	KHS13	200	140-145	2.22±0.02	7.29±0.04	1.40±0.01		3.44±0.24		2.61±0	8	3.81		0.76±0.05
NL-915	KHO4-2			170-175	2.20±0.05	7.58±0.09	1.43±0.05		3.39±0.23		5.96±0.08	8	6.51		1.76±0.12
NL-916	KHO5-1	KHS17	60	25-30	2.58±0.03	11.67±0.09	2.06±0.04		4.11±0.21		17.12±2.16	8	16.24		4.17±0.57
NL-917	KHO5-2			45-50	2.75±0.07	10.40±0.25	1.88±0.02		4.00±0.21		35.86±0.92	8	13.13		8.98±0.53
NL-918	KHO6-1	KHS25	115	50-55	2.45±0.01	9.23±0.03	1.66±0.06		3.70±0.22		24.24±0.12	8	11.45		6.54±0.39
NL-919	KHO6-2			73-76	2.17±0.04	8.14±0.07	1.48±0.02		3.53±0.23		26.55±0.08	8	6.51		7.51±0.49
NL-920	KHO6-3			105-110	2.11±0.02	6.02±0.02	1.16±0.03		3.08±0.23		22.84±2.1	8	5.21		7.41±0.88
NL-921	KHO7-1	KHS26	320	38-43	2.26±0.03	7.77±0.07	1.48±0.02		3.72±0.26		32.17±0.4	8	0.77		8.64±0.61
NL-922	KHO7-2			137-142	2.34±0.02	7.22±0.02	1.50±0.03		3.66±0.26		33.53±1.14	8	0.68		9.17±0.72
NL-923	KHO7-3			240-245	2.26±0.01	7.29±0.01	1.53±0.01		3.45±0.23		34.31±0.52	8	5.85		9.95±0.68
NL-924	KHO7-4			300-305	2.31±0.02	8.53±0.06	1.60±0.05		3.43±0.21		35.37±1.06	8	11.20		10.3±0.71
NAA obtained (used in this study)															
NJU-1995	KH4-1	KH4	300	240	1.56±0.07	5.45±0.19	1.34±0.05	2.15±-0.15	2.49±0.15	6.34±0.21	10.9±0.39	10/11	5.14	**2.95±0.23**	4.38±0.31
NJU-1996	KH4-2			160	1.99±0.08	6.82±0.22	1.66±0.05	2.24±0.15	2.58±0.16	1.6±0.17	1.7±0.03	10/6	4.88	0.72±0.09	**0.66±0.04**
NJU-1997	KH4-3			70	2.14±0.09	6.21±0.2	1.54±0.05	2.24±0.15	2.58±0.16	1.26±0.13	0.98±0.03	9/9	2.41	0.56±0.07	**0.38±0.03**
NJU-1998	KH4-4			20	1.96±0.08	7.5±0.24	1.46±0.05	2.34±0.15	2.68±0.16	0.91±0.06	0.64±0.02	8/9	2.84	0.39±0.04	**0.24±0.02**
NL-904	KHO1-1	KHS6	400	125	2.94±0.11	7.33±0.23	1.15±0.05		3.43±0.26		1.09±0.04	8	2.50		0.32±0.03
NL-905	KHO1-2			180-185	2.83±0.1	6.96±0.23	1.15±0.05		3.27±0.24		1.77±0.03	8	5.04		0.54±0.04
NL-906	KHO1-3			245-250	2.23±0.09	6.46±0.21	1.16±0.05		3.07±0.24		2.42±0.01	8	4.98		0.79±0.06
NL-907	KHO1-4			320	1.95±0.08	6.15±0.21	1.07±0.05		2.89±0.24		4.15±0.06	8	3.64		1.44±0.12
NL-908	KHO2-1	KHS7	165	70-75	1.87±0.08	7.15±0.23	1.13±0.05		3.19±0.25		0.86±0.02	8	1.91		0.27±0.02
NL-909	KHO2-2			145-150	1.84±0.08	6.34±0.21	1.14±0.05		3.00±0.23		3.66±0.07	8	5.41		1.22±0.10
NL-910	KHO2-3			125-130	2.26±0.09	7.39±0.24	1.27±0.05		3.24±0.23		1.71±0.03	8	7.84		0.53±0.04
NL-911	KHO3-1	KHS15	190	75-80	2.05±0.09	7.45±0.24	1.27±0.05		3.27±0.23		1.70±0.11	8	6.09		0.52±0.05
NL-912	KHO3-2			110-115	2.33±0.09	7.20±0.23	1.22±0.05		3.21±0.23		1.31±0.03	8	7.78		0.41±0.03
NL-913	KHO3-3			160-165	2.30±0.09	7.45±0.24	1.16±0.05		3.10±0.22		5.62±0.33	8	9.27		1.81±0.17
NL-914	KHO4-1	KHS13	200	140-145	2.07±0.09	6.76±0.22	1.18±0.05		3.16±0.24		2.61±0	8	3.81		0.83±0.06
NL-915	KHO4-2			170-175	1.98±0.08	7.32±0.23	1.27±0.05		3.17±0.23		5.96±0.08	8	6.51		1.88±0.14
NL-916	KHO5-1	KHS17	60	25-30	2.70±0.10	10.90±0.31	1.68±0.06		3.77±0.21		17.12±2.16	8	16.24		4.54±0.63
NL-917	KHO5-2			45-50	2.68±0.10	10.30±0.29	1.78±0.06		3.89±0.22		35.86±0.92	8	13.13		9.23±0.57
NL-918	KHO6-1	KHS25	115	50-55	2.34±0.09	9.28±0.27	1.50±0.05		3.55±0.22		24.24±0.12	8	11.45		6.83±0.42
NL-919	KHO6-2			73-76	2.25±0.09	8.00±0.24	1.31±0.05		3.39±0.23		26.55±0.08	8	6.51		7.84±0.54
NL-920	KHO6-3			105-110	1.92±0.08	5.63±0.20	0.99±0.05		2.86±0.23		22.84±2.1	8	5.21		7.99±0.98
NL-921	KHO7-1	KHS26	320	38-43	2.18±0.09	7.21±0.23	1.37±0.05		3.55±0.26		32.17±0.4	8	0.77		9.05±0.67
NL-922	KHO7-2			137-142	2.12±0.09	7.00±0.22	1.36±0.05		3.44±0.26		33.53±1.14	8	0.68		9.74±0.80
NL-923	KHO7-3			240-245	2.24±0.09	6.84±0.23	1.30±0.05		3.20±0.23		34.31±0.52	8	5.85		10.71±0.80
NL-924	KHO7-4			300-305	2.10±0.09	7.61±0.24	1.46±0.05		3.21±0.21		35.37±1.06	8	11.20		11.04±0.80

4. Minerals

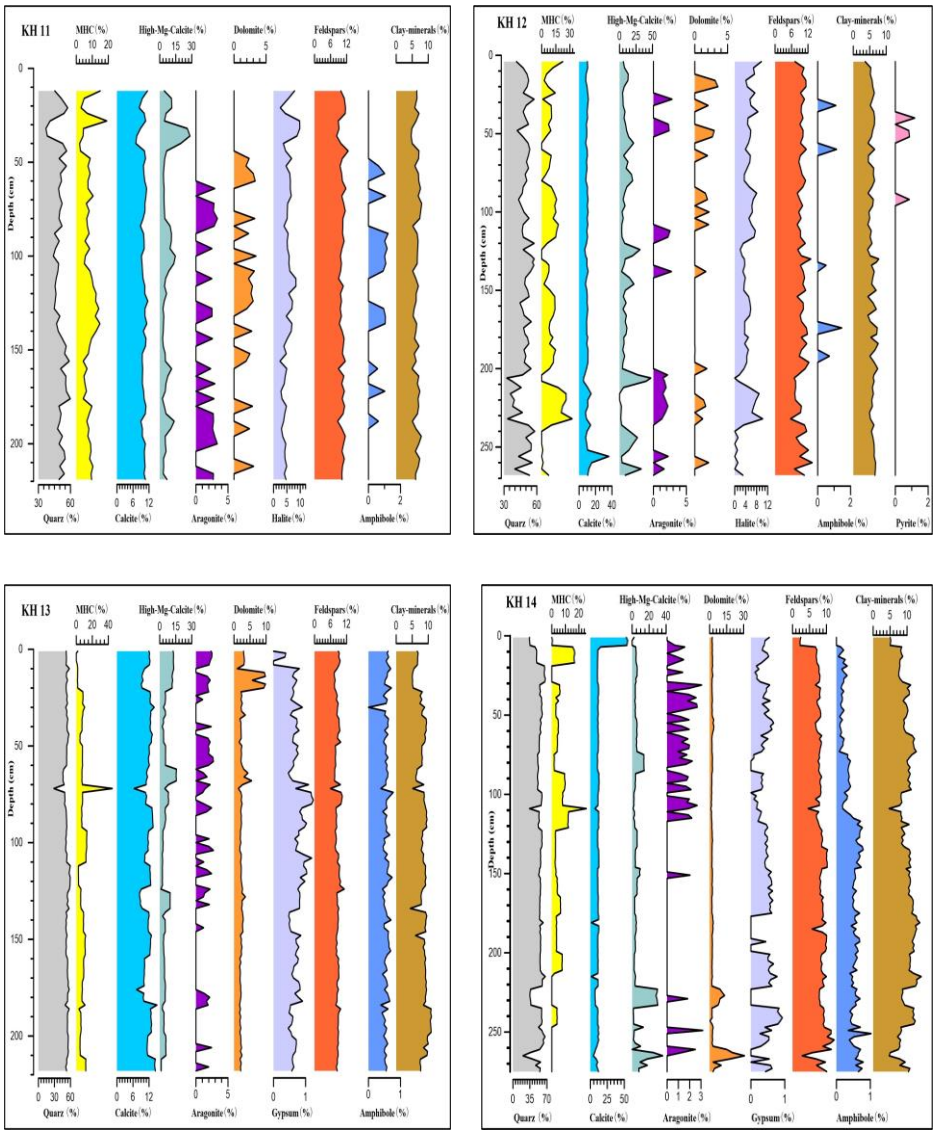

Fig. App.II 2 Minerals distributions against depth in sediment cores KH11-14 in Kuhai Lake.

5. Ostracods

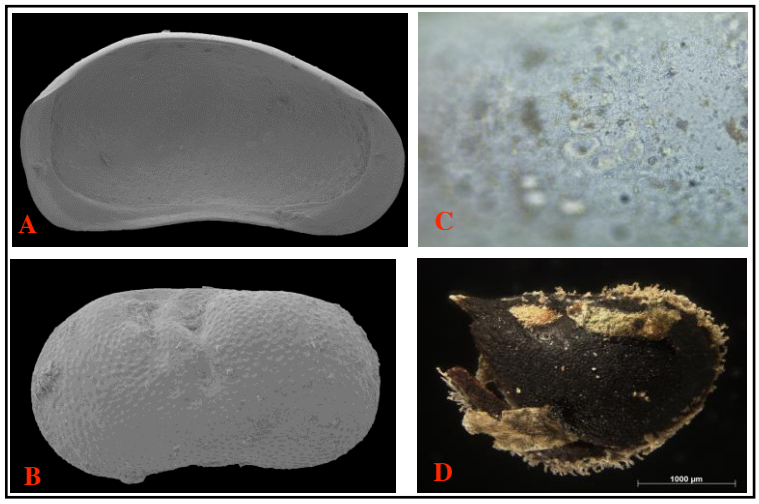

Fig. App.II 3 SEM (A-B) and transmitted light microscope photos (C-D) of additional ostracods and seed in Kuhai Lake area. (A) *Fabaeformiscandona rawsoni* (KHS27-5), f. lv. int. 1.18 mm. (B). *Ilyocypris* spec. (KHS27-15), lv.ext. 0.82 mm. (C) *Fabaeformiscandona rawsoni* f.lv., scars. (D) *Ruppia maritima* seed, KH16-206-20, 2.5x. **Abbreviations**: f.=female; lv= left valve; int.= internal view; ext.= external view. Specimens Friedrich-Schiller-Universität Jena, Germany. All samples are stored at Nanjing University.

6. Sections—description and photos of additional sections in Kuhai Lake area

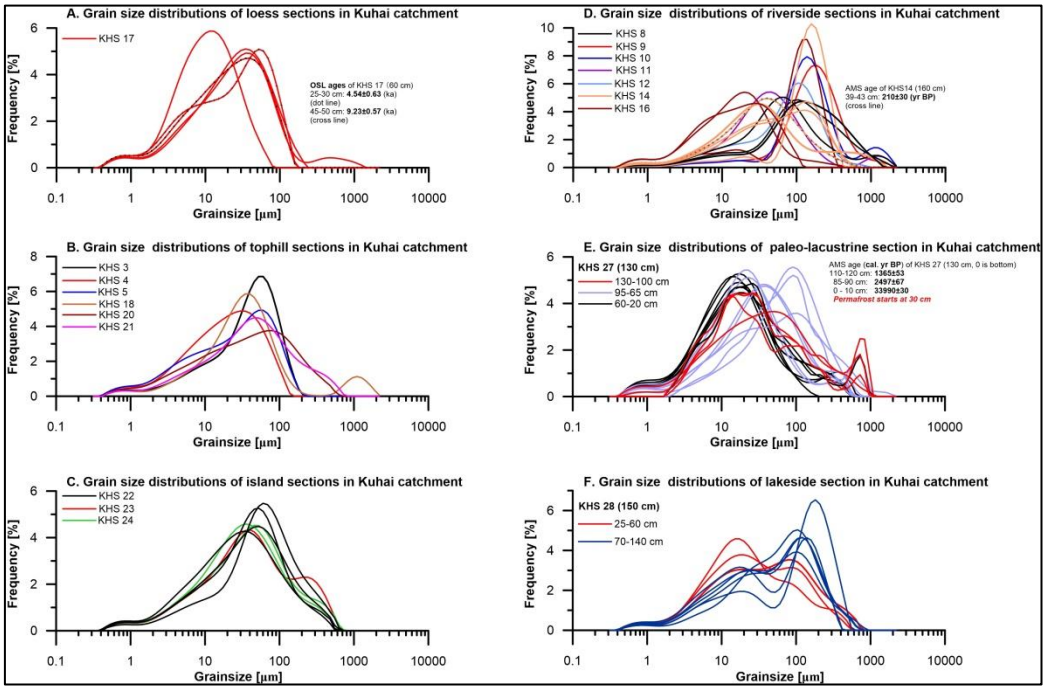

Fig. App.II 4 Grainsize distribution curves of most sections in Kuhai Lake area.

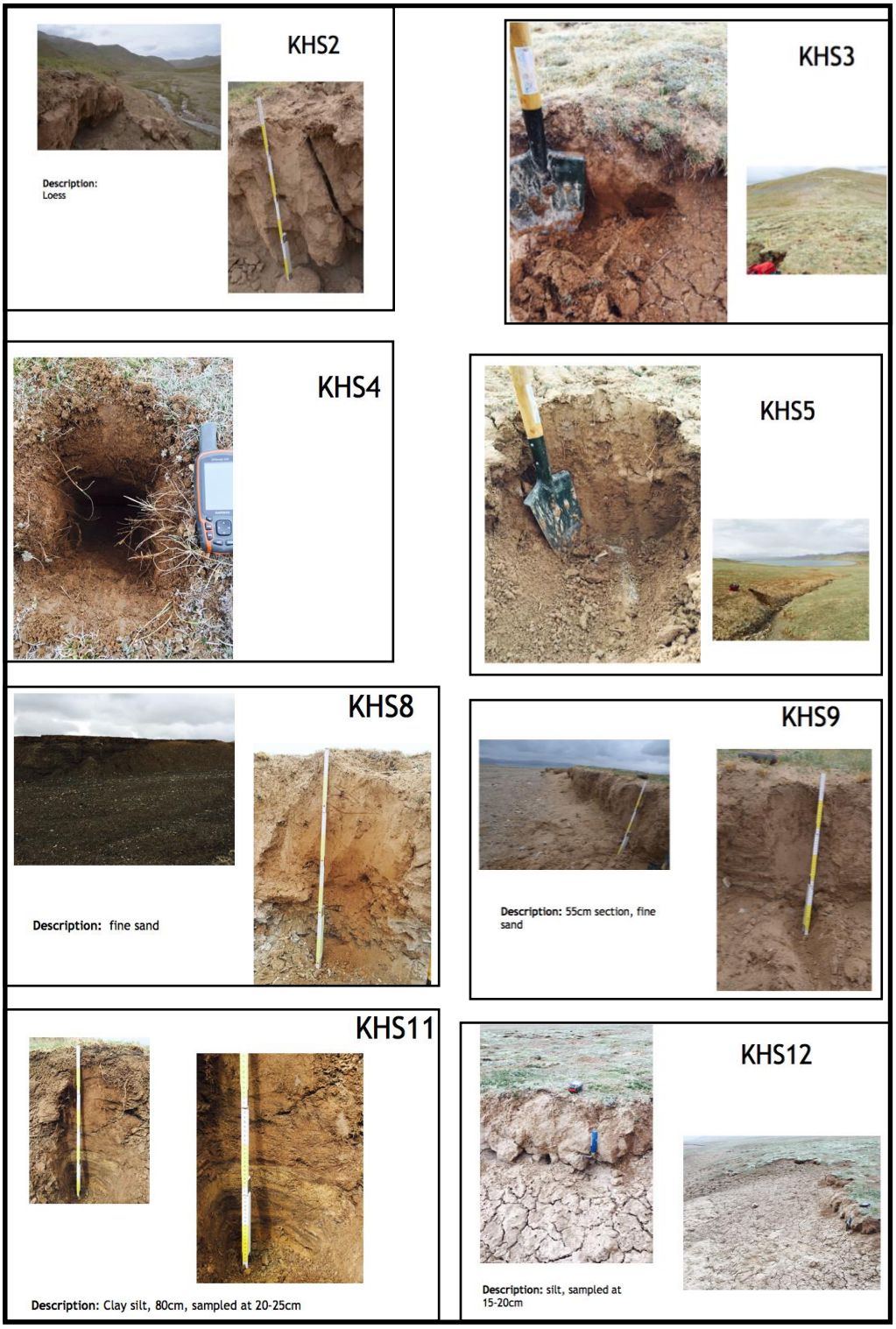

Fig. App.II 5a Photos and descriptions of sections KHS 2-5, KHS8-9 and KHS11-12.

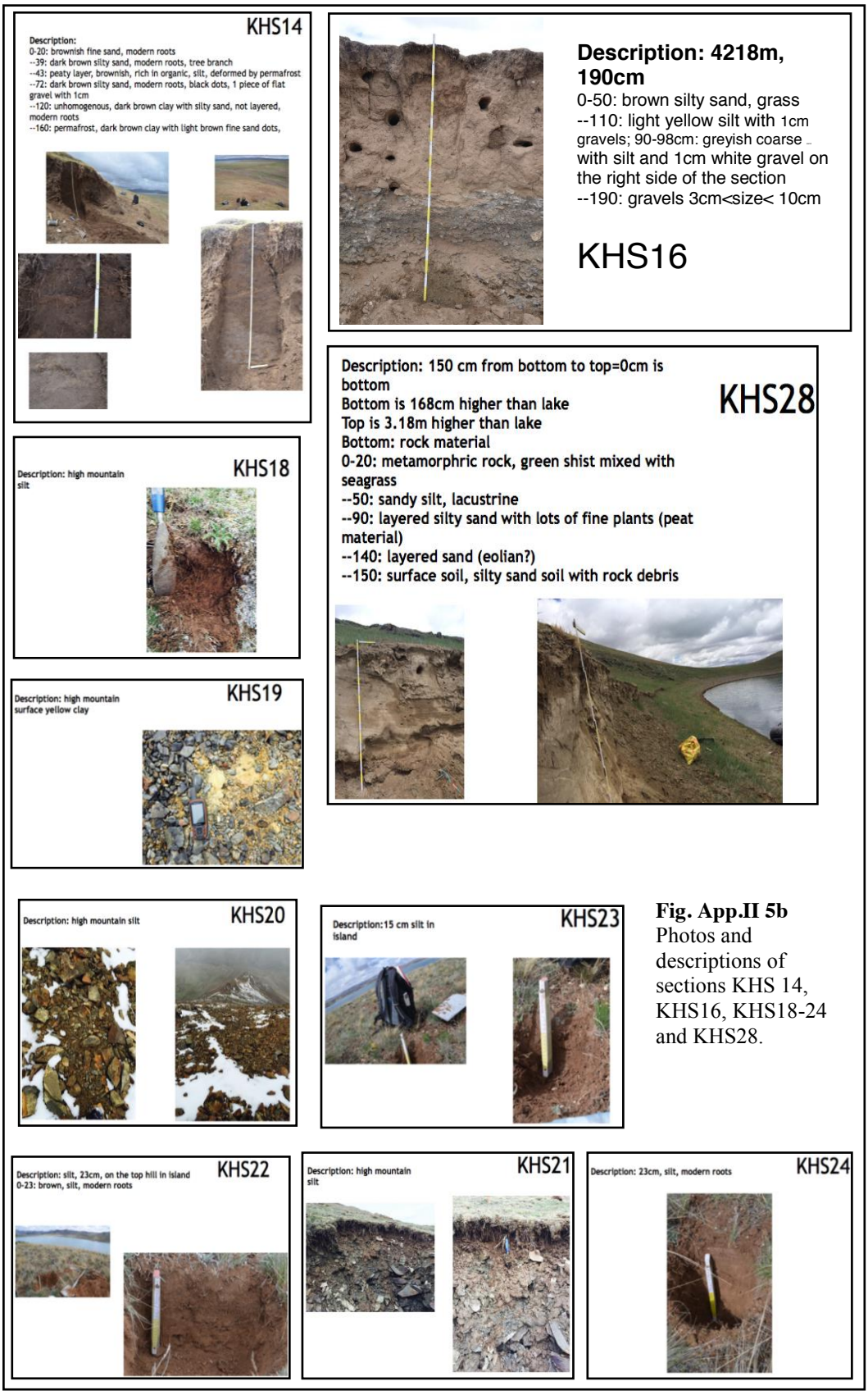

Fig. App.II 5b Photos and descriptions of sections KHS 14, KHS16, KHS18-24 and KHS28.

Publications

Yan, D., Wünnemann, B., Hu Y., Frenzel P., Zhang Y., Chen K., (in rev.). Wetland evolution in the Qinghai Lake area, China, in response to hydrodynamic and eolian processes during the past 1,100 year. ***Quaternary Science Reviews*** 162, 42-59.

Gupta, A., Dutt, S., Wünnemann,B**., Yan, D**.,(in rev). A long arid interlude in the NW Himalaya during ~4350-3450 cal. yrs BP and collapse of the Indus Valley civilization. ***Geophysical Research Letters*** (In review).

Ramisch, A., Lockot,G., Haberzettl, T., Hartmann, K.,Kuhn, G., Lehmkuhl, F.,Schimpf, S., Schulte, P., Stauch, G., Wang, R., Wünnemann,B., **Yan, D.**, Zhang, Y.,Diekmann B., 2016. A persistent northern boundary of Indian Summer Monsoon precipitation over Central Asia during the Holocene. ***Scientific Report*** 6, 25791.

Wünnemann, B., **Yan, D.**, Ci, R., 2015. Morphodynamics and lake level variations at Paiku Co, southern Tibetan Plateau, China. ***Geomorphology***. 246, 489-501.

Yan, D., Wünnemann, B., 2014. Late Quaternary water depth changes in Hala Lake, northeastern Tibetan Plateau, derived from ostracods assemblage and sediment propertied in multiple sediment records. ***Quaternary Science Reviews*** 95, 95-114.

Yan, D., Wuennemann, B., Stauch, G., Zhang, Y., E, C., Chen, K., Cao, G., Wang, J., 2014. Later Quaternary lake-catchment processes in Hala Lake, northern Tibetan Plateau, and their effects on lake evolution. ***AGU***, Oral presentation.

Wünnemann, B., Wagner, J., Zhang, Y., **Yan, D.**, Wang, R., Shen, Y., Fang, X., Zhang, J., 2012. Implications of diverse sedimentation patterns in Hala Lake, Qinghai Province, China for reconstructing Late Quaternary climate. ***Journal of Paleolimnology*** 48 (4), 725-749.

Declaration

I hereby declare that all parts of this dissertation were done by myself only with support of listed references therein.

Berlin, 30.01.2017

Dada YAN